LUT
Lappeenranta
University of Technology

Mehdi Hasan

PURIFICATION OF AQUEOUS ELECTROLYTE SOLUTIONS BY AIR-COOLED NATURAL FREEZING

Thesis for the degree of Doctor of Science (Technology) to be presented with due permission for public examination and criticism in the Suvorov auditorium of Technopolis at Lappeenranta University of Technology, Lappeenranta, Finland on the 19th of October, 2016, at noon.

Acta Universitatis
Lappeenrantaensis 717

Supervisors Professor Marjatta Louhi-Kultanen
LUT School of Engineering Science
Lappeenranta University of Technology
Finland

Associate Professor Jaakko Partanen
LUT School of Engineering Science
Lappeenranta University of Technology
Finland

Reviewers Professor Joachim Ulrich
Department of Thermal Process Technology
Martin Luther University Halle-Wittenberg
Germany

Associate Professor, Dr. Elif Genceli Güner
Department of Chemical Engineering
Istanbul Technical University
Turkey

Opponents Professor Joachim Ulrich
Department of Thermal Process Technology
Martin Luther University Halle-Wittenberg
Germany

Professor Henrik Saxén
Department of Chemical Engineering
Åbo Akademi University
Finland

ISBN 978-952-335-004-5
ISBN 978-952-335-005-2 (PDF)
ISSN-L 1456-4491
ISSN 1456-4491

Lappeenrannan teknillinen yliopisto
Yliopistopaino 2016

Abstract

Mehdi Hasan
Purification of aqueous electrolyte solutions by air-cooled natural freezing
Lappeenranta 2016
78 p.
Acta Universitatis Lappeenrantaensis
Diss. Lappeenranta University of Technology
ISBN 978-952-335-004-5
ISBN 978-952-335-005-2 (PDF)
ISSN-L 1456-4491
ISSN 1456-4491

Freeze crystallization is a particular type of a purification method where the solvent freezes out, which constricts the volume of the solution, leaving thus behind a more concentrated solution. In the case of freezing an aqueous solution, water is the solvent which crystallizes and can be separated from the concentrated solution by the virtue of buoyancy. In an ideal situation, freeze crystallization of an aqueous solution produces ice crystals that do not contain any of the impurities present in the original solution. As the process continues, the original solution becomes more concentrated and the freezing temperature declines progressively.

Freezing point depression (FPD) is of vital importance in characterising the freezing behaviour of any solution. Due to this necessity, a new calculation method to predict FPD is presented in this work. In this method, designated ion-interaction parameters for the Pitzer model are extracted from reliable FPD data found in the literature, other than calorimetric data. The extracted parameters from FPD data are capable of predicting the freezing point more accurately than those resulted from the calorimetric data. The calculation method is exemplified for numerous 1-1 and 1-2 types of electrolytes.

Impurities in excess of the maximum recommended limits must be removed from wastewater prior to discharge because of their persistent bio-accumulative and detrimental nature. Natural freezing is suggested in the present work as a purification technique to treat huge volumes of wastewater in a sustainable and energy-efficient manner. The efficiency of freeze crystallization in the purification of wastewater by imitating natural freezing in a developed winter simulation with the provision of altering winter conditions is scrutinized in this thesis. Hence, natural freezing is simulated experimentally for ice crystallization from unsaturated aqueous Na_2SO_4 and $NiSO_4$ solutions to assess the feasibility of such a technique to be used to purify wastewaters containing electrolytes. This work presents a series of data in similitude of natural freezing of water from aqueous Na_2SO_4 and $NiSO_4$ solutions in various concentrations and freezing conditions. The influence of solution concentration and different freezing conditions, such as ambient temperature, freezing time and freezing rate, on the efficiency of the purification process is investigated by analysing the effective distribution

coefficient (K) of the solute between ice and the solution. The experimental results demonstrate clearly that high purity ice can be obtained from slow freezing of the solution with the concentration typically found in industrial wastewater.

During freeze crystallization, the diffusion of impurities from the solid-liquid interface to the bulk of the solution, along with the growth mechanism of the solid phase play an important role in determining the purity of the ice layer. Therefore, a calculation method is introduced to estimate the concentration of the solution at the advancing ice–solution interface in terms of the limiting distribution coefficient (K^*) from experimental K values at different growth conditions. The heat transfer -controlled growth rate of the ice limited by the free convective heat transfer coefficient of air (h_{air}) rather than the thermal conductivity of the ice (k_{ice}) and the heat transfer coefficient of the solution (h_{sol}) was found to prevail over the mass transfer of rejected solute molecules from the ice–solution interface to the bulk solution of experimental interest. A simplified and robust model is developed to estimate the thickness and growth rate of the ice layer formed from solutions at different freezing conditions, and the model is validated with experimental results. In addition, inclusion formation within the ice matrix during freezing is investigated for various solution concentrations, both macroscopically and microscopically.

Keywords: Freeze crystallization, eutectic point, purification of wastewater, natural freezing, crystal growth kinetics, suspension crystallization, static layer crystallization, electrolyte, Pitzer model, freezing point depression, heat transfer, mass transfer, distribution coefficient, ice growth rate, ice purity.

Acknowledgements

All praise to THE MOST EXALTED for providing me the wisdom, intellect, patience, perseverance, wiliness, enthusiasm, strength, and health with other innumerable bounties to accomplish the goal of my doctoral study well ahead of the schedule. Even a million thanks would belittle the contribution of Prof. Marjatta Louhi-Kultanen for generating the theme of the dissertation, and sorting out scientific challenges and financial supports. I would like to acknowledge Dr. Jaakko Partanen for his initiatives, expert guidance, and supports with endless manoeuvres.

As this study was carried out in the Thermal Unit Operations research group of the School of Engineering Science at Lappeenranta University of Technology (LUT), I am hence grateful to all staffs of this unit. Special thanks to exchange students - Thomas Regal, Mael L'Hostis, Bolormaa Bayarkhuu, Nirina Ramanoarimanana, and Olaya Aranguren, LUT student – Mikko Brotell, and Rasmus Peltola, and LUT graduate MSc. Kaisa Suutari for helping me by performing the experiments and sharing their insight. I would like to remember the assistance of the late Mr. Markku Maijanen during the building of the experimental setups and also Ms. Anne Marttinen for her help in administrative formalities.

I am grateful to Prof. Ville Alopaeus, Dr. Rüdiger U. Franz von Bock und Polach of Aalto University, Prof. Alison Lewis's group in the Crystallization and Precipitation Unit (CPU) of the University of Cape Town (UCT), especially to Mr. Jemitias Chivavava, Mr. Edward Peter, and Mr. Dereck Ndoro for their scientific discretion and the fruitful discussions. Thanks to Ariful Islam Jewel and the staffs of UCT, and countrymen for supporting me with everything during my research visit in South Africa.

I would like to convey my gratitude to the Academy of Finland, the Graduate School of Chemical Engineering (GSCE), the LUT foundation, and LUT graduate school for supporting my research work financially.

I am thankful to my friends – Hasnat Amin, Ashraf khan, Muhammad Adeel Maan, Hafiz Maan, Fahad Rezwan, Fayaz Ahmad, and Jitu Kumar for all their help and support.

Last but not least, my sincerest thanks go to my wife, parents, brother, and relatives for their perpetual encouragement and compassionate understanding, patience and continuous support during my doctoral study.

Mehdi Hasan
October 2016
Lappeenranta, Finland

Contents

List of publications

This thesis is based on the following papers. The rights have been granted by the publishers to include the papers in the thesis.

I. Hasan, M., Louhi-Kultanen, M., 2016. Water purification of aqueous nickel sulfate solutions by air cooled natural freezing. *Chem. Eng. J.*, 294, pp. 176–184.

II. Hasan, M., Louhi-Kultanen, M., 2015. Ice growth kinetics modelling of air-cooled layer crystallization from sodium sulfate solutions. *Chem. Eng. Sci.*, 133, pp. 44–53.

III. Partanen, J.I., Hasan, M., Vahteristo, K.P., Louhi-Kultanen, M., 2014. Determination of the Pitzer interaction parameters at 273.15 K from the freezing-point data available for solutions of uni-univalent electrolytes. *Ind. Eng. Chem. Res.*, 53, pp. 19351–19358.

IV. Hasan, M., Louhi-Kultanen, M., 2014. Determination of Pitzer parameters for 1-1 nitrate and 1-2 sulfate Solutions from freezing Point Data. *Chem. Eng. Technol.*, 37, pp. 1340–1346.

V. Hasan, M., Partanen, J.I., Vahteristo, K.P., Louhi-Kultanen, M., 2014. Determination of the Pitzer interaction parameters at 273.15 K from the freezing-point data available for NaCl and KCl solutions. *Ind. Eng. Chem. Res.*, 53, pp. 5608–5616.

Author's contribution

The author planned all experiments, made the calculations, and explained the results for Publications I, II, IV and V. The author wrote the manuscripts together with the other co-authors. The author also took actively part in the modelling and calculation of Publication III.

Nomenclature

a	Chemical activity ($mol \cdot dm^{-3}$)
A_φ	Debye-Hückel constant (-)
b	Electrolyte independent constant term in Pitzer equation $(mol \cdot kg^{-1})^{-0.5}$
B, B^ϕ	Electrolyte terms as explicit functions of ionic strength $(mol \cdot kg^{-1})^{-1}$
C	Solute concentration (wt-%)
$C^*_{p,m}$ (A,l)	Heat capacity at constant pressure of pure solvent in liquid phase at the freezing temperature ($J \cdot K^{-1} \cdot mol^{-1}$)
$C^*_{p,m}$ (A,s)	Heat capacity at constant pressure of pure solvent in solid phase at the freezing temperature ($J \cdot K^{-1} \cdot mol^{-1}$)
C^ϕ, C_{MX}	Pitzer mixed parameter $(mol \cdot kg^{-1})^{-2}$
C_p	Heat capacity ($J \cdot kg^{-1} \cdot K^{-1}$)
D	Diffusion coefficient ($m^2\ s^{-1}$)
E	Separation efficiency (wt-%)
f^γ	Function of ion strength
G	Growth rate ($m\ s^{-1}$)
H	Latent heat of freezing of impure ice ($J \cdot kg^{-1}$)
h_{air}	Heat transfer coefficient of air ($W\ m^{-2}\ K^{-1}$)
H_f	Latent heat of freezing of pure ice ($J \cdot kg^{-1}$)
h_{sol}	Heat transfer coefficient of solution ($W\ m^{-2}\ K^{-1}$)
I	Ionic strength ($mol \cdot kg^{-1}$)
i	Index number
K	Effective distribution coefficient (-)
k	Thermal conductivity ($W\ m^{-1}\ K^{-1}$)
k	Mass transfer coefficient ($m\ s^{-1}$)
K*	Limiting distribution coefficient (-)
k_{ice}	Thermal conductivity of ice ($W\ m^{-1}\ K^{-1}$)
L_C	Characteristic length (m)
m	Molality of the solution ($mol \cdot kg^{-1}$)
M	Molecular weight ($kg \cdot mol^{-1}$)
R	Universal gas constant ($J \cdot mol^{-1} \cdot K^{-1}$)
R_F	Freezing ratio (wt-%)
R_h	Heat transfer resistance ($s\ K\ m^{-1}$)
R_m	Mass transfer resistance ($s\ K\ m^{-1}$)
t	Freezing time (s)
T_a	Air temperature inside freezer (°C, K)
T_f	Freezing point of solution (°C, K)
T_f^*	Freezing temperature of pure solvent (°C, K)
ΔT	Degree of undercooling from solution's freezing point (°C, K)
ΔT_f	Freezing point depression (°C, K)
U	Overall heat transfer coefficient ($W\ m^{-2}\ K^{-1}$)
V	Volume (m^3)
X	Ice layer thickness (m)

x	Coordinate in a positive direction into the melt
z	Charge number (-)

Greek symbols

α	Constant term in Pitzer equation (-)
β^0, β^1, β^2	Pitzer parameters $(mol \cdot kg^{-1})^{-1}$
ϕ	Osmotic coefficient (-)
γ	Activity coefficient (-)
ν	Kinematic viscosity ($m^2\ s^{-1}$)
δ	Boundary layer thickness (m)
ρ	Density ($kg \cdot m^{-3}$)
ν	Stoichiometric coefficients (-)

Dimensionless numbers

Nu	Nusselt number
Gr	Grashof number
Pr	Prandlt number
Sc	Schmidt number

Subscripts

A	solvent
W	water
s	solid
b	bulk
i	interface
O	initial
M, c	Cation
X, a	Anion
T	thermal
C	concentration

Abbreviations

Burton-Prim-Slichter	BPS
Crystal size distribution	CSD
Differential mass transfer model	DMTM
Eutectic freeze crystallization	EFC
Freeze crystallization	FC
Freezing point depression	FPD
Natural freezing	NF
Solid-liquid equilibrium	SLE

PART I: Overview of the thesis

1 Introduction

1.1 Background

Water is one of the vital resources on the earth that is so far not produced synthetically for consumption. In addition to groundwater as a raw water source, rivers and lakes are mostly the sources of fresh surface water. Surface water forms only 0.007% (9.37×10^4 km^3) of the total water on the earth of 1.34×10^9 km^3 (Gleick, 1998). Auspiciously, this small fraction of easily accessible water is sufficient to fulfil human requirements by natural replenishment through the water cycle. The rapid deterioration of the quality of fresh surface water due to industrial discharge, coupled with depletion of groundwater resources and insatiable demand makes the whole world to confront a major challenge of securing adequate fresh water supplies to meet the demand.

Water and energy are highly intertwined and interdependent. Manipulation in one domain can affect the other greatly. Like water consumption, the energy requirement is also increasing day by day. Processing more fossil fuel and nuclear power to satiate the augmented energy demand will eventually contaminate the water bodies substantially. Besides, intense mining activities resulting from increasing global metal consumption and subsequent pollution of natural water resources exacerbates the water problem further. In mining and metallurgical industries, mostly sulfuric acid and nitric acid are used as the leaching agent, which ends up with SO_4^{2-} and NO_3^- containing effluents. Over the permissible level both are considered as threats to the environment (Primo et al., 2009, Silva et al., 2010). Effluents emitted from bioleaching processes *viz*. Talvivaara in Finland are also detrimental when dispersed in the environment due to their high sulfate concentrations and low pH values (Nurmi et al., 2010). Moreover, mining activities also contaminate ground water. For instance, Hitura mine in Finland reports contamination of groundwater with nickel and sulfate contents around the tailings impoundment. The amount of accumulated tailings was around 12 million tons with the average nickel content of 0.22 wt-% after 36 years of operation. Contamination of ground water by nickel and sulfate has been observed around the tailings area. Due to the elevated Ni^{2+} and SO_4^{2-} concentrations, the nearby household water resource for local residents has been abandoned (Heikkinen and Räisänen, 2008). The exploitation of sulfide minerals generally takes in the chemical and/or biological oxidation of sulfur and has consequences in the formation of acidic sulfate -containing wastewaters, termed as acid mine drainage, AMD (Kaksonen et al., 2006). Depending on the nature of the ore, the discharge of mining industries may contain different types of dissolved metal ions as well.

1.2 Problem statement

Wastewater needs to be treated before dispersing in the environment. Stringent legislation is being imposed on industrial wastewater worldwide for the protection of water bodies from pollution. Therefore, suitable purification techniques are also being adopted based on the type of constituents, concentration level and source of wastewater. These purification techniques are mostly associated with energy and chemical utilization, which might worsen the situation further. Various types of physical-chemical separation methods, such as ion exchange, adsorption, chemical precipitation, electrochemical treatment, evaporative recovery, pressure driven membrane filtration, etc. have been used to treat wastewater in recent years (**Publication I**). The downsides of these conventional separation techniques are listed in **Table 1.1**.

Table 1.1 Conventional separation technologies, principles and drawbacks.

Separation method	Principle of separation	Drawback
Ion exchange/adsorption	Removal of dissolved ions by replacing them with similarly charged ions/to adhere on the adsorbent	-Limited to small scale applications -Thermal sensitivity of resin -Further need for chemicals to regenerate resins -High cost -Efficient only for a dilute solution
Precipitation	Addition of chemicals to reduce solubility.	-Extra usage of chemicals -High cost due to mixing and separation -Suitable only for small scale applications
Membrane filtration	Selective membrane only allows the solvent to pass through it.	-Fouling of membrane -Efficient only for a dilute solution -Energy-intensive
Evaporation	Vaporization of the solvent to attain supersaturation and thus crystallizing the solute.	-High energy consumption -Not suitable for a very low solution

By and large, the quantities of wastewater generated from mining industries are quite significant, *ca.* above 1 million tons annually in Finland. It is discernible in **Table 1.1** that none of the conventional methods is suitable for the treatment of very dilute and voluminous wastewater simultaneously. So, there is a great need to treat this huge volume of wastewater in an energy-efficient manner in other ways than using the conventional methods.

Natural freezing (NF) could be one of the potential options to solve this problem. The ambient temperature is the key parameter to influence NF behaviour. For instance, the average temperature in Finland during the winter season is usually under 0˚C. Depending on the location, winter starts in the range of middle of October to middle of November and prevails 110 days to 190 days. **Figure 1.1** shows the average temperature of whole Finland during the winter 2016.

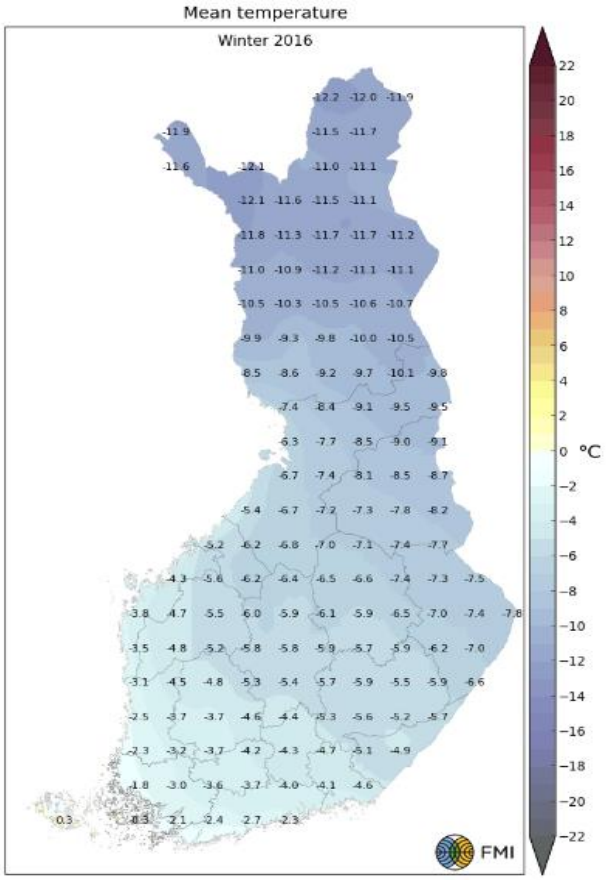

Figure 1.1 The average ambient temperature in Finland during the winter 2016 [Adopted from the Finnish Meteorological Institute].

Figure 1.1 shows clearly that Finland is rich in cooling capacity. Therefore, layer crystallization ensued by natural freezing of wastewater could be a very cost-effective purification technique in cold regions like Finland. The interest in natural freezing of wastewater is increasing, but hitherto the research achievements are very limited (Bu et al., 2011). For practical implementation of natural freezing, the basic principle and possible applications and influencing factors should be investigated, which is done in this work.

1.3 Objectives of the thesis

If the nature could be employed as a bounty to freeze wastewater, the problems associated with energy and chemical usages would be solved in a very sustainable and green manner. Natural freezing could be used, especially, in places where the temperature goes down to the sub-zero level during the winter season. Wastewater can be purified through the formation of a less contaminated ice layer by natural freezing. Freezing concentrates and thus reduces the volume of wastewater. Furthermore, if natural freezing is continued until the so called eutectic point at which ice and solute crystallization happen simultaneously, extra financial value can be added in terms of saleable solute recovery. Separation of ice from salt from the residual solution becomes very easy because of the significant density difference between them. Although freezing as a separation technique has been already experimented with in the diverse sectors mentioned above, this is yet to be done for mining wastewater. A fundamental study of the mass and energy transfer based on the solid-liquid equilibrium (SLE) is also of importance to aid the design of natural freezing as a novel purification method. In view of this challenge, the paramount objective of this work is to justify the efficacy of natural freezing to treat wastewater by the formation of an ice layer of higher purity on the surface of wastewater ponds in cold climate regions where the temperature goes below 0˚C during winter. The influence of solution concentration and freezing conditions, such as ambient temperature, freezing rate and freezing time on the efficiency of the purification process are investigated in this study. The kinetics of ice crystallization during freezing is also studied. A robust model is developed to depict the ice growth rate at different freezing conditions and the model is validated with experimental data. Furthermore, the formation of inclusion as a main source of impurity within the ice matrix while freezing a solution is investigated both macroscopically and microscopically.

1.4 Potential exploitations

Low energy requirement (Liu et al., 1997), high product quality and good separation efficiency (Kapembwa et al., 2013) are the main avails of FC. Typically, a solid-liquid phase equilibrium (SLE) prevails during freezing, and is of crucial importance in industrial processes like wastewater treatment, desalination and crystallization (Mohs et al., 2011, Marliacy et al., 1998). Therefore, an accurate model for predicting the freezing point of these systems is very important in the application of FC. In the case of eutectic freeze crystallization (EFC), solubility modelling in the sub-zero temperature range is also indispensable.

Sodium sulfate (Na_2SO_4) is present multifariously in effluents emanating from the use of detergents, in textile, glass and mining industries, kraft pulping (Garnett, 2001) and the ash of marine fossil fuels (Lin and Pan, 2001). On the other hand, nickel (II) ion in excess of the maximum allowable limits is found in many wastewaters discharged from electroplating, electronics, metal cleaning and textile industry sites, and due to toxicity, such wastewaters can cause serious water pollution if not treated before disposal (Shang et al., 2014). Because of their appearance in diverse wastewaters, natural freezing is simulated experimentally for Na_2SO_4 (aq) and $NiSO_4$ (aq) solutions in this work.

1.5 Plan of development

This thesis comprises six main chapters. **Chapter 2** provides the basic theory of freeze crystallization (FC), its classification, thermodynamics and kinetics behind FC as a purification and concentration method based on natural freezing (NF). **Chapter 3** introduces the Pitzer model to predict the freezing points of various 1-1 and 1-2 types electrolytes of practical interest. The virial coefficients of the Pitzer model mostly found in the literature at the temperature of interest for FC are acquired from isopiestic data. The extraction of these ion-interaction parameters from freezing point data which can be measured more accurately makes it possible to predict the freezing point more precisely. This is done by a novel calculation method, and the utilization of these parameters ameliorates the accuracy level of freezing point prediction. **Chapter 4** discusses all the relevant thermodynamic and physical properties of Na_2SO_4 (aq) and $NiSO_4$ (aq) solutions by which the efficiency of natural freezing as a purification method is simulated. These data sets are utilized for freezing kinetics exposition. **Chapter 5** presents the methodology of the experimental set-up and experimental procedure to simulate natural freezing with Na_2SO_4 (aq) and $NiSO_4$ (aq) solutions of different concentrations under different freezing conditions. The influence of different factors on the efficiency of the purification process according to the experimental results, kinetics of ice crystallization from solution by NF, and ice layer morphology analysis, along with explanations with reference to the literature are discussed in **Chapter 6**.

2 Freeze crystallization kinetics and ice purity

2.1 Introduction

Crystallization refers to the formation of solid phase/s from a solution at a certain operation condition. It is one of the most commonly employed techniques with multifarious functionalities used in purification, concentration and solidification -related industrial processes. Nucleation and growth rate are the two principle kinetic phenomena that happen during the crystallization process based on the thermodynamic driving force designated as supersaturation. Besides operating conditions, these two parameters are the determinants of crucial product quality, such as crystal size distribution (CSD) and the purity of any crystallization process. Generally, supersaturation is defined as a deviation from the thermodynamic equilibrium condition (Ulrich and Stelzer, 2011). Supersaturation is typically expressed in terms of concentration and temperature.

Nucleation is the generation of nanoscopically small crystalline bodies from a supersaturated fluid (Kashchiev, 2000, Mullin, 2001). There are two different types of nucleation: primary nucleation, which occurs spontaneously in the absence of any crystal (known as homogeneous nucleation) or in the presence of foreign particles (heterogeneous nucleation), and secondary nucleation which is induced by the presence of already-existing crystals in the solution. The attainment of critical sized nuclei is followed by growth, which means a layer-by-layer attachment of solute molecules on crystal surfaces. The attachment of a molecule onto a crystal surface is followed by its adsorption onto the surface and diffusion along the surface to the step or kink site for incorporation into the lattice. The kink is the most favourable location of attachment since the surface free energy is minimized there (Myerson, 2002).

Two frequently used terms in crystallization processes are solution crystallization and melt crystallization. The distinction between these two crystallization techniques can't be drawn very accurately. However, categorization can be made based on applied techniques used for these two cases. In general, the portion of the crystallizing component in melt crystallization is higher than all the other components present in the mixture. Consequently, the viscosity of the melt increases and the heat transfer becomes the rate dominating factor (Ulrich and Stelzer, 2013).

2.2 Freeze crystallization

2.2.1 Basic concept of freeze crystallization

Freeze crystallization (FC) is one kind of melt crystallization process where the solvent is crystallized out of the melt. Briefly, the freezing of a solvent out of the solution at its freezing point is known as freeze crystallization. **For instance, ice crystallization from the aqueous solution at its freezing point can be categorized as freeze crystallization of water**. The phase diagram in **Figure 2.1** shows that eutectic conditions are obtainable

either by continued ice crystallization until the salt solubility line is attained (A) or by continued salt crystallization until the ice crystallization line is reached (B) (Pronk et al., 2008).

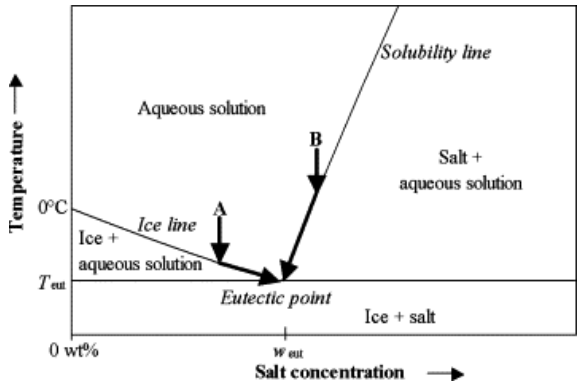

Figure 2.1 Phase diagram of a simple two-component system [Adopted from Pronk et al., 2008].

It is clear from **Figure 2.1** that the eutectic point is the intersection point of the ice line and the solubility line. At the eutectic point, both ice and salt crystallize simultaneously. Ice floats on the top and salt settles in the bottom and thereby, separation becomes very easier. The ice line designates the freezing point as a function of solute concentration.

Theoretically, it is possible to produce pure ice or pure salt by cooling the solution until the eutectic point is reached. Except for solid-solution formation, during freezing the solute molecules in a solution cannot fuse in the solid phase owing to constraints of their size/charge (Petrich and Eicken, 2009), and thereby only the solvent molecules metamorphose to the solid phase. Lowering of the freezing temperature of a solution below that of the pure solvent (water in **Figure 2.1**) in the presence of electrolytes or other types of solutes is known as freezing point depression (FPD). In general, the higher the concentration, the greater the FPD. This is one of the colligative properties of solution which results from different types of interaction between the solute and the solvent in the solution.

2.2.2 Advantages of freeze crystallization

Freeze crystallization has some advantages over conventional evaporative concentration due to the fact that the heat of fusion (6.01 $kJ \cdot mol^{-1}$) is almost seven times less than the heat of evaporation (40.6 $kJ \cdot mol^{-1}$). The low temperature condition makes it possible to use inexpensive construction material for freeze crystallization. No poisonous fumes are usually generated at lower temperatures, and bacterial growth can be controlled easily (Genceli, 2008). Pure enough ice resulting from FC can also be used as a cooling storage (Randall et al., 2011). FC does not require any pre-treatment method for separation or chemicals, and is thereby free of the disposal of toxic chemicals to the environment. The

low temperature declines sensitivity to biological fouling and issues of scaling and corrosion in pipe systems (Williams et al., 2015). It is also possible to obtain higher yield and separation efficiency compared to conventional membrane and evaporative concentrations (Sánchez et al., 2010).

2.2.3 Classification of freeze crystallization

In general, there are two ways to form ice crystal from aqueous solutions (Müller and Sekoulov, 1992, Ratkje and Flesland, 1995, Wakisaka et al., 2001, Miyawaki, 2001), suspension crystallization and layer crystallization. As with other crystallization processes, both of these methods involve the formation of ice nuclei from the solution followed by their growth. In suspension freeze crystallization, the solution is cooled in an agitated vessel by circulating the coolant through the jacket, and thus, below the freezing temperature of the solution, ice crystals are generated in the suspension, from where the ice crystals are then separated (Rahman and Al-Khusaibi, 2014). Usually, scrapers are employed in this type of a crystallizer to thwart ice scaling on the subcooled surface, which might reduce the heat transfer rate drastically. High investment and maintenance costs in the wake of using the scraper is the limitation of such a process (Stamatiou et al., 2005). On the other hand, during layer crystallization, the ice crystallites in the solution cluster together to form a single ice layer on the cold surface. No need for moving parts and simple operation and handling advocate layer crystallization as a potential purification technique. However, in the case of rapid crystallization rate, the impurity level of the formed ice layer is usually high, which vacillates the practical implementation of this method (Raventós et al., 2012). A moderate growth condition is the prerequisite for forming a very pure ice layer from solutions.

Among the various types of layer-melt crystallization processes which are also induced by indirect-contact freezing, e.g., layer crystallization on a rotating drum, dynamic layer growth, both falling film type and circular tube type, and progressive freeze crystallization, the non-stirred static layer growth system is the simple one without any need of moving parts and solid-liquid separation devices. In this process, the crystal mass (ice) is grown from a stagnant solution. As the main mode of heat and mass transfer during this process is free convection, the residence time is extended and the growth rate of the layer is very low ($<10^{-7}$ ms^{-1}), which promotes high purification efficiency. Fast crystallization results in impure ice crystals. There are two possible mechanisms of growing a layer by this process: (i) the crystals grow larger by free convective heat or mass transfer resistance, and (ii) agglomeration of crystals and subsequent fusion of agglomerates into a very large ice crystal due to extended residence time (Rahman et al., 2006). A large volume of a solution can be frozen in a batch-wise mode and the growth rate can be low (Shirai et al., 1987, Shimoyamada et al., 1997) by this method. A plate-type contact surface opts to increasing the crystal-solution interface per unit volume.

2.3 Influence of heat and mass transfer on crystal growth kinetics of freeze crystallization

For the attainment of any solid-liquid equilibrium (SLE) like freezing, the chemical potential of the solvent must be equal between the liquid and the solid phases (**Publication V**). In the case of an aqueous system where the solute molecules/ions are not able to integrate into the ice crystal lattice, redistribution of the solute ensues during ice crystallization from the solution. The diffusion of the solute away from the ice-solution interface predisposes the redistribution of the solute in the solution during freezing (Butler, 2002).

Like other crystallization processes, freeze crystallization happens under a driving force known as undercooling. Theoretically, at a very low growth rate, the solute has enough time to diffuse away from the interface of the growing crystal (unless it has crystallographic similarities with the growing crystal that is prone to adsorption), leading to a pure crystal and highly enriched solution. On the other hand, at a high growth rate, the solute is unable to diffuse away from the growing crystal and is entrapped within the crystal layer, leading to an impure crystal. At a transitional growth rate, which covers many practical circumstances, some solute is incorporated into the crystal and some is rejected. Similar phenomena also transpire in the case of solution inclusion in the crystal layer. A typical freezing profile of a solution in shown in **Figure 2.2**.

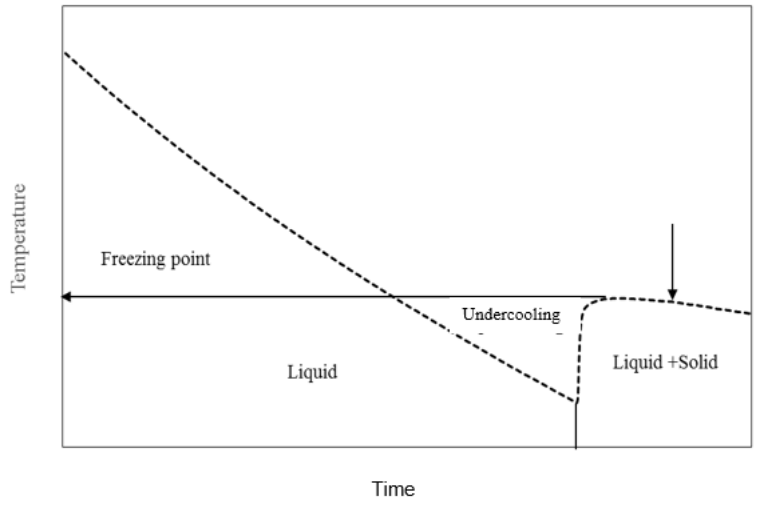

Figure 2.2 Freezing profile of a solution.

A solution can be cooled down to a temperature lower than the anticipated freezing point, i.e., 0°C in the case of pure water, without any phase change or ice formation. This is called undercooling. After a while, nucleation occurs and ice starts to form stochastically. Adding ice seeds is a technique to subdue the extent of undercooling. This is commonly

known as seeding. Momentarily, the temperature of the system increases in spite of continuous cooling due to the evolution of heat of crystallization. Then, the temperature of the ice-solution mixture starts to decrease very slowly with the course of time, which indicates that progressing freezing is concentrating and thus lowering the freezing point of the solution.

Cold air can be used as a medium for the static layer crystallization process to resolve the problem of impurity in the wake of rapid crystal growth, owing to a very low heat transfer coefficient which can vary from 12 $Wm^{-2}K^{-1}$ to 29 $Wm^{-2}K^{-1}$ in variation with stagnant to 6.7 ms^{-1} air velocity (Adams et al., 1960, Anderson, 1961). Therefore, the overall heat transfer coefficient of an indirect-contact solidification process induced by cold air would be low enough to ensure very low layer growth rate, and thus a highly efficient separation technique. This methodology is analogous to freezing wastewater in ponds during freezing days. The temperature and concentration profile of freezing a solution by cold air and the corresponding boundary layers are illustrated in **Figure 2.3.**

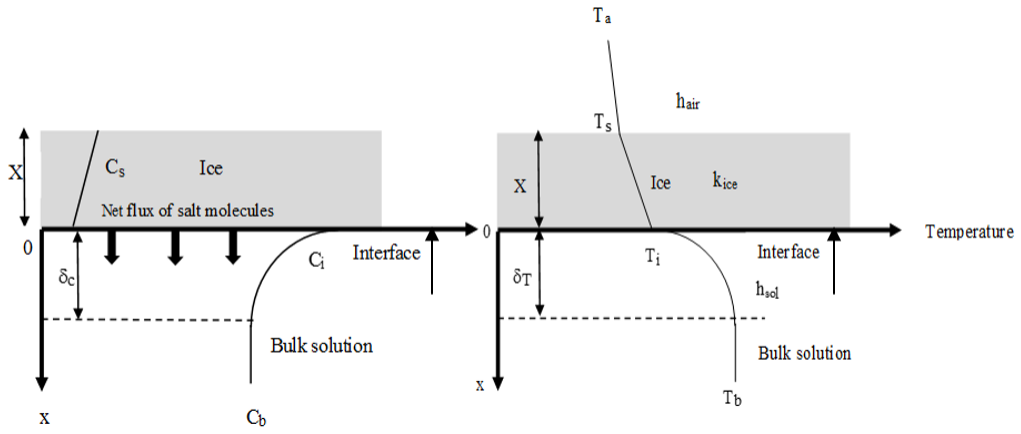

(a) (b)

Figure 2.3 Schematic depiction of (a) the concentration profile and (b) temperature profile of natural freezing of a solution (**Publication II**) in macroscale level.

Recent studies by Genceli et al., 2009 and Genceli et al., 2015 discover that the temperature profile at the ice-solution interface is not continuous. Consequently, the concentration might also be discontinuous at the ice-solution interface. Due to the exothermic nature of ice crystallization, the temperature jump across the interface is reported (Genceli et al., 2009). However, the temperature and concentration are assumed as continuous functions across the interface in order to avoid associated complexity while developing the model in this work.

After the onset of freezing, the latent heat of fusion rapidly raises the temperature very close to the thermodynamic equilibrium/freezing temperature. The effect of release of latent heat and redistribution of the solute during freezing a solution create temperature and concentration gradients in the liquid phase adjacent to the solid–liquid interface, thus generating thermal and mass boundary layers. Slow freezing is favourable for growing larger crystallites and minimizing solution occlusion (Glasgow and Ross, 1956) within the crystal matrix. Therefore, the purity of the ice crystals formed by freezing a solution is dependent on the growth rate (Butler, 2002).

2.3.1 Differential mass transfer model

During the growth of the crystal from melt, the extent of the concentration gradient in the locality of the advancing solid-liquid interface depends upon several factors, e.g., the solidification rate, the effective distribution coefficient K and the nature of the fluid flow (Weeks and Lofgren, 1967). The differential mass transfer model (DMTM) presented by Burton et al., (1953) is commonly used to construe the mass transfer of solute molecules between a single crystal and the melt. In their model, the solution concentration in the radial direction perpendicular to the growth condition a) is assumed to be uniform, b) the fluid is incompressible and uniform beyond the boundary layer, and c) the coordinates move at the same rate as the growing ice layer for being fixed to the solid-liquid interface, i.e., at x = 0, and extends in a positive direction into the melt (**see Figure 2.3**).

With an exception of the flow normal to the interface produced by ice growth, no fluid velocity exists at the ice-solution interface. Therefore, the flow can be assumed to be laminar at the interface and the fluid velocity is small enough for molecular diffusion to be the main means of transporting the rejected solute molecules away from the growing ice layer (Weeks and Lofgren, 1967). According to the BPS (Burton-Prim-Slichter) theory, the prevailing diffusion equation for a one-dimensional steady state system is

$$D\frac{d}{dx}\left(\frac{dC(x)}{dx}\right)+G\frac{dC(x)}{dx}=0 \qquad (2.1)$$

where D is the diffusion coefficient of the solute, x is the distance from the interface towards the melt, C(x) is the solution concentration within the boundary layer as a function of x, and G is the growth rate of the advancing ice front. Based on the assumption that diffusion in the solid phase is unlikely to happen and applying boundary conditions for steady-state growth

$$\left(C_i - C_s\right)G+D\frac{dC(x)}{dx}=0 \qquad \text{at } x = 0 \text{ and}$$

$$C\left(x\right)=C_b \text{at } x \geq \delta_c$$

Burton et al. (1952) proposed the solution of **Eq. (2.1)** at x = 0 as

$$K=\frac{K^*}{K^*+(1-K^*)\exp\left(-\frac{G}{k_l}\right)} \tag{2.2}$$

where $k_l = D/\delta_c$ is the mass transfer coefficient and δ_c is the boundary layer thickness for the concentration gradient at the ice-solution interface. **Eq. (2.2)** can be rearranged as

$$\ln\left(\frac{\frac{1}{K^*}-1}{\frac{1}{K}-1}\right)=\frac{G}{k_l} \tag{2.3}$$

2.3.2 Solute balance at the ice-solution interface

During the course of ice formation from the solution, the growth rate varies as the freezing advances and the solution becomes gradually more concentrated. However, for dilute solutions and/or if the volume of the solution is large enough (e.g., freezing huge volumes of effluents emanating from mining industries), then the increase in the concentration over a freezing time of experimental interest (the maximum freezing time was 24 h in this work) can be considered to be negligible, and the quasi-steady-state approximation would be rational. During the advancement of the ice layer from the solution, only a part of the solute molecules is fused into the ice as solution and the remainder is rejected at the progressively growing ice-solution interface. The rejected salt molecules are taken away from the interface by means of diffusion towards the boundary layer, δ_C. Under quasi steady state conditions, according to the solute balance at the ice –solution interface, the amount of rejected solute molecules per unit time and unit area, $G(C_i\text{-}C_s)$, should be equal to the diffusion flux of the solute molecules in the boundary layer (Kuroda, 1985) and can be expressed as

$$G(C_i-C_s)=k_l(C_i-C_b) \tag{2.4}$$

In **Eq. (2.4)**, the mass transfer resistance (R_m) of the average growth rate, G is $(C_i\text{-}C_s)/k_l$ (wt-% sm^{-1}) or $(C_i\text{-}C_s)\varphi/k_l$ (Ksm^{-1}), where the conversion factor is $\varphi = \rho_{ice}\alpha/\rho_b$ (Louhi-Kultanen, 1996). Here, α (Kwt-$\%^{-1}$) is the slope (α) of the liquid curve of the phase diagram of Na_2SO_4 - H_2O and the $NiSO_4$ - H_2O system is 0.27 K·wt-$\%^{-1}$ and 0.13 K·wt-$\%^{-1}$ in this work, and ρ_b and ρ_{ice} (kg·m^{-3}) represent the density of the bulk solution and the ice, respectively. After rearranging, **Eq. (2.4)** becomes

$$\left(\frac{1-\frac{K^*}{K}}{1-K^*}\right)=\frac{G}{k_l} \tag{2.5}$$

2.3.3 Overall heat balance

At the advent of ice crystallization from a solution, the removal of heat from the solution to the surrounding area is poised by the release of the heat of crystallization to the solution under quasi steady state condition, assuming that the change in the temperature of the solution as freezing proceeds is negligible (Kuroda, 1985) and thereby

$$G\rho_{ice}\Delta H=U(T_b-T_a) \tag{2.6}$$

where ρ_{ice} is the density of the ice layer, ΔH is the latent heat of freezing, and T_b and T_a are the temperatures of the bulk solution and ambient air, respectively. The heat transfer resistance (R_h) for the ice growth rate, G, in **Eq. (2.6)** is $\rho_{ice}\Delta H/U$ (Ksm^{-1}). The overall heat transfer coefficient, U, can be defined as **Eq. (2.7)**:

$$\frac{1}{U}=\left(\frac{1}{h_{sol}}+\frac{X}{k_{ice}}+\frac{1}{h_{air}}\right) \tag{2.7}$$

Here, X is the ice layer thickness, h_{sol} is the free convective heat transfer coefficient of the solution, h_{air} is the free convective heat transfer coefficient of air, and k_{ice} is the thermal conductivity of the ice. Under the assumption of no heat flux for radiation, sublimation and sensible heat loss, and replacement of the average ice growth rate, i.e., G = dx/dt, throughout the course of the ice layer formation, **Eq. (2.6) and Eq. (2.7)** generate

$$\int_0^X \rho_{ice}\Delta H dX=\int_0^t U(T_b-T_a)dt \tag{2.8}$$

$$\frac{X^2}{2k_{ice}}+\left(\frac{1}{h_{sol}}+\frac{1}{h_{air}}\right)X-\frac{\Delta Tt}{\rho_{ice}\Delta H}=0 \tag{2.9}$$

In the case of pure water **Eq. (2.9**) becomes

$$\frac{X^2}{2k_{ice}}+\left(\frac{1}{h_w}+\frac{1}{h_{air}}\right)X-\frac{\Delta Tt}{\rho_{ice}\Delta H_f}=0 \tag{2.10}$$

where h_w is the free convective heat transfer coefficient of water and $\Delta T = T_b - T_a$. The value of the latent heat of freezing of pure water, $\Delta H_f = 3.34\times10^5$ J·kg^{-1} (Osborne, 1939). Assuming no temperature difference between ice and water at the freezing condition, $T_b = T_i$ or $h_w \approx \infty$, **Eq. (2.10)** results in Stefan's formula (Ashton, 1989) as

$$\frac{X^2}{2k_{ice}}+\frac{X}{h_{air}}-\frac{\Delta Tt}{\rho_{ice}\Delta H_f}=0 \tag{2.11}$$

The free convective heat transfer coefficient (h_{sol}) and free convective mass transfer coefficient (k_l) at the interface of the horizontal ice layer and aqueous solution can be determined by using the following free convection correlations (Cengel, 2002)

$$Nu=0.27(Gr\cdot Pr)^{0.25} \quad 10^5<Gr\cdot Pr<10^{11} \tag{2.12}$$

$$Sh=0.27(Gr\cdot Sc)^{0.25} \quad 10^5<Gr\cdot Sc<10^{11} \tag{2.13}$$

Here, the Nusselt number, $Nu=\frac{h_{sol}\cdot L_c}{k}$, Grashof number, $Gr=\frac{g(C_i-C_b)L_c^3}{C\nu^2}$, Prandtl number, $Pr=\frac{C_p\nu\rho}{k}$, Schmidt number, $Sc=\frac{\nu}{D}$ and Sherwood number, $Sh=\frac{k_l.L_c}{D}$. Characteristic length, acceleration due to gravity, thermal conductivity, and specific heat at constant pressure, kinematic viscosity and density of the solution are designated by L_c, g, k, C_p and ρ, respectively. In the correlation, physical and thermodynamic properties are estimated at an average of interface and bulk concentration, $C=\frac{(C_i+C_b)}{2}$

Due to liquid inclusion in the ice layer, the latent heat of fusion for impure ice, ΔH is less than that of pure ice, ΔH_f. Malmgren has introduced an expression to determine the latent heat of fusion of impure ice based on the impurity level by assuming phase transition at thermodynamic equilibrium and constant bulk concentration (Petrich and Eicken, 2009). **Eq. (2.14)** comes from Malmgren's formula (Anderson, 1958)

$$\Delta H=\Delta H_f\left(1-\frac{C_s}{C_b}\right) \tag{2.14}$$

Based on heat and mass transfer, a calculation method has been developed to estimate K^* (**Publication II**) from experimental K values and thermo-physical properties of solutions at different freezing conditions. A flow chart for estimating K^* is shown in **Figure. 2.4**.

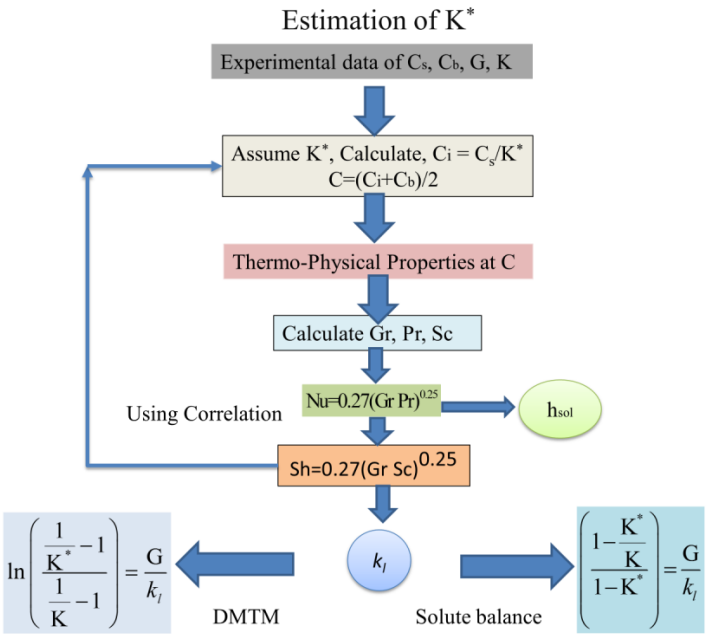

Figure 2.4 Flow chart of a calculation method to estimate K^*.

The estimated K^* values in variation with freezing conditions and electrolyte concentration are discussed elaborately later in the Results and discussion (section 6.2.5).

2.4 Freeze crystallization as a purification and separation method

Freeze crystallization refers to a separation technique in which a solvent crystallizes and thereby concentrates the residual solution in the solute. Freeze crystallization has a wide range of applications, e.g., in fruit juice concentration (O'Concubhair and Sodeau, 2013), protein crystallization (Ryu and Ulrich, 2012), solute concentration, and wastewater purification processes (Huige and Thijssen, 1972). FC has potential for successful commercial applications in chemical and petroleum industry, pulp and paper industry, the desalination process, food processing industry and biotechnology, waste minimization (Englezos, 1994), treatment of wastewater effluents (Lorain et al., 2001) from of mining and other industrial sectors, efficient recovery of different salts from reverse osmosis retentate of complex brine (Lewis et al., 2010), recycling industry, agricultural industry, etc. Apart from these, freeze crystallization also has the potential to be used to remove pharmaceutically active compounds from water (Gao and Shao, 2009), to polish secondary effluents in refineries (Gao et al., 2008), and to inactivate pathogens (Sanin et al., 1994).

During the freezing of the solution, impurities are rejected by the advancing solid phase, depending on the kinetics. Impurity can be (a) fused in the crystal, (b) carried by the entrapment of the mother solution between crystallites or (c) an adhering layer of solution on the crystal surface (Wieckhusen and Beckmann, 2013). Possible sources of impurity during freezing a solution are illustrated in **Figure. 2.5**.

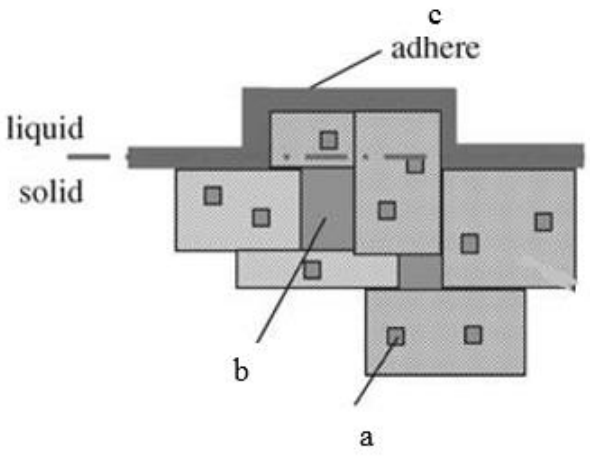

Figure 2.5 Different mechanism of impurities while freezing a solution: a) impurity fused in the crystal, b) impurity entrapped and c) impurity adhered to the surface (Wieckhusen and Beckmann, 2013).

The inclusion of the mother solution within the crystal lattice is considered as a volume defect which largely determines the properties of the crystals, such as mechanical strength or electric conductivity (Wieckhusen and Beckmann, 2013). Macroscopic level volume defect is visible in the ice layer obtained by freezing 4 wt-% Na_2SO_4 (aq) solution (**Figure. 2.6**).

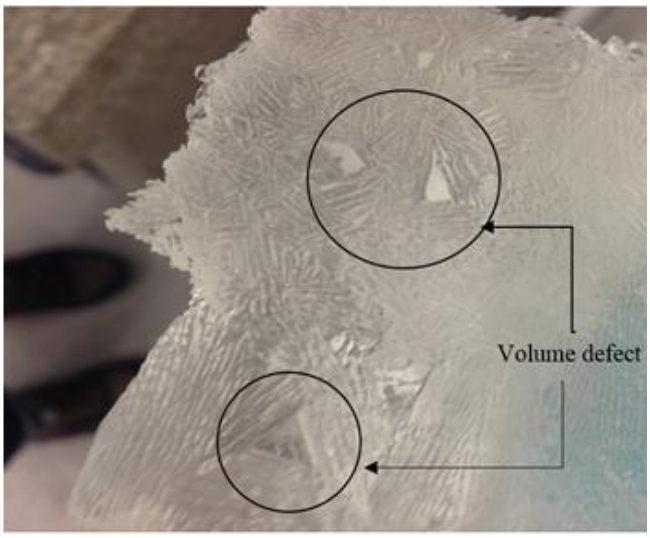

Figure. 2.6 Macroscopic level volume defect in the ice layer formed by freezing 4 wt-% Na_2SO_4 (aq) solution.

The adhering mother solution from the crystal surface can be removed by washing. **Figure. 2.7** displays the removal of an adhered $NiSO_4$ (aq) solution from the ice surface by spraying (from a squeeze wash bottle) pure water cooled down to 0ºC in ice-water suspension.

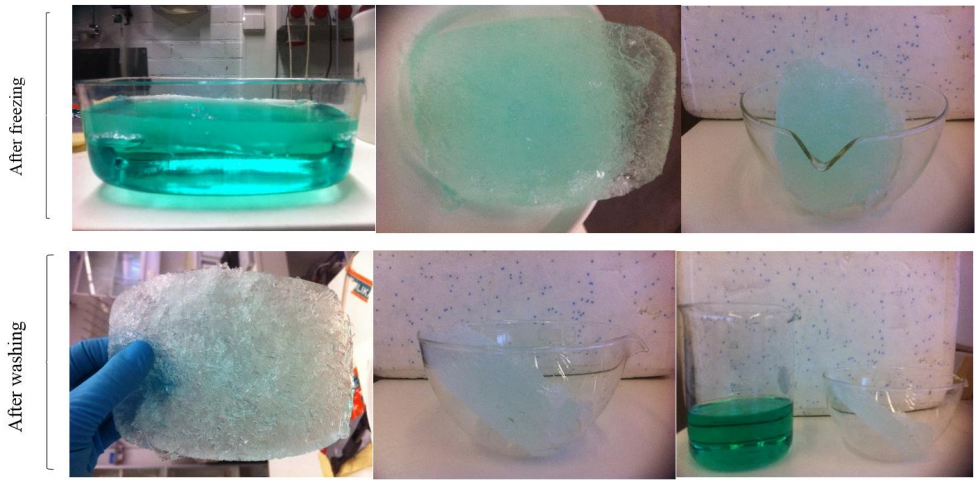

Figure 2.7 Removal of impurity by washing the ice layers form from a $NiSO_4$ (aq) solution.

It is evident in **Figure. 2.7**, that proper washing can increase the purity of the ice layer quite significantly. However, the entrapped mother solution cannot be washed and remains as the main source of impurity in the ice layer.

The occlusion of the solution during freezing is enhanced by constitutional undercooling, which ensues due to faster transport of heat from the bulk to the interface compared to molecular diffusion from the solid-liquid interface to the bulk (Terwilliger and Dizon, 1970, Petrich and Eicken, 2009). Thus, a thin layer is established below the interface, which is cooled further below the freezing point of the solution, but the interfacial solution concentration is only slightly enriched above the bulk level. Constitutional undercooling results in dendritic growth (**Figure 2.8**), which is susceptible to incorporating the solution within the crystal matrix.

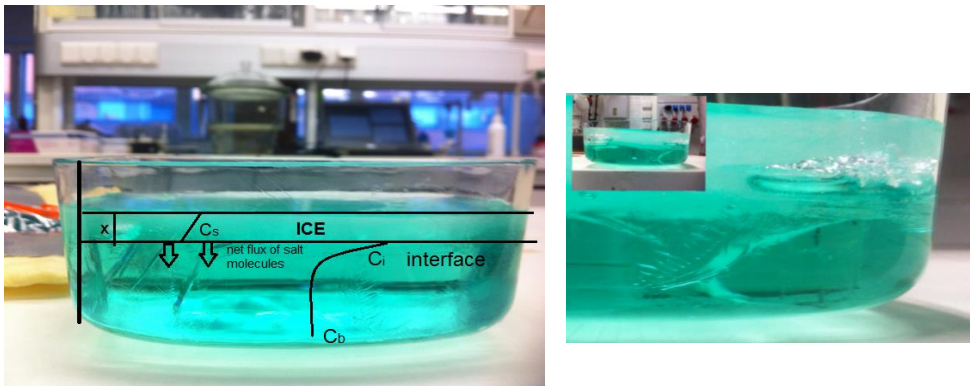

Figure 2.8 Constitutional undercooling and dendrite formation while freezing a $NiSO_4$ (aq) solution.

On the other hand, in the case of planar growth, the solution is mostly driven out with the advancement of crystallization. The growth rate of ice crystals during freezing is determined by transport phenomena. The coupled heat and mass transfer -induced growth mechanism of an air-cooled static layer crystallization process is described in detail in the previous section.

The migration of liquid inclusion of impure melt in crystalline layer happens during melt crystallization. The migration of entrapped brine through the sea-ice layer was first reported by Whitman, 1926. The migration of liquid inclusion is found to be influenced by the existing temperature gradient between the ice layer and the melt (Silventoinen et al., 1988). Henning and Ulrich, 1997 found that inclusions migrate through the layer towards warm side and migration rates increase with the increasing temperature gradients. However, the migration of liquid inclusion through ice layer during freeze crystallization was outside the scope of this work.

2.5 Conclusion

Different aspects of FC, along with its working principle, influential parameters and potential as a separation and purification technique were discussed in this chapter. Among different types of FC methods, static layer freeze crystallization is notable for its simple operation and efficient purification strategy. The underlying thermodynamics and kinetics of this method, based on heat and mass transfer were investigated elaborately in this section. Theoretically, very pure ice should be produced by freezing solutions. Thus, this technique has the potential to be adopted in geographical locations when the temperature level goes down to sub-zero level for the treatment and constriction of voluminous wastewater collected in a pond. Static layer ice crystallization from wastewater by natural freezing (NF) can be named as a sustainable and green purification method, which is devoid of using chemicals and thus of secondary effluents. Depending on the circumstances, this nature-aided purification method can be fused with other conventional techniques to make it even more feasible for industrial applications.

3 Solid-liquid equilibrium of aqueous electrolyte solutions below 0˚C

As discussed in the previous chapter, during natural freezing of a solution, the growth rate, and subsequently the purity of the ice layer relies greatly on the level of undercooling related to the freezing temperature of the corresponding solution. On the other hand, in the case of eutectic freeze crystallization, the issue of solubility modelling at sub-zero temperatures also becomes very important. Therefore, proper understanding of the thermodynamics of the solution and solid-liquid equilibrium (SLE) is necessary regarding industrial processes, such as wastewater treatment by freezing. Accurate models describing the phase behaviour of such systems are very demanding for the analysis, designing and optimizing such processes. Parameterization of thermochemical data, e.g., freezing point depression data (see for example Gibbard and Gossmann, 1974), osmotic and/or activity coefficient data (Pitzer and Mayorga, 1973) in aqueous solution, and flowing amalgam cell measurements (Harned and Nims, 1932, Harned and Cook, 1937) with binary salt systems provide important reference data that enable accurate prediction of the properties solution (Reardon, 1989).

In 1973, Pitzer presented a virial coefficient based ion-interaction model for the excess Gibbs energy (Pitzer, 1973, Pitzer and Mayorga, 1973). This model has been applied to an extensive range of applications (May et al., 2011). Numerous electrolyte-water systems have been modelled with it, but mostly at 25°C (Kim and Frederick, 1988; Pitzer, 1991). It has also been applied to predict solubilities in intricate geochemical systems from 25°C to high pressures and temperatures (see examples from Sippola, 2015). However, for studying the chemical potential of the solvent in the electrolyte solution, which is the key factor in phase equilibria modelling, the freezing point method is more precise than the most commonly used isopiestic method (Gibbard and Gossmann, 1974). In order to get Pitzer parameters at 273.15K for freezing point depression or solubility prediction at a sub-zero temperature, a lot of information, like the heat of the solution / heat of the dilution, along with osmotic and / or activity coefficient data are required (Silvester and Pitzer, 1978, Pitzer, 1991). Therefore, a simple model has been developed in the present study to determine the parameter values for the Pitzer equations at 273.15 K for sodium chloride (NaCl) and potassium chloride (KCl) aqueous solutions by using freezing point data. The resulting values have been tested with all relevant thermodynamic data available in the literature. The new parameter values obtained from the developed model generate better precision with both the freezing point data and the cell-potential difference data. For the best cases, the accuracy level for the formal data is close to being within 0.0001 K. The corresponding high-quality model has been applied for solutions of all salts which have been so far reliably measured using this cryoscopic method in the literature.

3.1 Theory

In the electrolyte solution, the solutes are dissociated into ions. The dissolution of the solute in the solvent entails a negative change in Gibbs energy, thereby most often a negative change in enthalpy and positive change in entropy. The alteration in interaction forces between ions and water is the reason for the change in enthalpy. Entropy is changed due to increased disorder in the water phase while dissolving the solute, which subsequently changes the water activity (a_w) (Jøssang and Stange, 2001). Physically, a_w is a scale to measure how easily the water content may be utilized, i.e., water activity = water availability. Theoretically, a_w describes the equilibrium amount of available water for hydration. In the case of a pure solvent, $a_w = 1$, and thorough unavailability of water means, $a_w = 0$. Unavailability of water incurs due to its interaction with existing dissociated ions in the solution, which infers that the addition of solutes depresses the water activity (De Vito et al., 2015; Smith et al., 1981).

Short-range interactions between pairs of ions in the electrolytes, triple ion interactions at high concentrations, and long-range electrostatic interactions in real solutions are the underlying reasons for the deviation from the ideal solution behaviour. The ratio of experimentally obtained osmotic pressures (Π) with the ideally expected osmotic pressure (Π_0) as from Raoult's law is known as the osmotic coefficient, ϕ (=Π/Π_0) (Stadie and Sunderman, 1931).

3.2 Prediction of the freezing point

The solid-liquid equilibrium (SLE) model equates the chemical potentials of the solvent and corresponding solid phase at the freezing temperature of the solution with basic thermodynamic formula pertinent to Gibbs energy, enthalpy and the entropy of fusion. The model correlates the activity of the solvent (a_A) and the freezing temperature of the solution (T_f) as follows (**Publications IV** & **V**):

$$-R \ln a_A = y = \Delta H^* \left(\frac{1}{T_f} - \frac{1}{T_f^*} \right) + \Delta C_{p,m} \left[\frac{(T_f - T_f^*)}{T_f} - \ln \left(\frac{T_f}{T_f^*} \right) \right] \qquad (3.1)$$

where A refers to the solvent (water in this case), R denotes the universal gas constant, T_f^* is the freezing point of the pure solvent (in this study, water), ΔH is the enthalpy of fusion at T_f^*, and $\Delta C_{p,m} (= C_{p,m}^*(A,l) - C_{p,m}^*(A,s))$ is the difference between the heat capacity at constant pressure of the pure solvent (water) in the liquid phase (denoted by $C_{p,m}^*(A,l)$) and the solid (ice) phase ($C_{p,m}^*(A,s)$) at the freezing temperature.

The activity of the solvent (a_A) is related to the osmotic coefficient (ϕ) as

$$\ln a_A = -\nu M_A m\phi \tag{3.2}$$

where $\nu = \nu_M + \nu_X$, ν_M and ν_X denote the stoichiometric coefficients of the cation and anion of the salt, respectively. The definitive model for calculating the osmotic coefficient of electrolytes is the Pitzer model with the following form (Pitzer and Mayorga, 1973)

$$\phi - 1 = -|z_M z_X| \frac{A_\phi I^{1/2}}{1 + bI^{1/2}} + 2\left(\frac{\nu_M \nu_X}{\nu}\right) m\left[\beta^0 + \beta^1 \exp(-\alpha_1 I^{1/2}) + \beta^2 \exp(-\alpha_2 I^{1/2})\right] + \left(\frac{2(\nu_M \nu_X)^{3/2}}{\nu}\right) m^2 C^\phi \tag{3.3}$$

where z_M and z_X are the charge of the cation and anion, A_ϕ is the Debye-Hückel constant (at temperature 273.15 K and pressure 101.325 kPa this value is 0.37642 $(\text{mol·kg}^{-1})^{-0.5}$ (Archer and Wang, 1990), b = 1.2 $(\text{mol·kg}^{-1})^{-0.5}$, $\alpha_1 = \alpha = 2.0$ $(\text{mol·kg}^{-1})^{-0.5}$, $\alpha_2 = 0$ and $\beta^2 = 0$ for 1-1 and 2-1 types of electrolytes. On the other hand for 2-2 type of electrolytes, α_1=1.4 $(\text{mol·kg}^{-1})^{-0.5}$, α_2=12 $(\text{mol·kg}^{-1})^{-0.5}$ and β^2 is electrolyte specified. The ionic strength can be formulated as, $I = 0.5\sum m_i z_i^2$. The term m refers to the molality (mol·kg^{-1}) of the solution, M_A is the molar mass of the solvent (for water 0.018015 kg·mol^{-1}). Calculated a_w at 25˚C by using **Eqs. 3.2 & 3.3** for different sulfate solutions of practical relevance are shown in **Figure 3.1.**

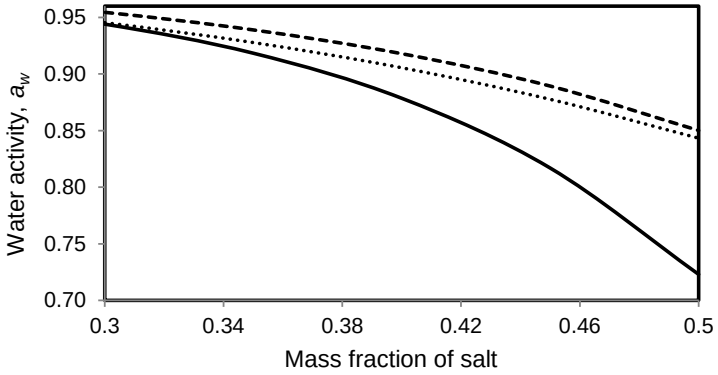

Figure 3.1 Calculated a_w with varying solution concentration for different electrolytes at 25˚C. The solid (—), dotted (⋯) and dash (---) lines indicate Na_2SO_4, $(NH_4)_2(SO_4)$ and K_2SO_4 (aq) solutions, respectively.

The ionic radii of Na^+, K^+ and NH_4^+ are 0.76Å, 1.36Å (Badger et al., 1994) and 1.38Å (Gautier et al., 2010) respectively. **Figure 3.1** displays that the water activity, a_w increases with the increased ionic radius. This trend of a_w is general for cations and is in accordance with Jøssang and Stange (2001).

After mathematical manipulation of **Eq. (3.1)** and **Eq. (3.2)**, an expression for freezing point depression of the solution ($\Delta T_f = T_f^* - T_f$) can be deduced as

$$\Delta T_f = \frac{\nu R T_f^* M_A m\phi}{\nu R M_A m\phi + \frac{\Delta H^*}{T_f^*}} + \frac{\Delta C_{p,m}\Delta T_f + \Delta C_{p,m}(T_f^* - \Delta T_f)\ln\left(\frac{T_f^* - \Delta T_f}{T_f^*}\right)}{\nu R M_A m\phi + \frac{\Delta H^*}{T_f^*}} \qquad (3.4)$$

From the osmotic coefficients of the solutions, it is possible to solve ΔT_f from **Eq. (3.4)** iteratively. This requires adjustable parameters when the Pitzer model is used. In the calculations, $T_f^* = 273.15$ K, $\Delta H = 6009.5$ J·mol^{-1} and $\Delta C_{p,m} = 37.87$ J·K^{-1}·mol^{-1} (Osborne, 1939, Osborne et al., 1939) are used. In **Publication V**, it has been shown that for NaCl and KCl solutions, the temperature dependency of $\Delta C_{p,m}$ has no effect on the temperature-dependent Pitzer parameters obtained from the freezing point data for dilute solutions up to 0.5 mol·kg^{-1}. Moreover, there are inconsistencies among reported $C_{p,m}^*$ (A,l) values of subcooled water in the literature (**Publication V**). Therefore, in the present work, constant $\Delta C_{p,m}$ value is considered. Ge and Wang (2009) have derived an equation to predict the freezing point of the electrolyte in a similar fashion, i.e., considering the chemical potential of the solvent is equal between the liquid and solid phases when the solution is in solid-liquid equilibrium. By using the Gibbs-Helmholtz equation and after mathematical manipulations, the freezing point depression of a solution can be expressed as

$$\Delta T_f = \frac{\Delta H^* - 2RT_f^* \ln a_w - \sqrt{2\Delta C_{p,m}^* T_f^{*2} R \ln a_w + (\Delta H^*)^2}}{2\left(\frac{\Delta H^*}{T_f^*} + 0.5\Delta C_{p,m}^* - R\ln a_w\right)} \qquad (3.5)$$

But **Eq. 3.4** is more theoretical and contains less approximation and therefore it was used in **Publications III, IV & V.** However, Eq. 3.5 gives practically almost same results. In the present work, the FPD of several electrolytes has been calculated as a function of molality with the model by using Pitzer ion-interaction parameters and A_φ at 25˚C and those for 0˚C (Pitzer, 1991) to compare the accuracy level with the experimental data. The outcomes are illustrated in **Figure. 3.2** for several electrolytes.

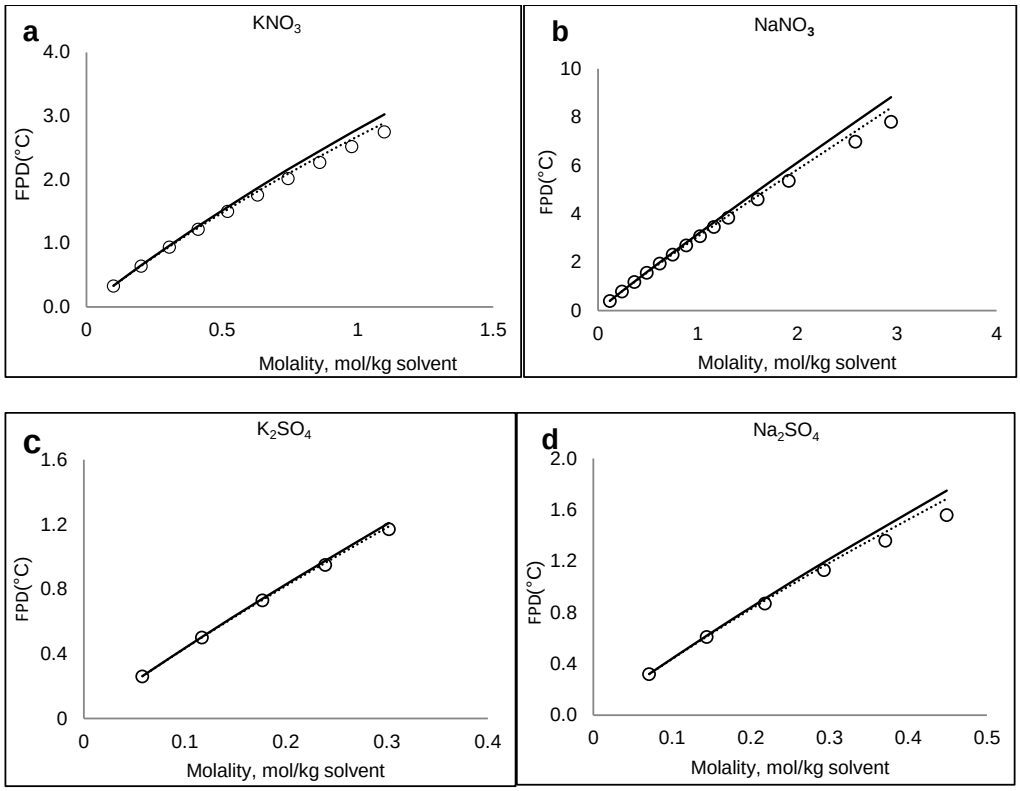

Figure 3.2 Prediction of FPD by **Eq. (3.5)** for solutions: (a) KNO_3, (b) $NaNO_3$, (c) K_2SO_4, (d) Na_2SO_4, as function of molality. The symbol (○) represents FPD data obtained from the literature and the solid line (—) represents the calculated FPD by using the ion-interaction parameter and Debye-Hückel constant at 25˚C and the dotted line (⋯) for 0˚C.

The deviation between the calculated and literature data can be defined by average absolute relative deviation (AARD) percentage as

$$\mathrm{AARD\%} = 100 \times \frac{1}{n_p}\left(\sum_{i=1}^{n_p} \frac{\left|V_i^{Cal} - V_i^{lit}\right|}{V_i^{lit}}\right) \tag{3.6}$$

where i is the index number, V^{cal}, V^{lit} and n_p designate the freezing point calculated by **Eq. (3.5)**, the freezing point obtained from the literature and the number of data points in the literature, respectively. **Figure 3.3** displays the AARD of freezing points of our case electrolytes.

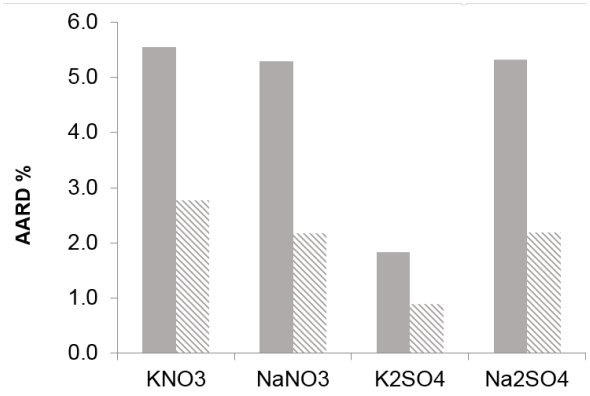

Figure 3.3 Average absolute relative deviation for predicting the freezing points of electrolytes based on the temperature dependency of the Pitzer-ion interaction parameters and the Debye-Hückel constant. The solid fill and pattern fill indicate Pitzer-ion interaction parameters and A_ϕ at 25°C and those at 0°C, respectively. Here the maximum concentration for each compound is same as shown in **Figure 3.2**.

In the case of 1-1 and 1-2 electrolyte solutions, AARD decreases by around 50% when the Pitzer ion interaction parameters are taken into account at 0°C than those at 25°C. This indicates that the temperature dependency of Pitzer parameters can influence FPD modelling significantly, which motivates for the extraction Pitzer ion-interaction parameters at a lower temperature, i.e., 0˚C from very reliable freezing point data available in the literature. The available temperature derivatives of these parameters have been extracted from calorimetric data, which might not be very accurate in the sub-zero temperature range during freezing.

3.3 Extraction of ion-interaction parameters from freezing point depression data

A calculation method for estimating Pitzer ion-interaction parameters from SLE data is presented in this section. **Eq. (3.3)** can be rearranged by using quantity y in **Eq. (3.1)** for the interaction parameter β^0 as a function of β^1, C^ϕ and molality, m.

$$\beta^0 = \frac{\nu}{2m\nu_M\nu_X}\left[\frac{|z_M z_X|A_\phi I^{1/2}}{1+bI^{1/2}} + \frac{\mathrm{y}}{\mathrm{R}\nu M_A m} - 1\right] - \beta^1\exp(-\alpha I^{1/2}) - (\nu_M\nu_X)mC^\phi \qquad (3.7)$$

By excluding the C^ϕ term, which is a rational assumption for dilute solutions up to 0.5 mol·kg^{-1} (Pitzer, 1991), **Eq. (3.7)** becomes

$$\beta^0 = \frac{\nu}{2m\nu_M\nu_X}\left[\frac{|z_M z_X| A_\phi I^{1/2}}{1+bI^{1/2}} + \frac{y}{RvM_A m} - 1\right] - \beta^1 \exp(-\alpha I^{1/2}) \qquad (3.8)$$

3.3.1 Determination of Pitzer parameters for a dilute solution

In order to solve β^0 from **Eq. (3.8)**, parameter β^1 must first be estimated. The value of β^1 that yielded the least value of standard deviation from the mean value of the experimental β^0 values at different molalities was chosen. For instance, the deviation of the freezing point of NaCl solutions found in the literature from prediction by the Pitzer parameter, estimated by using $\varepsilon(\Delta T) = T_f^*(\text{experiment}) - T_f^*(\text{model})$ is shown in **Figure 3.4.**

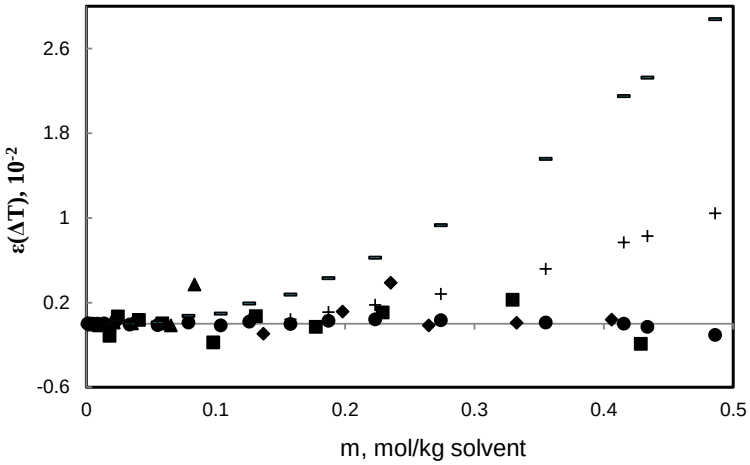

Figure 3.4 Deviation between the observed and predicted freezing-point depressions in NaCl solutions as a function of molality, m. The observed values have been measured by Scatchard and Prentiss(1933) (symbol ●), Gibbard and Gossmann (1974) (♦), Harkins and Roberts (1916) (▲), and Momicchioli et al. (1970) (■) for Pitzer parameters at 25˚C (-), and Pitzer parameters at 0˚C has also been used for the set of Scatchard and Prentiss (1933) calculated by using the temperature derivatives mentioned in Pitzer, 1991 (+).

Figure 3.4 clearly shows that with the Pitzer parameters obtained by our model, accurate prediction of FPD is possible. Based on the availability of reliable freezing point data for a dilute solution (ca. m<0.5 molality) in the literature, the values of the Pitzer parameter in **Eq. (3.8)** are listed for 26 different electrolytes at 273.15K in **Table 3.1.**

Table 3.1 Values of Pitzer parameters from **Eq. (3.8)** in dilute (m<0.5 mol·kg^{-1}) solutions of different electrolytes.

Electrolyte	β^0	β^1
NaCl	0.2801	0.0396
KCl	0.1919	0.0239
LiCl	0.243	0.1612
LiBr	0.387	0.163
KBr	0.25	0.0138
$LiNO_3$	0.348	0.118
$NaNO_3$	0.196	-0.055
KNO_3	-0.098	-0.129
$LiClO_3$	0.373	0.136
$NaClO_3$	0.195	-0.0149
$KClO_3$	0.081	-0.1500
$LiClO_4$	0.469	0.1654
$NaClO_4$	0.244	0.0025
Li-Formate	0.221	0.0751
Na-Formate	0.323	0.0482
K-Formate	0.337	0.0605
Li-Acetate	0.284	0.1141
Na- Acetate	0.428	0.1062
K- Acetate	0.412	0.1335
NH_4Cl	0.003	0.0778
NH_4Br	-0.072	0.1164
NH_4I	0.19	0.0456
NH_4NO_3	-0.0418	0.0332
Na_2SO_4	-0.1789	1.1900
K_2SO_4	-0.0128	0.5738
$(NH_4)_2SO_4$	0.0133	0.3140

3.3.2 Determination of Pitzer parameters for a less dilute solution

The same value of β^1 was used for less dilute solutions as for dilute solutions by ignoring the C^ϕ term. The reason for adapting this approach was that using the β^1 value obtained from dilute solutions yielded good results with the Pitzer equation for hydrochloric acid extended up to 16 mol.kg^{-1} (Partanen et al., 2007). After determining β^1, parameter C^ϕ was chosen in such a way that the least standard deviation was attained for β^0, values at different molalities, m (or ionic strength, I) from **Eq. (3.7)**. An error plot similar to **Figure 3.4** can be seen in **Publication V**. The values of the Pitzer parameter from **Eq. (3.7)** are listed for different less dilute electrolytes (*ca.* m<1.5 mol.kg^{-1}) at 273.15 K in **Table 3.2.**

Table 3.2 Values of Pitzer parameters from **Eq. (3.7)** in less dilute (m<1.5 mol·kg^{-1}) solutions of different electrolytes.

Electrolyte	β^0	β^1	C^ϕ
NaCl	0.0379	0.2801	0.00698
KCl	0.0239	0.1919	-
LiBr	0.1583	0.387	0.0195
KBr	0.0121	0.25	0.0081
$LiNO_3$	0.1163	0.348	0.0121
$NaNO_3$	-0.0561	0.1963	0.0107
$LiClO_3$	0.1339	0.373	0.011
$NaClO_3$	-0.0142	0.195	-0.004
$LiClO_4$	0.16	0.469	0.028
K-Formate	0.0589	0.337	0.0084
Li-Acetate	0.1123	0.284	0.0111
Na-Acetate	0.1037	0.428	0.014
K-Acetate	0.1301	0.412	0.016
NH_4NO_3	-0.0410	0.0332	-0.0020
$(NH_4)_2SO_4$	0.0138	0.3140	-0.0007

The freezing point depression, osmotic coefficient, activity coefficient for different salts as a function of molality with new parameter values and for the electrolytes mentioned in **Table 3.1** and **Table 3.2** can be found in **Publications III, IV & V**.

3.4 Solubility modelling

Solubility is the maximum amount of solute that a solvent can dissolve at a certain temperature and pressure. This is another type of an SLE system. Solubility data are very important for any kind of crystallization and precipitation related processes. Solubility modelling is of great importance in the case of salt recovery by using the eutectic freeze crystallization (EFC) process. Solubility data of many pure substances are available in databases or reported in the literature, which is not the case for the multicomponent system of practical interest. However, obtaining reliable solubility data needs extensive experimental investigations, and will thereby become time-consuming and costly (Han, 2015). Therefore, a solubility model as a predictive tool is very useful. Alike freezing point prediction, Pitzer's ion interaction model can be used in predicting the solubility of different systems.

Based on the Debye-Hückel equation for the dilute solution domain, the mean activity coefficient (γ), and the concentration dependence of the electrolyte terms B^{ϕ} and B electrolytes (Pitzer , 1991 & Kim and Frederick, 1988) can be calculated from **Eqs. (3.9-3.13)**.

$$\ln \gamma_{\pm} = \left|z_M z_X\right| f^{\gamma} + 2m\left(\frac{\nu_M \nu_X}{\nu}\right)\left(B^{\phi}_{MX} + B_{MX}\right) + 3m^2 \frac{\left(\nu_M \nu_X\right)^{3/2}}{\nu} C^{\phi}_{MX} \qquad (3.9)$$

$$f^{\gamma} = -A_{\phi}\left[\frac{I^{1/2}}{1+bI^{1/2}} + \left(\frac{2}{b}\right)\ln\left(1+bI^{1/2}\right)\right] \qquad (3.10)$$

$$B^{\phi}_{MX} = \beta^0 + \beta^1 \exp\left(-\alpha_1 I^{0,5}\right) + \beta^2 \exp\left(-\alpha_2 I^{0,5}\right) \qquad (3.11)$$

$$B_{MX} = \beta^0 + \beta^1 g\left(\alpha_1 I^{0,5}\right) + \beta^2 g\left(\alpha_2 I^{0,5}\right) \qquad (3.12)$$

$$g(x) = \frac{2(1-(1+x)e^{-x})}{x^2} \qquad (3.13)$$

The activity coefficient of a cation and an anion in the presence of various other cations and anions can be estimated by **Eq. (3.14)** and **Eq. (3.15)** (Pitzer, 1991) respectively

$$\ln \gamma_M = z_M^2 f^\gamma + \sum_a m_a (2B_{Ma} + ZC_{Ma}) + \sum_c m_c (2\theta_{Mc} + \sum_a m_a \psi_{Mca}) + \sum_a \sum_{a<a'} m_a m_{a'} \psi_{Maa'} + |z_M| \sum_c \sum_a m_c m_a C_{ca} + z_M^2 f'(B) \quad (3.14)$$

$$\ln \gamma_X = z_X^2 f^\gamma + \sum_c m_c (2B_{cX} + ZC_{cX}) + \sum_a m_a (2\theta_{Xa} + \sum_c m_c \psi_{cXa}) + \sum_c \sum_{c<c'} m_c m_{c'} \psi_{cc'X} + |z_X| \sum_c \sum_a m_c m_a C_{ca} + z_c^2 f'(B) \quad (3.15)$$

The subscripts M and X refer to the cation and anion examined currently, while subscripts c and a refer to the other cations and anions in the system. The terms θ and ψ are mixing parameters specific to the electrolyte system. Ionic strength, $I = \frac{1}{2}(\sum_a Z^2 m_a + \sum_c Z^2 m_c)$ and $Z = \sum_i m_i |z_i|$

Parameter B_{MX} is calculated by

$$B_{MX} = \beta_{MX}^0 + \beta_{MX}^1 f_2 + \beta_{MX}^2 f_2 \quad (3.16)$$

where, β_{MX}^0 , β_{MX}^1 and β_{MX}^2 are ion interaction parameters specific to the combination of ions in the system. The term β_{MX}^2 is used in case of 2-2 type electrolyte (e.g., $NiSO_4$). Parameter C_{MX} is calculated by

$$C_{MX} = \frac{C^\phi}{2\sqrt{|z_M z_X|}} \quad (3.17)$$

Here, C^ϕ is again an ion interaction parameter specific to the electrolyte. The other parameters in **Eqs. (3.14-3.15)** can be calculated by **Eqs. (3.18-3.20**).

$$f_2 = \frac{1}{2I^2}\left[1 - \left(1 + 2\sqrt{I}\right)e^{-2\sqrt{I}}\right] \quad (3.18)$$

$$f_3 = \frac{1}{2I^2}\left[-1 + \left(1 + 2\sqrt{I} + 2I\right)e^{-2\sqrt{I}}\right] \quad (3.19)$$

$$f'(B) = \sum_{MX} m_M m_X \beta_{MX}^1 f_3 \quad (3.20)$$

3.4.1 Calculation method

The program blocks used to predict the solubility of a specific electrolyte in a multicomponent system with these Pitzer equations are described as follows:

1. To calculate the average activity coefficient ($\gamma_{\pm}$) of that specific electrolyte (MX) in the solution in variation with different molalities by using **Eqs. (3.9-3.13)**.
2. To calculate the solubility product constant ($K_{sp,MX}$) of that specific electrolyte based on the solubility data in molality and the corresponding average activity coefficient.
3. To calculate the activity coefficient of cation (γ_M) and anion (γ_X) of that specific electrolyte in the mixed system by using **Eqs. (3.14-3.15)**.
4. To estimate the solubility MX in variation with the concentration of other ions in the solution by backward iteration and considering the same $K_{sp,MX}$ for the mixed system as calculated in step 2, because the solubility product depends only on the temperature. Therefore $K_{sp,MX}$ is constant under isothermal conditions regardless of a pure or a multicomponent system.

3.4.2 Example calculation with a K_2SO_4-Na_2SO_4-H_2O system

The development of accurate solubility models of multicomponent systems is of fundamental importance for modelling industrial processes like crystallization. Therefore, this kind of modelling is exemplified here with a multicomponent K_2SO_4-Na_2SO_4-H_2O system by following the program blocks as described above in the wake of viewing the influence of Na_2SO_4 as impurity on the solubility of K_2SO_4 in water.

Firstly, $\gamma_{K_2SO_4}$ in variation with solution molality are calculated (step 1) and compared with experimental data obtained from the literature (CRC handbook) as shown in **Table 3.3.** The constant terms and ion-interaction parameters of the Pitzer equations have been adopted from Pitzer (1991).

Table 3.3 Comparison of $\gamma_{K_2SO_4}$ at 25˚C obtained by the Pitzer model and experimental data found in the literature.

Molality	γ_{lit}	γ_{cal}	$\left(\frac{\gamma_{lit}-\gamma_{cal}}{\gamma_{lit}}\right)\times 100\%$
0.001	0.885	0.8850	0.002
0.002	0.844	0.8443	-0.038
0.005	0.772	0.7733	-0.172
0.01	0.704	0.7059	-0.271
0.02	0.625	0.6280	-0.475
0.05	0.511	0.5146	-0.702
0.1	0.424	0.4275	-0.828
0.2	0.343	0.3454	-0.708
0.5	0.251	0.2529	-0.760

It can be seen in **Table 3.3** that the Pitzer model is capable of predicting $\gamma_{K_2SO_4}$ quite accurately in variation with a solution concentration of up to 0.5 mol·kg^{-1}.

Secondly, $\gamma_{K_2SO_4}$ was calculated for the solubility concentration of K_2SO_4 in water at 25˚C (=0.69 molality), as presented in the literature (Haynes, 2014). When dissolving K_2SO_4 in water, the following equilibrium system can be considered.

$$K_2SO_4(s) \rightleftharpoons 2K^+(aq)+SO_4^{2-}(aq)$$

$$K_{sp,K_2SO_4} = \frac{(a_K)^2(a_{SO_4^{2-}})}{a_{K_2SO_4(s)}}$$

$$= (m_{K^+})^2(\gamma_{K^+})^2(m_{SO_4^{2-}})(\gamma_{SO_4^{2-}})$$

Thirdly, γ_{K^+}, γ_{Na^+} and $\gamma_{SO_4^{2-}}$ were calculated by **Eqs. 3.21, 3.22,** and **3.23** derived from **Eqs. 3.14** and **3.15** for the mixed system of K-Na-SO_4-H_2O (step 3).

$$\ln\gamma_{K^+} = f^\gamma + m_{SO_4}(2B_{K,SO_4} + ZC_{K,SO_4}) + m_{Na}(2\theta_{K,Na} + m_{SO_4}\psi_{K,Na,SO_4}) + (m_{Na}m_{SO_4}C_{Na,SO_4} + m_K m_{SO_4}C_{K,SO_4}) + f'(B) \quad (3.21)$$

$$\ln\gamma_{Na^+} = f^\gamma + m_{SO_4}(2B_{Na,SO_4} + ZC_{Na,SO_4}) + m_K(2\theta_{K,Na} + m_{SO_4}\psi_{K,Na,SO_4}) + (m_K m_{SO_4}C_{K,SO_4} + m_{Na}m_{SO_4}C_{Na,SO_4}) + f'(B) \quad (3.22)$$

$$\ln\gamma_{SO_4^{2-}} = 4f^\gamma + 2(m_K B_{K,SO_4} + m_{Na}B_{Na,SO_4}) + Z(m_K C_{K,SO_4} + m_{Na}C_{Na,SO_4}) + m_K m_{Na}\psi_{K,Na,SO_4} + 2(m_{Na}m_{SO_4}C_{Na,SO_4} + m_K m_{SO_4}C_{K,SO_4}) + 4f'(B) \quad (3.23)$$

Then the solubility K_2SO_4 in variation with the concentration of Na_2SO_4 in the solution was determined by backward iteration and considering the same $K_{sp,K_2SO_4} = 0.01651$ for the mixed system as calculated in step 2. The calculated solubility is compared with solubility found in the literature (Seidell, 1919 and Stephen & Stephen, 1964) and in **Figure 3.5**. The ion-interaction and mixing parameters used in the calculation have been collected from Pitzer (1991).

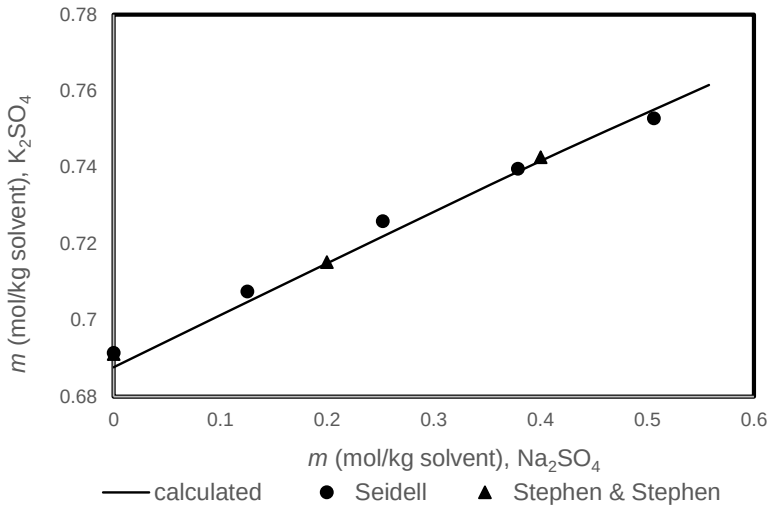

Figure 3.5 Solubility of K_2SO_4 in water at 25˚C in presence of Na_2SO_4.

Figure 3.5 shows that the solubility of K_2SO_4 in the presence of Na_2SO_4 in the solution validates that the developed methodology is good enough to predict solubility quite efficiently for a multi-component system. The effect of common ion in decreasing the solubility is not the case for K_2SO_4-Na_2SO_4-H_2O system. The experimental results show that K_2SO_4 and Na_2SO_4 form $K_3Na(SO_4)_2$ which dissolves only Na_2SO_4 (Seidell, 1999).

3.5 Conclusion

In this chapter, two possible solid-liquid equilibria, e.g., water-solution and salt-solution that can exist during freezing an electrolyte, were modelled thermodynamically. From the engineering perspective, these models can predict the freezing point and solubility quite efficiently, which would be vital for the use of freezing as a purification and separation technique and in the case of recovering salt from wastewater. Furthermore, by using freezing point data, Pitzer ion-interaction parameters were extracted for a wide range of 1-1 and 1-2 types of electrolytes. With these parameters, the freezing point can be predicted more accurately than with those currently available in the literature.

4 Compilation of thermodynamic and physical properties used in freeze crystallization calculations

4.1 Data of freezing point depression and physical properties

Thermodynamics of solid-liquid equilibria and the physical properties of crystals and solutions are the core data required for modelling any crystallization process. These factors include freezing point data, density, viscosity, specific heat capacity, diffusivity, thermal conductivity, water activity, osmotic coefficient, etc. In this section, all the required principal properties are compiled as a function of solution concentration before investigating the freezing behaviour of Na_2SO_4 and $NiSO_4$ solutions at different conditions.

Freezing point depression (FPD) data, along with various other thermodynamic and physical properties of Na_2SO_4 (aq) and $NiSO_4$ (aq) solutions in the range of 1 wt-% - 4 wt-% are collated (except for thermal conductivity, which was calculated from a correlation) and compared in **Figure 4.1**. References for these data are mentioned in **Publications I** & **II** for $NiSO_4$ (aq) and Na_2SO_4 (aq) solutions, respectively.

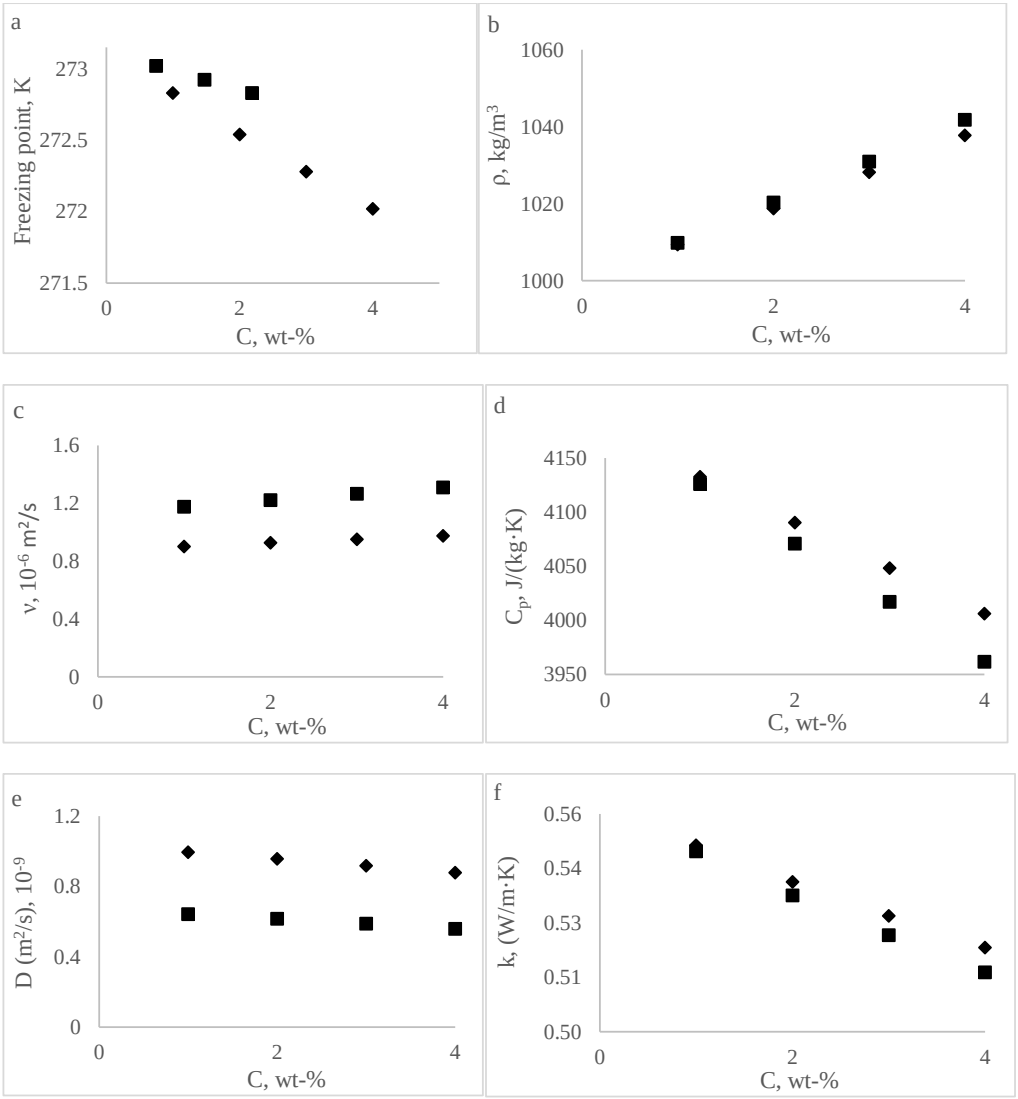

Figure 4.1 Physical properties of Na_2SO_4 (aq) (symbol ♦) and $NiSO_4$ (aq) (symbol ■) solutions as a function of solute concentration, (a) freezing point; (b) density; (c) kinematic viscosity; (d) specific heat capacity at constant pressure; (e) diffusion coefficient ; (f) thermal conductivity.

In most cases, these properties are available at 25˚C, with the exception of densities, which are available at 0˚C and 15˚C for the Na_2SO_4 (aq) and $NiSO_4$ (aq) solutions, respectively. The calculated water activity (a_w), the activity coefficient (γ) and the osmotic coefficient (ϕ) in variation with solution concentration at 25˚C with the Pitzer equation are shown and compared in **Figure 4.2**. The Pitzer parameters have been adopted

from Pitzer and Mayorga (1973) and Kim and Frederick Jr (1988) for the Na_2SO_4 and $NiSO_4$ solutions, respectively.

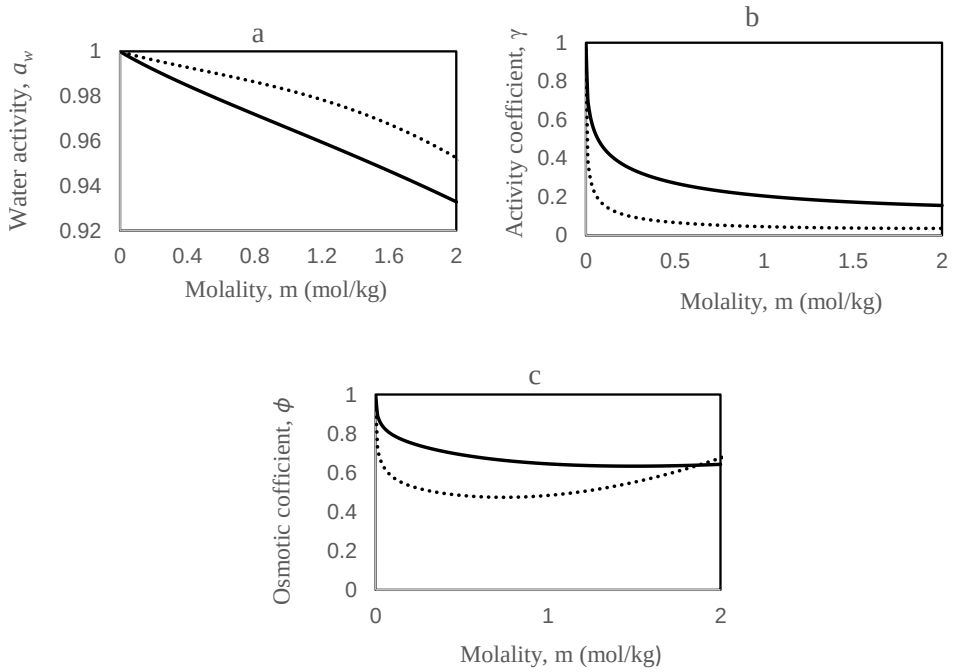

Figure 4.2 Water activity (a_w), activity coefficient (γ) and osmotic coefficient (ϕ) at different solution concentrations. Na_2SO_4 (aq) and $NiSO_4$ (aq) solutions are indicated by a solid line (—) and (⋯) dotted line, respectively.

The trend of a_w indicates non-ideal behaviour (**Figure 4.2a**). It is also evident from the calculated γ (**Figure 4.2b**) and ϕ (**Figure 4.2c**) which refer to deviation from ideal behaviour. For pure water, which is very likely to act like an ideal solution, $\gamma = 1$ and $\phi = 1$. At a given molality, the calculated γ and ϕ for $NiSO_4$ (aq) are smaller than those for Na_2SO_4 (aq), which also indicates that more deviation from ideal behaviour is apparent in the case of the $NiSO_4$ (aq) solution. For a very dilute solution (e.g., m<0.5 mol·kg^{-1}), water activity of both solutions shows a linear trend.

However, at a given molality a_w is higher in the case of the $NiSO_4$ (aq) solution than that of the Na_2SO_4 (aq) solution (**Figure 4.2a**), which hints that at a specific solution concentration less water interacts with ions in the case of the $NiSO_4$ (aq) solution, and therefore more water is available to transfer from the $NiSO_4$ (aq) solution to the solid phase (ice) while freezing. Due to the easiness in mobility, freezing point depression from a pure solvent is lower in the $NiSO_4$ (aq) solution at a certain concentration than that of the Na_2SO_4 (aq) solution (**Figure 4.1a**). At certain concentrations a_w of the $NiSO_4$ (aq)

solution is found higher than that of the Na_2SO_4 (aq) solution. On the contrary, γ and ϕ are found lower for $NiSO_4$ (aq) solutions.

4.2 Conclusion

The freezing point and thermo-physical properties of two electrolytes (i.e., Na_2SO_4 and $NiSO_4$ with which the freezing tests have been done in this work) were listed in this chapter. Even though some properties were not available at the temperatures of experimental interest, this kind of elaborate data set is vital to predict basic freezing behaviour and its efficiency as a purification technique and in designing such a system.

5 Methodology developed for freeze crystallization investigations

FPD is the core of any kind of freezing study which defines the level of undercooling at a certain freezing condition. *A priori* knowledge of FPD is vital in using freezing as a separation and purification method, especially in the case of natural freezing. Industrial wastewaters are typically multi-component ones with a wide range of variety, and hence the underlying thermodynamics (as discussed in Chapter 3) can be very complex. In this regard, a simple and accurate freezing point measuring device is of crucial importance before subjecting to freezing as a purification method. In the following sections, an experimental setup is introduced which can be utilized to measure the FPD of wastewater.

5.1 Experimental setup

5.1.1 Method

As the freezing temperature of a solution plays a key role while freezing, a simple setup was built to measure the freezing points of different solutions. The detection of the freezing point from the freezing profile of a solution was discussed in section 2.3.

5.1.2 Materials

A solution of NaCl was made by dissolving 99.5% pure NaCl (purchased from J.T. Backer) in deionized water (conductivity = 0.1 µS/cm, total organic carbon = 1ppb). NaCl (aq) solutions of 2wt-%, 3wt-%, 5wt-%, 12wt-% NaCl were used as reference solutions to compare the FPD data with the literature. Dissolution was accomplished at a relatively higher than room temperature (50°C) under vigorous mixing conditions (500 rpm) for 30 min.

5.1.3 Apparatus

The experiments were carried out in a 2L jacketed and insulated vessel with a scraper. A Vacon variable speed control motor with a four-blade impeller was used to provide sufficient mixing. The impeller and the scrapers were fixed to the same shaft. Monoethylene Glycol (freezing point -36°C) was used as the cooling liquid. A Lauda Proline RP 855 thermostat circulated the coolant through the jacket of the vessel continuously. The temperature of the solution was measured by a PT 100 sensor (with 0.015 °C accuracy level) and monitored by a tailor-made Matlab-programmed temperature logging device. It was possible to control the cooling rate via a Matlab command. **Figure 5.1** displays the experimental setup used in measuring FPD.

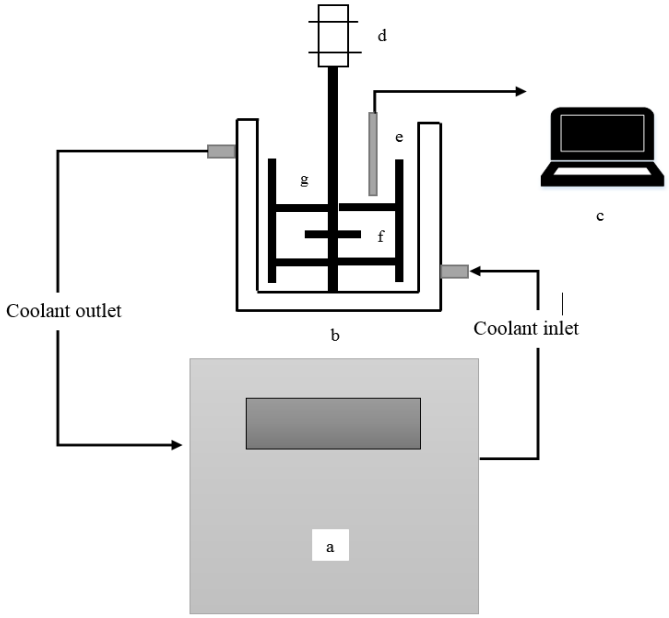

Figure 5.1 Experimental setup for measuring the freezing point of a solution, (a) Lauda proline RP 855 thermostat; (b) vessel; (c) data logging device; (d) motor; (e) Pt 100 thermosensor; (f) four-blade impeller; (g) scraper blade.

5.1.4 Experimental Procedure

Each experiment was initiated by adding 1L of solution to the vessel. The set-point of the thermostat cooling the liquid was fixed at 2.5°C to 3.0°C lower than the freezing point mentioned in the literature. The lower temperature was selected for the confirmation of ice formation. A scraper speed of 20 rpm was used. The rotational speed was measured by a Peak Tech – 2795 digital tachometer. A slow cooling rate ($0.01°K{\cdot}s^{-1}$) was used because a fast cooling rate could supercool the solution to a higher extent without any phase change. In the beginning, the coolant and solution temperature measurements were calibrated with an ice-water mixture of 0°C.

There was a temperature jump at a certain point in spite of cooling due to release of heat of ice crystallization and solution temperature remained constant for a while. This stable temperature indicated the freezing point of that solution. After that, the set temperature was increased to melt down all formed ice, followed by cooling the solution again. This procedure was repeated 4-5 times to ensure that the stable temperatures were approximately the same. Undercooling was high at the first run. During subsequent runs, there could be microscopic ice crystals from the first run (although not visible), which might have acted as seeds to initiate ice formation at the freezing point during the

following runs by subduing the undercooling level. A representative freezing profile of 4 wt-% NaCl (aq) solution is shown in **Figure 5.2**.

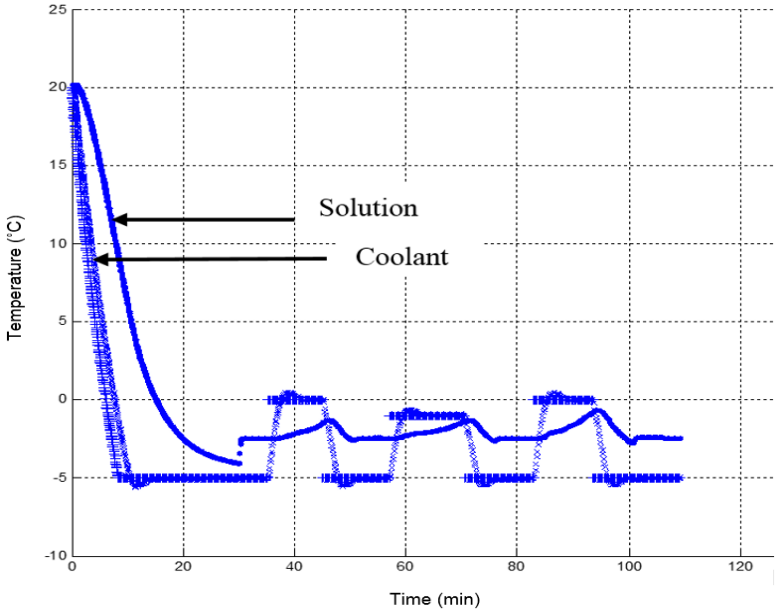

Figure 5.2 Freezing profile of 4 wt-% NaCl (aq) solution.

The solution was cooled down from 20˚C to -4˚C without any phase transition. After adding ice seeds at 30 min, the solution temperature rose abruptly due to the release of latent heat and became stable at -2.41˚C, which was the freezing point of this solution. Then, the solution temperature was raised to -1˚C by increasing the coolant temperature to ensure melting of all ice crystals within the solution. The solution was again cooled and became stable at -2.41˚C. This time no ice seeds were added. Nevertheless, the very small undercooling level (≈0.1˚C) inferred that microscopic ice crystals (which were not visible to naked eye) present in the solution might have acted as seeds in the second run to subdue the level of undercooling. The same procedure was followed two more times. In every case, the solution temperature stabilized at -2.41˚C, which can be considered the freezing temperature of the solution.

The freezing points of NaCl, $NiSO_4$ and $CoSO_4$ (aq) solutions in variation with concentration were measured experimentally with the existing setup and compared with the freezing points found in Haynes (2014) for NaCl (aq) solutions and Jones and Getman (1904) for $NiSO_4$ and $CoSO_4$ (aq) solutions.

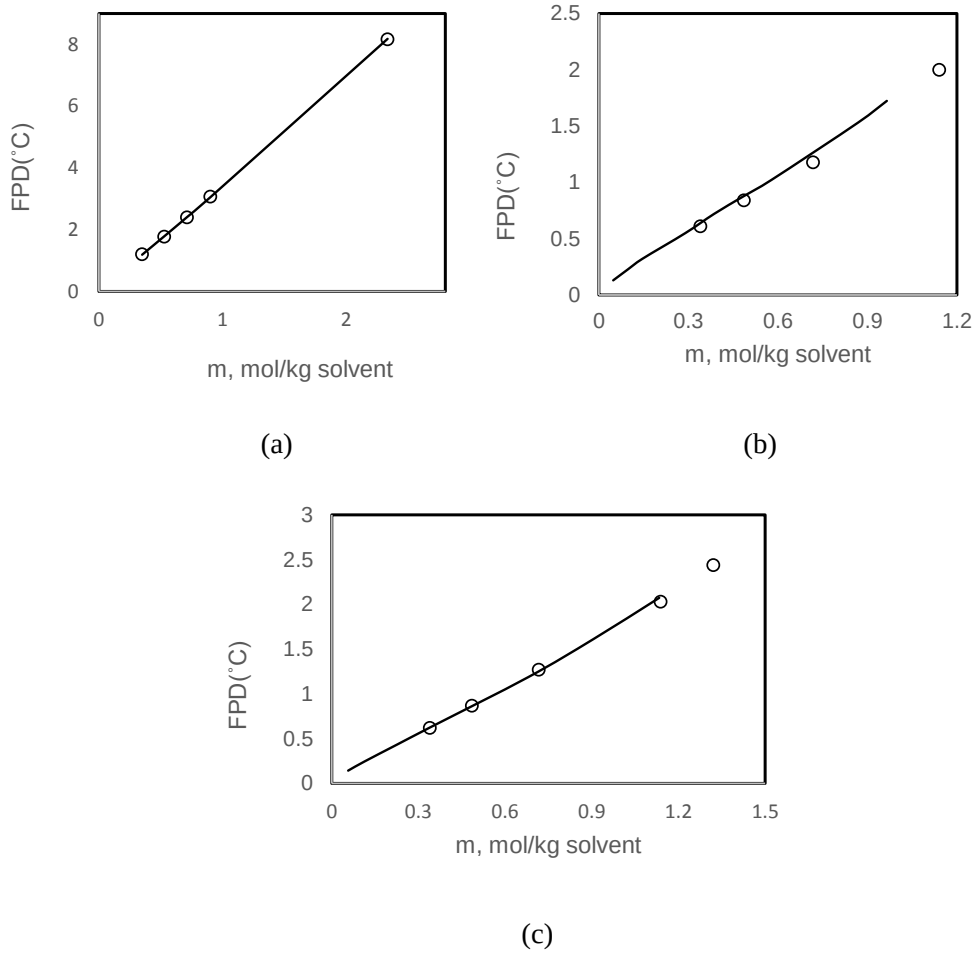

Figure 5.3 Freezing point of electrolyte solutions in variation with concentration, (a) NaCl; (b) $NiSO_4$; (c) $CoSO_4$ (aq). Symbols ○ and — represent experimental and literature freezing points, respectively.

The measured freezing points were found in good agreement with the literature data and within experimental limitations (**Figure 5.3**).

The very simple experimental setup and procedure presented in this chapter was capable of determining the freezing point quite correctly from the engineering point of view. Thus, this methodology can be adopted as a reliable scheme to determine the freezing point of complex multi-component wastewaters as the core issue to justify the efficacy of freezing as a purification technique.

6 Natural freezing as a purification technique

As discussed in the previous sections, nature could theoretically be utilized quite efficiently as a purification technique to treat and constrict huge volumes of wastewater collected in ponds. A developed winter simulator with the provision to replicate different freezing conditions was employed to epitomize natural freezing (NF) as a purification technique. The effect of different parameters and freezing conditions on the separation efficiency is explained thoroughly in this chapter. The varieties of ice morphologies with solution concentration and freezing conditions are also presented. The experimental setup of the winter simulator, including freezing test results in relation to theoretical knowledge are discussed in the following sections.

6.1 Experimental setup for simulating natural freezing

6.1.1 Materials and methods

1 wt%, 2 wt%, 3 wt% and 4 wt% Na_2SO_4 (aq) solutions were prepared by dissolving 99% pure anhydrous Na_2SO_4 (purchased from Merck), and 0.1 wt.%, 1 wt.% and 2 wt.% $NiSO_4$ (aq) solutions were prepared by dissolving 99% pure $NiSO_4 \cdot 6H_2O$ (analytical grade, manufactured by Merck) in deionized water (conductivity = 0.1 $\mu S\ cm^{-1}$, total organic carbon=1 ppb). Dissolution was performed at room temperature under vigorous mixing conditions (500 rpm) for 30 min.

6.1.2 Experimental setup and procedure for simulating natural freezing

The detailed experimental setup to treat the model aqueous electrolyte solutions by simulating natural freezing is presented in **Figure 6.1**. A 710 ml rectangular plastic vessel (14 cm × 8.74 cm × 5.8 cm) was used as the crystallizer. In order to promote ice layer growth merely on the top surface, the top surface of the crystallizer was exposed to cold air in a freezer box where the air temperature (T_a) was controlled by a Lauda proline RP 850 thermostat. Inside the freezer, an air circulation rate of 0.24 ms^{-1} was applied for better heat transfer and to ensure homogeneous temperature distribution throughout the freezer.

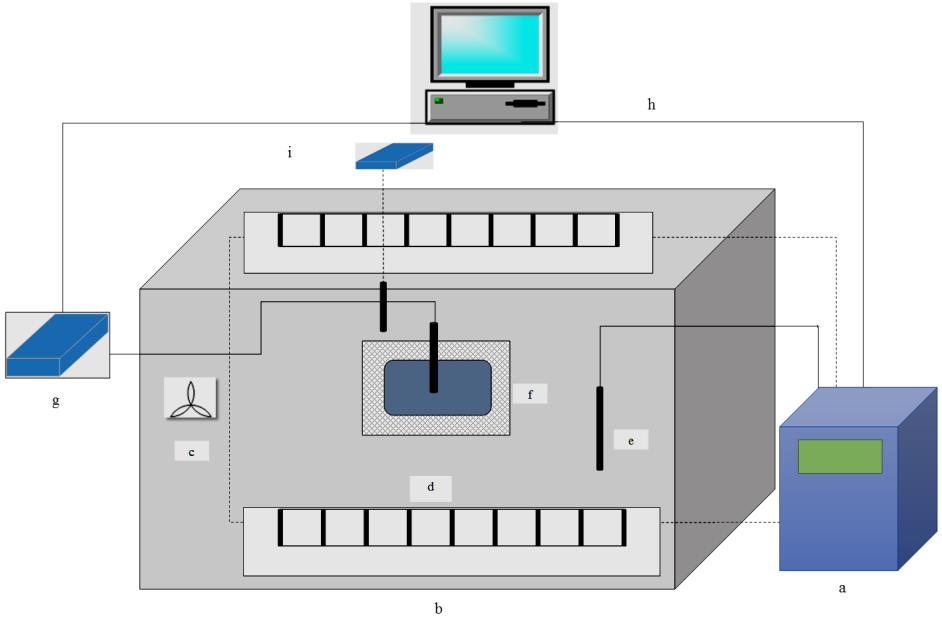

Figure 6.1 Experimental setup for freezing a solution. (a) Lauda proline RP 855 thermostat; (b) freezer box; (c) fan; (d) heat exchanger; (e) Pt 100 thermosensor; (f) crystallizer with insulation; (g) Pico logger; (h) data monitoring and storage device; (i) anemometer. The electric wire and coolant flow pipe are represented by a solid line (—) and dotted line (⋯), respectively.

A 500 ml sample solution was precooled by keeping it in a freezing room at -15 °C. When the solution arrived its freezing temperature, small ice crystal platelets appeared on the liquid at its surface and the solution was relocated to the crystallizer within the freezer box. The existence of ice platelets indicated accomplishment of the freezing temperature of the solution, and the platelets worked as seed crystals to prevent subsequent undercooling. The temperature inside the freezer was maintained at a constant temperature a few degrees lower (e.g., ΔT=1 °C, 2 °C, 3 °C) than the freezing temperature of the solution, by means of a Lauda proline RP 850 thermostat. After a certain freezing time (5 h, 10 h, 15 h, 24 h, 48h, 72h), the ice layer that had formed by freezing the solution was collected from the crystallizer. The ice layer was washed with distilled water at 0 °C to circumvent melting during washing. The volume and density of the residual solution were measured. After measuring the thickness and mass of the collected ice layer, ice impurities were analysed with the thermogravimetric method. The growth rate of ice crystallization (G) was measured from the thickness of the ice layer (X) formed after a certain freezing time (t).

The thermogravimetric method was used to measure the amount of Na_2SO_4 and $NiSO_4$ entrapped in the ice layer formed from Na_2SO_4 (aq) and $NiSO_4$ (aq) solutions at 100˚C

and 400 °C for 24 h, respectively. The ice layers obtained at different freezing conditions were observed microscopically under a calibrated Olympus BH2-UMA microscope to characterize the ice structure and ice inclusion. This was illustrated by the $NiSO_4$ (aq) solution because of its monochromatic green colour which could be detected easily. The captured images were handled with an image processing tool (analySIS). Furthermore, thin ice layers were examined through a polarized light source (by Edmund optics) to visualize ice grains within the polycrystalline ice layer. The ice layers formed in the $NiSO_4$ (aq) solutions were used for characterization.

6.2 Results and discussion

6.2.1 Determination of h_{air}

The heat transfer coefficient of air (h_{air}) while freezing is a significant factor for characterizing the freezing behaviour of a solution, interdependent on air velocity. In this work, air circulation rate during freezing was maintained at 0.24 m s^{-1} to substantiate the assumption of free convection rather than forced convection, which replicates quiescent weather conditions. At this air velocity, h_{air} was acquired as 23.5 $Wm^{-2}K^{-1}$, on average, inside the freezer. The heat transfer coefficient values indicated in the literature (Ashton, 1989) between the ice layer and air varied between 10 to 30 $Wm^{-2}K^{-1}$ depending on air velocity, which was consistent with the heat transfer coefficient obtained experimentally.

6.2.2 Measured solution temperature over time during natural freezing

In this work, the steady state condition was assumed during the modelling of freezing kinetics, even though the temperature and concentration of the solution varied with the advancement of the freezing process. At the sufficiently low freezing rate of experimental interest, the rate of changing temperature and concentration of the solution with freezing were insignificant enough to ignore. For instance, even at the experimental condition of the freezing of 3 wt% Na_2SO_4 (aq) for 24 h at comparatively higher ΔT=3 °C, where the bulk solution temperature T_b was most likely to be time-dependent, the alteration of T_b due to progressive freezing from -0.87 °C to -1.1 °C is unsubstantial. The temperature profile was almost flat over the 24 h freezing period, as illustrated in **Figure 6.2**.

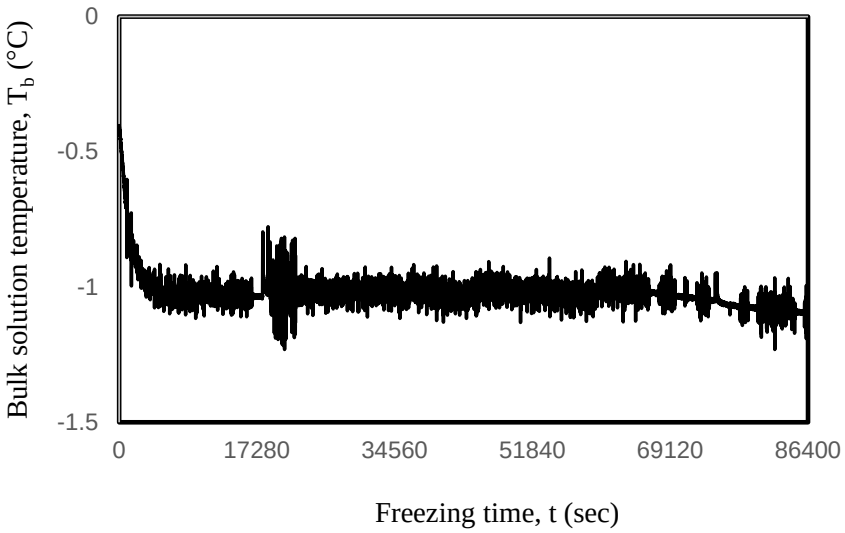

Figure 6.2 The change of T_b of 3 wt% Na_2SO_4 (aq) solution at ΔT=3 °C, over 24 h freezing time (t).

The same was also applicable for the other solutions and freezing conditions. Therefore, it is quite rational to consider steady-state condition during the modelling.

6.2.3 Growth rate as a function of freezing time, concentration and freezing point

The growth rate of the ice layer (G) from Na_2SO_4 (aq) and $NiSO_4$ (aq) solutions of different concentrations were manipulated by altering the freezing time (t) and the level of undercooling of air from the freezing point (ΔT) of the corresponding solution. The variation of G with solution concentration, t and ΔT simulating different freezing conditions are demonstrated comprehensively in **Publications I & II** for $NiSO_4$ (aq) and Na_2SO_4 (aq) solutions, respectively. Experimentally, G varied from 3.5×10^{-8} ms^{-1} to 4.5×10^{-7} ms^{-1} in different freezing conditions. This wide range of G replicates how weather conditions result in deflecting G. The experimental results showed that G decreased mostly with the advancement of freezing because of the heat transfer resistance exerted by the growing ice layer.

6.2.4 Effective distribution coefficient as a function of growth rate

Ice impurity (C_s) compared with the concentration (C_b) of the bulk solution is quite often expressed in terms of the effective distribution coefficient (K). Experimental K values, along with the corresponding growth conditions are presented in **Figure 6.3**. Considering the Na_2SO_4 (aq) and $NiSO_4$ (aq) solutions of different concentrations, K increased 0.0033-0.36 for the increase 3.5×10^{-8} ms^{-1} - 4.5×10^{-7} ms^{-1} in G. This indicates that at a higher G, the solutes in the solution are prone to be entrapped in the ice layer rather than dispersing from the ice-solution interface to the bulk solution. The dependency of solution

concentration rather than the type of solution on K was also clearly visible. For lower G values, especially in proximity of G≈5×10^{-8} ms^{-1}, K dropped significantly and the purity of the ice layer was very high. For instance, in the case of 1 wt-% $NiSO_4$ (aq) solution at G value 3.5×10^{-8} ms^{-1}, the corresponding K value was 0.00332, which implies that the formed ice layer was about 300 times purer than the solution from which it had formed. In the case of Na_2SO_4 (aq) solution of higher concentration, i.e., 4 wt-%, K was found to be 0.037 at G value 5.7×10^{-8} ms^{-1}. These experimental results indicate how uncontrollable weather conditions affect the freezing of a solution and thus control the impurity of the formed ice layer.

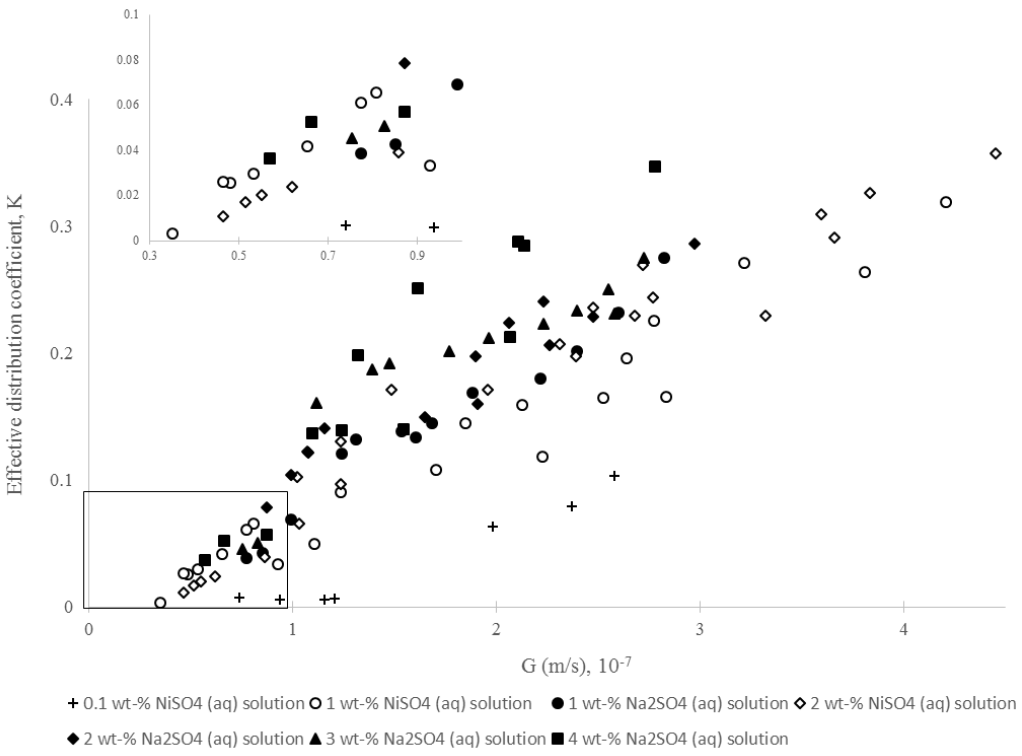

Figure 6.3 Effective distribution coefficient, K, for Na_2SO_4 and $NiSO_4$ solutions as a function of ice layer growth rate, G.

It can be seen in **Figure 6.3** that for the same solution concentration at a certain G, K is little bit higher in the case of the Na_2SO_4 (aq) solution than that of the $NiSO_4$ (aq) solution. A similar trend was also observed by Matsuda et al. (1999). They found that the solutes of larger molecular weights were more difficult to capture than the solutes of small molecular weights under the same initial solution concentration. This can also be explained in terms of water activity (a_w) as described in section 4.1.

6.2.5 Estimating the limiting distribution coefficient

Ice impurity (C_s) compared with the interfacial solution concentration (C_i) is known as the limiting distribution coefficient (Weeks and Lofgren, 1967). Burton et al., (1953) proposed a model to determine K^* from a set of experimental G and corresponding K values (as shown in **Figure 6.3**) by considering the constant K^* value regardless of G. However, Louhi-Kultanen et al., 1988 found that K^* is a function of G. Furthermore, it was inferred from the experimental results and also from the literature data for freezing sea-water that K values drop abruptly at a lower G (Weeks and Lofgren, 1967). Therefore, a calculation method was introduced to estimate the concentration of the solution at the advancing ice-solution interface in terms of the limiting distribution coefficient (K^*) from experimental K values at different growth conditions. Details of this method can be found in **Publication II**.

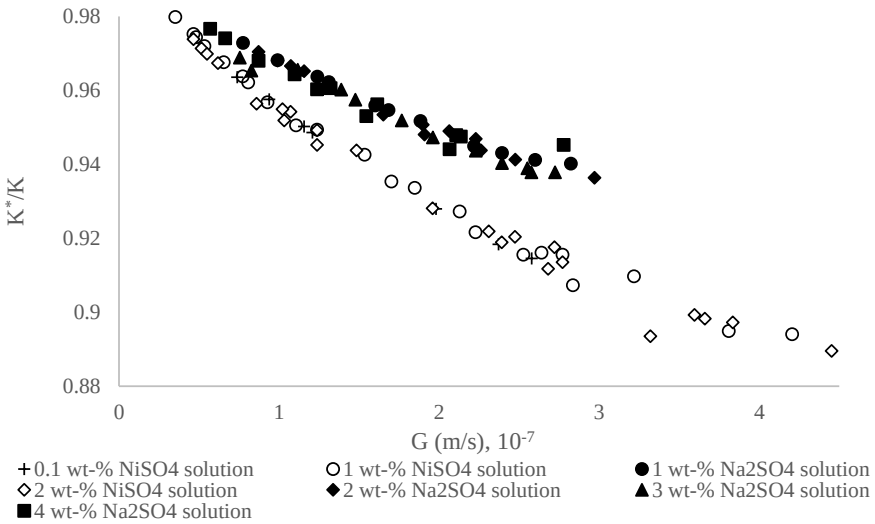

Figure 6.4 Ratio of the limiting and effective distribution coefficient of Na_2SO_4 and $NiSO_4$ (aq) solutions as a function of ice layer growth rate, G.

The values of K^*/K are independent of solution concentration and dependent on the type of solution. This is possibly due to the difference between the thermodynamic and physical properties of the Na_2SO_4 (aq) and $NiSO_4$ (aq) solutions. **Figure 6.4** also indicates that at very low growth conditions, e.g., $G<10^{-7}$ m s^{-1}, the solute gets enough time to diffuse from the ice-solution interface to the bulk solution, which eventually results in $K \approx K^*$. As the growth rate increased, incorporation of solutes in the solution at the advancing ice front also increased and the K^* value decreased.

6.2.6 Heat and mass transfer resistance

The heat (R_h) and mass transfer (R_m) resistances to advancing the ice front of the Na_2SO_4 (aq) and $NiSO_4$ (aq) solutions are presented as a function of initial concentration, t and ΔT in **Table 6.1** and **Table 6.2,** respectively.

Table 6.1 Influence of heat and mass transfer resistance on the t of the Na_2SO_4 (aq) solution at different freezing conditions.

Solution concentration, wt-%	ΔT	time, t (hr)	Heat transfer Resistance (sKm^{-1}), 10^7	Mass transfer Resistance (sKm^{-1}), 10^5
1	1	5	1.23	0.79
		10	1.31	0.89
		15	1.37	0.97
		24	1.40	1.03
	2	5	1.17	0.72
		10	1.24	0.80
		15	1.29	0.86
		24	1.35	0.96
	3	5	1.04	0.62
		10	1.15	0.72
		15	1.24	0.83
		24	1.36	1.02
2	1	5	1.20	1.62
		10	1.24	1.71
		15	1.28	1.84
		24	1.35	2.04
	2	5	1.07	1.36
		10	1.13	1.48
		15	1.20	1.67
		24	1.33	2.01
	3	5	1.03	1.27
		10	1.16	1.50
		15	1.24	1.68
		24	1.39	2.06
3	1	5	1.14	2.31
		10	1.19	2.54
		15	1.36	3.58
		24	1.40	3.69
	2	5	1.08	2.10
		10	1.13	2.32
		15	1.20	2.54
		24	1.27	2.86
	3	5	1.04	1.99
		10	1.13	2.25
		15	1.20	2.53
		24	1.32	2.97
4	1	5	1.21	3.41
		10	1.33	3.93
		15	1.35	4.18
		24	1.41	4.51
	2	5	1.01	2.73
		10	1.10	3.06
		15	1.21	3.33
		24	1.35	3.71
	3	5	0.94	2.31
		10	1.08	2.88
		15	1.23	3.38
		24	1.42	3.44

Table 6.2 Influence of heat and mass transfer resistance on the t of the $NiSO_4$ (aq) solution at different freezing conditions.

Solution concentration, wt-%	ΔT(˚C)	time, t (hr)	Heat transfer Resistance ($K{\cdot}s{\cdot}m^{-1}$), 10^7	Mass transfer Resistance ($K{\cdot}s{\cdot}m^{-1}$), 10^5
0.1 wt-%	1	24	1.50	0.07
	2	24	1.49	0.08
	3	24	1.50	0.08
	4	24	1.48	0.08
	0.8	24	1.67	0.07
	0.8	48	1.67	0.09
	0.9	72	1.67	0.11
1 wt-%	1	5	1.21	0.52
	1	10	1.30	0.58
	1	15	1.38	0.66
	1	24	1.43	0.72
	2	5	1.19	0.50
	2	10	1.30	0.57
	2	15	1.29	0.59
	2	24	1.40	0.71
	3	5	1.05	0.43
	3	10	1.16	0.51
	3	15	1.25	0.59
	3	24	1.39	0.77
	4	5	1.00	0.41
	4	15	1.21	0.60
	4	24	1.42	0.83
	0.2	48	1.46	0.82
	0.2	72	1.51	0.91
	0.4	48	1.45	0.80
	0.4	72	1.53	0.93
	0.6	72	1.52	1.05
	0.8	48	1.47	0.82
	0.8	72	1.60	0.97
2 wt-%	1	5	1.16	1.04
	1	10	1.24	1.15
	1	15	1.27	1.22
	1	24	1.34	1.36
	2	5	1.04	0.90
	2	10	1.14	1.03
	2	15	1.22	1.16
	2	24	1.33	1.41
	3	5	1.03	0.88
	3	10	1.14	1.03
	3	15	1.24	1.19
	3	24	1.30	1.48
	4	5	0.94	0.81
	4	10	1.05	0.96
	4	15	1.13	1.12
	4	24	1.36	1.76
	0.2	48	1.48	1.67
	0.2	72	1.54	1.92
	0.4	48	1.49	1.70
	0.4	72	1.55	1.95
	0.8	48	1.52	1.86
	0.8	72	1.62	2.39
	1.3	48	1.51	1.96

It can be seen in **Tables 6.1** and **6.2** that in most of the cases, R_m increased with the increasing concentration of the solution, whereas R_h is likely to be concentration-independent. It is apparent that R_h is of the order of 10^7 $K{\cdot}s{\cdot}m^{-1}$ and R_m is of the order of 10^5 $K{\cdot}s{\cdot}m^{-1}$, which indicates that heat transfer dominates the kinetics of freezing.

The calculated thermal boundary layer, δ_T (=k/h_{sol}) and mass boundary layer, δ_c (=D/k_{sol}) for the Na_2SO_4 (aq) and $NiSO_4$ (aq) solutions are displayed in **Figure 6.5**.

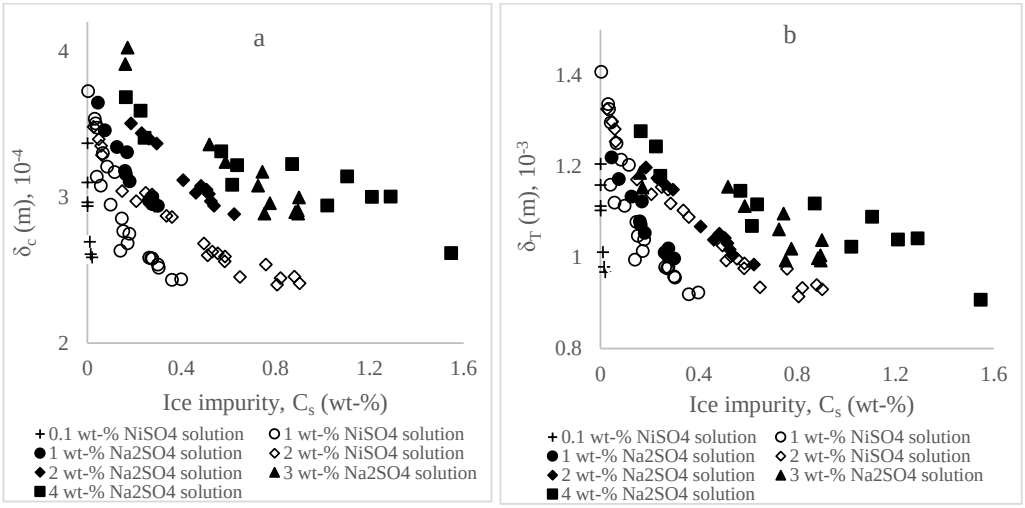

Figure 6.5 Influence of (a) mass boundary (δ_c) layer and (b) thermal boundary layer (δ_T) on ice impurity C_s formed of Na_2SO_4 (aq) and $NiSO_4$ (aq) solutions of different concentrations.

δ_T was found approximately 3.4 and 3.8 times higher than δ_c with the variation of the Na_2SO_4 (aq) and $NiSO_4$ (aq) solutions of different concentrations and freezing conditions, respectively, which further indicates that ice crystallization was limited by the heat transfer. **Figure 6.5** depicts the inverse relation between boundary layer thickness and ice impurity. For thinner boundary layers, heat and mass transfer occurred more readily, and G was therefore higher than for thicker boundary layers, and consequently the impurity of the ice layer was higher. **Figure 6.5** also shows that the ice layer formed of the more concentrated solution was more susceptible to inclusion of impurities at the same boundary layer thickness.

6.2.7 Freezing ratio and separation efficiency

The term separation efficiency (E) is defined as the ratio between the amount of solute in the residual solution after freezing and the total amount of solute in the initial solution that is subjected to freezing, as shown in **Eq. (6.1)**. The freezing ratio (R_F) is defined as in **Eq. (6.2)**

$$E(\%)=\left(1-\frac{C_s V_s}{C_0 V_0}\right)\times 100\% \tag{6.1}$$

$$R_F=\left(\frac{V_s}{V_0}\right) \tag{6.2}$$

where C_0 and V_0 stand for the concentration and volume of the initial solution, respectively, and V_s refers to the volume of the ice layer after melting. E as a function of R_F is for the Na_2SO_4 (aq) and $NiSO_4$ (aq) solutions of different concentrations are shown in **Figure 6.6.**

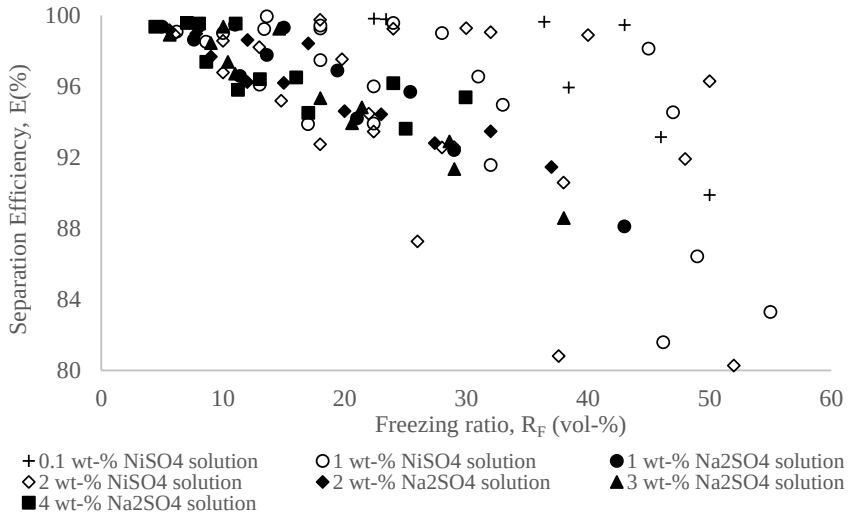

Figure 6.6 Influence of freezing ratio (RF) on separation efficiency (E).

Figure 6.6 shows that E is influenced by the initial concentration of the solution. For the very dilute solution, i.e., 0.1 wt-% $NiSO_4$ (aq) solution, E did not change significantly even after half of the solution was frozen. Considering all solutions, E was above 92% until R_F = 25%, which means that solution enrichment was dominant within this range, and therefore the ice layer was very pure. Even above R_F = 50%, E was above 80%. This result implicates that within these concentration profiles and freezing conditions, the volume of wastewater can be reduced up to 50% with separation efficiency higher than 80%.

6.2.8 Ice layer characteristics

In practice, the natural freezing based purification method in wastewater ponds would integrate some other post-freezing processes, e.g., ice breaking, ice collection, how the formed ice layer could be removed and transported from the pond to the post-processing

unit, and so on. Thus, it becomes very important to investigate the underlying reasons that might affect the morphology and mechanical properties of the ice layer.

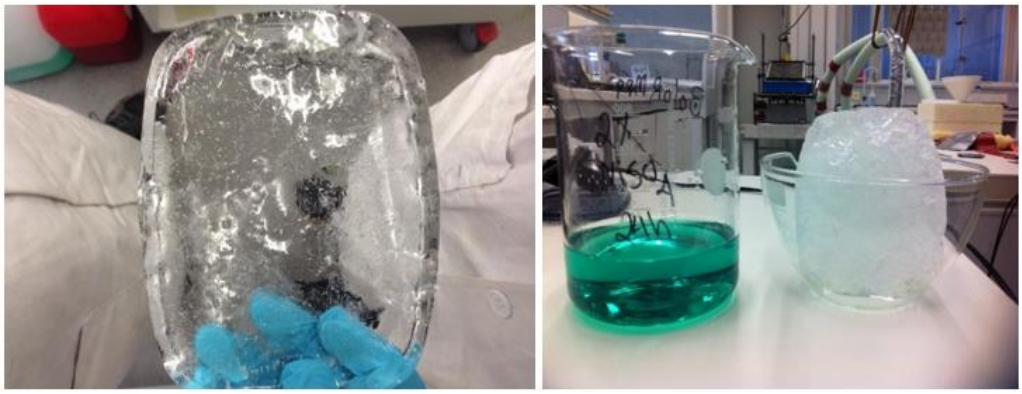

(a) (b)

Figure 6.7 Difference between transparency levels of ice layers formed of (a) 0.1 wt-% $NiSO_4$ (aq) solution and (b) 2 wt-% $NiSO_4$ (aq) solution.

The transparency of the ice layer formed of a very dilute solution (e.g., 0.1 wt-% $NiSO_4$ (aq)) was akin to that formed from pure water, which reflects the high purity of the ice layer formed of the 0.1 wt-% solution evident in **Figure 6.7**. On the other hand, the ice layers formed by freezing the 1 wt-% and 2 wt-% $NiSO_4$ (aq) solutions and 1 wt-% - 4 wt-% Na_2SO_4 (aq) solutions were opaque. Solution inclusion within the ice layer raises the albedo, which explains the difference in transparency between the ice layers of the different solutions.

Microscopic images showed that the upper surface of ice layers were planar regardless of solution type and concentration, as shown in **Figure 6.8** for different $NiSO_4$ (aq) solutions.

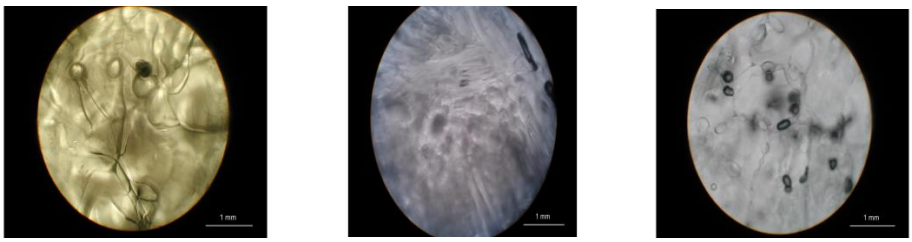

(a) (b) (c)

Figure 6.8 Microscopic view of the upper surface of the ice layer obtained of (a) 0.1 wt.%; and (b) 1 wt-%; (c) 2 wt-% $NiSO_4$ (aq) solution, respectively. The scale bar represents 1 mm at 1.5 magnification (**Publication I**).

The microscopic images also revealed that, unlike the upper surface, the lower surface of the ice layer was not always planar but varied with the concentration of the solution of which it had formed. The lower surfaces of the ice layers formed from 1 wt-% and 2 wt-% $NiSO_4$ (aq) solutions were sutured (**Figure. 6.9b and 6.9c**). This difference in the interfacial texture can be explained by constitutional undercooling (Hurle, 1993; Nishinaga, 2014) that ensues due to faster transport of heat from the bulk to the interface compared with molecular diffusion from the interface to the bulk (Petrich and Eicken, 2009). Thus, a thin layer is established below the interface, which is cooled further below the freezing point of the solution, but the interfacial solution concentration is only slightly enriched above the bulk level. For very dilute solutions (in our case the 0.1 wt-% aqueous $NiSO_4$ solution), molecular diffusion is not noteworthy, so constitutional undercooling is unlikely to affect the structure of the lower surface. Therefore, a planar interface can be anticipated as freezing proceeds at a much lower growth rate. Conversely, with the higher concentrated solutions of the 1 wt-% and 2 wt-% $NiSO_4$(aq) solutions, the morphology of the ice-solution interface (lower surface of the ice layer) can be cellular or lamellar, as shown in **Figure 6.9b and Figure 6.9c**, because of the formation of a constitutionally undercooled layer. This difference in the interfacial texture could also be interpreted as an increase in solute extraction with increasing solute content in the solution, making the lower surface of the ice layer (which was in contact with the solution) more sutured (Hirata et al., 2000).

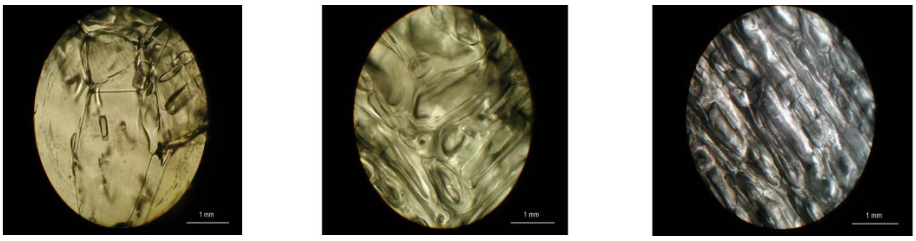

(a) (b) (c)

Figure 6.9 Microscopic view of the lower surface of the ice layer obtained from (a) 0.1 wt-%; and (b) 1 wt-%; (c) 2 wt-% $NiSO_4$ (aq) solution, respectively. The scale bar represents 1 mm at 1.5 magnification (**Publication I**).

Solution incorporation within the ice layer was observed only at the upper surface (**Figures. 6.8a to 6.8c**) but not in the lower surface (**Figures 6.9a to 6.9c**). This was due to the fact that the upper surface formed at the beginning of the freezing, which implied the highest ice growth rate. Later, during the remaining freezing time, the growth rate dropped because of the additional heat resistance of the formed ice layer, and thus the lower surface formed at a lower growth rate. It is evident from **Figure 6.3** that the growth rate influences the corresponding K value greatly.

The ice layers were polycrystalline by nature and comprised many crystal families (grains) of different sizes. The grains can be seen in **Figure 6.10**, which shows thin ice layers, illuminated with cross-polarized light, from freezing the $NiSO_4$ (aq) solutions.

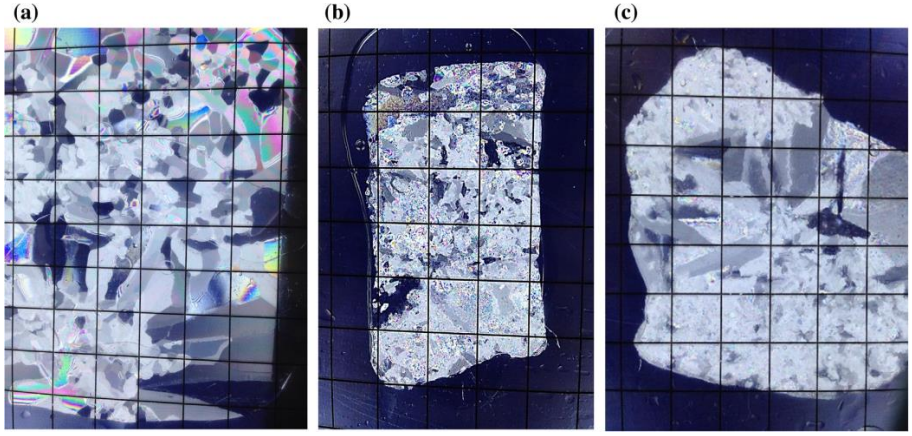

Figure 6.10 Macroscopic view of thin ice layers obtained from (a) 0.1 wt.%; (b) 1 wt.%; and (c) 2 wt.% $NiSO_4$ (aq) solutions, photographed through cross-polarized light. The grid scale is 1 cm in both horizontal and vertical direction (**Publication I**).

It is visible that the average ice crystallite size formed in the dilute solution are higher than those of the more concentrated solution and prone to solution incorporation. Therefore, at the same freezing conditions, the ice layer formed of the concentrated solution had a higher K value (higher impurity) than that of the dilute solution (**Figure 6.3**).

Entrapment of the $NiSO_4$ (aq) solution within the interstitial of crystallites is illustrated in **Figure 6.11.**

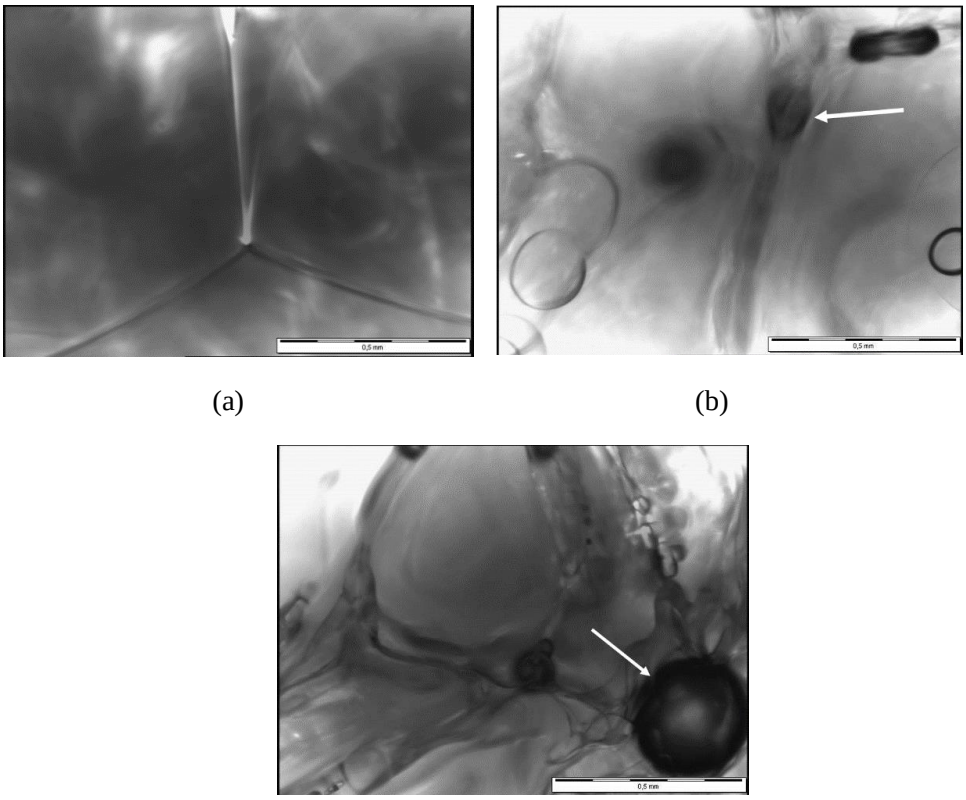

(a) (b)

(c)

Figure 6.11 Photomicrograph of solution incorporation (marked by arrows) in the interstitial of ice grains from freezing (a) 0.1 wt-%; (b) 1 wt-%; and (c) 2 wt-% $NiSO_4$ (aq) solution, respectively. The scale bar represents 0.5 mm at 5.0 magnification (**Publication I**).

In the almost pure ice that was produced by freezing the 0.1 wt-% $NiSO_4$ (aq) solution, the grain boundaries were too thin to accommodate solution entrapment. The grain boundaries of the ice of the 1 wt-% and 2 wt-% $NiSO_4$ (aq) solutions were spacious enough to permit inclusion. Entrapped inclusion influenced the mechanical properties of the ice layer. In **Figure. 6.11b**, some transparent bubbles are visible. It was difficult to categorize whether these were mother liquor voids or air bubbles. However, impurity analysis of the ice gave accurate data on the quantities of entrapped solute in the ice. The ice layer formed of the concentrated solution (2 wt-%) felt softer due to the greater volume fraction of inclusion than the ice layers obtained from the very dilute solution (0.1 wt-%). In the case of ice formation of the Na_2SO_4 (aq) solution (**Publication II**) and ethylene glycol solutions of different concentrations (Hirata et al., 2000), similar ice characteristics have been reported in the literature.

6.2.9 Modelling of ice layer thickness

In our previous work (**Publication II**), we developed a model to predict the ice growth rate G from ice thickness (X) at different ΔT and freezing time t, assuming steady state conditions, as in **Eq. (2.10)**.

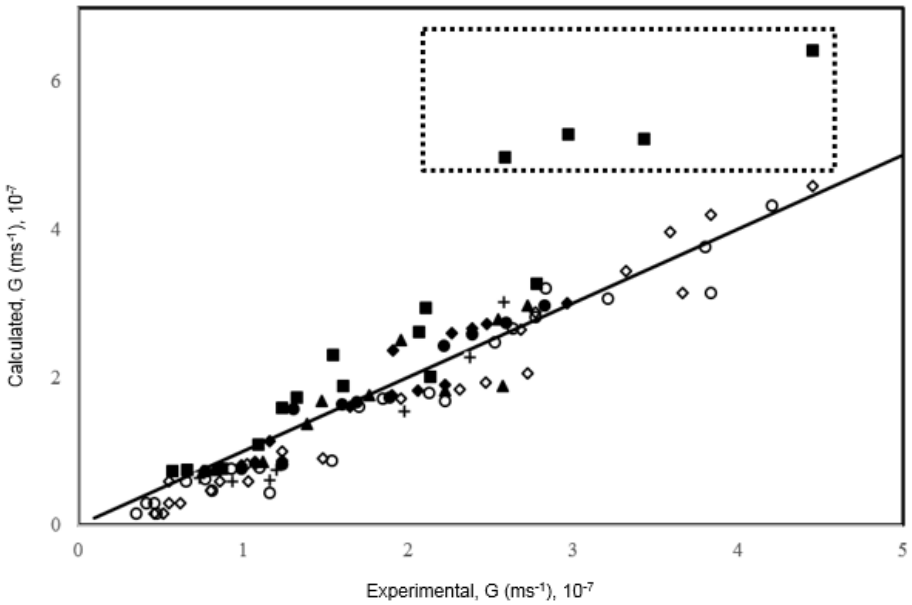

Figure 6.12 Comparison between experimental and model ice growth rate G from Na_2SO_4 (aq) and $NiSO_4$ (aq) solutions of different concentration. The solid line represents the condition where experimental results completely coincide with the model results. Symbols indicate same as they do in **Figure 6.3** – **Figure 6.6**.

G calculated with the model and experimental G at different ΔT and t are compared in **Figure 6.12**, which illustrates that the experimental data are in good agreement with calculated data. In most cases, the model values underestimate G slightly, which is probably due to the increment of T_b from the freezing point of the solution when transferring the solution from the freezing room to the ice crystallizer within the freezer. Even though the change of T_b due to solution enrichment while freezing was within experimental limitations, it lowered ΔT later during freezing. Hence, the model would be more accurate if the initial temperature of the solution at its freezing point could be controlled at the commencement of freezing and if ΔT could be adjusted constantly during the course of freezing. Furthermore, more precise prediction would be possible if physical and thermodynamic properties were available in the literature at the corresponding freezing point of the solution. In the case of the 4 wt% Na_2SO_4 (aq) solution, for some

freezing conditions (e.g., $\Delta T=4^{\circ}C$) not only ice crystallization occurred but also salt crystallization. As the model in this work is based on only ice crystallization, there are some outliers for the 4 wt% Na_2SO_4 (aq) solution in **Figure 6.12**, as highlighted by the dotted rectangular box.

6.3 Conclusion

Natural freezing (NF) of two different electrolytic solutions was explored in a developed winter simulator in this chapter. The experimental results were expounded by fundamental theories as described in **Chapter 2**. The influence of several factors on freeze crystallization and its efficiency as a purification technique were perused in varying freezing conditions replicating varying winter conditions. This kind of a study is of importance to be able to employ NF for the purpose of purifying real life wastewater emitting from a variety of industries.

Summary

Freeze crystallization has the potential to be applied in diverse purification techniques. In cold weather regions where the temperatures are below 0˚C, the acceptability of this method can even be more pronounced if nature can be used for freezing. Natural freezing has potential to be applied in ponds to treat the voluminous wastewater emitting from mining industries. The traditional methods of treating huge volumes of wastewater are either very energy-intensive or associated with secondary effluent generation. The present work promotes the concept of natural freezing in wastewater ponds. Natural freezing was epitomized in a laboratory-scale winter simulator with the possibility to manipulate the inside air temperature to freeze simple binary Na_2SO_4 (aq) and $NiSO_4$ (aq) solutions because of their common existence in wastewaters of different sources. Freezing efficiency in variation with freezing conditions analogous to varying weather conditions, as well as solution concentration and type were investigated in a detailed manner. The experimental results were interpreted on the basis of crystallization kinetics and thermodynamics of freezing. The purity and morphology of the ice layers formed at varying freezing conditions were analyzed thoroughly.

Comprehensive understanding of the solid-liquid equilibrium is the core factor in any freezing process. The level of undercooling by natural freezing at certain weather conditions relies on the freezing point of the solution, which influences the kinetics of freezing and thus controls the efficiency of the freezing process. Therefore, prior knowledge of the freezing temperature of a solution plays a key role in this regard. The freezing point of electrolyte solutions can be predicted by Pitzer's activity coefficient model. The virial coefficients of the Pitzer model and the temperature derivatives are usually extracted from isopiestic data, however. Very accurate freezing point data are available in the literature for different types of electrolytes in variation with solution concentration. In this work, a calculation method was developed to extract temperature derivatives of Pitzer ion-interaction parameters at 0˚C by utilizing the freezing point of NaCl and KCl (aq) solutions as a function of concentration, which is very pertinent for freezing. The validity of the parameters was also studied by using literature results of concentration cells without transference, in addition to the freezing-point data presented in the literature. In both cases, the new parameter values applied better than those of isopiestic data considered at 25˚C. Later this methodology was applied to obtain temperature derivatives of all 1-1 and 1-2 types of electrolytes for which reliable freezing point data were available in the literature. Furthermore, these parameters can also be used to predict the solubility of the solution at subzero temperature range, which is very important for the eutectic freeze crystallization process in which both ice and salts are produced simultaneously from the solution. This methodology can be protracted to predict the freezing temperature of a multi-component solution of practical interest very accurately.

Natural freezing of Na_2SO_4 (aq) and $NiSO_4$ (aq) solutions at different concentrations was investigated at a freezing rate ranging from approximately 3.5×10^{-8} ms^{-1} to 4.5×10^{-7} m s^{-1}. Ice impurity in terms of the effective distribution coefficient, K, was

measured experimentally. The growth rate of the advancing ice layer G, and the initial concentration of the solution were found as causative factors determining the ice impurity in terms of the effective distribution coefficient K. Freezing a solution of about 10000 ppm concentration at the rate in proximity of 3×10^{-8} m s^{-1} can produce an ice layer of about 250 times purer than the original solution. In the case of a dilute solution, a purer ice layer could be obtained at the same G. For dilute solutions of experimental interest, the kinetics of the solidification process was dominated by heat transfer rather than mass transfer. The thickness of the boundary layers that developed due to the thermal (δ_T) and concentration (δ_C) gradient at the interface was inversely related to the freezing rate. The overall heat transfer coefficient (U) is limited by the free convective heat transfer coefficient of the air (h_{air}) rather than the thermal conductance of the ice layer (k_{ice}) and the free convective heat transfer coefficient of the solution (h_{sol}).The thermal boundary layer tends to increase with the course of freezing because the heat resistance exerted by the growing ice layer inhibits the growth rate. This eventually allows for the solute molecules to diffuse through the boundary layer rather than being entrapped in the advancing ice layer. Therefore, remarkably low growth rates result in better separation. Ice formed of a concentrated solution has a tendency toward higher impurity at the same G because of the significant presence of solute molecules in the solution.

A calculation model was developed to estimate the concentration at the ice-solution interface, C_i, based on its variation with the growth rate. The model was built up with the differential mass transfer model (DMTM) and solute balance model at the ice–solution interface. The difference between these methods in estimating the limiting distributive coefficient, K^*, was negligible. With a very low G, K equals to K^*. A simplified model was developed based on the overall heat balance from the bulk solution to cold air to predict ice thickness at different growth conditions. The model worked quite well when there was only ice formation from the solution. However, when the eutectic point was reached, i.e., ice and salt started to crystallize simultaneously, the model showed discrepancies in estimating ice thickness. The accuracy of the model was hampered by a lack of knowledge about the thermo-physical properties of the solutions at temperatures below 25 °C. Usually, the concentration of Ni^{2+} in mine waters or in effluents emanating from nickel processing industries is very low, and this model would work very efficiently.

Natural freezing is potentially relevant for the remediation of wastewater contaminated by mining activities in geographic zones where the temperature drops below the freezing point of the treated solution. This approach has the advantage of good separation efficiency and low energy consumption. The mass and energy transfer occurring on the ice-solution interface is very crucial to elaborate the enrichment mechanism. Fundamental study of the mass and energy transfer based on the solid-liquid equilibrium is of importance to aid the design of such an efficient separation technique. As a first investigation of natural treatment of Na_2SO_4 (aq) and $NiSO_4$ (aq) solutions, this work answers the essential question on feasibility and provides a sufficient level of theoretical explanations

References

Adams, C. M., French, D. N., Kingery, W. D., 1960. Solidification of sea ice. *J. Glaciol.*, 3 (28), pp.745–761.

Anderson, D. L., 1961. Growth rate of sea ice. *J. Glaciol.*, 3 (30), pp. 1170–1172.

Anderson, D. L., 1958. A model for determining sea ice properties. *Arct. Sea Ice Natl. Acad. Sci. Wash. DC Natl. Res. Counc. Publ.*, 598, pp. 198–152.

Archer, D.G., Wang, P., 1990. The Dielectric Constant of Water and Debye-Hückel Limiting Law Slopes. *J. Phys. Chem. Ref. Data*, 19 (2), pp. 371–411.

Ashton, G.D., 1989. Thin ice growth. *Water Resour. Res.*, 25 (3), pp. 564–566.

Badger, J., Kapulsky, A., Gursky, O., Bhyravbhatla, B., Caspar, D.L., 1994. Structure and selectivity of a monovalent cation binding site in cubic insulin crystals. *Biophys. J.*, 66, pp. 286–292.

Bu, D., Xu, Y., Gu, W., Lin, Y., Tao, J., Zhang, X., 2011. Review of wastewater treatment by natural freezing, in: Remote Sensing, Environment and Transportation Engineering (RSETE), *International Conference on.* pp. 692–695. Nanjing: IEEE.

Burton, J. A., Prim, R. C., Slichter, W. P., 1953. The distribution of solute in crystals grown from the melt. Part I. Theoretical. *J. Chem. Phys.*, 21 (11), pp. 1987–1991.

Butler, M.F., 2002. Freeze concentration of solutes at the ice/solution interface studied by optical interferometry. *Cryst. Growth Des.*, 2 (6), pp.541–548.

CRC handbook of chemistry and physics, (2014) (ed. W. M. Haynes). CRC press, Boca Raton, FL, USA.

De Vito, F., Veytsman, B., Painter, P., Kokini, J. L., 2015. Simulation of the effect of hydrogen bonds on water activity of glucose and dextran using the Veytsman model. *Carbohydr. Polym.*, 117, pp. 236–246.

Englezos, P., 1994. The freeze concentration process and its applications. *Dev. Chem. Eng. Miner. Process*, 2 (1), pp. 3–15.

Gao, W., Shao, Y., 2009. Freeze concentration for removal of pharmaceutically active compounds in water. *Desalination*, 249 (1), pp. 398–402.

Gao, W., Smith, D.W., Habib, M., 2008. Petroleum refinery secondary effluent polishing using freezing processes—toxicity and organic contaminant removal. *Water Environ. Res.*, 80 (6), pp. 517–523.

Garnett, E. D., 2001. S*odium sulfate: Handbook of deposits, processing, properties, and use*. Academic Press, London, UK.

Gautier, M., Muller, F., Le Forestier, L., Beny, J. M., Guégan, R., 2010. NH_4-smectite: characterization, hydration properties and hydro mechanical behaviour. *Appl. Clay Sci.*, 49 (3), pp. 247–254.

Ge, X., Wang, X., 2009. Estimation of freezing point depression, boiling point elevation, and vaporization enthalpies of electrolyte solutions. *Ind. Eng. Chem. Res.*, 48 (4), pp. 2229–2235.

Genceli, F. E., Rodriguez Pascual, M., Kjelstrup, S., Witkamp, G. J. 2009. Coupled heat and mass transfer during crystallization of $MgSO_4 \cdot 7H_2O$ on a cooled surface. *Cryst. Growth Des.*, 9(3), pp. 1318-1326.

Genceli, F.E., 2008. *Scaling-up eutectic freeze crystallization.* Delft University of Technology (Ph.D. Dissertation), Delft, The Netherlands.

Gibbard, H. F. Jr., Gossmann, A. F., 1974. Freezing points of electrolyte mixtures. I. Mixtures of sodium chloride and magnesium chloride in water. *J. Solut. Chem.* 3, pp. 385–393.

Glasgow Jr., A. R., Ross, G., 1956. Purification of substances by a process of freezing and fractional melting under equilibrium conditions. *J. Res. Natl. Bur. Stand.*, 57 (3), pp. 137–142.

Gleick, P.H., 1998. *Water in Crisis: A Guide to the World's Freshwater Resources.* Oxford University Press, New York, USA.

Güner, F. E. G., Wåhlin, J., Hinge, M., Kjelstrup, S. 2015. The temperature jump at a growing ice–water interface. *Chem. Phys. Lett.*, 622, pp. 15–19.

Finnish Meteorological Institute (2016). Mean temperature maps from 1961 onwards: (Retrieved Jun. 28, 2016), url: http://en.ilmatieteenlaitos.fi/maps-from-1961–onwards

Han, B., 2015. *Influence of multi-phase phenomena on semibatch crystallization processes of aqueous solutions*. Acta Univ. Lappeenrantaensis 646, Finland.

Harkins, W. D., Roberts, W. A., 1916. The freezing-point lowerings in aqueous solutions of salts and mixtures of salts and of a salt with a nonelectrolyte. *J. Am. Chem. Soc.*, 38 (12), pp. 2676–2679.

Harned, H. S., Cook, M. A., 1937. The thermodynamics of aqueous potassium chloride solutions from electromotive force measurements. *J. Am. Chem. Soc.*, 59 (7), pp. 1290–1292.

Harned, H. S., Nims, L. F., 1932. The thermodynamic properties of aqueous sodium chloride solutions from 0 to 40. *J. Am. Chem. Soc.*, 54 (2), pp. 423–432.

Heikkinen, P. M., Räisänen, M. L., 2008. Mineralogical and geochemical alteration of Hitura sulphide mine tailings with emphasis on nickel mobility and retention. *J. Geochem. Explor*., 97 (1) , pp. 1–20.

Henning, S., Ulrich, J., 1997. Description of the Migration of liquid inclusions in growing crystalline layers. *Chem. Eng. Res. Des.*, 75 (2), pp. 233–236.

Hirata, T., Nagasaka, K., Ishikawa, M., 2000. Crystal ice formation of solution and its removal phenomena at cooled horizontal solid surface: Part I: ice removal phenomena. Int. J. Heat Mass Transf., 43 (3), pp. 333–339.

Huige, N. J. J., Thijssen, H. A. C., 1972. Production of large crystals by continuous ripening in a stirrer tank. J. Cryst. Growth, 13, pp. 483–487.

Hurle, D. T., 1993. *Handbook of crystal growth.* North Holland.

Jones, H. C., Getman, F. H., 1904. The nature of concentrated solutions of electrolytes. *Am. Chem. J*. 31, pp. 303–359.

Jøssang, A., Stange, E., 2001. A new predictive activity model for aqueous salt solutions. *Fluid Phase Equilibria*, 181 (1), pp. 33–46.

Kaksonen, A. H., Plumb, J. J., Robertson, W. J., Riekkola-Vanhanen, M., Franzmann, P. D., Puhakka, J. A., 2006. The performance, kinetics and microbiology of sulfidogenic fluidized-bed treatment of acidic metal-and sulfate-containing wastewater. *Hydrometallurgy*, 83 (1), pp. 204–213.

Kapembwa, M., Rodríguez-Pascual, M., Lewis, A. E., 2013. Heat and mass Transfer effects on ice growth mechanisms in pure water and aqueous solutions. *Cryst. Growth Des.*, 14 (1), pp. 389–395.

Kashchiev, D., 2000. *Nucleation: Basic theory with applications*. Butterworth-Heinemann, Oxford, UK.

Kim, H. T., Frederick, W. J. Jr., 1988. Evaluation of Pitzer ion interaction parameters of aqueous electrolytes at 25. degree. C. 1. Single salt parameters. *J. Chem. Eng. Data*, 33 (2), pp. 177–184.

Kuroda, T., 1985. Rate determining processes of sea ice growth. *Ann. Glaciol.*, 6, pp. 168–17.

Lewis, A. E., Nathoo, J., Thomsen, K., Kramer, H. J., Witkamp, G. J., Reddy, S. T., Randall, D. G., 2010. Design of a Eutectic Freeze Crystallization process for multicomponent waste water stream. *Chem. Eng. Res. Des.* 88 (9), pp. 1290–1296.

Lin, C. Y., Pan, J. Y., 2001. The effects of sodium sulfate on the emissions characteristics of an emulsified marine diesel oil-fired furnace. *Ocean Eng.*, 28 (4), pp. 347–360.

Liu, L., Miyawaki, O., Nakamura, K., 1997. Progressive freeze-concentration of model liquid food. *Food Sci. Technol. Int. Tokyo*, 3 (4), pp. 348–352.

Lorain, O., Thiebaud, P., Badorc, E., Aurelle, Y., 2001. Potential of freezing in wastewater treatment: soluble pollutant applications. *Water Res.*, 35 (2), 541–547.

Louhi-Kultanen, M., 1996. Concentration and purification by crystallization. *Acta Polytech. Scand., Chem. Technol. Ser.*, 241, pp. 1–112.

Louhi-Kultanen, M., Silventoinen, I., Palosaari, S., 1988. Purification of organic chemicals by zone melting. *Acta Polytech. Scand., Chem. Technol. Ser.*, Ser. 3–24, pp. 1-112.

Marliacy, P., Hubert, N., Schuffenecker, L., Solimando, R., 1998. Use of Pitzer's model to calculate thermodynamic properties of aqueous electrolyte solutions of Na_2SO_4 + NaCl between 273.15 and 373.15 K. *Fluid Phase Equilibria*, 148 (1), pp. 95–106.

Matsuda, A., Kenji K., and Hirohumi K., 1999. Freeze Concentration with Supersonic Radiation under Constant Freezing Rate. Effect of Kind and Concentration of Solutes. *J. Chem. Eng. Jpn.*, 32(5), pp. 569–572.

May, P. M., Rowland, D., Hefter, G., Königsberger, E., 2011. A generic and updatable Pitzer characterization of aqueous binary electrolyte solutions at 1 bar and 25˚C. *J. Chem. Eng. Data*, 56 (12), pp. 5066–5077.

Miyawaki, O., 2001. Analysis and control of ice crystal structure in frozen food and their application to food processing. *Food Sci. Technol. Res.*, 7 (1), pp. 1–7.

Mohs, A., Decker, S., Gmehling, J., 2011. The solid–liquid equilibrium of the binary system H_2O–DMSO and the influence of a salt (NaCl, KCl) on the thermodynamic behavior: Correlations using a revised LIQUAC model. *Fluid Phase Equilibria* 304 (1), pp. 12–20.

Momicchioli, F., Devoto, O., Grandi, G., Cocco, G., 1970. Thermodynamic Properties of Concentrated Solutions of Strong Electrolytes I. Activity Coefficients of Water From Freezing-Point Depressions for Alkali Chlorides. Berichte Bunsenges. *Für Phys. Chem.*, 74 (1), pp. 59–66.

Müller, M., Sekoulov, I., 1992. Waste water reuse by freeze concentration with a falling film reactor. *Water Sci. Technol.*, 26 (7-8), pp. 1475–1482.

Mullin, J. W., 2001. *Crystallisation*, 4th Edition. Butterworth-Heinemann, Oxford, UK.

Myerson, A., 2002. *Handbook of industrial crystallization*. Butterworth-Heinemann, Oxford, UK.

Nishinaga, T., 2014. *Handbook of Crystal Growth:* Fundamentals. Elsevier, Amsterdam, The Netherlands.

Nurmi, P., Özkaya, B., Sasaki, K., Kaksonen, A. H., Riekkola-Vanhanen, M., Tuovinen, O.H., Puhakka, J. A., 2010. Biooxidation and precipitation for iron and sulfate removal from heap bioleaching effluent streams. *Hydrometallurgy*, 101 (1), pp. 7–14.

O'Concubhair, R., Sodeau, J. R., 2013. The effect of freezing on reactions with environmental impact. *Acc. Chem. Res*., 46 (11), pp. 2716–2724.

Osborne, N. S., 1939. Heat of fusion of ice. A revision. *J. Res Natl Bur Stand*, 23, pp. 643–646.

Osborne, N. S., Stimson, H. F., Ginnings, D.C., 1939. Measurements of heat capacity and heat of vaporization of water in the range of 0° to 100°C. *J. Res Natl Bur Stand*, 23, pp. 197–260.

Partanen, J. I., Juusola, P. M., Vahteristo, K. P., de Mendonça, A. J. G., (2007). Re-evaluation of the activity coefficients of aqueous hydrochloric acid solutions up to a molality of 16.0 mol·kg-1 using the Hückel and Pitzer equations at temperatures from 0 to 50 °C. *J. Solution Chem.*, 36 (1), pp. 39−59.

Petrich, C., Eicken, H., 2009. *Growth, structure and properties of sea ice in Sea-Ice.* (eds Thomas, D. N., Dieckmann, G. S.), 2nd edition, Wiley-Blackwell, Oxford, UK.

Pitzer, K. S., 1991. *Activity coefficients in electrolyte solutions*. CRC press, Boca Raton, FL, USA.

Pitzer, K. S., 1973. Thermodynamics of electrolytes. I. Theoretical basis and general equations. *J. Phys. Chem.*, 77 (2), pp. 268–277.

Pitzer, K. S., Mayorga, G., 1973. Thermodynamics of electrolytes. II. Activity and osmotic coefficients for strong electrolytes with one or both ions univalent. *J. Phys. Chem.*, 77 (19), pp. 2300–2308.

Primo, O., Rivero, M. J., Urtiaga, A. M., Ortiz, I., 2009. Nitrate removal from electro-oxidized landfill leachate by ion exchange. *J. Hazard. Mater.*, 164 (1), pp. 389–393.

Pronk, P., Infante Ferreira, C. I., Witkamp, G. J., 2008. Prevention of crystallization fouling during eutectic freeze crystallization in fluidized bed heat exchangers. *Chem. Eng. Process: Process Intensif.*, 47 (2), pp. 2140–2149.

Rahman, M. S., Ahmed, M., Chen, X. D., 2006. Freezing-Melting Process and Desalination: I. Review of the State-of-the-Art. *Sep. Purif. Rev.*, 35, pp. 59–96.

Rahman, M. S. and Al-Khusaibi, M. (2014) *Freezing-melting desalination process, in desalination: Water from Water* (ed J. Kucera), John Wiley & Sons, Inc., Hoboken, NJ, USA.

Randall, D. G., Nathoo, J., Lewis, A. E., 2011. A case study for treating a reverse osmosis brine using Eutectic Freeze Crystallization-Approaching a zero waste process. *Desalination*, 266 (1), pp. 256–262.

Ratkje, S. K., Flesland, O., 1995. Modelling the freeze concentration process by irreversible thermodynamics. *J. Food Eng.*, 25 (4), pp. 553–568.

Raventós, M., Hernández, E., Auleda, J. M., 2012. Freeze Concentration Applications in Fruit Processing. *Adv. Fruit Process. Technol*., pp. 263-286.

Reardon, E. J., 1989. Ion interaction model applied to equilibria in the nickel (II) sulfate-sulfuric acid-water system. *J. Phys. Chem.*, 93 (11), 4630–4636.

Ryu, B. H., Ulrich, J., 2012. Controlled nucleation and growth of protein crystals by solvent freeze-out. *Cryst. Growth Des.*, 12 (12), 6126–6133.

Sánchez, J., Ruiz, Y., Raventos, M., Auleda, J. M., Hernandez, E., 2010. Progressive freeze concentration of orange juice in a pilot plant falling film. *Innov. Food Sci. Emerg. Technol.*, 11 (4), pp. 644–651.

Sanin, F. D., Vesilind, P. A., Martel, C. J., 1994. Pathogen reduction capabilities of freeze/thaw sludge conditioning. *Water Res.*, 28 (11), pp. 2393–2398.

Scatchard, G., Prentiss, S. S., 1933. The freezing points of aqueous solutions. IV. Potassium, sodium and lithium chlorides and bromides. *J. Am. Chem. Soc*., 55 (11), pp. 4355–4362.

Seidell, A., 1919. *Solubilities of inorganic and organic compounds*. Van Nostrand Company, NY, USA.

Shang, G., Zhang, G., Gao, C., 2014. Treatment of simulated dilute Ni^{2+} - containing wastewater by electrodeionisation with a bipolar membrane: Feasibility and current density distribution. *Desalination*, 353, pp. 1–7.

Shimoyamada, M., Shibata, M., Ishikawa, K., Watanabe, K., 1997. Preparation of large ice crystals by controlling the difference between solution and coolant temperatures and its application to freeze concentration. *J. Jpn Soc Food Sci.*, 44 (1), pp. 59–61.

Shirai, Y., Sugimoto, T., Hashimoto, M., Matsuno, R., 1987. Mechanism of ice growth in a batch crystallizer with an external cooler for freeze concentration. *Agric Biol Chem.*, 51 (9), pp. 2359–2366.

Silva, R., Cadorin, L., Rubio, J., 2010. Sulphate ions removal from an aqueous solution: I. Co-precipitation with hydrolysed aluminum-bearing salts. *Miner. Eng.*, 23 (15), pp. 1220–1226.

Silvester, L. F., Pitzer, K. S., 1978. Thermodynamics of electrolytes. X. Enthalpy and the effect of temperature on the activity coefficients. *J. Solut. Chem.*, 7 (5), pp. 327–337.

Silventoinen, I. K., Korhonen, J. T., Palosaari, S. M., 1988. A mathematical model for purification of a crystal layer by the temperature gradient method. *J. Chem. Eng. Jpn.*, 21 (3), pp. 311–315.

Sippola, H., 2015. Thermodynamic Modelling of Aqueous Sulfuric Acid, Aalto University (Phd dissertation), Finland.

Smith, D. S., Mannheim, C. H., Gilbert, S. G., 1981. Water sorption isotherms of sucrose and glucose by inverse gas chromatography. *J. Food Sci.*, 46 (4), pp. 1051–1053.

Stephen, H., Stephen, T., 1964. *Solubilities of inorganic and organic compounds. Vol. 2, Ternary and multicomponent systems*, Part 2, Pergamon Press, NY, USA.

Stadie, W.C., Sunderman, F.W., 1931. The osmotic coefficient of sodium in sodium hemoglobinate and of sodium chloride in hemoglobin solution. *J. Biol. Chem.*, 91 (1), pp. 227–241.

Stamatiou, E., Meewisse, J. W., Kawaji, M. (2005). Ice slurry generation involving moving parts. *Int. J. Refrig.*, 28(1), pp. 60–72.

Terwilliger, J. P., Dizon, S. F., 1970. Salt rejection phenomena in the freezing of saline solutions. *Chem. Eng. Sci.*, 25 (8), pp. 1331–1349.

Ulrich, J. and Stelzer, T. 2013. *Crystallization: Crystallization: basic concepts and industrial applications*. John Wiley & Sons, Inc., Hoboken, NJ, USA.

Ulrich, J. and Stelzer, T. 2011. *Crystallization. Kirk-Othmer Encyclopedia of Chemical Technology. 1–63*, John Wiley & Sons, Inc., Hoboken, NJ, USA.

Whitman, W. G. 1926. Elimination of salt from sea-water ice. *Am. J. Sci.*, 62, pp.126–132.

Wakisaka, M., Shirai, Y., Sakashita, S., 2001. Ice crystallization in a pilot-scale freeze wastewater treatment system. *Chem. Eng. Process: Process Intensif.*, 40 (3), pp. 201–208.

Weeks, W. F., Lofgren, G., 1967. The effective solute distribution coefficient during the freezing of NaCl solutions. (International Conference on Low Temperature Science Proceedings) *Phys. Snow Ice*, 1 (1), pp. 579–597.

Wieckhusen, D., Beckmann, W., 2013. *Crystallization: basic concepts and industrial applications*. John Wiley & Sons, Inc., Hoboken, NJ, USA.

Williams, P. M., Ahmad, M., Connolly, B.S., Oatley-Radcliffe, D. L., 2015. Technology for freeze concentration in the desalination industry. *Desalination*, 356, 314–327.

Cengel, Y. A., Cengel, 2002. *Heat transfer: a practical approach*, 2nd ed. McGraw-Hill, NY, USA.

PART II: Publications

Publication I

Hasan, M., Louhi-Kultanen, M

Water purification of aqueous nickel sulfate solutions by air cooled natural freezing.

Reprinted with permission from
Chemical Engineering Journal
Vol. 294, pp. 176-184, 2016

Chemical Engineering Journal 294 (2016) 176–184

Contents lists available at ScienceDirect

Chemical Engineering Journal

journal homepage: www.elsevier.com/locate/cej

Water purification of aqueous nickel sulfate solutions by air cooled natural freezing

M. Hasan *, M. Louhi-Kultanen

Thermal Unit Operations/Separation Technology, School of Engineering Science, Lappeenranta University of Technology, P.O. Box 20, FI-53851 Lappeenranta, Finland

HIGHLIGHTS

- Natural freezing is a potential treatment method for wastewaters containing $NiSO_4$.
- Suitable to replace expensive methods to treat dilute solution of heavy metals.
- Ice purity is determined by growth rate and solution concentration.
- Solution inclusion within ice crystallites is the main source of ice impurity.
- Solution concentration and freezing condition control ice characteristics.

ARTICLE INFO

Article history:
Received 22 January 2016
Received in revised form 25 February 2016
Accepted 27 February 2016
Available online 3 March 2016

Keywords:
Freeze crystallization
Distribution coefficient
Ice growth rate
Ice purity
Heat transfer
Wastewater treatment

ABSTRACT

Ni^{2+} in excess of maximum recommended limits must be removed from wastewater prior to discharge because of its persistent bio-accumulative and detrimental nature. Natural freezing is suggested as a purification technique to treat huge volumes of wastewater containing Ni^{2+} in a sustainable and energy efficient manner. In order to evaluate the feasibility of such a technique for purification of wastewater, natural freezing was simulated experimentally for ice crystallization from different $NiSO_4$ (aq) solutions. The impact of solution concentration at different freezing conditions such as different ambient air temperature, freezing time and freezing rate on the efficiency of the purification process was investigated. Experimental results demonstrated that at the growth rate (G) of 3.5×10^{-8} m/s, the ice layer formed from 1 wt.% (≈10,000 ppm) $NiSO_4$ (aq) solution incorporated only 0.0038 wt.% (≈38 ppm) $NiSO_4$ as impurity, i.e., the ice is more than 250 times pure than the original salt solution. In the case of freezing of very dilute solutions, e.g., 0.1 wt.% $NiSO_4$ (aq) solution, which is the dilution level of practical interest, the same growth condition is likely to produce an ice layer of even higher purity. For example, at G of 7.4×10^{-8} m/s, the ice layer impurity that had formed from 0.1 wt.% $NiSO_4$ (aq) solution was only 0.001 wt.% (≈10 ppm). For this reason, this purification technique has potential for implementation on the surface of wastewater ponds in cold climate regions where the temperature drops below 0 °C. In addition, inclusion formation within the ice matrix during freezing was investigated for various solution concentrations both macroscopically and microscopically.

1. Introduction

Lack of access and deterioration in water quality are major problems all over the world. Industrial discharge exacerbates water scarcity by polluting both the environment and water resources [1]. Mining and heavy industry produce substantial volumes of wastewater contaminated with heavy metal [2,3]. Release of wastewaters laden with heavy metals above thresholds defined in worldwide environmental legislation is harmful to the environment and deleterious to both flora and fauna [4].

It is common to find nickel (II) ion in excess of maximum allowable limits in many wastewaters discharged from electroplating, electronics, metal cleaning and textile industry sites and such wastewaters can cause serious water pollution if not treated before release [2]. Nickel is responsible for a number of pathological effects and is implicated in several severe and long-lasting disorders such as damage to lungs and kidneys, gastrointestinal distress, pulmonary fibrosis, renal edema and skin dermatitis [5]. In view of its toxicity, strict permissible limits have been set, e.g., the limit for potable water is 0.02 mg/L [6].

* Corresponding author. Tel.: +358 465969187.
E-mail address: Mehdi.Hasan@lut.fi (M. Hasan).

http://dx.doi.org/10.1016/j.cej.2016.02.114
1385-8947/

List of symbols

G	growth rate (m/s)
SLE	solid–liquid equilibrium
C_s	solute concentration in solid (ice) phase (wt.%)
C_b	solute concentration in the bulk solution (wt.%)
C_i	solute concentration at the ice-solution interface (wt.%)
C_0	concentration of initial solution to freeze (wt.%)
K	effective distribution coefficient
K^*	limiting distribution coefficient
DMTM	differential mass transfer model
FPD	freezing point depression (°C/K)
ρ	density (kg/m^3)
ν	kinematic viscosity (m^2/s)
D	diffusion coefficient (m^2/s)
C_p	heat capacity (J/kg/K)
k	thermal conductivity (W/m/K)
T_f	Freezing point of the solution (°C/K)
T_b	temperature of the bulk solution (°C/K)
T_a	air temperature inside the freezer (°C/K)
ΔT	degree of undercooling from solution's freezing point (°C/K)
t	freezing time (s)
δ	boundary layer thickness (m)
δ_T	thermal boundary layer (m)
δ_C	concentration boundary layer (m)
R_F	freezing ratio (%)
E	separation efficiency (%)
V_s	volume of solid (ice) phase after mixing (m^3)
V_0	volume of initial solution to freezing (m^3)
X	ice layer thickness (m)
h_{sol}	heat transfer coefficient of solution (W/m^2/K)
h_{air}	heat transfer coefficient of air (W/m^2/K)
k_{ice}	thermal conductivity of ice (W/m/K)
ΔH	latent heat of freezing of impure ice (J/kg)
ΔH_f	latent heat of freezing of pure ice (J/kg)
U	overall heat transfer coefficient (W/m^2/K)

A number of conventional physical–chemical separation methods, such as ion exchange, adsorption, chemical precipitation, electrochemical treatment, evaporative recovery, pressure driven membrane filtration, etc. have been used in recent years to treat Ni^{2+} containing wastewater.

Application of chemical precipitation, adsorption and ion exchange technologies is limited to small-scale. Membrane process is highly energy intensive, prone to fouling and efficient only for dilute solution. Inefficient metal removal, low separation efficiency, high costs for chemical reagents, high-energy requirements and the production of high volumes of secondary wastewater are shortcomings of these technologies [2,7]. On the other hand, due to toxicity the presence of high concentration of Ni^{2+} in the effluents impedes the direct application of biological methods in the treatment of nickel-containing wastewaters [8]. Due to aforementioned reasons, none of these methods is suitable for treatment of dilute and voluminous wastewater. For instance in Finland mine water effluents are usually very dilute and annual effluent volume in some mines can be even up to 10 million tons. Therefore, this huge volume of wastewater needs to be treated in an energy efficient manner rather than using conventional methods.

Ice formation from aqueous solutions by freeze crystallization has a wide range of applications in solute concentration and wastewater purification processes [9]. Freeze crystallization can overcome some of the limitations associated with the abovementioned technologies. The approach provides high product quality at good separation efficiency [10] and low energy requirements [11]. Of the two possible freeze crystallization methods, layer crystallization and suspension crystallization, the former is more advantageous in terms of ease of separation ability, based on density difference between the ice layer and residual solution [3].

Natural freezing can be used to treat wastewaters in ponds by ice crystallization in regions where ambient temperatures drop below 0 °C during winter time. The use of natural freezing in wastewater treatment facilitates volume reduction by forming pure ice layer and thus concentrate pollutants in the residual wastewater.

This work introduces ice crystallization as a purification technique to treat $NiSO_4$-laden wastewaters. Natural freezing was simulated experimentally for ice crystallization from unsaturated $NiSO_4$ (aq) solutions. The influence of solution concentration and different growth conditions on the efficiency of the purification process is also addressed in the present work.

Inclusion of concentrated solution within the ice layer during freezing is an important feature influencing the ice characteristics. With the exception of natural sea ice inclusion [12,13], the mechanisms of inclusion formation in the ice layer have not been studied extensively. From photomicrographs of sea ice, it is apparent that brine incorporates in the ice matrix as pockets [14,15]. The probable reason behind the difference in appearance and characteristics between sea ice and lake ice is the difference between the chemical compositions of water from these two sources [16]. Therefore, we also focus in this work on how the ice layer formed by freezing $NiSO_4$ (aq) solutions differs both macroscopically and microscopically with the variation of initial solution concentration.

2. Theoretical considerations

Ideal conditions for purification through freezing include (1) that the impurities do not form solid-solution with ice, (2) that the growth rate of ice layer is low enough to avoid occlusion of impurities, and (3) that the ice crystallites are large enough to minimize the amount of solution retained on their surfaces. For the attainment of any solid–liquid equilibrium (SLE), the chemical potential of the solvent must be equal between the liquid and solid phases [17]. During ice crystallization from a solution, redistribution of solute occurs and the extent of the redistribution is greatly influenced by the growth kinetics of the ice front and the ability of the solute to diffuse away from the ice-solution interface [18]. Usually, solute molecules/ions are unable to integrate into the ice crystal lattice owing to constraints imposed by their size/charge [16]. Thus, ions are mostly rejected by the progressing ice-solution interface.

The purity of the ice crystals formed from the solution relies on the growth rate of the ice crystallization [18]. At very low growth rates, only a very small portion of the solute gets incorporated into the ice layer and the major portion of the solute diffuses away from the advancing ice front into the bulk of the solution. Thus, the purity of the ice layer becomes very high and the remaining solution becomes solute – enriched. On the other hand, if the growth rate is too high for the solute to diffuse from the ice-solution interface, the solutes become entrapped in the ice layer, which eventually leads to impure ice crystals and no enrichment of the solution.

During freezing of the solution, the incorporation of solute in the crystal can be characterized by the redistribution of solute in

the solid phase (C_s) relative to that present in the bulk liquid phase (C_b). This is referred to as the effective distribution coefficient $K = C_s/C_b$. If the solute rejection rate by the advancing ice front is greater than the diffusion rate into the bulk of the solution, higher concentration of solute in the interface (C_i) than in the bulk solution, $C_i > C_b$, results. Thus, a concentration gradient develops adjacent to the ice-solution interface. The limiting distribution coefficient (K^*) is a specific form of distribution coefficient at the solid–liquid interface that is defined as $K^* = C_s/C_i$ [19,20].

During ice crystallization from a solution, removal of heat from the solution to the surrounding area is balanced by the heat of crystallization into the solution. Released heat diffused into the bulk solution coupled with the rejection of solutes leads to the formation of a concentration and thermal boundary layer in front of the advancing ice layer.

A differential mass transfer model (DMTM) presented by Burton et al., 1953 is frequently used to study the mass transfer of solute molecules between a single crystal and the melt. This model implies that the concentration gradient in the vicinity of the advancing solid–liquid interface during the crystal growth from melt depends upon several factors, namely, the freezing rate, the effective distribution coefficient, K, and the nature of the fluid flow [19]. In our previous work [3], an overall heat transfer based model was developed by equating removal of heat from the solution into the surrounding area for freezing and release of the heat of crystallization into the solution. In ice crystallization, surface kinetics is very fast due to the small molecular size of water. Hence, only at extreme conditions, i.e., below −143.15 °C amorphous ice can be formed [21].

3. Physical and thermodynamic properties of model $NiSO_4$ (aq) solutions

The binary phase diagram of $NiSO_4$–H_2O system is available in literature [22]. According to the phase diagram, eutectic point of $NiSO_4$–H_2O is at 26 wt.% and −3.18 °C. Natural freezing of wastewater was characterized with model $NiSO_4$ (aq) solutions. Freezing point depression (FPD) data along with various other thermodynamic and physical properties of $NiSO_4$ (aq) solutions in the range of 1 wt.%–4 wt.% were collated and correlated statistically by best fitting of data, except thermal conductivity, which was calculated from correlation. Table 1 lists these properties, which are used for further calculation in this work.

4. Method

4.1. Preparation of solution

0.1 wt.%, 1 wt.% and 2 wt.% $NiSO_4$ (aq) solutions were prepared by dissolving 99% pure $NiSO_4{\cdot}6H_2O$ (analytical grade, manufactured by Merck) in deionized water (conductivity = 0.1 μS/cm, total organic carbon = 1 ppb). Dissolution was performed at room temperature under vigorous mixing condition (500 rpm) for 30 min.

4.2. Experimental setup for simulating natural freezing

The detailed experimental setup to treat solutions by simulating natural freezing is presented in Fig. 1. A 710 ml rectangular plastic vessel (14 cm × 8.74 cm × 5.8 cm) was used as a crystallizer. To promote ice layer growth merely on the top surface, the top surface of the crystallizer was exposed to cold air in a freezer box where the air temperature (T_a) of the freezer box was controlled by a Lauda proline RP 850 thermostat. Inside the freezer, an air circulation rate of 0.24 m/s was applied for better heat transfer and to ensure homogeneous temperature distribution throughout the freezer.

4.3. Methods

The growth rate of ice crystallization (G) was measured from the thickness of ice layer (X) formed at a certain freezing time (t). In this work, the growth rate of ice crystallization from 500 ml $NiSO_4$ (aq) solution at its freezing temperature (T_f) was manipulated by altering the undercooling, ΔT ($=T_f - T_a$), from 0.2 °C to 4.0 °C and t from 5 h to 72 h. Prior to freezing, ice seeds were added to induce ice crystallization from the undercooled solution and prevent supercooling.

At first, the growth rate of the ice layer (G) formed from both 1 wt.% and 2 wt.% $NiSO_4$ (aq) solutions was manipulated by varying the freezing time (t) and level of undercooling (ΔT) from the corresponding solution's freezing point. As conventional methods for removal of heavy metals from dilute solution (⩽100 mg/L) are expensive [7] and the concentration of Ni^{2+} in typical wastewaters emanating from electroplating and textile industries may contain up to 1000 mg/L (≈0.1 wt.%) [23], which led us to do further freezing experiments with very dilute solutions, i.e., 0.1 wt.% $NiSO_4$ (aq) solution.

In our previous work [3], we developed a model to predict ice growth rate G from ice thickness (X) at different ΔT and freezing time t, assuming steady state conditions, as in Eq. (1):

$$\frac{X^2}{2k_{ice}} + \left(\frac{1}{h_{sol}} + \frac{1}{h_{air}}\right)X - \frac{\Delta T t}{\rho_{ice}\Delta H} = 0 \tag{1}$$

Derivation and notation for symbols are mentioned in Supplementary documents (Appendix 1).

$$\Delta H = \Delta H_f\left(1 - \frac{C_s}{C_b}\right) \tag{2}$$

The value of latent heat of freezing of pure water, $\Delta H_f = 3.34 \times 10^5$ (J/kg) [24].

Thermogravimetric method was used to measure the amount of $NiSO_4$ entrapped in the ice layer. In order to determine the quantity of anhydrous $NiSO_4$ in the ice accurately, the sample was dried at 400 °C for 24 h, because $NiSO_4$ completely dehydrates at 330 °C [25]. Thermal analysis by Netzsch thermal analyzer STA 449 C for the dried $NiSO_4$ sample showed that the mass of $NiSO_4$ by solid did not change after drying at 350 °C for 30 min, which implies that

Table 1
Thermodynamic and physical properties of $NiSO_4$ (aq) solutions.

Property	Unit	Correlation*	Refs.
Freezing point depression	°C	$FPD = -0.13 \times y - 0.019$	[26,30]
Density, ρ (at 25 °C)	kg/m^3	$\rho = 10.544 \times y + 999.28$	[27]
Kinematic viscosity, ν (at 25 °C)	m^2/s	$\nu = 4.431 \times 10^{-8} \times y + 1.133 \times 10^{-6}$	[27]
Diffusion coefficient, D (at 25 °C)	m^2/s	$D = -2.766 \times 10^{-11} \times y + 6.71 \times 10^{-10}$	[27]
Heat capacity, C_p (at 25 °C)	J kg^{-1} K^{-1}	$C_p = -54.687 \times y + 4180.7$	[28]
Thermal conductivity, k (at 25 °C)	W m^{-1} K^{-1}	$k = -0.011 \times y + 0.5553$	[29]

* $[y]$ = wt.% = y, g salt/100 g salt solution.

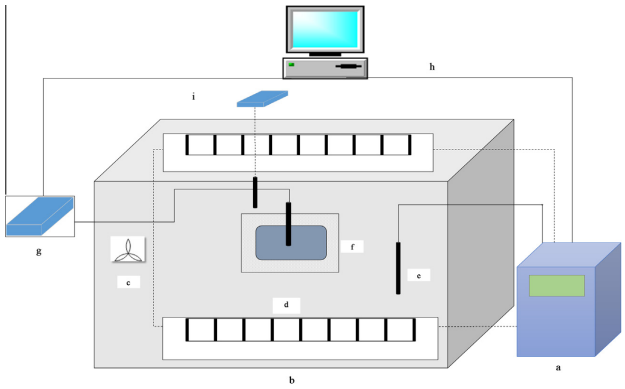

Fig. 1. Experimental setup for freezing of solution. (a) Lauda proline RP 855 thermostat; (b) freezer box; (c) fan; (d), heat exchanger; (e) Pt 100 thermosensor; (f) crystallizer with insulation; (g) Pico logger; (h) data monitoring and storage device; (i) anemometer. Electric wire and coolant flow pipe are represented by — and....., respectively.

$NiSO_4$ was in anhydrous form before the thermogravimetric (TG) analysis. The density and volume of the residual solution were also measured. Effective distribution coefficient (K) was calculated from the amount of $NiSO_4$ in the ice layer and in the bulk solution after freezing.

Ice layers obtained from $NiSO_4$ (aq) solutions at different freezing conditions were observed microscopically under calibrated Olympus BH2-UMA microscope to characterize ice structure and ice inclusion. Captured images were handled with image processing tool (analySIS). Furthermore, thin ice layers were examined through polarized light source (by Edmund optics) to visualize ice grains within polycrystalline ice layer.

5. Results and discussion

5.1. Ice growth rate (G) as a function of freezing time (t) and ΔT

Variation of ice growth (G) with solution's concentration, t and ΔT simulating different freezing conditions are summarized in Table 2. From Table 2, it can be seen that mostly G decreased as freezing proceeded. This behavior is due to added heat resistance of the formed ice layer by freezing. The decrease of G with freezing time (t) appears to be influenced by the magnitude of the freezing driving force ΔT, whereas the influence of the solution concentration was insignificant. For the experimental design matrix as presented in Table 2, G varied approximately from 3.5×10^{-8} m/s to 4.5×10^{-7} m/s in different freezing conditions. This wide range of G replicates how G can be varied with weather condition.

5.2. Ice impurity (C_s) and effective distribution coefficient (K) as a function of G

Ice impurity (C_s) compared with the bulk solution's concentration (C_b) is expressed in terms of the effective distribution coefficient (K). Experimental K values along with corresponding C_s values at different growth conditions are presented in Fig. 2.

The values of K increased 0.0032–0.35 for the increase in G 3.5×10^{-8} m/s–4.5×10^{-7} m/s (Fig. 2a), which indicates that at higher G, solutes in the solution are likely to be captured in the ice layer rather than dispersing from the interface to the bulk solution. Higher K values were obtained for 2 wt.% $NiSO_4$ (aq) solution than for 0.1 wt.% and 1 wt.% at around the same G. For G values less than 10^{-7} m/s, K dropped significantly and the purity of the ice layer was very high. For G values around 5×10^{-8} m/s, K values were roughly around 0.01 for both 1 wt.% and 2 wt.% $NiSO_4$ (aq) solution, which implies that the obtained ice layer was 100 times more pure (i.e., $K = C_s/C_b = 0.01 = 1/100$) than the residual freezing solution from which it had formed. For 1 wt.% $NiSO_4$ (aq) solution at G value 3.5×10^{-8} m/s, the corresponding K value was 0.0038, which is remarkably low, and an almost pure ice layer was found. From the concentration dependency of K values shown in Fig. 2(a), it can be expected that with the freezing conditions given in Table 2, K values would be very low for Ni^{2+} laden practical wastewaters. The dependency of C_s with G can be explained in the same manner as the trends are quite similar (Fig. 2b) which gives the idea how uncontrollable weather condition effects on ice layer impurity. Thus by knowing the average temperature of a freezing time we can get the idea about the ice layer impurity for a solution of specific Ni^{2+} concentration from our experimental data. In order to reach the legislation limit, conventional methods, e.g., ion exchange, adsorption or membrane filtration could be used in line after reducing the volume of wastewater significantly by natural freezing.

5.3. Boundary layer thickness (δ) and ice impurity (C_s)

In our previous work [3] a calculation method was introduced to estimate the concentration of Na_2SO_4 (aq) solution at the advancing ice-solution interface in terms of the limiting distribution coefficient (K^*) from experimental K values at different growth conditions using the physio-thermodynamic properties of corresponding solutions. The same procedure was followed also in this work for $NiSO_4$ (aq) solutions to extract useful information, e.g., heat transfer (R_h) and mass transfer resistance (R_m) during ice growth.

The calculated thermal boundary layer (δ_T) and concentration boundary layer (δ_c) from the heat (h_{sol}) and mass transfer coefficients (k_l) for 0.1 wt.%, 1 wt.% and 2 wt.% $NiSO_4$ (aq) solutions at different growth conditions and their impact on ice impurity are presented in Fig. 3.

δ_T was found 3.58–3.78 times higher than δ_c with the variation of $NiSO_4$ (aq) solution concentration and freezing conditions, which indicates that the ice crystallization is limited by the heat transfer. Fig. 3 depicts the inverse relation between boundary layer thickness and ice impurity. For thinner boundary layers, heat and mass transfer occurred more readily, and G was therefore higher

Table 2
Variation in ice growth rate (G) with solution concentration and freezing conditions.

Solution concentration, wt.%	ΔT (°C)	Freezing time, t (hr)	Growth rate, G (m/s), 10^{-7}
0.1	0.8	24	1.16
	0.8	48	0.94
	0.9	72	0.74
	1	24	1.21
	2	24	1.98
	3	24	2.37
	4	24	2.58
1	0.2	48	0.35
	0.2	72	0.48
	0.4	48	0.46
	0.4	72	0.53
	0.6	72	0.81
	0.8	48	0.77
	0.8	72	0.65
	1	5	1.53
	1	10	1.24
	1	15	1.10
	1	24	0.93
	2	5	2.13
	2	10	2.23
	2	15	1.85
	2	24	1.70
	3	5	3.22
	3	10	2.77
	3	15	2.64
	3	24	2.53
	4	5	4.21
	4	15	3.81
	4	24	2.83
2	0.2	48	0.46
	0.2	72	0.52
	0.4	48	0.62
	0.4	72	0.55
	0.8	48	1.03
	0.8	72	0.86
	1	5	1.48
	1	10	1.24
	1	15	1.07
	1	24	1.02
	1.3	48	1.24
	2	5	2.72
	2	10	2.47
	2	15	2.31
	2	24	1.96
	3	5	3.66
	3	10	2.77
	3	15	2.39
	3	24	2.68
	4	5	4.45
	4	10	3.83
	4	15	3.60
	4	24	3.32

than for thicker boundary layers, and consequently the impurity of the ice layer was higher. Fig. 3 also shows that the ice layer had formed from the more concentrated solution was more susceptible to inclusion of impurities at the same boundary layer thickness.

5.4. Freezing ratio (R_F) vs separation efficiency (E)

The term separation efficiency (E) is defined as the ratio between the amount of solute in the residual solution after freezing and the total amount of solute in the initial solution that is subjected to freezing, as shown in Eq. (3). The freezing ratio (R_F) is defined as in Eq. (4).

$$E(\%) = \left(1 - \frac{C_s V_s}{C_0 V_0} \times 100\right)\% \tag{3}$$

$$R_F = \left(\frac{V_s}{V_0}\right) \tag{4}$$

where C_0 and V_0 stand for the concentration and volume of the initial solution, respectively, and V_s refers to the volume of the ice layer after melting. Experimental E versus R_F for 0.1 wt.%, 1 wt.% and 2 wt.% $NiSO_4$ (aq) solution is shown in Fig. 4.

Fig. 4 shows that E is remarkably influenced by the initial concentration of the solution. For 0.1 wt.% $NiSO_4$ (aq) solution, E was unaffected by the change of freezing ratio (R_F). Until R_F = 20%, E did not change that much with the course of freezing 1 wt.% and 2 wt.% $NiSO_4$ (aq) solutions which implies that solute enrichment was happening in both cases. E was above 90% with 50% freezing of the 1 wt.% $NiSO_4$ (aq) solution. On the other hand, for 2 wt.% $NiSO_4$ (aq) solution, E declined to below 80% when 30% of the initial solution was frozen and after 50% freezing, E deteriorated significantly. This infers that after 20% freezing of 2 wt.% $NiSO_4$ (aq) solution, enrichment of solution started to be affected by the extent of solution entrapment within advancing ice layer. Above R_F = 50%, almost no enrichment happened, consequently, E dropped drastically.

5.5. Comparison between experimental and model ice layer thickness (X)

In the present work, overall heat transfer coefficient (U) varied from 17.34 (W m^{-2} K^{-1}) to 21.82 (W m^{-2} K^{-1}) depending on the freezing conditions of the $NiSO_4$ (aq) solutions.

The steady state assumption as freezing proceeded is reasonable because the change in the bulk solution temperature T_b due to solution enrichment with the progress of the freezing was negligible. For example, even at the experimental condition of freezing of 1 wt.% $NiSO_4$ (aq) for 24 h at ΔT = 4 °C, where T_b was most likely to be time dependent, the change of T_b due to solution concentration increase (from 1 wt.% to 1.83 wt.%) was insignificant, from −0.15 °C to −0.24 °C. Using the correlation in Table 1, thermodynamically the freezing point should be −0.258 °C for this enrichment of solution.

G calculated with the model and experimental G at different ΔT and t are compared in Fig. 5. Fig. 5 illustrates that experimental data are in good agreement with calculated data. In most cases, the model values slightly overestimate G, which is probably due to increment of T_b from the solution's freezing point while transferring the solution from the freezing room to the ice crystallizer within the freezer. Even though the change of T_b due to solution enrichment while freezing is within experimental limitations, it lowered ΔT later during freezing. Hence, the model would be more accurate if the initial temperature of the solution at its freezing point could be controlled at the commencement of freezing and if ΔT could be adjusted constantly during the course of freezing. Furthermore, more precise prediction would be possible if physical and thermodynamic properties were available in the literature at the corresponding freezing point of the solution.

5.6. Ice layer characteristics

The ice layer formed from 0.1 wt.% $NiSO_4$ (aq) solution was found to be very transparent unlike the less bright ice obtained from 1 wt.% and 2 wt.% $NiSO_4$ (aq) solutions. The upper ice surfaces obtained from 0.1 wt.%, 1 wt.% and 2 wt.% solutions were planar but not sutured. The same ice characteristics were observed regardless of the freezing conditions. Solution inclusion within the ice layer raises the albedo, which explains the difference in transparency between the ice layers of the different solutions.

Microscopic images showed that, unlike the upper surface, the lower surface of the ice layer was not always planar but varied with the concentration of solution from which it had formed, as illustrated in Fig. 6(a–c).

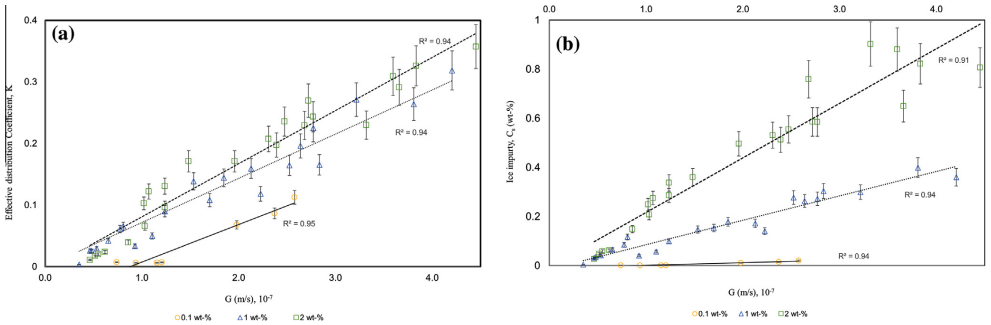

Fig. 2. Effective distribution coefficient K, g salt in ice/g salt in bulk solution (a); and ice layer impurity, C_s (b); as a function of ice layer growth rate G from $NiSO_4$ (aq) solution (○, 0.1 wt.%; Δ, 1 wt.%; □, 2 wt.%). A relationship is shown between G vs K and G vs C_s is shown by —, ... and —— for 0.1 wt.%, 1 wt.% and 2 wt.% $NiSO_4$ (aq) solutions, respectively. Error bars replicate 10% error in every case.

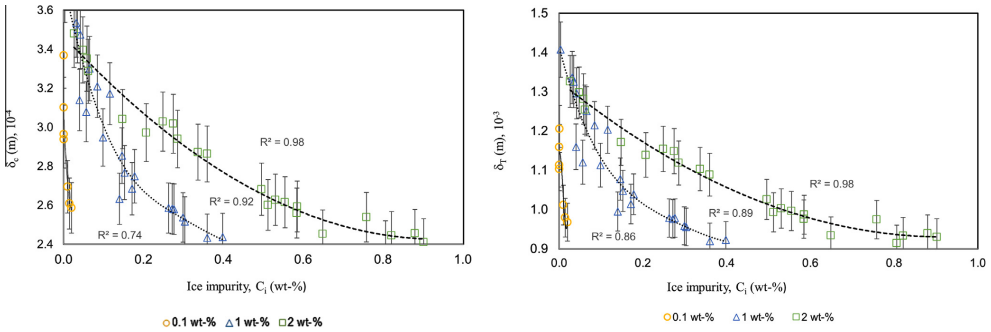

Fig. 3. Influence of concentration (δ_c) and thermal boundary layer (δ_T) on ice impurity C_s (○, 0.1 wt.%; Δ, 1 wt.%; □, 2 wt.%) for different $NiSO_4$ (aq) solution and correlation is represented by fitted line —, ... and —— for 0.1 wt.%, 1 wt.% and 2 wt.% $NiSO_4$ (aq) solutions, respectively. Error bars replicate 5% error in every case.

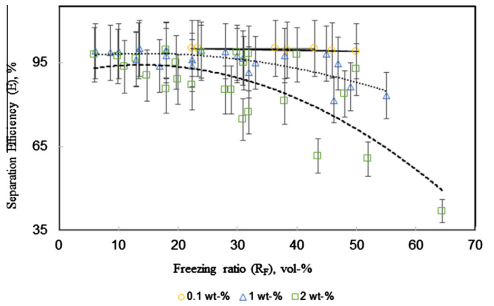

Fig. 4. Influence of freezing ratio (R_F%) of $NiSO_4$ (aq) solution (○, 0.1 wt.%; Δ, 1 wt.%; □, 2 wt.%) on separation efficiency (E%). Relationship between R_F and E is shown by fitted line —, ... and —— for 0.1 wt.%, 1 wt.% and 2 wt.% $NiSO_4$ (aq) solutions, respectively. Error bars replicate 10% error in every case.

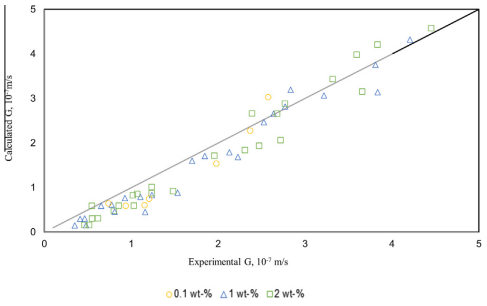

Fig. 5. Comparison between experimental and model ice growth rate G from $NiSO_4$ (aq) solution (○, 0.1 wt.%; Δ, 1 wt.%; □, 2 wt.%). The line represents the condition where experimental results completely coincide with the model results.

As seen in Fig. 6(a–d), both the lower surface and the upper surface of the ice layer from the 0.1 wt.% $NiSO_4$ (aq) solution were non-sutured. The lower surfaces of the 1 wt.% and 2 wt.% $NiSO_4$ (aq) solutions were sutured (Fig. 6b and c). This difference in interfacial texture can be explained by the constitutional supercooling that ensues due to faster transport of heat from the bulk to the interface compared with molecular diffusion from the interface to the bulk [16]. Thus, a thin layer is established below the interface, which is cooled further below the freezing point of the

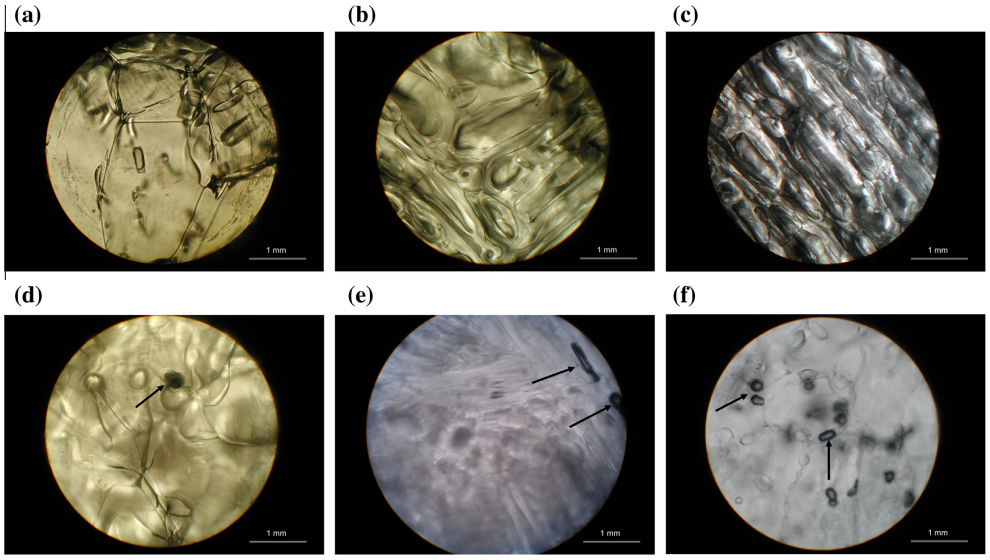

Fig. 6. Microscopic view of the lower surface of the ice layer obtained from (a) 0.1 wt.%; (b) 1 wt.%; (c) 2 wt.% $NiSO_4$ (aq) solution, respectively; and microscopic view of the upper surface of the ice layer obtained from (d) 0.1 wt.%; (e) 1 wt.%; (f) 2 wt.% $NiSO_4$ (aq) solution, respectively. Solution inclusion at upper surface is marked by arrows. Scale bar represents 1 mm at 1.5 magnification.

solution, but the interfacial solution concentration is only slightly enriched above the bulk level. For very dilute solutions (in our case 0.1 wt.% aqueous $NiSO_4$ solution) molecular diffusion is not significant, so constitutional supercooling is unlikely to affect the structure of the lower surface. Therefore, a planar interface can be expected as freezing proceeds at much lower growth rate. Conversely, with the higher concentrated solutions of 1 wt.% and 2 wt.% $NiSO_4$ (aq) solution, the morphology of the ice-solution interface (lower surface of the ice layer) can be cellular or lamellar, as shown in Fig. 6(b and c), because of the formation of the constitutionally undercooled layer.

Solution incorporation within the ice layer was observed only at the upper surface (Fig. 6(d–f) but not in the lower surface (Fig. 6a–c). This is due to the fact that the upper surface formed at the beginning of the freezing, which implies the fastest ice growth rate. Later, during the remaining freezing time, the growth rate declined

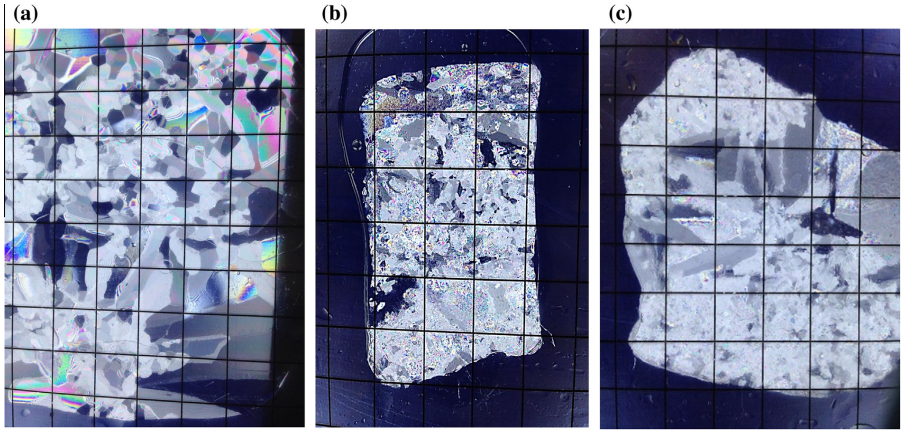

Fig. 7. Macroscopic view of thin ice layers obtained from (a) 0.1 wt.%; (b) 1 wt.%; (c) 2 wt.% $NiSO_4$ (aq) solutions, photographed through cross polarized light. Grid scale is 1 cm in both the horizontal and vertical direction.

(Table 2) because of the added heat resistance of the formed ice layer, and thus the lower surface formed at lower growth rate. It is evident from Fig. 2 that the growth rate greatly influences corresponding K value.

The ice formed from the $NiSO_4$ (aq) solutions was polycrystalline in nature and consisted of many crystal families (grains) of different size. The grains can be seen in Fig. 7, which shows thin ice layers, illuminated with cross polarized light, from freezing of the $NiSO_4$ (aq) solutions.

Due to its non-transparent nature and/or overlapping of grains, ice found by freezing 1 wt.% and 2 wt.% $NiSO_4$ (aq) solutions was not very distinguishable macroscopically. However, Fig. 7 (b and c) show clearly that grain sizes were smaller with higher salt concentrations of 1 wt.% and 2 wt.%.

Entrapment of $NiSO_4$ (aq) solution within the interstitial of crystallites is illustrated in Supplementary material (Appendix 2). In the almost pure ice that was produced by freezing 0.1 wt.% $NiSO_4$ (aq) solution, the grain boundaries were too thin to accommodate solution entrapment. But grain boundaries of the ice from the 1 wt.% and 2 wt.% $NiSO_4$ (aq) solutions were spacious enough to permit inclusion. Entrapped inclusion influenced the mechanical properties of the ice layer. In the figure (Appendix 2b), some transparent bubbles are visible. It was difficult to identify whether these were mother liquor voids or air bubbles. However, impurity analysis of the ice gave accurate data on the quantities of entrapped solute in the ice.

Theoretically, separation efficiency of a specific component within multi-component solution while freezing relies on the size, shape, ionic charge, concentration, diffusivity in the solution, and so on. Based on these characteristics, it might be possible to get selective separation by freezing. The influence of impurities can play a significant role on the ice structure, volume fraction of voids and inclusions, ice grain size etc. In variation with the type of industries/sources, the composition of wastewaters may vary significantly in presence of multiple components. This topic requires wider investigations and our aim in near future is to use real wastewaters and to compare ice structures and ice impurities which would form at different freezing conditions.

6. Conclusion

Natural freezing of $NiSO_4$ (aq) solutions at three different concentrations was simulated across a wide range of freezing rates, extending from roughly 3.5×10^{-8} m/s to 4.5×10^{-7} m/s. The growth rate of the ice layer G, and the initial concentration of the solution are causative factors determining the ice impurity in terms of the effective distribution coefficient K. If a dilute solution is permitted to freeze at a rate in the order of 10^{-8} m/s, then the formed ice layer can be expected to be highly purified. For very dilute solutions, the influence of mass transfer on ice purity could be overlooked compared with that of heat transfer. The thermal boundary layer tends to increase with the course of freezing because the heat resistance exerted by the growing ice layer inhibits the growth rate. This eventually allows for the solute molecules to diffuse through the boundary layer rather than being entrapped in the advancing ice layer. Therefore, remarkably low growth rates result in better separation. Ice formed from concentrated solution has a tendency toward higher impurity at the same G because of the significant presence of solute molecules in the solution. Usually, the concentration of Ni^{2+} in mine waters or in effluents emanating from nickel processing industries is very low. Therefore, natural freezing has the potential to be a sustainable purification technique in regions where temperatures drop to subzero levels and high-volume wastewater treatment capacities are required.

Acknowledgments

The authors are indebted to the Academy of Finland (Project No. 260141, 285064), the Graduate School of Lappeenranta University of Technology (LUT) and the Graduate School of Chemical Engineering (GSCE) for financial support. The contribution of Ms. Bolormaa Bayarkhuu and Mr. Nirina Ramanoarimanana during the experimental work is also acknowledged.

Appendix A. Supplementary data

Supplementary data associated with this article can be found, in the online version, at http://dx.doi.org/10.1016/j.cej.2016.02.114.

References

[1] D.G. Randall, J. Nathoo, A.E. Lewis, A case study for treating a reverse osmosis brine using eutectic freeze crystallization–approaching a zero waste process, Desalination 266 (1) (2011) 256–262.
[2] G. Shang, G. Zhang, C. Gao, Treatment of simulated dilute Ni^{2+}-containing wastewater by electrodeionisation with a bipolar membrane: feasibility and current density distribution, Desalination 353 (2014) 1–7.
[3] M. Hasan, M. Louhi-Kultanen, Ice growth kinetics modeling of air-cooled layer crystallization from sodium sulfate solutions, Chem. Eng. Sci. 133 (2015) 44–53.
[4] K.H. Ahn, K.G. Song, H.Y. Cha, I.T. Yeom, Removal of ions in nickel electroplating rinse water using low-pressure nanofiltration, Desalination 122 (1) (1999) 77–84.
[5] X. Zhang, X. Wang, Adsorption and desorption of nickel (II) ions from aqueous solution by a lignocellulose/montmorillonite nanocomposite, PLoS One 10 (2) (2015) e0117077.
[6] F. Fu, R. Chen, Y. Xiong, Comparative investigation of N, N′-bis-(dithiocarboxy) piperazine and diethyldithiocarbamate as precipitants for Ni (II) in simulated wastewater, J. Hazard. Mater. 142 (1) (2007) 437–442.
[7] L. Wang, H. Chua, P.K. Wong, W.H. Lo, P.H.F. Yu, Ni^{2+} removal and recovery from electroplating effluent by *Pseudomonas putida* 5-x cell biomass, J. Environ. Sci. Health Part A 38 (3) (2003) 521–531.
[8] A. Sochacki, J. Surmacz-Gorska, O. Faure, B. Guy, Polishing of synthetic electroplating wastewater in microcosm upflow constructed wetlands: effect of operating conditions, Chem. Eng. J. 237 (2014) 250–258.
[9] N.J.J. Huige, H.A.A. Thijssen, Production of large crystals by continuous ripening in stirred tank, J. Cryst. Growth 13–14 (1972) 483–487.
[10] M. Kapembwa, M. Rodriguez-Pascual, A.E. Lewis, Heat and mass transfer effects on ice growth mechanisms in pure water and aqueous solutions, Cryst. Growth Des. 14 (1) (2013) 389–395.
[11] L. Liu, O. Miyawaki, K. Nakamura, Progressive freeze concentration of model liquid, Food Sci. Technol. Int. 3 (4) (1997) 348–352.
[12] K.M. Golden, S.F. Ackley, V.I. Lytle, The percolation phase transition in sea ice, Science 282 (5397) (1998) 2238–2241.
[13] D.N. Thomas, G. Kattner, R. Engbrodt, V. Giannelli, H. Kennedy, C. Haas, G.S. Dieckmann, Dissolved organic matter in Antarctic sea ice, Ann. Glaciol. 33 (1) (2001) 297–303.
[14] D.L. Anderson, A Model for Determining Sea Ice Properties, Arctic Sea Ice, 598, National Academy of Sciences, National Research Council, Publication, Washington, DC, 1958.
[15] A. Kovacs, Sea ice. Part 1. Bulk salinity versus ice floe thickness (No. CRREL-96-7). Cold Regions Research and Engineering Lab Hanover NH, 1996.
[16] C. Petrich, H. Eicken, Growth, structure and properties of sea ice, in: D.N. Thomas, G.S. Dieckmann (Eds.), Sea Ice, second ed., Wiley-Blackwell, Oxford, UK, 2009.
[17] M. Hasan, J.I. Partanen, K.P. Vahteristo, M. Louhi-Kultanen, Determination of the Pitzer interaction parameters at 273.15 K from the freezing-point data available for NaCl and KCl solutions, Ind. Eng. Chem. Res. 53 (13) (2014) 5608–5616.
[18] M.F. Butler, Freeze concentration of solutes at the ice/solution interface studied by optical interferometry, Cryst. Growth Des. 2 (6) (2002) 541–548.
[19] W.F. Weeks, G. Lofgren, The effective solute distribution coefficient during the freezing of NaCl solutions. in: Physics of Snow and Ice: International Conference on Low Temperature Science Proceedings, 1 (1) University, 579–597.
[20] J.A. Burton, R.C. Prim, W.P. Slichter, The distribution of solute in crystals grown from the melt, Part 1. Theoretical, J. Chem. Phys. 21 (1953) 1987–1991.
[21] A. Kouchi, T. Yamamoto, T. Kozasa, T. Kuroda, J.M. Greenberg, Conditions for condensation and preservation of amorphous ice and crystallinity of astrophysical ices, Astron. Astrophys. 290 (1994) 1009–1018.
[22] X. Lu, Novel Applications of Eutectic Freeze Crystallization, Delft University of Technology, TU Delft, 2014.
[23] K. Dermentzis, Removal of nickel from electroplating rinse waters using electrostatic shielding electrodialysis/electrodeionization, J. Hazard. Mater. 173 (1) (2010) 647–652.

[24] N.S. Osborne, Heat of fusion of ice – a revision, J. Res. Nat. Inst. Stand. Technol. 23 (1939) 643–646.
[25] K. Lascelles, L.G. Morgan, D. Nicholls, D. Beyersmann, Nickel compounds, Ullmann's Encyclopedia of Industrial Chemistry, Germany, 2005.
[26] I. Remsen, American Chemical Journal, The Chemical Publishing Co., Printers, Easton, Pennsylvania, 1904.
[27] V.M. Lobo, J.L. Quaresma, Handbook of Electrolyte Solutions, vol. 41, Elsevier, The University of California, 1989.
[28] T. Chen, Physicochemical properties of nickel and cobalt sulphate solutions of hydrometallurgical relevance Doctoral dissertation, Department of Chemical and Metallurgical Engineering & Chemistry, Murdoch University, 2003.
[29] H. Ozbek, S.L. Phillips, Thermal conductivity of aqueous sodium chloride solutions from 20 to 330°C, J. Chem. Eng. Data 25 (3) (1980) 263–267.
[30] P.G.M. Brown, J.E. Prue, A study of ionic association in aqueous solutions of bi-bivalent electrolytes by freezing-point measurements, Proc. R. Soc. London Ser. A 232 (1190) (1955) 320–336.

Publication II

Hasan, M., Louhi-Kultanen, M

Ice growth kinetics modeling of air-cooled layer crystallization from sodium sulfate solutions.

Reprinted with permission from
Chemical Engineering Science
Vol. 133, pp. 44-53, 2015

Chemical Engineering Science 133 (2015) 44–53

Contents lists available at ScienceDirect

Chemical Engineering Science

journal homepage: www.elsevier.com/locate/ces

Ice growth kinetics modeling of air-cooled layer crystallization from sodium sulfate solutions

M. Hasan *, M. Louhi-Kultanen

Department of Chemical Technology, Lappeenranta University of Technology, PO Box 20, FI-53851 Lappeenranta, Finland

HIGHLIGHTS

- Natural freezing as a novel separation method is replicated experimentally.
- Natural freezing was epitomized by ice crystallization from Na_2SO_4 (aq) solutions.
- Robust model was developed to depict the influence of different factors.
- Natural freezing of solution was found to be heat transfer controlled.
- This process has adoptability in cold climate countries at wastewater pond regions.

ARTICLE INFO

Article history:
Received 2 September 2014
Received in revised form
21 January 2015
Accepted 23 January 2015
Available online 2 February 2015

Keywords:
Ice crystallization
Crystal growth kinetics
Crystal purity
Heat transfer
Mass transfer
Wastewater treatment

ABSTRACT

Natural freezing has the possible use to be used as a purification technique to treat wastewater. Natural freezing was simulated experimentally for ice crystallization from unsaturated Na_2SO_4 (aq) solutions to assess the feasibility of such a technique for being used to purify wastewater. The influence of solution concentration and different growth conditions, such as ambient temperature, freezing time and freezing rate, on the efficiency of the purification process was investigated by analysis of the effective distribution coefficient (K) of the solute between the ice and the solution. A calculation method is introduced to estimate the concentration of solution at the advancing ice–solution interface in terms of the limiting distribution coefficient (K^*) from experimental K values at different growth conditions. The heat transfer controlled growth rate of the ice limited by the free convective heat transfer coefficient of air (h_{air}) rather than the thermal conductivity of the ice (k_{ice}) and the heat transfer coefficient of the solution (h_{sol}) found to prevail over the mass transfer of rejected solute molecules from the ice–solution interface to the bulk solution. Advancement of the thermal (δ_T) and concentration boundary layer (δ_C) at the ice–solution interface was proportional to the square root of freezing time. A simplified model is developed to estimate the thickness of the ice layer formed from solutions at different freezing conditions and the model is validated with experimental results.

1. Introduction

Crystallization of water as ice from aqueous solutions by freeze crystallization has an extensive range of applications, especially in solute concentration and wastewater purification processes (Huige and Thijssen, 1972). High product quality, good separation efficiency (Kapembwa et al., 2013) and low energy requirement (Liu et al., 1997) have made freeze crystallization a promising method to address the treatment of wastewater (Lorain et al., 2001). If it is possible to form a single ice layer by natural freezing, ice crystallization treatment of wastewater would become a simple and cost effective approach, because separation of the ice layer is relatively easy as a result of the density difference between the ice and solution.

Redistribution of solute occurs during ice crystallization from a solution and the extent of redistribution is greatly influenced by the ability of the solute to diffuse away from the ice–solution interface (Butler, 2002). During ice crystallization from solution, usually solute molecules/ions are not able to incorporate into the ice crystal lattice owing to constraints of their size/charge (Petrich and Eicken, 2009). These ions are rejected by the advancing ice–solution interface. If the growth rate of the ice layer by natural freezing were low enough then only a small portion of the solute is incorporated into the ice layer and most of it is rejected and purity of the ice layer would be very high. Hence, almost pure water would be obtainable by separation of the ice layer formed on the

* Corresponding author. Tel.: +358 465 96 9187.
E-mail address: Mehdi.Hasan@lut.fi (M. Hasan).

http://dx.doi.org/10.1016/j.ces.2015.01.050
0009-2509/

surface of wastewater ponds in cold climate countries where the temperature goes below 0 °C during winter. In Finland, the mining industries produce significant amount of wastewater. Thus huge volume of wastewater (more than 1 million tons per year) need to be treated in an energy efficient manner. Mining operations are a potential source of seriously contaminated water that is difficult to treat. For example, sulfuric and nitric acid, commonly used as leaching agents in the mining and metallurgical industries, produce effluents containing sulfate (SO_4^{2-}) (Silva et al., 2010) and nitrate (NO_3^-) (Primo et al., 2008) ions. Both of these compounds are considered threats to the environment if present in high level.

Sodium sulfate (Na_2SO_4) is common in effluents emanating from the use of detergents, the textile, glass and mining industries, kraft pulping, (Garrett, 1998) and the ash of marine fossil fuels (Lin and Pan, 2001). This work introduces ice crystallization from Na_2SO_4 (aq) solution, as a model solution, with varying concentrations and ambient temperature imitating natural freezing of saline sea water. Separation efficiency is investigated in terms of a distribution coefficient as a function of solution concentration and different growth conditions. Concentration of the solution at the ice–solution interface and parameters describing the growth kinetics of the ice layer are estimated from experimental results. A model is derived to quantify the ice layer by natural freezing of Na_2SO_4 (aq) solutions. The model can also be used to study the dependency of the growth rate on the initial solution concentration, heat and mass transfer, difference between the solution's freezing point and ambient temperature and freezing time.

2. Theoretical considerations

At any solid–liquid equilibrium (SLE) the chemical potential of the solvent and the corresponding solid phase is equal (Hasan et al., 2014). Solidification of melt is associated with the release of heat from the crystallization and rejection of solutes from the ice–solution interface to the bulk solution. These effects create temperature and concentration gradients in the liquid phase adjacent to the solid–liquid interface, which in turn generate thermal and mass boundary layers. The temperature and concentration profile of natural freezing of a solution and the corresponding boundary layers are illustrated in Fig. 1.

The purity of the ice crystals formed in ice crystallization is dependent on the growth rate (Butler, 2002). If the ice growth rate is low enough for the solute to diffuse away from the advancing ice front, pure ice is formed and the solution becomes more concentrated. On the other hand, if the growth rate is so high that all solutes are entrapped in the ice, this leads to impure ice crystals and no enrichment of the solution.

When a melt solidifies, the distribution of solute in the solid phase, C_s (wt%), relative to that present in the bulk liquid phase, C_b (wt%), is referred to as the effective distribution coefficient, $K=C_s/C_b$, which is predominantly determined by the ability of the solute to diffuse away from the solid–liquid interface. A higher solute rejection rate of ice compared with the diffusion of solute from the ice–solution interface to the bulk solution results in a higher concentration of solute in the interface, C_i (wt%) than in the bulk solution, $C_i > C_b$. The limiting distribution coefficient (K^*) is a specific form of distribution coefficient at the solid–liquid interface, defined as $K^*=C_s/C_i$ (Weeks and Lofgren, 1967).

Knowledge of a diffusion model is necessary to describe the movement of rejected solute from the advancing solid–liquid interface into the bulk. In water crystallization, surface kinetics is very fast due to its small molecular size. This is the reason why amorphous ice can only be formed at extreme conditions, i.e., below −143.15 °C (Kouchi et al., 1994). Pronk et al. (2006) investigated ice crystallization with a freezing system equipped

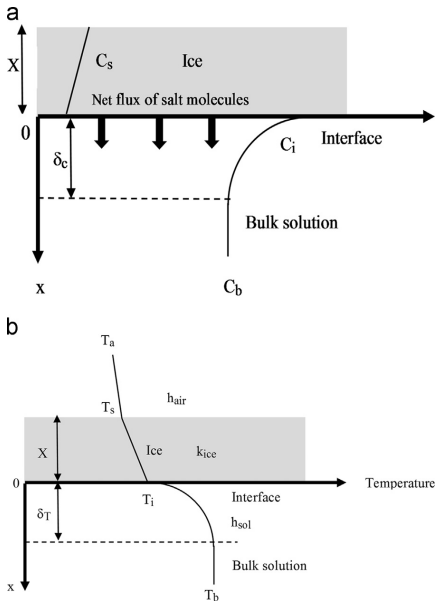

Fig. 1. Schematic depiction of and (a) the concentration profile and (b) temperature profile of ice crystallization by natural freezing from solution.

with a cooling heat exchanger. They investigated the factors dominating the ice crystal growth with the salt solutions. According to Pronk et al., at salt concentration higher than 1 wt%, the resistance of ice growth rate due to surface integration kinetics is ignorable compared with heat and mass transfer resistance. In the present work, the solution concentration was 1 wt% or above, so the surface kinetics was ignored.

2.1. Differential mass transfer model (DMTM)

The extent of the concentration gradient in the locality of the advancing solid–liquid interface during growth of the crystal from melt depends upon several factors, e.g., the solidification rate, the effective distribution coefficient, K and the nature of the fluid flow (Weeks and Lofgren, 1967). The mass transfer of solute molecules between a single crystal and the melt is commonly studied using a differential mass transfer model (DMTM) presented by Burton et al. (1953) and assuming that the solution concentration in the radial direction perpendicular to the growth condition is uniform, and that the fluid is incompressible and uniform beyond the boundary layer. It is assumed that the coordinates move at the same rate as the growing ice layer for being fixed to the solid–liquid interface, i.e., at $x=0$, and extends in a positive direction into the melt.

At the solid–liquid interface, there is no fluid velocity with an exception of the flow normal to the interface produced by crystal growth. Therefore, at the interface the flow is laminar and the fluid velocity is small enough for molecular diffusion to be the main means of transporting the rejected solute molecules away from the growing crystal (Weeks and Lofgren, 1967). According to BPS (Burton–Prim–Slichter) theory, the governing diffusion equation

for a one-dimensional steady state system the governing is:

$$D\frac{d}{dx}\left(\frac{dC(x)}{dx}\right)+G\frac{dC(x)}{dx}=0 \quad (1)$$

where, D ($m^2\ s^{-1}$) is the diffusion coefficient of the solute, x (m) is the distance from the interface, $C(x)$ (wt%) is the solution concentration within the boundary layer as a function of x, and G ($m\ s^{-1}$) is the growth rate of the advancing ice front. Assuming no diffusion in the solid phase and applying boundary conditions for steady-state growth:

$$(C_i-C_s)G+D\frac{dC(x)}{dx}=0,\ \text{at}\ x=0$$

and

$$C(x)=C_b\ \text{at}\ x\geq\delta_c$$

Burton et al., proposed the solution of Eq. (1) at $x=0$ as:

$$K=\frac{K^*}{K^*+(1-K^*)\exp(-G/k_l)} \quad (2)$$

where k_l ($m\ s^{-1}$)$=D/\delta_c$ is the mass transfer coefficient and δ_c (m) is the boundary layer thickness for the concentration gradient at the ice–solution interface. This equation can be rearranged as (Weeks and Lofgren, 1967):

$$\ln\left(\frac{(1/K^*)-1}{(1/K)-1}\right)=\frac{G}{k_l} \quad (3)$$

2.2. Solute balance at the ice–solution interface

During the course of ice formation from the solution, the growth rate varies as the freezing proceeds and the solution becomes progressively more concentrated. However, for dilute solutions and/or if the volume of the solution is significantly large (e.g., freezing the huge volumes of effluents emanating from mining industries), the increase in the concentration over a short freezing time (maximum freezing time was 24 h in this work) can be considered to be negligible, and the quasi-steady-state approximation can be considered reasonable. During the growth of the ice layer from the melt only a part of the solute molecules is incorporated into the ice and the remainder is rejected at the advancing ice–solution interface. The rejected salt molecules are carried away by diffusion in the boundary layer, δ_C. Under quasi steady state conditions, the amount of rejected solute molecules per unit time and unit area, $G(C_i-C_s)$, should be equal to diffusion flux of the solute molecules in the boundary layer (Kuroda, 1985):

$$G(C_i-C_s)=k_l(C_i-C_b) \quad (4)$$

From Eq. (4), the mass transfer resistance (R_m) of the **average** growth rate, G is $(C_i-C_s)/k_l$ ($wt\%\ s\ m^{-1}$) or $(C_i-C_s)\varphi/k_l$ ($K\ s\ m^{-}$), where the conversion factor is, $\varphi=\rho_{ice}\alpha/\rho_b$ (Louhi-Kultanen, 1996). Here, α ($K\ wt\%^{-1}$) is the slope of the liquidus curve of the phase diagram of Na_2SO_4–H_2O system ($\alpha=0.27\ K\ wt\%^{-1}$ in this work) and ρ_b and ρ_{ice} ($kg\ m^{-3}$) represent the density of the bulk solution and the ice, respectively. After rearranging, Eq. (4) becomes:

$$\left(\frac{1-(K^*/K)}{1-K^*}\right)=\frac{G}{k_l} \quad (5)$$

2.3. Overall heat balance

During ice crystallization from a solution, removal of heat from the solution to the surrounding area is balanced by release of the heat of crystallization to the solution under quasi steady state condition assuming the change in the temperature of the solution as freezing proceeds is negligible (Kuroda, 1985):

$$G\rho_{ice}\Delta H=U(T_b-T_a) \quad (6)$$

where ρ_{ice} ($kg\ m^{-3}$) is the density of the ice layer, ΔH ($J\ kg^{-1}$) is the latent heat of freezing, and T_b and T_a (°C/K) are the temperature of the bulk solution and ambient air, respectively. The heat transfer resistance (R_h) for ice growth rate, G, from Eq. (6) is $\rho_{ice}\Delta H/U$ ($K\ s\ m^{-1}$). The overall heat transfer coefficient, U ($W\ m^{-2}\ K^{-1}$), can be defined:

$$\frac{1}{U}=\left(\frac{1}{h_{sol}}+\frac{X}{k_{ice}}+\frac{1}{h_{air}}\right) \quad (7)$$

here X (m) is the ice layer thickness, h_{sol} ($W\ m^{-2}\ K^{-1}$) is the free convective heat transfer coefficient of the solution, h_{air} ($W\ m^{-2}\ K^{-1}$) is the free convective heat transfer coefficient of air, and k_{ice} ($W\ m^{-1}\ K^{-1}$) is the thermal conductivity of the ice. Assuming no heat flux for radiation, sublimation and sensible heat loss, and replacement of the average ice growth rate, i.e., $G=(dX/dt)$, throughout the course of the ice layer formation, Eq. (6), after integration gives:

$$\int_0^X\rho_{ice}\Delta H dX=\int_0^t U(T_b-T_a)dt \quad (8)$$

$$\frac{X^2}{2k_{ice}}+\left(\frac{1}{h_{sol}}+\frac{1}{h_{air}}\right)X-\frac{\Delta Tt}{\rho_{ice}\Delta H}=0 \quad (9)$$

In the case of pure water Eq. 9 becomes:

$$\frac{X^2}{2k_{ice}}+\left(\frac{1}{h_w}+\frac{1}{h_{air}}\right)X-\frac{\Delta Tt}{\rho_{ice}\Delta H_f}=0 \quad (10)$$

where h_w ($W\ m^{-2}\ K^{-1}$) is the free convective heat transfer coefficient of water and $\Delta T=T_b-T_a$. The value of latent heat of freezing of pure water, $\Delta H_f=3.34\times10^5$ ($J\ kg^{-1}$) (Osborne, 1939). Assuming no temperature difference between ice and water at the freezing condition, $T_b=T_i$ or $h_w\approx\infty$, Eq. (10) results in Stefan's formula (Ashton, 1989) as follows:

$$\frac{X^2}{2k_{ice}}+\frac{X}{h_{air}}-\frac{\Delta Tt}{\rho_{ice}\Delta H_f}=0 \quad (11)$$

The free convective heat transfer coefficient (h_{sol}) and free convective mass transfer coefficient (k_l) at interface of the horizontal ice layer and aqueous solution can be determined using the following free convection correlations (Cengel, 2002).

$$Nu=0.27(Gr\ Pr)^{0.25}\times10^5<GrPr<10^{11} \quad (12)$$

$$Sh=0.27(Gr\ Sc)^{0.25}10^5<GrSc<10^{11} \quad (13)$$

here the Nusselt number, $Nu=(h_{sol}\times L_c/k)$, Grashof number, $Gr=(g(C_i-C_b){L_c}^3/C\nu^2)$, Prandtl number, $Pr=(C_p\nu\rho/k)$, Schmidt number, $Sc=(\nu/D)$ and Sherwood number, $Sh=(k_l\times L_c/D)$. Characteristic length, acceleration due to gravity, thermal conductivity, specific heat at constant pressure, kinematic viscosity and density of the solution are designated by L_c (m), g ($m\ s^{-2}$), k ($W\ m^{-1}\ K^{-1}$), C_p ($J\ kg^{-1}\ K^{-1}$) and ρ ($kg\ m^{-3}$), respectively. In the correlation, physical and thermodynamic properties are estimated at an average of interface and bulk concentration, $C=((C_i+C_b)/2)$, and at 25 °C, with the exception of ρ, which is available in the literature for 0 °C.

As solute molecules are retained in the liquid inclusion in the ice layer, the latent heat of fusion for impure ice, ΔH ($J\ kg^{-1}$) is less than that of pure ice (ΔH_f). Malmgren introduced an expression to determine the latent heat of fusion of impure ice based on the impurity level by assuming phase transition at thermodynamic equilibrium and constant bulk concentration (Petrich and Eicken,

2009). According to Malmgreen's formula (Anderson, 1958):

$$\Delta H = \Delta H_f \left(1 - \frac{C_s}{C_b}\right) \quad (14)$$

2.4. Physical and thermodynamic properties of model Na_2SO_4 (aq) solutions

Natural freezing of wastewater was characterized by a model Na_2SO_4 (aq) solution. Freezing point depression (FPD) and various other thermodynamic and physical properties of Na_2SO_4 (aq) solutions in the range of 1 wt% to 4 wt% were collected and correlated statistically by best fitting of data. Table 1 lists these properties, which are used for further calculation in this work.

3. Experimental method

3.1. Materials and methods

1 wt%, 2 wt%, 3 wt% and 4 wt% Na_2SO_4 (aq) solutions were prepared by dissolving 99% pure anhydrous Na_2SO_4 (purchased from Merck) in deionized water (conductivity = 0.1 μS cm^{-1}, total organic carbon = 1 ppb). Dissolution was performed at room temperature under vigorous mixing condition (500 rpm) for 30 min.

3.2. Apparatus for ice layer crystallization

The experimental setup to simulate natural freezing is presented in Fig. 2. A 710 ml rectangular plastic vessel with Teflon coating (14 cm × 8.74 cm × 5.8 cm) acted as a crystallizer for ice layer crystallization from the Na_2SO_4 (aq) solution by natural freezing. In this vessel, heat transfer from the side and bottom surfaces was avoided by the use of extruded polystyrene foam and only the top surface was exposed for heat transfer to or from the solution to facilitate uni-dimensional ice layer growth. The crystallizer vessel was placed in a freezer box. The air temperature (T_a) of the freezer box was controlled by a Lauda proline RP 850 thermostat. Monoethylene glycol (freezing point, -36 °C) was used as a coolant. The coolant flowed at the rate of 23 l min^{-1} from the thermostat to the heat exchangers situated inside the freezer box for a set temperature. The temperature of the freezing solution in the vessel was measured by PT 100 element and monitored by

Table 1
Thermodynamic and physical properties of Na_2SO_4 (aq) solutions.

Property	Unit	Correlation*	Ref.
Freezing point depression	°C	$FPD = 0.269 \times y + 0.06$	Hasan and Louhi-Kultanen (2014), Haynes (2014–2015)
Density, ρ (at 0 °C)	kg m^{-3}	$\rho = 9.4765 \times y + 999.82$	Chen et al. (1980)
Kinematic viscosity, ν (at 25 °C)	m^2 s^{-1}	$\nu = 2.412 \times 10^{-8} \times y + 8.782 \times 10^{-7}$	Abdulagatov et al. (2005)
Diffusion coefficient, D (at 25 °C)	m^2 s^{-1}	$D = -3.89 \times 10^{-11} \times y + 1.03 \times 10^{-9}$	Rard and Miller (1979)
Heat capacity, C_p (at 25 °C)	J kg^{-1} K^{-1}	$C_p = -42.172 \times y + 4174.8$	Magalhaes et al. (2002)
Thermal conductivity, k (at 25 °C)	W m^{-1} K^{-1}	$k = -0.0094 \times y + 0.5554$	Ozbek and Phillips (1980)

* $[y]$ = wt% = y g salt/100 g salt solution.

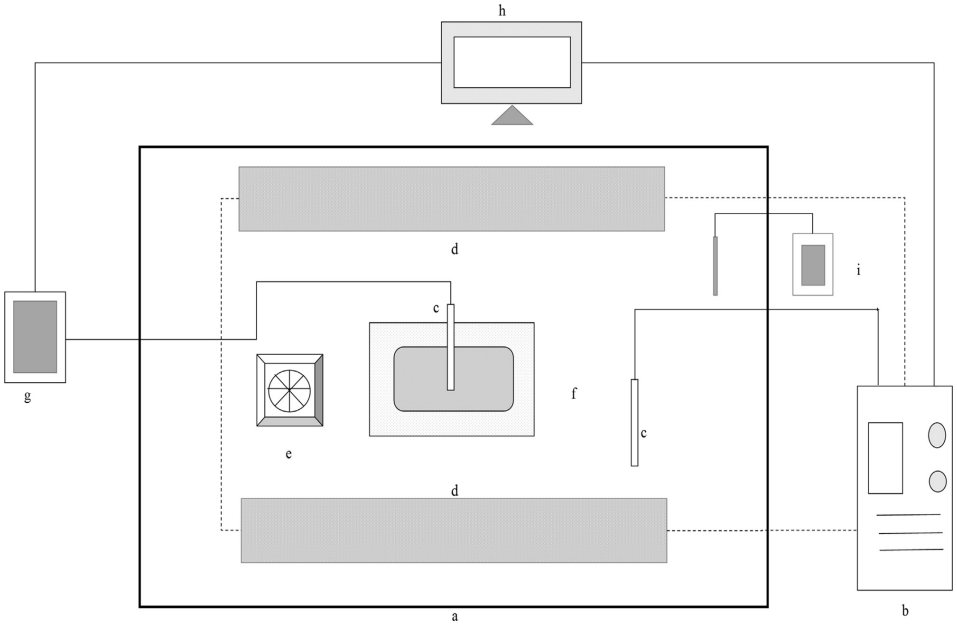

Fig. 2. Experimental setup for freezing of solution. (a) Freezer box; (b) Lauda proline RP 855 thermostat; (c) Pt 100 thermosensor; (d) heat exchanger; (e) fan; (f) crystallizer with insulation; (g) Pico logger; (h) data monitoring and storage device; (i) anemometer. Electric wire and coolant flow pipe are represented by — and ···, respectively.

Pico data logger. A central process unit (cpu) cooling fan ($80 \times 80 \times 25$ mm) operated by 12 V potential difference was used to maintain air circulation rate of 0.24 m s^{-1} (measured by Kimo anemometer) inside the freezer box in order to ensure a homogeneous temperature.

3.3. Experimental procedure

A 500 ml sample solution was precooled by keeping it in a freezing room at −15 °C. When the solution reached its freezing temperature, small ice crystal platelets appeared on the liquid surface and the solution was relocated to the crystallizer within the freezer box. The existence of ice platelets indicated attainment of the solution's freezing temperature and the platelets worked as seed crystals to prevent supercooling. The temperature inside the freezer was kept at a constant temperature a few degrees lower ($\Delta T = 1$ °C, 2 °C, 3 °C) than the freezing temperature of the solution by Lauda proline RP 850 thermostat. After a certain freezing time (5 h, 10 h, 15 h, 24 h), the ice layer that had formed by freezing the solution was collected from the crystallizer. The ice layer was washed with distilled water at 0 °C to avoid melting during washing. The volume and density of the residual solution were measured. After measuring the thickness and mass of the collected ice layer, ice impurities were analyzed by thermogravimetric method. Experiments were also performed in the same manner with pure water for ice crystallization.

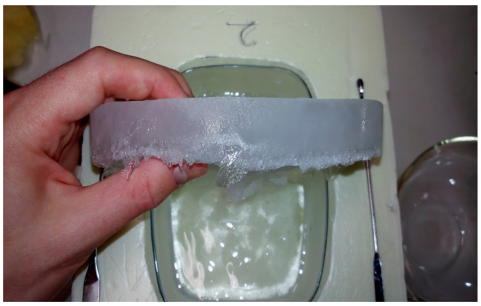

Fig. 3. Photo of ice crystal obtained by the freezing of Na_2SO_4 (aq) solution.

4. Results and discussion

4.1. Determination of h_{air}

Laminar airflow inside the freezer was required for the thermostat to maintain constant air temperature, T_a. The air circulation rate of 0.24 m s^{-1} in the freezer was low enough to assume free convection rather than forced convection and replicates quiescent weather conditions. Ice crystallization experiments by freezing pure water at different ΔT values were performed as described in the previous section. For instance, in the case of $\Delta T = 3$ °C, the thickness (X) of the ice layer was 1.8 cm after 24 h freezing time (t). Exporting the X, t and ΔT values along with $k_{ice} = 2.16$ W m^{-1} K^{-1}, $\rho_{ice} = 917$ kg m^{-3} (Haynes, 2014–2015), and $\Delta H_f = 3.34 \times 10^5$ J kg^{-1} (Osborne et al., 1939) at 0 °C into Eq. (9), h_{air} was obtained as 23.5 W m^{-2} K^{-1}, on average, inside the freezer. Heat transfer coefficient values reported in the literature (Ashton, 1989) between ice layer and air varied between 10 to 30 W m^{-2} K^{-1}, which was consistent with heat transfer coefficient obtained in the present work, i.e., 23.5 W m^{-2} K^{-1}. This value was used in further calculations.

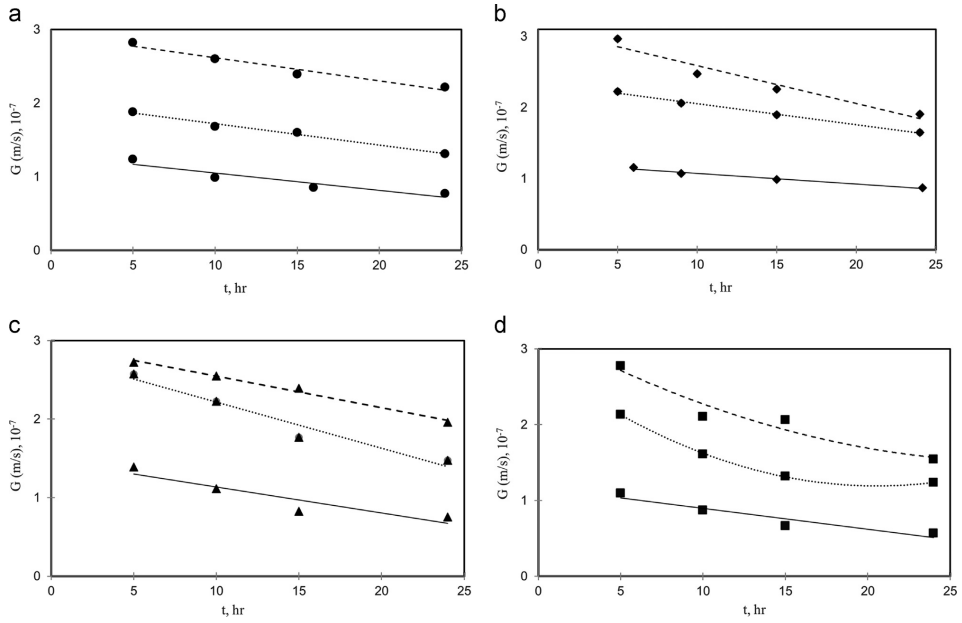

Fig. 4. Plot of ice growth rate, G vs freezing time, t as function of concentration of Na_2SO_4 solution (symbol ●, 1 wt% (a); ◆, 2 wt% (b); ▲, 3 wt% (c); ■, 4 wt% (d)). $\Delta T = 1$ °C, $\Delta T = 2$ °C and $\Delta T = 3$ °C is represented by —, ··· and - - -, respectively.

4.2. Characteristics of the ice layer

During the ice formation experiments, supercooling was subdued by platelets of ice crystals, and thus planar growth of the ice layer was observed rather than dendritic growth. It was also observed that the strength of the ice layer obtained from pure water was higher and more transparent than that of the Na_2SO_4 (aq) solutions. The lower surface of the pure ice layer was smooth. The impure ice layer obtained from the Na_2SO_4 (aq) solutions, on the other hand, was cloudy and soft and the lower surface was sutured. Transparency, hardness and smoothness of the ice layer decreased with increasing concentration of the initial solution. Fig. 3 shows an ice crystal obtained by freezing of the Na_2SO_4 (aq) solution. Differences in the ice characteristics can be considered as having been caused by an increase in solute extraction with increasing salt content in the solution. Similar ice characteristics have been reported in the literature during ice formation from ethylene glycol solution of different concentrations (Hirata et al., 2000). Retained solute molecules in the inclusion of the solution in the ice layer have very important consequences for the microstructure and properties of impure ice (Petrich and Eicken, 2009). It has also been reported that the tensile strength (σ) of sea ice decreases with the salinity of sea water which is in agreement with the changes in ice characteristics observed in this study (Anderson, 1958).

4.3. Growth rate (G) as a function of freezing time (t), concentration (wt%) and ΔT

During the experiments, the growth rate of the ice layer, G, from the different initial solutions was manipulated by altering ΔT=1 °C, 2 °C, 3 °C and t=5 h, 10 h, 15 h and 24 h. Experimental results are presented in Fig. 4.

For all values of ΔT in this study, G decreased linearly for 1 wt%, 2 wt% and 3 wt% Na_2SO_4 (aq) solutions. The formed ice layer itself acted as heat resistance for further freezing. Therefore, the overall heat transfer coefficient, U declines with ice layer thickness, X (see Eq. (7)), which consequently leads to a decrease in G. In most cases, the decline in G is influenced by the freezing driving force ΔT as well. Time dependent average growth rate at each growth condition was further used for estimating limiting distribution coefficient, K^* and the ice layer thickness, X.

For, 4 wt% Na_2SO_4 (aq) solution and ΔT=2 °C and ΔT=3 °C, G did not decrease greatly after 5 h of freezing time. For ΔT=2 °C and ΔT=3 °C, after 5 h of freezing time, the salts and ice started to crystallize simultaneously, that is, eutectic freeze crystallization (EFC) occurred. There is inconsistency between the reported eutectic points of Na_2SO_4 (aq) solution. According to Pronk (2007), the eutectic point of Na_2SO_4 (aq) solution is at 3.8 wt% and −1.2 °C. On the other hand, Randall and Lewis (2009) reported the eutectic point of Na_2SO_4 (aq) solution is at 4.19 wt% and −1.27 °C. Experimentally we observed the formation of salt crystals followed by ice crystallization while freezing only 4 wt% Na_2SO_4 (aq) solution. The latter reference is more in accordance with our experimental observation. Crystallization of the salt reduces the solute mass transfer limitation, which nullifies the increasing resistance of the growing ice front.

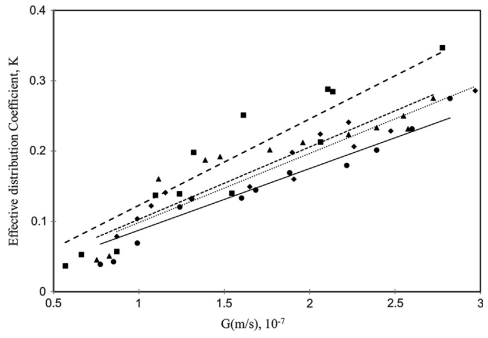

Fig. 5. Effective distribution coefficient, K as a function of ice layer growth rate, G from Na_2SO_4 solution (●, 1 wt%; ◆, 2 wt%; ▲, 3 wt%; ■, 4 wt%. A linear relationship is shown between G and K by, —, ····, —, and - - - for 1 wt%, 2 wt%, 3 wt% and 4 wt%, respectively.

4.4. Effective distribution coefficient (K)

The effective distribution coefficient, K, is a very important parameter for freeze crystallization and determines the solute separation efficiency. In this study, K was determined empirically (by altering ΔT and t as mentioned earlier) at different growth conditions of the advancing ice front of the Na_2SO_4 (aq) solutions. The results are shown in Fig. 5.

K was found to rise with the increase in G, indicating that at higher G, solutes are likely to be entrapped in the ice layer rather than diffusing from the interface to the bulk solution. At around the same G, the K values increased with the increasing concentration of the solution. For G values less than 10^{-7} m s^{-1}, K dropped significantly and the purity of the ice layer was very high.

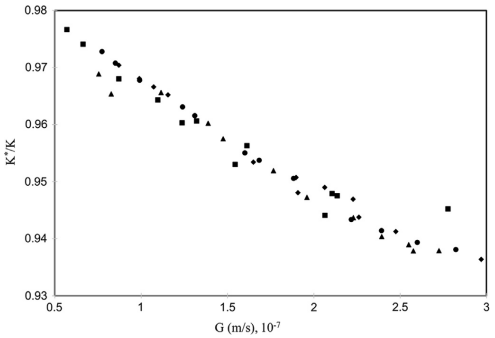

Fig. 6. Ratio of limiting and effective distribution coefficient as a function of ice layer growth rate, G. Symbols: ●, 1 wt%; ◆, 2 wt%; ▲, 3 wt%; ■, 4 wt% of Na_2SO_4 (aq) solution, respectively.

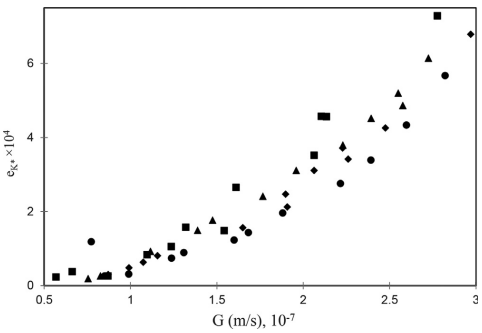

Fig. 7. Plot of e_{K^*} as a function of ice layer growth rate, G from Na_2SO_4 (aq) solution. Symbols: ●, 1 wt%; ◆, 2 wt%; ▲, 3 wt%; ■, 4 wt% Na_2SO_4 solution.

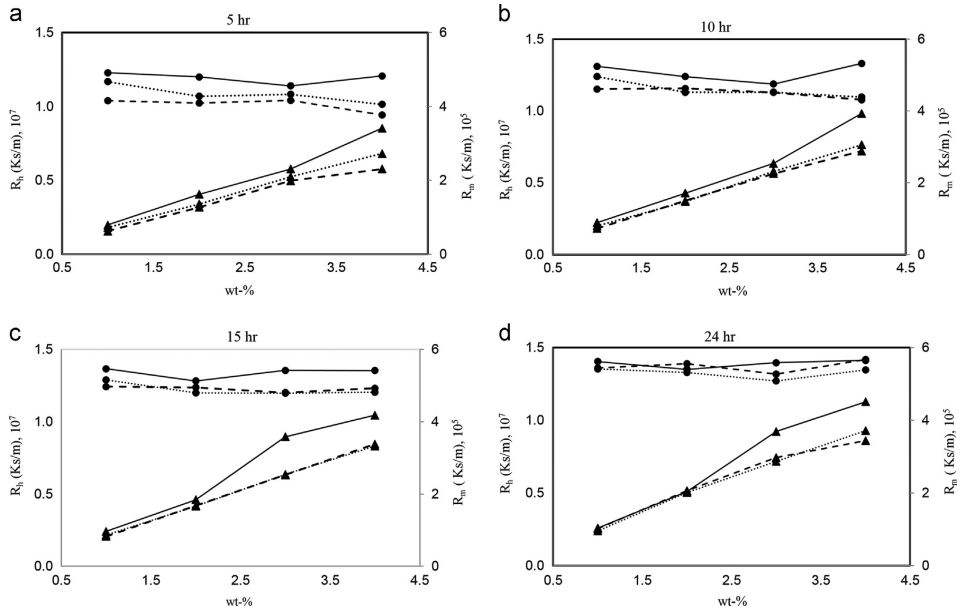

Fig. 8. Influence of heat (R_h, symbol, ●) and mass transfer (R_m, symbol, ▲) resistance on ice growth rate (G) from Na_2SO_4 (aq) solutions of different concentration with course of time. ─, ···, and - - - represent ΔT=1 °C, ΔT=2 °C, and ΔT=3 °C, respectively.

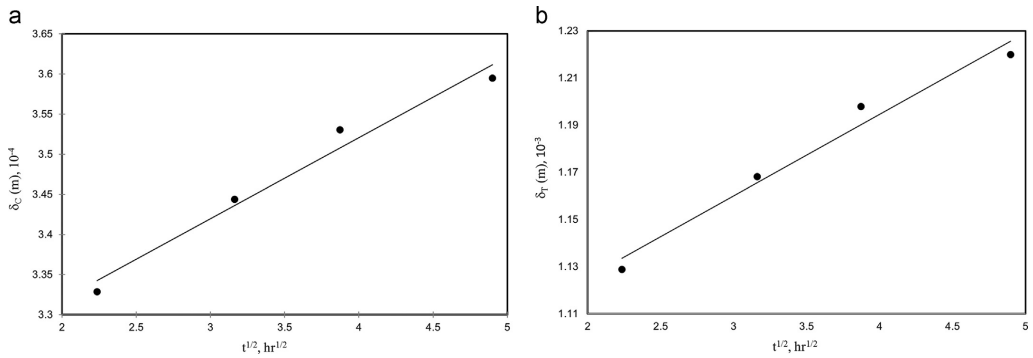

Fig. 9. Developed boundary layers due to, (a) concentration gradient; (b) temperature gradient at the ice–solution interface for 1 wt% initial solution with freezing time, t.

4.5. Estimating limiting distribution coefficient (K^*)

By mathematical manipulation Eq. (2) can be rewritten as

$$\ln\left(\frac{1}{K}-1\right) = \ln\left(\frac{1}{K^*}-1\right) - \left(\frac{G}{k_l}\right) \tag{15}$$

From the intercept of the plot of $\ln(1/K-1)$ vs G, the limiting distribution coefficient, K^*, can be determined by considering the constant K^* value regardless of growth rate. However, Louhi-Kultanen et al. (1988) found that K^* is a function of G. Furthermore, it has been inferred from experimental results and also from literature data for freezing sea-water that K values drop abruptly at lower G (Weeks and Lofgren, 1967). As a result, the ordinate of the plot from Eq. (14) increases exponentially, which degrades the goodness of fitting of experimental points into a straight line. Therefore, K^* was estimated iteratively using experimental values of K at different growth conditions and G by equating mass transfer coefficient values (k_l) obtained from Eqs. (3) and (13) and also from Eqs. (5) and (13) for the differential and interfacial mass balance of the solute, respectively. A similar trend as in Fig. 5 was obtained from the calculated K^* values as a function of G. Fig. 6 presents the trend at different growth conditions.

The values of K/K^* are independent of solution concentration. Fig. 6 also intimates that at very low growth conditions, e.g., $G < 10^{-7}$ m s^{-1}, the solute gets enough time to diffuse from the ice–solution interface to the bulk solution, and then $K \approx K^*$. This can be validated by limiting the growth condition, i.e., $G \to 0$ in Eq. (2). At zero growth rate, K^* approaches to K and thus K^*/K approaches to 1.

As the growth rate increases, incorporation of solute in the advancing ice front also increases and the K^* value reduces. The difference between calculated K^* values by differential mass transfer model (DMTM), as in Eq. (3), and by mass balance of the solute at the interface, as in Eq. (5), is expressed by an error function as follows

$$e_{k^*} = K^*(\text{DMTM}) - K^*(\text{solute} - \text{balance}) \quad (16)$$

An error plot as a function of G is presented in Fig. 7 as an example. From Fig. 7, it can be inferred that either model can be used at experimental growth conditions ranging from 5×10^{-8} to 3.0×10^{-7} m s^{-1}.

4.6. Heat (R_h) and mass transfer resistance (r_m)

The heat transfer (R_h) and mass transfer (R_m) resistances to advancing ice front from Na_2SO_4 (aq) solutions are represented as a function of initial concentration, t and ΔT in Fig. 8.

In all cases, R_m increases with increasing concentration of the solution, whereas R_h is concentration independent. It is apparent that R_h is of the order of 10^7 K s m^{-1} and R_m is of the order of 10^5 K s m^{-1}, which indicates that heat transfer dominates the kinetics of freezing. It was not possible to calculate accurate resistances because physical and thermodynamic properties were used at 25 °C (only density values of solution are available at 0 °C). If properties were available at 0 °C or at even lower temperatures more accurate results could be estimated.

Calculated δ_T ($=k/h_{sol}$) and δ_c ($=D/k_l$) for 1 wt% Na_2SO_4 (aq) solution at $\Delta T=1$ °C (best in terms of the temperature dependency of the physical and thermodynamic properties because its freezing point is higher than other solutions) as a function of t is shown in Fig. 9.

In both cases, interfacial positions are found to be proportional to the square root of time. Terwilliger and Dizio (1970) found a similar trend for δ_T with respect to the square root of time during freezing of brine solution. Boundary layer thickness for all growth conditions are shown in Table 2.

Boundary layers appear to develop with freezing time (t), decrease with the increase of ΔT and be loosely linked with the initial concentration of the solution. The ratio between the thermal and concentration boundary layer (δ_T/δ_C) is around 3.41 for all growth conditions and solutions.

4.7. Modeling of ice thickness (X)

Ice layer thickness (X) can be predicted after a certain freezing time, t and freezing condition ΔT if h_{sol} and k_{ice} are known from Eq. (9). Because of very low salt entrapment, k_{ice} was used as that of pure ice at 0 °C. The change of overall heat transfer coefficient, U due to thicker ice layer formation at different growth conditions can be taken into account in the model. The calculated results are shown in Table 3 as a function of the ice thickness (X). From the table, it is evident that the change of U with the change of X was quite insignificant. The difference between the experimental and calculated thickness was higher at higher solution concentration and ΔT.

The change of T_b due to solution enrichment with the course of freezing was insignificant. For instance, even at the experimental condition of freezing of 3 wt% Na_2SO_4 (aq) for 24 h at $\Delta T=3$ °C, where, T_b was most likely to be time dependent, the change of T_b due to progressive concentration from −0.87 °C to −1.1 °C is unsubstantial, as illustrated in Fig. 10.

Even though the change of T_b due to solution enrichment while freezing is within experimental limitations, the model would work better if ΔT could be adjusted constantly during the course of experiment. More accurate prediction would be possible if physical and thermodynamic properties as a mean of h_{sol} were calculated at the corresponding freezing point of the solution. In the case of the 4 wt% solution not only ice crystallization occurred but also salt crystallization.

Table 2
Boundary layer thickness at different growth condition for ice crystallization from Na_2SO_4 (aq) solutions.

Concentration	t (h)	ΔT (°C)	δ_C (m) 10^{-4}	δ_T (m) 10^{-3}
1 wt%	5	1	3.33	1.13
	10		3.44	1.17
	15		3.53	1.20
	24		3.59	1.22
	5	2	3.09	1.05
	10		3.14	1.07
	15		3.16	1.07
	24		3.29	1.12
	5	3	2.91	0.99
	10		2.93	0.99
	15		2.95	1.00
	24		2.98	1.01
2 wt%	5	1	3.37	1.15
	10		3.40	1.16
	15		3.44	1.17
	24		3.50	1.20
	5	2	3.02	1.03
	10		3.05	1.04
	15		3.08	1.05
	24		3.12	1.07
	5	3	2.88	0.98
	10		2.94	1.01
	15		2.97	1.02
	24		3.03	1.04
3 wt%	5	1	3.24	1.11
	10		3.36	1.16
	15		4.02	1.15
	24		3.91	1.19
	5	2	2.89	0.99
	10		2.96	1.02
	15		3.08	1.06
	24		3.17	1.10
	5	3	2.89	0.99
	10		2.90	1.00
	15		2.91	1.00
	24		3.00	1.04
4 wt%	5	1	3.31	1.15
	10		3.40	1.18
	15		3.59	1.24
	24		3.68	1.28
	5	2	3.00	1.04
	10		3.14	1.09
	15		3.23	1.12
	24		3.22	1.12
	5	3	2.62	0.91
	10		3.00	1.04
	15		2.94	1.02
	24		3.08	1.07

As the model in this work is based on only ice crystallization, 4 wt% Na_2SO_4 (aq) solutions were excluded from the comparison.

5. Conclusion

Natural freezing of Na_2SO_4(aq) solutions at different concentration was investigated at a freezing rate ranging from approximately 5×10^{-8} to 3.0×10^{-7} m s^{-1}. Ice purity in terms of the effective distribution coefficient, K, was measured experimentally and was found to be affected by the growth rate, G. A calculation model was developed to estimate the concentration at the ice–solution interface, C_i, based on its variation with the growth rate. The model was built up both by differential mass transfer model (DMTM) and solute balance model at the ice–solution interface. The difference between these methods in estimating the limiting distributive coefficient, K^*, was negligible. With very low G, $K \approx K^*$. The kinetics of the solidification process was dominated by heat transfer rather than mass transfer. The thickness of the boundary layers that developed due to the thermal (δ_T) and concentration (δ_C) gradient

Table 3
Comparison between observed and calculated ice thickness (X) obtained from solution Na_2SO_4 (aq) solutions of different concentration and growth conditions.

Concentration	ΔT (°C)	Freezing time, t (h)	Overall heat transfer coefficient, U (W m^{-2} K^{-1})	X (experimental) (m) 10^{-2}	X (calculated) (m) 10^{-2}
1 wt%	1	5	21.90	0.22	0.22
		10	21.75	0.36	0.28
		15	21.45	0.46	0.40
		24	20.95	0.67	0.63
	2	5	21.77	0.34	0.31
		10	21.15	0.61	0.6
		15	20.59	0.86	0.87
		24	19.64	1.13	1.36
	3	5	21.35	0.51	0.53
		10	20.43	0.94	0.98
		15	19.67	1.29	1.39
		24	18.48	1.92	2.09
2 wt%	1	5	21.91	0.21	0.21
		10	21.70	0.39	0.3
		15	21.40	0.53	0.43
		24	20.90	0.75	0.66
	2	5	21.71	0.4	0.34
		10	21.03	0.74	0.66
		15	20.46	1.02	0.94
		24	19.61	1.43	1.39
	3	5	21.33	0.53	0.54
		10	20.42	0.89	0.98
		15	19.64	1.22	1.4
		24	18.52	1.65	2.05
3 wt%	1	5	21.82	0.25	0.25
		10	21.65	0.4	0.31
		15	21.44	0.45	0.41
		24	20.93	0.65	0.64
	2	5	21.73	0.46	0.34
		10	21.03	0.8	0.66
		15	20.42	0.95	0.94
		24	19.45	1.27	1.45
	3	5	21.31	0.49	0.53
		10	20.36	0.92	1.01
		15	19.54	1.29	1.44
		24	18.31	1.69	2.17

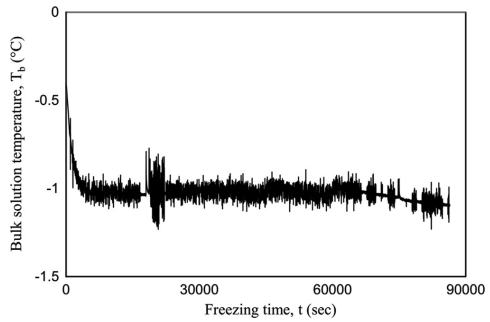

Fig. 10. The change of T_b of 3 wt% Na_2SO_4 (aq) solution at $\Delta T = 3$ °C, over 24 h freezing time (t).

at the interface was inversely related to the freezing rate. The overall heat transfer coefficient (U) is limited by the free convective heat transfer coefficient of the air (h_{air}) rather than the thermal conductance of the ice layer (k_{ice}) and the free convective heat transfer coefficient of the solution (h_{sol}). A simplified model was developed based on the overall heat balance from the bulk solution to cold air to predict ice thickness at different growth conditions. The model worked quite well when there was only ice formation from the solution. However, when the eutectic point is reached, i.e., ice and salt start to crystallize simultaneously, then the model shows discrepancies in estimating ice thickness. The accuracy of the model is hampered by a lack of knowledge about the thermo-physical properties of solutions at temperatures below 25 °C.

Acknowledgement

The authors are indebted to the Academy of Finland (Project no. 260141), the Graduate School of Lappeenranta University of Technology (LUT) and the Graduate School of Chemical Engineering (GSCE) for financial support. The contribution of Mr. Mikko Brotell during the experimental work is also acknowledged.

References

Abdulagatov, I.M., Zeinalova, A., Azizov, N.D., 2005. Viscosity of aqueous Na_2SO_4 solutions at temperatures from 298 to 573 K and at pressures up to 40 MPa. Fluid Phase Equilib. 227 (1), 57–70.
Anderson, D.L., 1958. A model for determining sea ice properties. In:Arctic Sea Ice, Publ., pp. 148-152.
Ashton, G.D., 1989. Thin ice growth. Water Resour. Res. 25 (3), 564–566.
Burton, J.A., Prim, R.C., Slichter, W.P., 1953. The distribution of solid in crystals grown from the melt, Part 1. Theoretical. J. Chem. Phys. 21, 1987–1991.
Butler, M.F., 2002. Freeze concentration of solutes at the ice/solution interface studied by optical interferometry. Cryst. Growth Des. 2 (6), 541–548.
Cengel, Y.A., 2002. Heat Transfer—A Practical Approach, second ed. McGraw-Hill Companies, Inc., New York, NY.
Chen, C.T.A., Chen, J.H., Millero, F.J., 1980. Densities of sodium chloride, magnesium chloride, sodium sulfate, and magnesium sulfate aqueous solutions at 1 atm from 0 to 50 °C and from 0.001 to 1.5 m. J. Chem. Eng. Data 25 (4), 307–310.
Garrett, D.E., 1998. Sodium Sulfate—Handbook of Deposits, Processing, Properties and Use. Academic Press, London, UK.
Hasan, M., Partanen, J.I., Vahteristo, K.P., Louhi-Kultanen, M., 2014. Determination of the Pitzer interaction parameters at 273.15 K from the freezing-point data available for NaCl and KCl solutions. Ind. Eng. Chem. Res. 53 (13), 5608–5616.
Hasan, M., Louhi-Kultanen, M., 2014. Determination of pitzer parameters for 1-1 nitrate and 1-2 sulfate solutions from freezing point data. Chem. Eng. Technol. 37 (8), 1340–1346.
Haynes, W.M., 2014–2015. CRC Handbook of Chemistry and Physics (Ed:), 95th ed. CRC Press, Boca Raton, FL.
Hirata, T., Nagasaka, K., Ishikawa, M., 2000. Crystal ice formation of solution and its removal phenomena at cooled horizontal solid surface: Part I: Ice removal phenomena. Int. J. Heat Mass Transfer 43 (3), 333–339.
Huige, N.J.J., Thijssen, H.A.A., 1972. Production of large crystals by continuous ripening in stirred tank. J. Cryst. Growth 13–14, 483–487.
Kapembwa, M., Rodriguez-Pascual, M., Lewis, A.E., 2013. Heat and mass transfer effects on ice growth mechanisms in pure water and aqueous solutions. Cryst. Growth Des. 14 (1), 389–395.
Kouchi, A., Yamamoto, T., Kozasa, T., Kuroda, T., Greenberg, J.M., 1994. Conditions for condensation and preservation of amorphous ice and crystallinity of astro-physical ices. Astron. Astrophys. 290, 1009–1018.
Kuroda, T., 1985. Rate determining processes of sea ice growth. Ann. Glaciol. 6, 168–170.
Lin, C.Y., Pan, J.Y., 2001. The effects of sodium sulfate on the emissions characteristics of an emulsified marine diesel oil-fired furnace. Ocean Eng. 28 (4), 347–360.
Liu, L, Miyawaki, O., Nakamura, K., 1997. Progressive freeze concentration of model liquid. Food Sci. Technol. Int. 3 (4), 348–352.
Lorain, O., Thiebaud, P., Badorc, E., Aurelle, Y., 2001. Potential of freezing in wastewater treatment: soluble pollutant applications. Water Res. 35 (2), 541–547.
Louhi-Kultanen, M., Silventoinen, I., Palosaari, S., 1988. Purification of organic chemicals by zone melting. Acta Polytech. Scand., Chem. Technol. Ser. 182, 3–24.
Louhi-Kultanen, M., 1996. Concentration and purification by crystallization. Acta Polytech. Scand., Chem. Technol. Ser. 241, 1–112.
Magalhaes, M.C.F., Konigsberger, E., May, P.M., Hefter, G., 2002. Heat capacities of concentrated aqueous solutions of sodium sulfate, sodium carbonate, and sodium hydroxide at 25 °C. J. Chem. Eng. Data 47 (3), 590–598.
Ozbek, H., Phillips, S.L., 1980. Thermal conductivity of aqueous sodium chloride solutions from 20 to 330 °C. J. Chem. Eng. Data 25 (3), 263–267.
Osborne, N.S., Stimson, H.F., Ginning, D.C., 1939. Measurements of heat capacity and heat of vaporization of water in the range 0° to 100 °C. J. Res. Natl. Bur. Stand. 23, 197–260.
Osborne, N.S., 1939. Heat of fusion of ice—a revision. J. Res. Natl. Bur. Stand. 23, 643–646.
Petrich, C., Eicken, H., 2009. Growth, Structure and Properties of Sea Ice, in Sea Ice. In: Thomas, D.N., Dieckmann, G.S. (Eds.), second ed. Wiley-Blackwell, Oxford, UK.

Primo, O., Rivero, M.J., Urtiaga, A.M., Ortiz, I., 2008. Nitrate removal from electro-oxidized landfill leachate by ion exchange. J. Hazard. Mater. 164 (1), 389–393.
Pronk, P., Ferreira, C.A.I., Witkamp, G.J., 2006. Influence of solute type and concentration on ice scaling in fluidized bed ice crystallizers. Chem. Eng. Sci. 61 (13), 4354–4362.
Pronk, P., 2007. Fluidized Bed Heat Exchangers to Prevent Fouling in Ice Slurry Systems and Industrial Crystallizers (Ph.D. Dissertation). Delft University of Technology, The Netherlands.
Randall, D.G., Lewis, A.E., 2009. Seeding for selective salt recovery during Eutectic Freeze Crystallization. In: International Mine Water Conference, 19–22 October, Pretoria, South Africa, pp. 639–646.
Rard, J.A., Miller, D.G., 1979. The Mutual diffusion coefficients of Na_2SO_4–H_2O and $MgSO_4$–H_2O at 25 °C from Rayleigh interferometry. J. Sol. Chem. 8 (10), 756–765.
Silva, R., Cadorin, L., Rubio, J., 2010. Sulphate ions removal from an aqueous solution: I. Co-precipitation with hydrolysed aluminum-bearing salts. Miner. Eng. 23 (15), 1220–1226.
Terwilliger, J.P., Dizio, S.F., 1970. Salt rejection phenomena in the freezing of saline solutions. Chem. Eng. Sci. 25 (8), 1331–1349.
Weeks, W.F., Lofgren, G., 1967. The effective solute distribution coefficient during the freezing of NaCl solutions (International Conference on Low Temperature Science Proceedings). Phys. Snow Ice 1 (1), 579–597.

Publication III

Partanen, J. I., Hasan, M., Vahteristo, K.P., Louhi-Kultanen, M.,

Determination of the Pitzer interaction parameters at 273.15 K from the freezing-point data available for solutions of uni-univalent electrolytes.

Reprinted with permission from
Industrial and Engineering Chemistry Research
Vol. 53, pp. 19351–19358, 2014

I&EC research
Industrial & Engineering Chemistry Research

Article

pubs.acs.org/IECR

Determination of the Pitzer Interaction Parameters at 273.15 K from the Freezing-Point Data Available for Solutions of Uni-Univalent Electrolytes

Jaakko I. Partanen,* Mehdi Hasan, Kari P. Vahteristo, and Marjatta Louhi-Kultanen

Department of Chemical Technology, Lappeenranta University of Technology, P.O. Box 20, FIN-53851 Lappeenranta, Finland

Supporting Information

ABSTRACT: A novel calculation method (see the article in *Ind. Eng. Chem. Res.* **2014**, *53*, 5608−5616) was applied in this work to evaluate the ion interaction parameters for the Pitzer model from freezing points of aqueous solutions of pure electrolytes. The freezing-point depression data from aqueous solutions of salts consisting of chloride, bromide, nitrate, chlorate, perchlorate, formate, and acetate ions as anions and lithium, sodium, and potassium ions as cations were used in the present study. The literature data from the research group of Scatchard (*J. Am. Chem. Soc.* **1932**, *54*, 2676−2695; **1933**, *55*, 4355−4362; and **1934**, *56*, 805−811) were available for the calculations. Additionally, the parameters for salts of ammonium ion with chloride, bromide, iodide, and nitrate ions were determined but the data of this group (*J. Am. Chem. Soc.* **1932**, *54*, 2696−2705) are probably not reliable in these cases. The parameter values obtained using this method for solutions of the other salts than those of ammonium salts predict more accurately the experimental data than the ordinarily used Pitzer parameters and their temperature derivatives. Up to a molality of 0.5 mol·kg^{-1} in the former case, the errors are usually less than ±0.001 K, but in the latter case, they can be as high as ±0.02 K. The ordinarily used parameter values have been most often determined using calorimetric measurements.

INTRODUCTION

In a previous study,[1] the parameter values for the Pitzer equations at 273.15 K have been determined for sodium and potassium chloride solutions using freezing-point depression data, and the resulting values were tested with all relevant thermodynamic data available in the literature. Also, new calculations methods were developed in this connection and tested comprehensively. As explained in that study,[1] many new and promising technical processes have been recently developed where the accurate calculation of freezing-points in solutions is decisive. The calculation methods developed in the previous study for NaCl and KCl solutions are comparable in accuracy with the best thermodynamic methods available for all temperatures in dilute solutions. It is additionally probable that the equations of these methods can be extended by adding in a reasonable way new parameters into these equations when more concentrated solutions or even mixtures of concentrated solutions are considered in practical problems encountered in industrial process development. Of course in these connections, the accuracy and theoretical requirements are not as high as they are in the previous study. The accuracy requirement cannot be satisfied in the concentrated solutions because the freezing points in these solutions are much below zero degrees Celsius where pure water is not thermodynamically stable as liquid. This problem was considered in detail in ref 1. The models like those determined in this reference can serve as the accurate limiting models for dilute solutions in the new parametrization procedures necessary for the more complex systems. In that reference, additionally, the freezing points in the sets[2] used in the parameter estimation were compared with those obtained with the commonly used Pitzer parameters together with their temperature dependencies. In the present study, all of these calculations were made and reported with the other precise freezing point data available in the literature for solutions of uni-univalent electrolytes. Most of these data have been measured by the research group of Scatchard.[2−7] The freezing-point sets reported in these studies cover uniformly for almost all of the electrolytes tested with very many points the molality range from 0 to about 1.3 mol·kg^{-1}, and the precision of the data seem to be in most cases better than ±0.001 K. Some preliminary results[8] of the new calculations for $NaNO_3$, KNO_3, and NH_4NO_3 solutions were already presented in the 20th International Workshop on Industrial Crystallization (BIWIC 2013).

THEORY

In ref 1, it was shown that the following equation is valid at the freezing point T_f of an electrolyte solution

$$-R\ln a_A = y = \Delta H^*\left(\frac{1}{T_f} - \frac{1}{T_f^*}\right) + \Delta C_{p,m}\left[\frac{(T_f - T_f^*)}{T_f} - \ln\left(\frac{T_f}{T_f^*}\right)\right] \quad (1)$$

where A refers to the solvent (water in this case), T_f^* is the freezing point of pure solvent (asterisk symbol, *), and a is the activity. Quantities ΔH^* and $\Delta C_{p,m}$ are defined by equations

$$\Delta H^* = \Delta H_{m,fus}(A, T_f^*) \quad (2)$$

Received: August 12, 2014
Revised: November 14, 2014
Accepted: November 14, 2014
Published: November 14, 2014

$$\Delta C_{p,m} = C^*_{p,m}(A, l) - C^*_{p,m}(A, s) \quad (3)$$

where $\Delta H_{m,fus}(A, T_f^*)$ is the enthalpy of the fusion at T_f^* and $C_{p,m}$ refers to the molar heat capacity at a constant pressure. As earlier,[1] the following values for these quantities were used: ΔH^* = 6009.5 J·mol^{-1} (Osborne et al.[9]), and ΔC_p = 37.87 J·K^{-1}·mol^{-1} (Osborne[10] and Osborne et al.[9]), and the latter value can be regarded as a constant up to a salt molality of about 0.5 mol·kg^{-1}. In eq 1, it is possible to calculate directly the values of quantity y from the experimental freezing point data. The freezing point depression (ΔT_f) is defined in the following ordinary way

$$\Delta T_f = T_f^* - T_f \quad (4)$$

The definition of the osmotic coefficient of the solvent (ϕ) is based on the solvent activity in solutions of a uni-univalent electrolyte as follows:

$$\ln a_A = -2mM_A\phi \quad (5)$$

where m is the molality of the solution and M_A is the molar mass of solvent (for water it is 0.018015 kg·mol^{-1}). The following equation can be derived for ΔT_f:

$$\Delta T_f = \frac{2RT_f^{*}M_A m\phi}{2RM_A m\phi + \frac{\Delta H^*}{T_f^*}} + \frac{\Delta C_{p,m}\Delta T_f + \Delta C_{p,m}(T_f^* - \Delta T_f)\ln\left(\frac{T_f^* - \Delta T_f}{T_f^*}\right)}{2RM_A m\phi + \frac{\Delta H^*}{T_f^*}} \quad (6)$$

This equation requires iterative calculations and it was presented for the first time for the thermodynamic considerations of NaCl solutions based on the more empirical Hückel equation to describe the nonideality.[11]

In the present study, the Pitzer equations are used in the treatment of nonideality. For the osmotic coefficient in an aqueous solution of a uni-univalent electrolyte, the Pitzer equation[12,13] has the form

$$\phi = 1 - \frac{A_\varphi\sqrt{m}}{1 + b\sqrt{m}} + (\beta^0 + \beta^1 e^{-\alpha\sqrt{m}})(m/m^o) + C^\phi(m/m^o)^2 \quad (7)$$

where m^o = 1 mol·kg^{-1} and A_ϕ is the Debye−Hückel constant which depends on the temperature. According to Archer and Wang,[14] its value at 273.15 K and at 101.325 kPa is 0.37642 (mol·kg^{-1})$^{-1/2}$. The following common Pitzer parameter values are now used in eq 7: b = 1.2 (mol·kg^{-1})$^{-1/2}$ and α = 2.0 (mol·kg^{-1})$^{-1/2}$. In this equation, β^0, β^1, and C^ϕ are the parameters that depend on the electrolyte, and they were determined in the present study for 273.15 K for solutions of uni-univalent electrolytes. In the literature are given Pitzer parameters and their temperature dependencies for many uni-univalent electrolytes. The most important Pitzer parameter values at 298.15 K (i.e., those determined by Pitzer and Mayorga[13]) are additionally presented in Table S1, and this table is given in Supporting Information. Also, the temperature dependencies of these parameters are included in the table when available. These derivatives have been determined by Silvester and Pitzer.[15] Based on these values, the resulting Pitzer parameter values at 273.15 K were obtained by using the linear relationship and they are also given in Supporting Information Table S1.

RESULTS AND DISCUSSION

Determination of Pitzer Parameters for Dilute Solutions and Tests of the Resulting Equation. In dilute solutions, eq 7 is valid without the C^ϕ term and the parameters for the tested electrolytes are first determined for the case. It was shown in ref 1 that the resulting two-parameter equation applies up to a molality of 0.5 mol·kg^{-1}. The following method was used in this determination, as in that article: to solve experimental β^0 values, it is possible to arrange eq 7 without the C^ϕ term in the following form using eq 5 and quantity y in eq 1

$$\beta^0 = \frac{ym^o}{2RM_A m^2} - \frac{m^o}{m} + \frac{A_\varphi m^o}{\sqrt{m}(1 + b\sqrt{m})} - \beta^1 e^{-\alpha\sqrt{m}} \quad (8)$$

The data from the research group of Scatchard (see refs 2−7) were used in the parameter estimation and these data for all electrolytes are similar to those of Scatchard and Prentiss[2] used in ref 1 for NaCl and KCl solutions. The results and the range of the experimental points included in the determination are given in Supporting Information as Table S2. For the calculations based on eq 8, the value of parameter β^1 was estimated as in ref 1: the value was chosen that gives the least value for the standard deviation about the mean of the experimental β^0 values. In several cases, the two-parameter model is only needed because all data can be explained quite well with the model.

The β^0 values obtained in this way for NaBr solutions[2] and for NH_4NO_3 solutions[5] from the data of Scatchard and Prentiss are not sufficiently constant for a reliable determination. This is shown in Figure 1 where the β^0 values in a reasonable range are

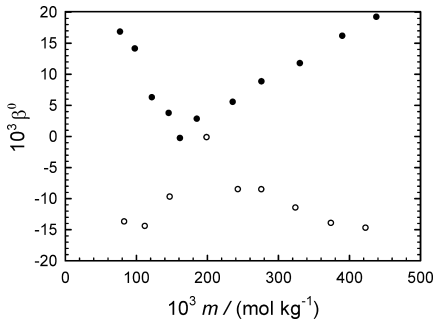

Figure 1. Values of Pitzer parameter β^0 obtained from eq 8 as a function of molality m from the freezing point depression sets of NaBr (symbol ●) and NH_4NO_3 (○) of Scatchard and Prentiss (refs 2 and 5, respectively) in the case where the following best values are used for parameter β^1: 0.489 (NaBr) and −0.062 (NH_4NO_3).

shown as a function of the molality in the case where the best value of parameter β^1 is used for both salt. Therefore, the results of these two salts are not considered here further. Additionally, the nonideality results reported in ref 8 for NH_4NO_3 solutions at 273.15 K are not reliable, as also suspected in that paper. The experimental freezing point depressions for the other sets reported by Scatchard et al. were then reproduced with the new models using eqs 6 and 7. The errors calculated by

$$e_T = \Delta T_f(\text{observed}) - \Delta T_f(\text{predicted}) \quad (9)$$

are then presented as a function of the molality. The resulting error plots for all salts up to a molality of about 0.3 mol·kg^{-1} are shown in graphs A of Figures 2 to 8 for alkali metal chlorides,

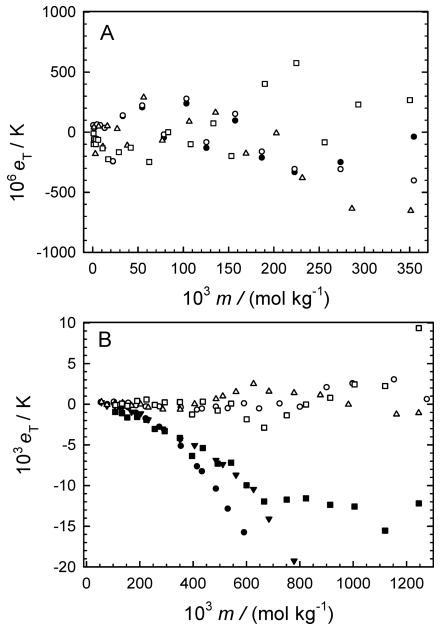

Figure 2. Plot of e_T (eq 9), the deviation between the observed and predicted freezing-point depressions in NaCl, KCl, and LiCl solutions as a function of molality m. The observed values have been measured by Scatchard and Prentiss[2] and the predicted values were determined from eq 6 where either the two-parameter Pitzer equation (eq 7 without the C^ϕ term) or the three-parameter Pitzer equation (eq 7) was used for the osmotic coefficients. Graph A shows the results for dilute solutions and graph B for less dilute solutions. Symbols for graph A: ●, NaCl, the new two-parameter equation where $\beta^0 = 0.0396$ and $\beta^1 = 0.2801$ (Supporting Information Table S2); ○, NaCl, the new three-parameter equation where $\beta^0 = 0.0379$, $\beta^1 = 0.2801$, and $C^\phi = 0.00698$ (Supporting Information Table S3); △, KCl, the new equation where $\beta^0 = 0.0239$ and $\beta^1 = 0.1919$ (Supporting Information Table S2); □, LiCl, the new equation where $\beta^0 = 0.1612$ and $\beta^1 = 0.243$ (Supporting Information Table S2). Symbols for graph B: ●, NaCl, the literature equation where $\beta^0 = 0.0586$, $\beta^1 = 0.2489$, and $C^\phi = 0.00391$ (Supporting Information Table S1); ○, NaCl, the new three-parameter eq (Supporting Information Table S3); ▼, KCl, the literature equation where $\beta^0 = 0.03386$, $\beta^1 = 0.1854$, and $C^\phi = 0.000434$ (Supporting Information Table S1); △, KCl, the new eq (Supporting Information Table S2); ■, LiCl, the literature equation where $\beta^0 = 0.1536$, $\beta^1 = 0.2940$, and $C^\phi = 0.00472$ (Supporting Information Table S1); □, LiCl, the new eq (Supporting Information Table S2). For KCl and LiCl solutions, only the two-parameter equations were estimated in this study.

bromides, nitrates, chlorates, perchlorates, formates, and acetates, respectively. Graph A in Figure 9 contains the results for ammonium salts in dilute solutions. The parameter values used in the calculations are given in the captions of the figures (in addition to in Supporting Information Table S2). This applies later also to all parameters used in the determination of the errors for the plots in Figures 2 to 9. These plots in all eight figures

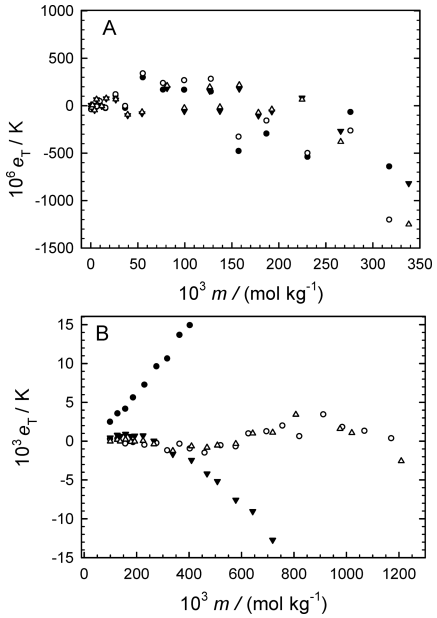

Figure 3. Plot of e_T (eq 9), the deviation between the observed and predicted freezing-point depressions in LiBr and KBr solutions as a function of molality m. The observed values have been measured by Scatchard and Prentiss[2] and the predicted values were determined from eq 6 where either the two-parameter Pitzer equation (eq 7 without the C^ϕ term) or the three-parameter Pitzer equation (eq 7) was used for the osmotic coefficients. Graph A shows the results for dilute solutions and graph B for less dilute solutions. Symbols for graph A: ●, LiBr, the new two-parameter equation where $\beta^0 = 0.163$ and $\beta^1 = 0.387$ (Supporting Information Table S2); ○, LiBr, the new three-parameter equation where $\beta^0 = 0.1583$, $\beta^1 = 0.387$, and $C^\phi = 0.0195$ (Supporting Information Table S3); ▼, KBr, the new two-parameter equation where $\beta^0 = 0.0138$ and $\beta^1 = 0.250$ (Supporting Information Table S2); △, KBr, the new three-parameter equation where $\beta^0 = 0.0121$, $\beta^1 = 0.250$, and $C^\phi = 0.0081$ (Supporting Information Table S3). Symbols for graph B: ●, LiBr, the literature equation where $\beta^0 = 0.1793$, $\beta^1 = 0.2381$, and $C^\phi = 0.006$ (Supporting Information Table S1); ○, LiBr, the new three-parameter eq (Supporting Information Table S3); ▼, KBr, the literature equation where $\beta^0 = 0.03843$, $\beta^1 = 0.1777$, and $C^\phi = -0.00005$ (Supporting Information Table S1); △, KBr, the new three-parameter eq (Supporting Information Table S3).

reveal that the new two-parameter Pitzer models generally apply well to the experimental data used in the estimation. Almost all absolute errors are smaller than ±0.001 K and they very often form a random pattern. In the dilute solutions considered in graphs A of Figures 2 to 9, the limit of an acceptable error for a model seems to be close to the value of ±0.001 K, but also the randomness of the pattern of errors is an important factor in this evaluation. The latter factor is more important than the limit in very dilute solutions where the freezing point depressions and also their errors are already small. Only the data for ammonium salts in Figure 9A do not, therefore, support clearly within their full precision the new Pitzer models in the molality range from (0 to 0.15) mol·kg^{-1}. It is well known that the data of Scatchard et al.[5] for ammonium salts are not reliable in dilute solutions, see for

dx.doi.org/10.1021/ie503201m | Ind. Eng. Chem. Res. 2014, 53, 19351−19358

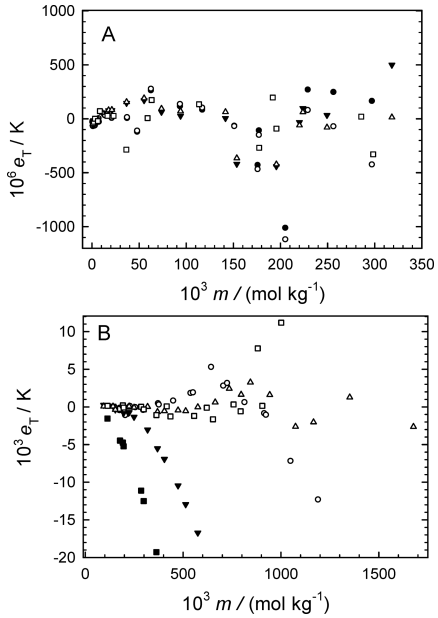

Figure 4. Plot of e_T (eq 9), the deviation between the observed and predicted freezing-point depressions in $LiNO_3$, $NaNO_3$, and KNO_3 solutions as a function of molality m. The observed values have been measured by Scatchard and Prentiss[4] and the predicted values were determined from eq 6 where either the two-parameter Pitzer equation (eq 7 without the C^ϕ term) or the three-parameter Pitzer equation (eq 7) was used for the osmotic coefficients. Graph A shows the results for dilute solutions and graph B for less dilute solutions. Symbols for graph A: ●, $LiNO_3$, the new two-parameter equation where $\beta^0 = 0.118$ and $\beta^1 = 0.348$ (Supporting Information Table S2); ○, $LiNO_3$, the new three-parameter equation where $\beta^0 = 0.1163$, $\beta^1 = 0.348$, and $C^\phi = 0.0121$ (Supporting Information Table S3); ▼, $NaNO_3$, the new two-parameter equation where $\beta^0 = -0.055$ and $\beta^1 = 0.196$ (Supporting Information Table S2); △, $NaNO_3$, the new three-parameter equation where $\beta^0 = -0.0574$, $\beta^1 = 0.196$, and $C^\phi = 0.0116$ (Supporting Information Table S3); □, KNO_3, the new equation where $\beta^0 = -0.129$ and $\beta^1 = -0.098$ (Supporting Information Table S2). Symbols for graph B: ○, $LiNO_3$, the new three-parameter eq (Supporting Information Table S3); ▼, $NaNO_3$, the literature equation where $\beta^0 = -0.02485$, $\beta^1 = 0.1268$, and $C^\phi = 0.00507$ (Supporting Information Table S1); △, $NaNO_3$, the new three-parameter eq (Supporting Information Table S3); ■, KNO_3, the literature equation where $\beta^0 = -0.08675$, $\beta^1 = -0.11185$, and $C^\phi = -0.00333$ (Supporting Information Table S1); □, KNO_3, the new eq (Supporting Information Table S2). For KNO_3, only the two-parameter equation was estimated in the present study.

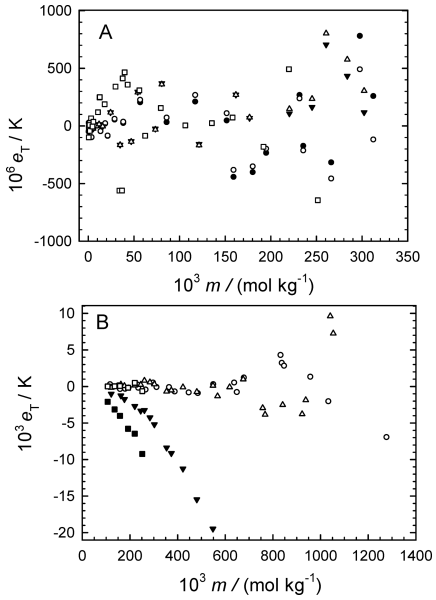

Figure 5. Plot of e_T (eq 9), the deviation between the observed and predicted freezing-point depressions in $LiClO_3$, $NaClO_3$, and $KClO_3$ solutions as a function of molality m. The observed values have been measured by Scatchard et al.[6] and the predicted values were determined from eq 6 where either the two-parameter Pitzer equation (eq 7 without the C^ϕ term) or the three-parameter Pitzer equation (eq 7) was used for the osmotic coefficients. Graph A shows the results for dilute solutions and graph B for less dilute solutions. Symbols for graph A: ●, $LiClO_3$, the new two-parameter equation where $\beta^0 = 0.136$ and $\beta^1 = 0.373$ (Supporting Information Table S2); ○, $LiClO_3$, the new three-parameter equation where $\beta^0 = 0.1339$, $\beta^1 = 0.373$, and $C^\phi = 0.0110$ (Supporting Information Table S3); ▼, $NaClO_3$, the new two-parameter equation where $\beta^0 = -0.0149$ and $\beta^1 = 0.195$ (Supporting Information Table S2); △, $NaClO_3$, the new three-parameter equation where $\beta^0 = -0.0142$, $\beta^1 = 0.195$, and $C^\phi = -0.004$ (Supporting Information Table S3); □, $KClO_3$, the new equation where $\beta^0 = -0.1500$ and $\beta^1 = 0.081$ (Supporting Information Table S2). Symbols for graph B: ○, $LiClO_3$, the new three-parameter eq (Supporting Information Table S3); ▼, $NaClO_3$, the literature equation where $\beta^0 = -0.000975$, $\beta^1 = 0.19783$, and $C^\phi = 0.002723$ (Supporting Information Table S1); △, $NaClO_3$, the new three-parameter eq (Supporting Information Table S3); ■, $KClO_3$, the literature equation where $\beta^0 = -0.1457$ and $\beta^1 = 0.1686$ (Supporting Information Table S1); □, $KClO_3$, the new eq (Supporting Information Table S2). For $KClO_3$, only the two-parameter equation was estimated in this study. The errors of the points ($m = 1.1684$ mol·kg^{-1}, $\Delta T_f = 3.60888$ K) and (1.2852, 3.95484) for the new equation in the $NaClO_3$ set are outside the scale of graph B. These errors are 0.02131 and 0.04139 K, respectively.

example the textbook of Harned and Owen.[16] In the present study, the parameters were not estimated from the data of very dilute solutions, and therefore, these parameters were also tested using data from other sources. Garnsey and Prue[17] measured freezing points for dilute NH_4Cl and NH_4Br solutions (33 and 23 points, respectively), but these data extend only up to a molality of 0.1 mol·kg^{-1}. Using the new parameter values, these data were predicted and the results are shown as error plots in graph B of Figure 9. Also the parameter values of Pitzer and Mayorga[13] at 298.15 K for these electrolytes were included in the calculations and the results are shown in this graph. In general, the data from these very dilute solutions can be usually predicted well also with the Pitzer parameters at 298.15 K. In the present case, according to Figure 9B, the freezing points from ref 17 can be predicted in a much better way with the parameters at 298.15 K than with the new Pitzer parameters determined for 273.15 K in the present study. These new parameters are not reliable, and therefore, the ammonium salt data are not considered here further.

dx.doi.org/10.1021/ie503201m | Ind. Eng. Chem. Res. 2014, 53, 19351−19358

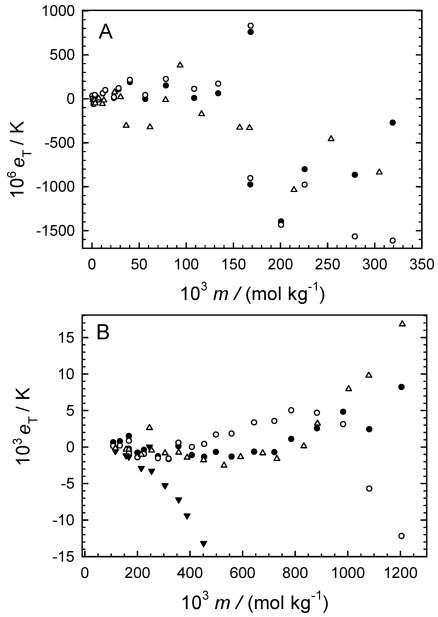

Figure 6. Plot of e_T (eq 9), the deviation between the observed and predicted freezing-point depressions in $LiClO_4$ and $NaClO_4$ solutions as a function of molality m. The observed values have been measured by Scatchard et al.[6] and the predicted values were determined from eq 6 where either the two-parameter Pitzer equation (eq 7 without the C^ϕ term) or the three-parameter Pitzer equation (eq 7) was used for the osmotic coefficients. Graph A shows the results for dilute solutions and graph B for less dilute solutions. Symbols for graph A: ●, $LiClO_4$, the new two-parameter equation where $\beta^0 = 0.1654$ and $\beta^1 = 0.469$ (Supporting Information Table S2); ○, $LiClO_4$, the new three-parameter equation where $\beta^0 = 0.1600$, $\beta^1 = 0.469$, and $C^\phi = 0.028$ (Supporting Information Table S3); △, $NaClO_4$, the new equation where $\beta^0 = 0.0025$ and $\beta^1 = 0.244$ (Supporting Information Table S2). Symbols for graph B: ●, $LiClO_4$, the literature equation where $\beta^0 = 0.1963$, $\beta^1 = 0.3821$, and $C^\phi = 0.00273$ (Supporting Information Table S1); ○, $LiClO_4$, the new three-parameter eq (Supporting Information Table S3); ▼, $NaClO_4$, the literature equation where $\beta^0 = 0.023$, $\beta^1 = 0.2181$, and $C^\phi = 0.00288$ (Supporting Information Table S1); △, $NaClO_4$, the new eq (Supporting Information Table S2). For $NaClO_4$, only the two-parameter equation was estimated in the present study. The error of the point ($m = 0.24548$ mol·kg^{-1}, $\Delta T_f = 0.82938$ K) for the new equation in the $NaClO_4$ set is outside the scale of graph A. This error is 0.00262 K.

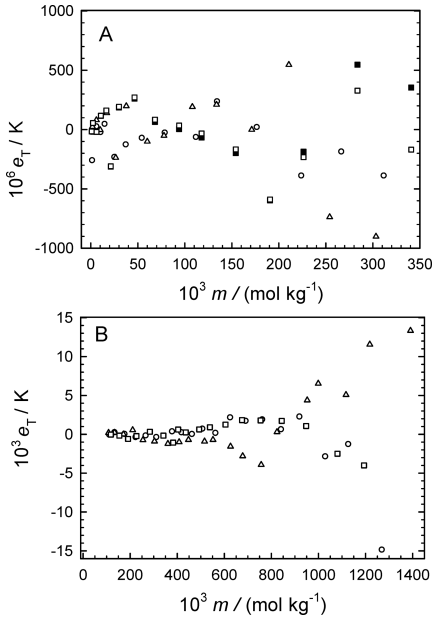

Figure 7. Plot of e_T (eq 9), the deviation between the observed and predicted freezing-point depressions in lithium, sodium, and potassium formate solutions as a function of molality m. The observed values have been measured by Scatchard and Prentiss[7] and the predicted values were determined from eq 6 where either the two-parameter Pitzer equation (eq 7 without the C^ϕ term) or the three-parameter Pitzer equation (eq 7) was used for the osmotic coefficients. Graph A shows the results for dilute solutions and graph B for less dilute solutions. Symbols for graph A: ○, Li formate, the new equation where $\beta^0 = 0.0751$ and $\beta^1 = 0.221$ (Supporting Information Table S2); △, Na formate, the new equation where $\beta^0 = 0.0482$ and $\beta^1 = 0.323$ (Supporting Information Table S2); ■, K formate, the new two-parameter equation where $\beta^0 = 0.0605$ and $\beta^1 = 0.337$ (Supporting Information Table S2); □, K formate, the new three-parameter equation where $\beta^0 = 0.0589$, $\beta^1 = 0.337$, and $C^\phi = 0.0084$ (Supporting Information Table S3). Symbols for graph B: ○, Li formate, the new eq (Supporting Information Table S2); △, Na formate, the new eq (Supporting Information Table S2); □, K formate, the new three-parameter eq (Supporting Information Table S3). For Li and Na formate, only the two-parameter equations were estimated in the present study.

Determination of Pitzer Parameters for Less Dilute Solutions and Tests of the Resulting Equation. In the less dilute solutions, the following equation is valid for parameter β^0

$$\beta^0 = \frac{ym^\circ}{2RM_A m^2} - \frac{m^\circ}{m} + \frac{A_\varphi m^\circ}{\sqrt{m}(1 + b\sqrt{m})} - \beta^1 e^{-\alpha\sqrt{m}} - \frac{C^\phi m}{m^\circ} \quad (10)$$

This equation is used here in the determination of the Pitzer parameters from the data of Scatchard group for more concentrated solutions in case the two-parameter equation is not satisfactory for these solutions. In the evaluations, as earlier,[1] it is first assumed that parameter β^1 has the same value as that used for dilute solutions (see Supporting Information Table S2) for each salt. The experimental points from the lower limit in Supporting Information Table S2 to the strongest solution available was usually included in the determination for each case. The value of parameter C^ϕ was chosen in the same way as earlier,[1] that is, the value was taken that gives the least value for the standard deviation about the mean of the experimental β^0 values. The results of this estimation are also given in Supporting Information Table S3, which consists of these parameter values. The standard deviation for the estimated β^0 parameters are also reported in the table. The new three-parameter Pitzer equations thus apply to all data given by Scatchard et al. (in the best case up to 1.7 mol·kg^{-1}), but theoretically, the two-parameter Pitzer equations (see Supporting Information Table S2) are better

dx.doi.org/10.1021/ie503201m | Ind. Eng. Chem. Res. 2014, 53, 19351−19358

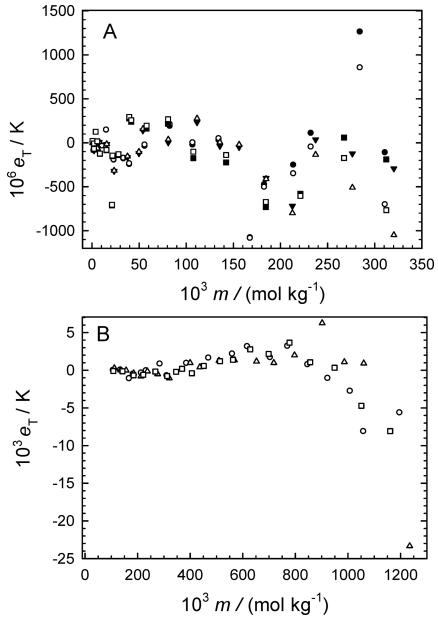

Figure 8. Plot of e_T (eq 9), the deviation between the observed and predicted freezing-point depressions in lithium, sodium, and potassium acetate solutions as a function of molality m. The observed values have been measured by Scatchard and Prentiss[7] and the predicted values were determined from eq 6 where either the two-parameter Pitzer equation (eq 7 without the C^ϕ term) or the three-parameter Pitzer equation (eq 7) was used for the osmotic coefficients. Graph A shows the results for dilute solutions and graph B for less dilute solutions. Symbols for graph A: ●, Li acetate, the new two-parameter equation where $\beta^0 = 0.1141$ and $\beta^1 = 0.284$ (Supporting Information Table S2); ○, Li acetate, the new three-parameter equation where $\beta^0 = 0.1123$, $\beta^1 = 0.284$, and $C^\phi = 0.0111$ (Supporting Information Table S3); ▼, Na acetate, the new two-parameter equation where $\beta^0 = 0.1062$ and $\beta^1 = 0.428$ (Supporting Information Table S2); △, Na acetate, the new three-parameter equation where $\beta^0 = 0.1037$, $\beta^1 = 0.428$, and $C^\phi = 0.014$ (Supporting Information Table S3); ■, K acetate, the new two-parameter equation where $\beta^0 = 0.1335$ and $\beta^1 = 0.412$ (Supporting Information Table S2); □, K acetate, the new three-parameter equation where $\beta^0 = 0.1301$, $\beta^1 = 0.412$, and $C^\phi = 0.016$ (Supporting Information Table S3). Symbols for graph B: ○, Li acetate, the new three-parameter eq (Supporting Information Table S3); △, Na acetate, the new three-parameter eq (Supporting Information Table S3); □, K acetate, the new three-parameter eq (Supporting Information Table S3).

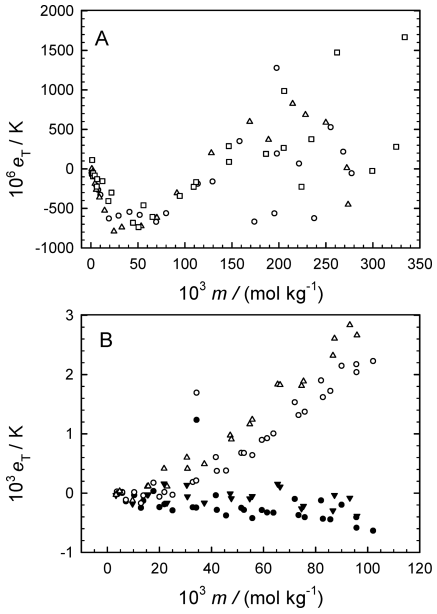

Figure 9. Plot of e_T (eq 9), the deviation between the observed and predicted freezing-point depressions in NH_4Cl, NH_4Br, and NH_4I solutions as a function of molality m. The observed values have been measured by Scatchard et al.[5] (graph A) and Garnsey and Prue[17] (graph B) and the predicted values were determined from eq 6 where either the two-parameter Pitzer equation (eq 7 without the C^ϕ term) or the literature Pitzer equation of Pitzer and Mayorga for 298.15 K (see Supporting Information Table S1 and eq 7) was used for the osmotic coefficients. Symbols for graph A: ○, NH_4Cl, the new equation where $\beta^0 = 0.0778$ and $\beta^1 = 0.003$ (Supporting Information Table S2); △, NH_4Br, the new equation where $\beta^0 = 0.1164$ and $\beta^1 = -0.072$ (Supporting Information Table S2); □, NH_4I, the new equation where $\beta^0 = 0.0456$ and $\beta^1 = 0.19$ (Supporting Information Table S2). Symbols for graph B: ●, NH_4Cl, the literature equation where $\beta^0 = 0.0522$, $\beta^1 = 0.1918$, and $C^\phi = -0.00301$ (Supporting Information Table S1); ○, NH_4Cl, the new eq (Supporting Information Table S2); ▼, NH_4Br, the literature equation where $\beta^0 = 0.0624$, $\beta^1 = 0.1947$, and $C^\phi = -0.00436$ (Supporting Information Table S1); △, NH_4Br, the new eq (Supporting Information Table S2). The points ($m = 0.02698$ mol·kg^{-1}, $\Delta T_f = 0.0914$ K) and (0.00843, 0.0339) in the NH_4Cl and NH_4Br sets, respectively, have been omitted as outliers in graph B.

because the parameters of these equations are associated closely with the temperature of 273.15 K (see above) and describe only the interactions between species at this constant temperature.

The new parameter values were first tested using in different sets the same points as those used for the two-parameter models, and these results are shown in graphs A of Figures 2 to 8. The two- and three-parameter models give almost the same results in these dilute solutions. In the case of the more concentrated solutions, the resulting error plots for the sets[2−7] used in the parameter estimation are shown in graphs B of Figures 2 to 8. These plots reveal that the new Pitzer models apply well to these data because almost all absolute errors are smaller than ±0.003 K. In the case of the results for the less dilute solutions in these graphs, the larger error limit is acceptable because the freezing point depressions in those are larger.

The values of the Pitzer parameters at 273.15 K from Silvester and Pitzer,[15] based on calorimetric data, are shown in Supporting Information Table S1. These values were also tested with the data of Scatchard's group in the same way as the new parameter values. The results are shown in graphs B of Figures 2 to 6. According to these graphs, the Pitzer parameters determined for 273.15 K using the calorimetric data from the values of Pitzer and Mayorga at 298.15 K do not explain the freezing point data of the Scatchard's group well. The only exceptions are the LiCl data in Figure 2 and the $LiClO_4$ data in Figure 6. In general, the present freezing point data seem to be very precise (despite of problems with solutions of some salts considered above) and the high-precision freezing point data (where the experimental errors are

often quite close to ±0.0001 K) give the thermodynamic quantities (as if they are isothermally determined) at 273.15 K within their full precision up to about 0.5 mol·kg^{-1}. Therefore, it is clear that the calorimetric data (where results from various temperatures are needed) cannot compete in accuracy with these data, and the temperature dependence of the Pitzer parameters can be determined much more accurately from these data than from the calorimetric data. The temperature derivatives of the Pitzer parameters were based here on the values of Pitzer and Mayorga[13] at 298.15 K and on the new values at 273.15 K, and these values are given in Supporting Information Table S1. Recently, also, the parameter values of Pitzer and Mayorga at 298.15 K have been critically tested with the traceable Hückel parameters for different uni-univalent electrolytes.[18−24] In the most cases, the Pitzer parameters at 298.15 K apply well to the experimental data available for the different salts. In Supporting Information Table S1 are also given the citations to these Pitzer parameter tests for the salt solutions considered in the table.

Recommended Freezing Point Depressions. On the basis of the evidence provided by the tests of the present study (see Figures 2 to 8), the suggested Pitzer parameters explain well the freezing point depressions available for most salt solutions considered. The exception are the results for NaBr, NH_4Cl, NH_4Br, NH_4I, and NH_4NO_3 solutions. The freezing point depressions for NaCl and KCl solutions have been tabulated in ref 1. New tables of these values for the other salts at rounded molalities are given in Supporting Information of the present study. Supporting Information Table S4 contains there the results for LiCl, LiBr, KBr, $LiNO_3$, $NaNO_3$, and KNO_3. In Supporting Information Table S5 are presented the ΔT_f values for $LiClO_3$, $NaClO_3$, $KClO_3$, $LiClO_4$, and $NaClO_4$, and finally in Supporting Information Table S6 for lithium, sodium, and potassium formates and acetates. The values in these tables were based on the new three-parameter Pitzer equations. It was shown in graphs A of Figures 2 to 7 that the two-parameter Pitzer equation gives in dilute solutions almost the same values as those tabulated. The freezing points were also determined with the Pitzer parameters suggested in ref 8 for $NaNO_3$ and KNO_3 solutions (see Supporting Information Table S1). These freezing points are included in Supporting Information Table S4 and they are very close to the values recommended in this table.

CONCLUSIONS

Pitzer parameters for solutions of 17 uni-univalent electrolytes were determined here for 273.15 K by a new calculation method from the best freezing point data available in the literature. It was proved in ref 1 that the accuracy of the new two-parameter Pitzer equations are affected by no means by the fact that the freezing point data are not isothermal and these equations apply within experimental error up to a molality of 0.5 mol·kg^{-1}. The results obtained with the new Pitzer equations are compared to those obtained by the corresponding equations where the parameter values have been determined using calorimetric data from the values recommended for 298.15 K. The new parameter values apply much better to the data used here in the parameter estimation. Up to a molality of 0.5 mol·kg^{-1} in the case of the new parameters, the freezing-point depression errors are usually less than ±0.001 K, but in the case of the literature parameters, they can be as high as ±0.02 K. If these freezing-point data are high-precision data (as they seem to be for solutions of the most electrolytes considered here), the calorimetric data for these salt solutions are probably only semiquantitative and must be used with care in any mathematical treatment of chemical thermodynamics.

ASSOCIATED CONTENT

Supporting Information

Tables S1 to S6 as described in the text. This material is available free of charge via the Internet at http://pubs.acs.org/.

AUTHOR INFORMATION

Corresponding Author

*Fax: +358 5 411 7201. E-mail: jpartane@lut.fi.

Notes

The authors declare no competing financial interest.

ACKNOWLEDGMENTS

The authors are indebted to the Academy of Finland (Project No. 260141) and to the Graduate School and Research Foundation of Lappeenranta University of Technology for financial support.

REFERENCES

(1) Hasan, M.; Partanen, J. I.; Vahteristo, K. P.; Louhi-Kultanen, M. Determination of the Pitzer interaction parameters at 273.15 K from the freezing-point data available for NaCl and KCl solutions. *Ind. Eng. Chem. Res.* **2014**, *53*, 5608−5616.

(2) Scatchard, G.; Prentiss, S. S. The freezing points of aqueous solutions. IV. Potassium, sodium and lithium chlorides and bromides. *J. Am. Chem. Soc.* **1933**, *55*, 4355−4362.

(3) Scatchard, G.; Jones, P. T.; Prentiss, S. S. The freezing points of aqueous solutions. I. A freezing point apparatus. *J. Am. Chem. Soc.* **1932**, *54*, 2676−2690.

(4) Scatchard, G.; Prentiss, S. S.; Jones, P. T. The freezing points of aqueous solutions. II. Potassium, sodium and lithium nitrates. *J. Am. Chem. Soc.* **1932**, *54*, 2690−2695.

(5) Scatchard, G.; Prentiss, S. S. The freezing points of aqueous solutions. III. Ammonium chloride, bromide, iodide, nitrate, and sulfate. *J. Am. Chem. Soc.* **1932**, *54*, 2696−2705.

(6) Scatchard, G.; Prentiss, S. S.; Jones, P. T. The freezing points of aqueous solutions. V. Potassium, sodium and lithium chlorates and perchlorates. *J. Am. Chem. Soc.* **1934**, *56*, 805−807.

(7) Scatchard, G.; Prentiss, S. S. The freezing points of aqueous solutions. VI. Potassium, sodium and lithium formates and acetates. *J. Am. Chem. Soc.* **1934**, *56*, 807−811.

(8) Hasan, M.; Louhi-Kultanen, M. Determination of Pitzer parameters for 1−1 nitrate and 1−2 sulfate solutions from freezing point data. *Chem. Eng. Technol.* **2014**, *37*, 1340−1346.

(9) Osborne, N. S.; Stimson, H. F.; Ginnings, D. C. Measurements of heat capacity and heat of vaporization of water in the range 0 to 100 °C. *J. Res. Natl. Bur. Stand.* **1939**, *23*, 197−260.

(10) Osborne, N. S. Heat of fusion of ice. A revision. *J. Res. Natl. Bur. Stand.* **1939**, *23*, 643−646.

(11) Partanen, J. I.; Minkkinen, P. O. Activity and osmotic coefficients of dilute sodium chloride solutions at 273 K. *J. Chem. Eng. Data* **1991**, *36*, 432−435.

(12) Pitzer, K. S. Thermodynamics of electrolytes. I. Theoretical basis and general equations. *J. Phys. Chem.* **1973**, *77*, 268−277.

(13) Pitzer, K. S.; Mayorga, G. Thermodynamics of electrolytes. II. Activity and osmotic coefficients for strong electrolytes with one or both ions univalent. *J. Phys. Chem.* **1973**, *77*, 2300−2308.

(14) Archer, D. G.; Wang, P. The dielectric constant of water and Debye-Hückel limiting law slopes. *J. Phys. Chem. Ref. Data* **1990**, *19*, 371−411.

(15) Silvester, L. F.; Pitzer, K. S. Thermodynamics of electrolytes. X. Enthalpy and effects of temperature on the activity coefficients. *J. Solution Chem.* **1978**, *7*, 327−337.

(16) Harned, H. S.; Owen, B. B. *The Physical Chemistry of Electrolytic Solutions*, 3rd ed.; Reinhold Publishing Corporation: New York, 1958; pp 726−727.
(17) Garnsey, R.; Prue, J. E. Cryoscopic determination of osmotic coefficients for ammonium chloride and bromide. *Trans. Faraday Soc.* **1966**, *62*, 1265−1270.
(18) Partanen, J. I.; Covington, A. K. Re-evaluation of the thermodynamic activity quantities in aqueous sodium and potassium chloride solutions at 25 °C. *J. Chem. Eng. Data* **2009**, *54*, 208−219.
(19) Partanen, J. I. Re-evaluation of the thermodynamic activity quantities in aqueous lithium chloride solutions at 25 °C up to a molality of 6.0 mol·kg^{-1}. *J. Chem. Eng. Data* **2009**, *54*, 882−889.
(20) Partanen, J. I. Re-evaluation of the thermodynamic activity quantities in aqueous alkali metal bromide solutions at 25 °C. *J. Chem. Eng. Data* **2010**, *55*, 2202−2213.
(21) Partanen, J. I. Re-evaluation of the thermodynamic activity quantities in aqueous alkali metal nitrate solutions at T = 298.15 K. *J. Chem. Thermodyn.* **2010**, *42*, 1485−1493.
(22) Partanen, J. I. Re-evaluation of the thermodynamic activity quantities in pure aqueous solutions of chlorate, perchlorate, and bromate salts with lithium, sodium or potassium ions at 298.15 K. *J. Solution Chem.* **2012**, *41*, 271−293.
(23) Partanen, J. I.; Covington, A. K. Re-evaluation of the thermodynamic activity quantities in aqueous solutions of uni-univalent alkali metal salts of aliphatic carboxylic acids and thallium acetate at 25 °C. *J. Chem. Eng. Data* **2011**, *56*, 4524−4543.
(24) Partanen, J. I. Mean activity coefficients and osmotic coefficients in aqueous solutions of salts of ammonium ions with univalent anions at 25 °C. *J. Chem. Eng. Data* **2012**, *57*, 2654−2666.

Publication IV

Hasan, M., Louhi-Kultanen, M., 2014.

Determination of Pitzer Parameters for 1-1 Nitrate and 1-2 Sulfate Solutions from Freezing Point Data.

Reprinted with permission from
Chemical Engineering and Technology
Vol. 37, pp.1340–1346, 2014

Mehdi Hasan
Marjatta Louhi-Kultanen

Department of Chemical Technology, Lappeenranta University of Technology, Lappeenranta, Finland.

Determination of Pitzer Parameters for 1-1 Nitrate and 1-2 Sulfate Solutions from Freezing Point Data

Freezing point depression (FDP) modeling was performed for selected aqueous nitrate and sulfate salt solutions to evaluate Pitzer ion interaction parameter values at 273.15 K. 1-1 and 1-2 electrolyte solutions of $NaNO_3$, KNO_3, NH_4NO_3, Na_2SO_4, K_2SO_4, and $(NH_4)_2SO_4$ were studied. New Pitzer parameter values of β^0, β^1, and C^ϕ were obtained for the studied electrolyte solutions. FDP modeling was also used to determine temperature derivatives of interaction parameters for the Pitzer model for selected salt solutions. Osmotic and activity coefficients using the new parameter values are also presented.

Keywords: Freezing point depression, Freeze crystallization, Ion interaction parameter, Pitzer model, Solid-liquid equilibrium

Received: March 29, 2014; *revised:* May 09, 2014; *accepted:* May 12, 2014

DOI: 10.1002/ceat.201400202

1 Introduction

The freezing temperature of a pure solvent is depressed in the presence of electrolytes or other solutes. Freezing point depression (FPD) is one of the colligative properties of solvents, and higher electrolyte concentrations generally decrease the freezing point even further. FPD is correlated with the solute concentration by a proportional constant termed the cryoscopic constant, K_f ($K\,kg\,mol^{-1}$), in the case of an ideally dilute solution [1]. Different types of interactions between the constituent ions of the solution are the fundamental reason for deviations from the ideally dilute behavior of real solutions [2]. It is worthwhile to perform a critical analysis of various sets of electrolyte data for aqueous solutions over wide ranges of temperature and pressure to meet the needs of chemistry, chemical engineering, geochemistry, oceanography, boiler engineering [3], petroleum engineering [4], oil recovery systems [3], and food engineering [5]. Solid-liquid equilibria in electrolyte solutions are of crucial importance in industrial processes such as wastewater treatment, desalination, and crystallization [6, 7]. Accurate prediction of the freezing point is of vital importance in freeze concentration (FC) and eutectic FC (EFC), in which separation occurs on the basis of the freezing temperature of the solutions. EFC is considered a separation and concentration technique with great potential because of its ability to recover ice and salt crystals simultaneously, with high purities, by operating under eutectic conditions [8]. Precise models of the thermodynamic behavior in the phases of these systems will permit improved analysis, design, and optimization of processes and equipment [4]. The parameters of thermodynamic models of binary salt systems and mixed solutions are usually determined from very accurate experimental data, like FPD [9], isopiestic equilibrium [10], vapor pressure [11], and cell potential difference data [12–15]. The Pitzer virial-coefficient model to interpret thermodynamic properties of electrolyte solutions mostly uses osmotic and activity coefficient data at 298.15 K for parameterization. In order to obtain Pitzer parameters at temperatures lower than 298.15 K, e.g., at 273.15 K, the heat of solution and the heat of dilution are required, along with osmotic and activity coefficient data [16, 17]. This demand can be met by using only freezing point data of the electrolytes. Determination of the freezing temperature of a solution is a very accurate method and its accuracy is comparable with that of the isopiestic method. The fact that the method is not isothermal can be overlooked if only dilute solutions ($< 0.5\,mol\,kg^{-1}$) are taken into account, because the extent of FPD is very small within this range. Interaction parameters for the Pitzer model at 273.15 K have recently been determined for aqueous solutions of NaCl and KCl using freezing point data [18].

Sulfuric acid and nitric acid are commonly used as leaching agents in the mining and metallurgical industries, often resulting in effluents containing sulfate (SO_4^{2-}) and nitrate (NO_3^-) ions. Such effluents are considered a potential threat to the environment [19, 20]. EFC is a potential candidate for the treatment of SO_4^{2-}- and NO_3^--bearing effluents because it exhibits advantageous features compared with other possible approaches such as ion exchange and membrane separation techniques which require additional handling and disposal and are energy intensive and costly [21]. To enable utilization of EFC in process stream treatment of such solutions, precise prediction of

Correspondence: Mehdi Hasan (Mehdi.Hasan@lut.fi), Department of Chemical Technology, Lappeenranta University of Technology, P.O. Box 20, 53850 Lappeenranta, Finland.

the thermodynamics properties of the solutions is vital. In this study, $NaNO_3$, KNO_3, NH_4NO_3, Na_2SO_4, K_2SO_4, and $(NH_4)_2SO_4$ were chosen as model sulfate and nitrate solutions.

The present study determines parameters values for Pitzer equations at 273.15 K for the above nitrate and sulfate solutions using freezing point data available in the literature. The predicted freezing points in the sets used for parameter estimation are compared to those obtained with conventional Pitzer parameters, together with their temperature dependencies. Temperature derivatives of the Pitzer parameters are not available in the literature for ammonium sulfate and nitrate solutions. Hence, a significant outcome of the present work is the generation of associated temperature derivatives of these solutions based on the determination of Pitzer parameters at 273.15 K using freezing point data.

2 Theory

The solid-liquid equilibrium (SLE) model used in the present work equates the chemical potentials of the solvent and corresponding solid phase at the freezing temperature of the solution with a basic thermodynamic formula pertinent to the Gibbs energy, enthalpy and the entropy of fusion. The model correlates the activity of the solvent (a_A) and the freezing temperature of the solution (T_f) [18] as follows:

$$-R\ln a_A = y = \Delta H^{\star}\left(\frac{1}{T_f} - \frac{1}{T_f^{\star}}\right) + \Delta C_{p,m}\left[\frac{(T_f - T_f^{\star})}{T_f} - \ln\left(\frac{T_f}{T_f^{\star}}\right)\right] \quad (1)$$

where R denotes the universal gas constant, $T_f^{\star}$ is the freezing point of the pure solvent (in this study, water), $\Delta H^{\star}$ is the enthalpy of fusion at $T_f^{\star}$, and $\Delta C_{p,m}(=C^{\star}_{p,m}(A,l) - C^{\star}_{p,m}(A,s))$ is the difference between the heat capacities at constant pressure of the pure solvent (water) in the liquid phase (denoted by $C^{\star}_{p,m}(A,l)$) and the solid (ice) phase ($C^{\star}_{p,m}(A,s)$) at the freezing temperature. The activity of the solvent is related to the osmotic coefficient (ϕ) as

$$\ln a_A = -\nu M_A m\phi \quad (2)$$

where m refers to the molality (mol kg^{-1}) of the solution, M_A is the molecular weight of the solvent (for water, 0.018015 kg mol^{-1}), and $\nu = \nu_M + \nu_X$ denotes the stoichiometric coefficients of the cation and anion of the salt, respectively. After mathematical manipulation, an expression for the FPD of the solution ($\Delta T_f = T_f^{\star} - T_f$) can be defined as [18]

$$\Delta T_f = \frac{\nu R T_f^{\star} M_A m\phi}{\nu R M_A m\phi + \frac{\Delta H^{\star}}{T_f^{\star}}} + \frac{\Delta C_{p,m}\Delta T_f + \Delta C_{p,m}(T_f^{\star} - \Delta T_f)\ln\left(\frac{T_f^{\star} - \Delta T_f}{T_f^{\star}}\right)}{\nu R M_A m\phi + \frac{\Delta H^{\star}}{T_f^{\star}}} \quad (3)$$

From the osmotic coefficients of the solutions, it is possible to solve Eq. (3) iteratively, which additionally requires adjustable parameters when the Pitzer model is used. In the calculations, $T_f^{\star} = 273.15$ K, $\Delta H^{\star} = 6009.5$ J mol^{-1}, and $\Delta C_{p,m} = 37.87$ J K^{-1}mol^{-1} [22, 23] were used. Previous work [18] had shown that, for NaCl and KCl solutions, the temperature dependency of $\Delta C_{p,m}$ has no effect on the temperature-dependent Pitzer parameters obtained from the freezing point data for dilute solutions up to 0.5 mol kg^{-1}. Moreover, there are inconsistencies among reported $C^{\star}_{p,m}(A,l)$ values of subcooled water in the literature [18]. Therefore, in the present work, a constant $\Delta C_{p,m}$ value was considered.

The definitive model for calculating the osmotic coefficient of 1-1 and 1-2 electrolytes is the Pitzer model with the following form [24]:

$$\phi - 1 = -|Z_M Z_X|\frac{A_\phi I^{1/2}}{1 + bI^{1/2}} + 2\left(\frac{\nu_M \nu_X}{\nu}\right)m\left[\beta^0 + \beta^1\exp(-\alpha I^{1/2})\right] + \frac{2(\nu_M\nu_X)^{3/2}}{\nu}\Bigg)m^2 C^{\phi} \quad (4)$$

where, Z_M and Z_X are the valences of the cation and anion, respectively, A_ϕ is the Debye-Hückel constant (at a temperature of 273.15 K and a pressure of 101.325 kPa, this value is 0.37642 (mol kg^{-1})$^{-0.5}$ [25]), $b = 1.2$ (mol kg^{-1})$^{-0.5}$, $\alpha = 2.0$ (mol kg^{-1})$^{-0.5}$, and $I = 0.5\sum m_i Z_i^2$ is the ionic strength. The interaction parameters β^0, β^1, and C^{ϕ} are electrolyte-dependent Pitzer parameters, which in this work are determined for $NaNO_3$, KNO_3, NH_4NO_3, Na_2SO_4, K_2SO_4, and $(NH_4)_2SO_4$ solutions at 273.15 K. Eqs. (5)–(8) describe the Debye-Hückel equations for the dilute solution domain, the stoichiometric mean activity coefficient (γ), and the concentration dependence of the electrolyte terms B^{ϕ} and B, respectively, for 1-1- and 1-2-type electrolytes [26].

$$f^{\gamma} = -A_\phi\left[\frac{I^{1/2}}{(1 + bI^{1/2})} + \left(\frac{2}{b}\right)\ln(1 + bI^{1/2})\right] \quad (5)$$

$$\ln\gamma = |Z_M Z_X|\left[f^{\gamma} + 2m\left(\frac{\nu_M\nu_X}{\nu}\right)(B^{\phi} + B) + 3m^2\left(\frac{\nu_M {\nu_X}^{3/2}}{\nu}\right)\right]C^{\phi} \quad (6)$$

$$B^{\phi} = \beta^0 + \beta^1\exp(-\alpha I^{1/2}) \quad (7)$$

$$B = \beta^0 + \beta^1 g(\alpha I^{1/2}) \quad (8a)$$

$$g(x) = \frac{2(1 - (1 + x)e^{-x})}{x^2} \quad (8b)$$

3 Results and Discussion

Excluding the C^{ϕ} term, which is a rational assumption for dilute solutions up to 0.5 mol kg^{-1} [17], Eq. (4) can be rearranged using quantity y in Eq. (1) for the interaction parameter β^0 as a function of β^1 and molality m:

$$\beta^0 = \frac{v}{2mv_M v_X}\left[\frac{|Z_M Z_X| A_\phi I^{1/2}}{1+bI^{1/2}} + \frac{y}{RvM_A m} - 1\right] - \beta^1 \exp(-aI^{1/2}) \quad (9)$$

In order to solve β^0 from Eq. (9), parameter β^1 must first be estimated. β^1 was chosen as the value that yielded the least standard deviation value from the mean value of the experimental β^0 values at different molalities. Freezing point data for dilute solutions of Na_2SO_4 and K_2SO_4 can be found in the literature [27, 28]. The highest limit for Na_2SO_4 solutions was about 0.1 mol kg^{-1}, and 0.3 mol kg^{-1} for K_2SO_4 solutions. Experimental freezing points in the range of 0.0058–0.1034 mol kg^{-1} for Na_2SO_4 solutions and in the range of 0.177–0.302 mol kg^{-1} for K_2SO_4 were used for the estimation of β^0 and β^1. Using Eq. (9) the following parameters were obtained: $\beta^0(Na_2SO_4)$ = –0.1789, $\beta^0(K_2SO_4)$ = –0.0128, $\beta^1(Na_2SO_4)$ = 1.190, and $\beta^1(K_2SO_4)$ = 0.5738, with a standard deviation from the mean β^0 values of 0.043 for Na_2SO_4 solutions and 0.007 for K_2SO_4. The reliability of the obtained parameters was corroborated through an error function as follows

$$e_T = \Delta T_f(\text{observed}) - \Delta T_f(\text{predicted}) \quad (10)$$

Error plots as a function of molality m are presented in Fig. 1 a for both salts. The absolute error of < 0.0040 K for both salts confirms that the obtained parameters correlate well with the experimental data.

The interaction parameter C^{ϕ} was taken into account for solution concentrations above 0.5 mol kg^{-1}. Considering term C^{ϕ} for less dilute solutions up to 1.5 mol kg^{-1}, the modified version of Eq. (9) is

$$\beta^0 = \frac{v}{2mv_M v_X}\left[\frac{|Z_M Z_X| A_\phi I^{1/2}}{1+bI^{1/2}} + \frac{y}{RvM_A m} - 1\right] - \beta^1 \exp(-aI^{1/2}) - (v_M v_X) m C^{\phi} \quad (11)$$

For less dilute solutions, the same value of β^1 was used as for dilute solutions, by ignoring the C^{ϕ} term. The reason for adopting this approach is that using the β^1 value from dilute solutions yielded good results with the Pitzer equation for hydrochloric acid extending up to 16 mol kg^{-1} [29]. After determining β^1, parameter C^{ϕ} was chosen in such a way that the lowest standard deviation was attained for β^0 values at different molalities m (or ionic strength I) from Eq. (11). The same strategy has previously been followed to determine β^0, β^1, and C^{ϕ} at 273.15 K for NaCl and KCl solutions using freezing point data [18].

Experimental data points in the range of 0.07369–1.3514 mol kg^{-1} for $NaNO_3$ solutions [30], 0.06327–1.001 mol kg^{-1} for KNO_3 solutions [30], 0.2763–1.4035 mol kg^{-1} for NH_4NO_3 solutions [31], and 0.2671–1.2141 mol kg^{-1} for $(NH_4)_2SO_4$ [31] solutions were used for parameter estimation. The following parameters were obtained: $\beta^0(NaNO_3)$ = –0.0561, $\beta^0(KNO_3)$ = –0.1316, $\beta^0(NH_4NO_3)$ = –0.0410, $\beta^0((NH_4)_2SO_4)$ = 0.0138, $\beta^1(NaNO_3)$ = 0.1963, $\beta^1(KNO_3)$ = –0.0966, $\beta^1(NH_4NO_3)$ = 0.0322, $\beta^1((NH_4)_2SO_4)$ = 0.3140, $C^{\phi}(NaNO_3)$ = 0.0107, $C^{\phi}(KNO_3)$ = 0.0035, $C^{\phi}(NH_4NO_3)$ = –0.002, $C^{\phi}((NH_4)_2SO_4)$ = –0.0007, with standard deviations of 0.002, 0.001, 0.0004, and 0.001 for $NaNO_3$, KNO_3, NH_4NO_3, and $(NH_4)_2SO_4$ solutions, respectively.

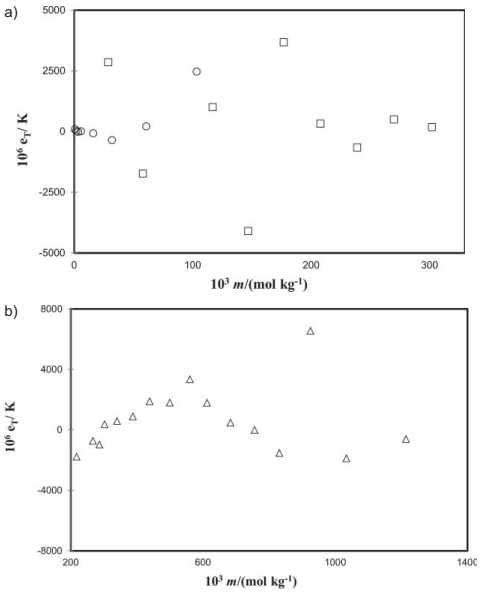

Figure 1. Plot of e_T (Eq. 10) depicting the deviation between the observed and predicted FPD in Na_2SO_4 (graph A, symbol ○), K_2SO_4 (A, □), and $(NH_4)_2SO_4$ (B, △) solutions as a function of molality m. The observed values were measured by Randall and Scott [27] for Na_2SO_4 and by Scatchard and Prentiss [31] for $(NH_4)_2SO_4$, and adopted from the literature [28] for K_2SO_4 solutions. The predicted values were determined from Eq. (3), in which osmotic coefficients were calculated from Eq. (4) with $\beta^0(Na_2SO_4)$ = –0.1789, $\beta^1(Na_2SO_4)$ = 1.1900, $\beta^0(K_2SO_4)$ = –0.0128, $\beta^1(K_2SO_4)$ = 0.5738, $\beta^0((NH_4)_2SO_4)$ = 0.0138, $\beta^1((NH_4)_2SO_4)$ = 0.3140, and $C^{\phi}((NH_4)_2SO_4)$ = –0.0007.

The new parameter values were tested with experimental freezing point data by Eq. (10). Error plots as a function of molality m of all nitrate salt and $(NH_4)_2SO_4$ solutions are displayed in Figs. 2 and 1 b, respectively. The absolute error value was found to be smaller than 0.007 K for all solutions below 1.5 mol kg^{-1}, which confirms the high level of accuracy.

The parameters acquired by the method presented in this paper, Pitzer parameters at 298.15 K, temperature derivatives, and calculated Pitzer parameters at 273.15 K from temperature

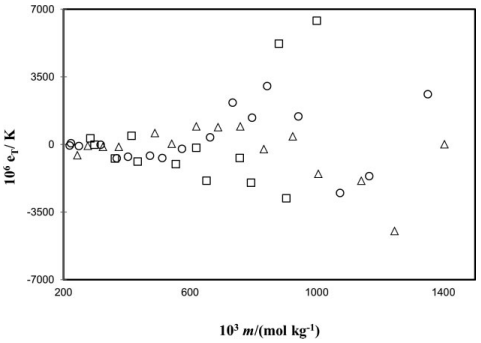

Figure 2. Plot of e_T (Eq. 10) depicting the deviation between the observed and predicted FPD in $NaNO_3$ (○), KNO_3 (□), and NH_4NO_3 (Δ) solutions as a function of molality *m*. The observed values were adopted from the literature [30, 31] and the predicted values were determined from Eq. (3), in which osmotic coefficients were calculated from Eq. (4) with $\beta^0(NaNO_3)$ = –0.0561, $\beta^0(KNO_3)$ = –0.1316, $\beta^0(NH_4NO_3)$ = –0.0410, $\beta^1(NaNO_3)$ = 0.1963, $\beta^1(KNO_3)$ = –0.0966, $\beta^1(NH_4NO_3)$ = 0.0332, $C^\phi(NaNO_3)$ = 0.0107, $C^\phi(KNO_3)$ = 0.0035, and $C^\phi(NH_4NO_3)$ = –0.0020.

dependencies are given in Tab. 1. The temperature derivatives for NH_4NO_3 and $(NH_4)_2SO_4$ solutions cannot be found in the literature and it was therefore not possible to estimate the parameters at 273.15 K for these solutions. Measurement of the freezing point with very high precision is very difficult, owing to the fact that it comprises several stages where errors can occur. Lower measurement precision explains the scatter in the error plots.

Figs. 3 and 4 present error plots of the nitrate and sulfate solutions, respectively, in which the predicted values were calculated from Eq. (3) on the basis of the Pitzer parameters obtained from calorimetric data. The comparatively higher order of errors indicates that the experimental data are not in good agreement with the values calculated with the Pitzer parameter values. However, the Pitzer parameter values introduced in this work exhibit better validity for solutions of both < 0.5 and < 1.5 mol kg^{-1}. It can be concluded that the Pitzer interaction parameters at 273.15 K obtained from calorimetric data cannot compete in terms of accuracy level with those from freezing point data as presented in this work. The osmotic (ϕ) and activity coefficient (γ) values, calculated as a function of *m* (mol kg^{-1}) at 273.15 K from Eqs. (4) and (6), respectively, using the estimated parameter values from the freezing point data, are listed in Tabs. 2–5.

Table 1. Values of the Pitzer parameters for Eq. (9) in dilute (< 0.5 mol kg^{-1}) solutions of Na_2SO_4 and K_2SO_4 and for Eq. (11) in less dilute (< 1.5 mol kg^{-1}) solutions of $NaNO_3$, KNO_3, NH_4NO_3 and $(NH_4)_2SO_4$ at 273.15 K, and the temperature dependencies of the Pitzer values at 298.15 K.

	β^0	β^1	C^ϕ	$10^4(d\beta^0/dT)_P$	$10^4(d\beta^1/dT)_P$	$10^5(dC^\phi/dT)_P$
$NaNO_3$	0.0068[b]	0.1783[b]	–0.00072[b]	12.33[a]	20.6[a]	–23.1[a]
	–0.02495[c]	0.1268[c]	0.005055[c]			
	–0.0561[d]	0.1963[d]	0.0107[d]	25.16	–7.2	–45.68
KNO_3	–0.0816[b]	0.0494[b]	0.0066[b]	2.06[a]	64.5[a]	39.7[a]
	–0.08675[c]	–0.1118[c]	–0.003325[c]			
	–0.1316[d]	–0.0966[d]	0.0035[d]	20	58.4	12.4
NH_4NO_3	–0.0154[b]	0.112[b]	–0.00003[b]			
	–0.0410[d]	0.0332[d]	–0.0020[d]	10.24	31.51	7.88
Na_2SO_4	0.0196[b]	1.113[b]	0.0057[b]	23.6[a]	56.3[a]	–48.8[a]
	–0.0395[c]	0.9722[c]	0.0179[c]			
	–0.1789[d]	1.1900[d]				
K_2SO_4	0.0499[b]	0.7793[b]		14.4	66.8	
	0.0139[c]	0.6124[c]				
	–0.0128[d]	0.5738[d]				
$(NH_4)_2SO_4$	0.0409[b]	0.6585[b]	–0.0012[b]			
	0.0138[d]	0.3140[d]	–0.0007[d]	10.86	137.82	–2.00

a) Temperature derivative of Pitzer parameters taken from [17].
b) Determined by Pitzer [17] at 298.15 K.
c) Calculated values at 273.15 K using the temperature dependencies given by Pitzer [17].
d) Recommended values at 273.15 K determined in the present work using the freezing point data of the solutions.

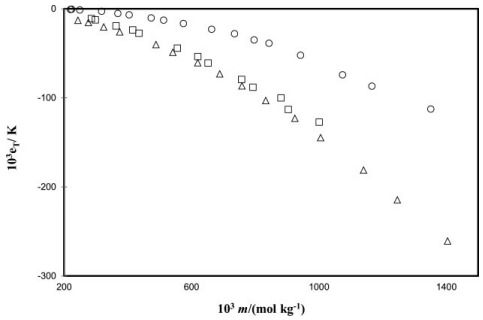

Figure 3. Plot of e_T (Eq. 10) depicting the deviation between the observed and predicted FPD in $NaNO_3$, KNO_3, and NH_4NO_3 solutions as a function of molality *m*. The observed values were adopted from the literature [30, 31] and the predicted values were determined from Eq. (3), in which osmotic coefficients were calculated from Eq. (4) with parameter values shown in Tab. 1. (○) $NaNO_3$ at 273.15 K by Pitzer [17], (□) KNO_3 at 273.15 K by Pitzer [17], (Δ) NH_4NO_3 at 298.15 K by Pitzer [17].

Table 2. Values presented for osmotic coefficients ϕ in aqueous $NaNO_3$, KNO_3, NH_4NO_3, and $(NH_4)_2SO_4$ solutions determined from Eq. (4) using recommended values of the Pitzer model (from Eq. 11) at 273.15 K obtained from the present work as a function of molality *m*.

m [mol kg^{-1}]	ϕ_{NaNO_3}	ϕ_{KNO_3}	$\phi_{NH_4NO_3}$	$\phi_{(NH_4)_2SO_4}$
0.01	0.967	0.964	0.966	0.895
0.02	0.956	0.950	0.954	0.863
0.05	0.937	0.924	0.933	0.811
0.1	0.918	0.895	0.911	0.767
0.2	0.895	0.856	0.885	0.719
0.3	0.879	0.827	0.866	0.690
0.4	0.866	0.802	0.852	0.669
0.5	0.854	0.779	0.839	0.654
0.6	0.844	0.759	0.828	0.641
0.7	0.834	0.740	0.818	0.630
0.8	0.825	0.722	0.808	0.621
0.9	0.817	0.704	0.799	0.613
1	0.810	0.688	0.790	0.606
1.1	0.803	0.672	0.782	0.601
1.2	0.796	0.656	0.774	0.595
1.3	0.790	0.641	0.767	0.591
1.4	0.784	0.626	0.759	0.587
1.5	0.778	0.611	0.752	0.583

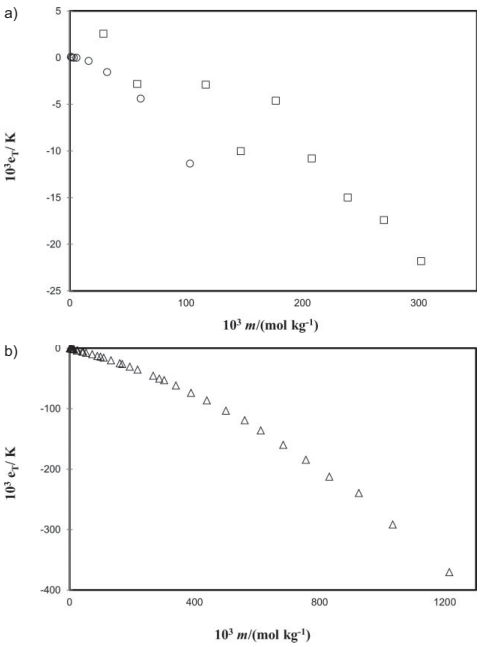

Figure 4. Plot of e_T (Eq. 11) depicting the deviation between the observed and predicted FPD in Na_2SO_4, $(NH_4)_2SO_4$, and K_2SO_4 solutions as a function of molality *m*. The observed values were measured by Randall and Scott [27] for Na_2SO_4 and by Scatchard and Prentiss [31] for $(NH_4)_2SO_4$, and adopted from the literature [28] for K_2SO_4 solutions. The predicted values were determined from Eq. (3), in which osmotic coefficients were calculated from Eq. (4) with parameter values shown in Tab. 1. Na_2SO_4 (graph A, symbol ○) at 273.15 K by Pitzer [17], K_2SO_4 (A, □) at 273.15 K by Pitzer [17], $(NH_4)_2SO_4$ (B, Δ) at 298.15 K by Pitzer [17].

Table 3. Values presented for osmotic coefficients ϕ in aqueous Na_2SO_4 and K_2SO_4 solutions determined from Eq. (4) using recommended values of the Pitzer model (from Eq. 9) at 273.15 K obtained from the present work as a function of molality *m*.

m [mol kg^{-1}]	$\phi_{Na_2SO_4}$	$\phi_{K_2SO_4}$
0.01	0.901	0.897
0.02	0.872	0.867
0.05	0.826	0.818
0.10	0.780	0.775
0.20	0.717	0.727
0.30	0.666	0.695

Table 4. Values presented for activity coefficients γ in aqueous $NaNO_3$, KNO_3, NH_4NO_3, and $(NH_4)_2SO_4$ solutions determined from Eq. (6) using recommended values of the Pitzer model (from Eq. 11) at 273.15 K obtained from the present work as a function of molality *m*.

m [mol kg^{-1}]	γ_{NaNO_3}	γ_{KNO_3}	$\gamma_{NH_4NO_3}$	$\gamma_{(NH_4)_2SO_4}$
0.01	0.903	0.897	0.900	0.713
0.02	0.869	0.859	0.866	0.635
0.05	0.812	0.790	0.805	0.520
0.1	0.759	0.722	0.746	0.430
0.2	0.695	0.637	0.678	0.343
0.3	0.654	0.580	0.633	0.296
0.4	0.622	0.537	0.599	0.264
0.5	0.596	0.501	0.571	0.241
0.6	0.573	0.471	0.548	0.223
0.7	0.554	0.444	0.528	0.209
0.8	0.537	0.421	0.510	0.197
0.9	0.521	0.400	0.494	0.187
1	0.507	0.381	0.479	0.178
1.1	0.495	0.363	0.465	0.170
1.2	0.483	0.348	0.453	0.164
1.3	0.472	0.333	0.441	0.158
1.4	0.462	0.319	0.430	0.152
1.5	0.452	0.306	0.420	0.147

Table 5. Values presented for activity coefficients γ in aqueous Na_2SO_4 and K_2SO_4 solutions determined from Eq. (6) using recommended values of the Pitzer model (from Eq. 9) at 273.15 K obtained from the present work as a function of molality *m*.

m [mol kg^{-1}]	$\gamma_{Na_2SO_4}$	$\gamma_{K_2SO_4}$
0.01	0.722	0.716
0.02	0.649	0.640
0.05	0.540	0.528
0.1	0.450	0.439
0.2	0.356	0.352
0.3	0.298	0.304

4 Conclusions

Freezing point data from the literature were used to determine Pitzer parameters at 273.15 K for selected 1-1 nitrate and 1-2 sulfate salt solutions. For dilute solutions up to 0.5 mol kg^{-1}, where FPD is relatively low, the Pitzer equation with the new parameter values predicted the freezing-point within the experimental error. It was further found that the freezing point of these dilute solutions can be predicted with the new Pitzer parameters given in the present work and the obtained modeling results can be compared to parameters determined using calorimetric data from values obtained at 298.15 K. Using the new parameter values, activity and osmotic coefficients at rounded molalities for 273.15 K were also presented. The obtained parameter values for studied salt solutions based on literature freezing point depression data seemed to yield mainly results with high accuracy, whereas in the case of ammonium nitrate and ammonium sulfate solutions, the freezing point depression data likely had lower accuracy. The accuracy of thermodynamic models based on calorimetric data and freezing point depression data from literature will be further studied in our future work.

The thermodynamic model introduced in this work provides vital thermodynamic data for these aqueous nitrate and sulfate salt solutions. This thermodynamic background is of interest when designing separation and purification processes such as desalination, FC, and EFC.

Acknowledgment

The authors are indebted to the Academy of Finland (Project No. 260141), the Graduate School of Lappeenranta University of Technology (LUT) and the Graduate School of Chemical Engineering (GSCE) for financial support.

The authors have declared no conflict of interest.

Symbols used

a_A	[mol dm^{-3}]	activity of the solvent
A_ϕ	[(mol kg^{-1})$^{-0.5}$]	Debye-Hückel constant
b	[(mol kg^{-1})$^{-0.5}$]	electrolyte independent constant term in Pitzer equation
B, B^ϕ	[(mol kg^{-1})$^{-1}$]	electrolyte terms as explicit functions of ionic strength
C^ϕ	[(mol kg^{-1})$^{-2}$]	Pitzer parameters
$C^\star_{p,m}(A, l)$	[J K^{-1}mol^{-1}]	heat capacity at constant pressure of the pure solvent in the liquid phase at the freezing temperature
$C^\star_{p,m}(A, s)$	[J K^{-1}mol^{-1}]	heat capacity at constant pressure of the pure solvent in the solid phase at the freezing temperature
$\Delta C_{p,m}$	[J K^{-1}mol^{-1}]	difference between the heat capacities
e_T	[K]	error function of FPD as defined in Eq. (10)
$\Delta H^\star$	[J mol^{-1}]	enthalpy of fusion at $T_f^\star$
I	[mol kg^{-1}]	ionic strength
m	[mol kg^{-1}]	molality of the solution

M_A	[kg mol^{-1}]	molecular weight of the solvent
R	[J mol^{-1}K^{-1}]	universal gas constant
T_f	[K]	freezing temperature of the solution
T_f^*	[K]	freezing point of the pure solvent
ΔT_f	[K]	freezing point depression
Z_M, Z_X	[–]	valences of the cation and anion

Greek symbols

α	[(mol kg^{-1})$^{-0.5}$]	constant term in Pitzer equation
β^0, β^1	[(mol kg^{-1})$^{-1}$]	Pitzer parameters
γ	[–]	activity coefficient
ν	[–]	stoichiometric coefficients
ϕ	[–]	osmotic coefficient

Subscripts

A	solvent
f	freezing point
M	cation
X	anion

References

[1] R. A. Robinson, R. H. Stokes, *Electrolyte Solutions*, 2nd ed., Butterworths, London **1959**.
[2] K. S. Pitzer, *J. Phys. Chem.* **1973**, *77 (2)*, 268.
[3] D. R. Schreiber, K. DeWyse, L. C. Shreiber, T. Tung, *J. Solution Chem.* **1999**, *28 (5)*, 567.
[4] H. Haghighi, A. Chapoy, B. Tohidi, *Ind. Eng. Chem. Res.* **2008**, *47 (11)*, 3983.
[5] M. S. Rahman, N. Guizani, M. Al-Hinai, S. A. Al-Maskri, S. A. Al-Hammani, *Food Hydrocolloids* **2002**, *16*, 653.
[6] P. Marliacy, N. Hubert, L. Schuffenecker, R. Solimando, *Fluid Phase Equilib.* **1998**, *148 (1/2)*, 95.
[7] A. Mohs, S. Decker, J. Gmehling, *Fluid Phase Equilib.* **2011**, *304 (1/2)*, 12.
[8] F. van der Ham, G. J. Witkamp, J. de Graauw, G. van Rosmalen, *J. Cryst. Growth* **1999**, *198/199 (1)*, 744.
[9] G. Scatchard, S. S. Prentiss, *J. Am. Chem. Soc.* **1933**, *55 (11)*, 4355.
[10] R. A. Robinson, *Trans. R. Soc. N. Z.* **1945**, *75 (2)*, 203.
[11] H. F. Gibbard, Jr., G. Scatchard, R. A. Rousseau, J. L. Creek, *J. Chem. Eng. Data* **1974**, *19 (3)*, 281.
[12] G. J. Janz, A. R. Gordon, *J. Am. Chem. Soc.* **1943**, *65 (2)*, 218.
[13] A. S. Brown, D. A. MacInnes, *J. Am. Chem. Soc.* **1935**, *57 (7)*, 1356.
[14] W. J. Hornibrook, G. J. Janz, A. R. Gordon, *J. Am. Chem. Soc.* **1942**, *64 (3)*, 513.
[15] T. Shedlovsky, D. A. MacInnes, *J. Am. Chem. Soc.* **1937**, *59 (3)*, 503.
[16] F. Silverster, K. S. Pitzer, *J. Solution Chem.* **1978**, *7 (5)*, 327.
[17] *Activity Coefficients in Electrolyte Solutions* (Ed: K. S. Pitzer), 2nd ed., CRC Press, Boca Raton, FL **1991**.
[18] M. Hasan, J. I. Partanen, K. P. Vahteristo, M. Louhi-Kultanen, *Ind. Eng. Chem. Res.* **2014**, *53 (13)*, 5608.
[19] R. Silva, L. Cadorin, J. Rubio, *Miner. Eng.* **2010**, *23 (15)*, 1220.
[20] O. Primo, M. J. Rivero, A. M. Urtiage, *J. Hazard. Mater.* **2009**, *164 (1)*, 389.
[21] J. Nathoo, R. Jivanji, A. E. Lewis, *Proc. of the Int. Mine Water Conf.* (Ed: A. E. Lewis), Curran Associates, Red Hook, NY **2010**.
[22] N. S. Osborne, H. F. Stimson, D. C. Ginning, *J. Res. Natl. Bur. Stand.* **1939**, *23*, 197.
[23] N. S. Osborne, *J. Res. Natl. Bur. Stand.* **1939**, *23*, 643.
[24] K. S. Pitzer, G. Mayorga, *J. Phys. Chem.* **1973**, *77 (2)*, 268.
[25] D. G. Archer, P. Wang, *J. Phys. Chem. Ref. Data* **1990**, *19*, 371.
[26] H. T. Kim, J. F. William, Jr., *J. Chem. Eng. Data* **1988**, *33 (2)*, 177.
[27] M. Randall, G. N. Scott, *J. Am. Chem. Soc.* **1927**, *49 (3)*, 647.
[28] *CRC Handbook of Chemistry and Physics* (Ed: W. M. Haynes), 94th ed., CRC Press, Boca Raton, FL **2013**.
[29] J. I. Partanen, P. M. Juusola, K. P. Vahteristo, A. J. G. de Mondonca, *J. Solution Chem.* **2007**, *36 (1)*, 39.
[30] G. Scatchard, S. S. Prentiss, P. T. Jones, *J. Am. Chem. Soc.* **1932**, *54 (7)*, 2690.
[31] G. Scatchard, S. S. Prentiss, *J. Am. Chem. Soc.* **1932**, *54 (7)*, 2696.

Publication V

Hasan, M., Partanen, J.I., Vahteristo, K.P., Louhi-Kultanen, M.,

Determination of the Pitzer interaction parameters at 273.15 K from the freezing-point data available for NaCl and KCl solutions.

Reprinted with permission from
Industrial and Engineering Chemistry Research
Vol. 53, pp.5608-5616, 2014

I&EC research
Industrial & Engineering Chemistry Research

Article

pubs.acs.org/IECR

Determination of the Pitzer Interaction Parameters at 273.15 K from the Freezing-Point Data Available for NaCl and KCl Solutions

Mehdi Hasan, Jaakko I. Partanen,* Kari P. Vahteristo, and Marjatta Louhi-Kultanen

Department of Chemical Technology, Lappeenranta University of Technology, P.O. Box 20, FIN-53851 Lappeenranta, Finland

Supporting Information

ABSTRACT: A novel calculation method is presented in this work to evaluate the ion interaction parameters for the Pitzer model from freezing points of aqueous solutions of pure electrolytes. The freezing-point depression data from aqueous solutions of sodium chloride and potassium chloride are used to epitomize this method. The parameter values obtained using this method predict more accurately the experimental data than the most often used values for the Pitzer method up to a molality of 1.5 mol·kg^{-1}. The parameters obtained by the freezing-point technique are associated with the solutions which are below the temperature of 273.15 K. It is verified in the present study that the temperature dependences of these parameters between the two temperatures are, however, practically negligible at molalities less than 0.5 mol·kg^{-1}. In addition to the freezing-point data existing in the literature, the validity of the parameters was also studied using the literature results from concentration cells without transference.

INTRODUCTION

In the presence of electrolytes or other solutes, the freezing temperature of a solution is lower than that of the pure solvent. In general, the higher is the electrolyte concentration, the greater is the freezing point depression. As it is one of the colligative properties of the solvent, the relative amount of anions and cations with respect to the amount of solvent is the key factor that determines its value. In the case of ideally dilute solutions, the freezing point depression can be estimated by a simple linear relation between this quantity and the solute concentration where the constant is called the cryoscopic constant (see, e.g., ref 1). Short-range interactions between pairs of ions in the electrolyte and triple ion interactions at high concentration, and long-range electrostatic interactions prevailing in dilute solutions are the underlying reasons for the deviation from the ideally dilute behavior.[2] Accurate electrolyte data for aqueous solutions over wide ranges of temperatures and pressures are needed, for example, in chemistry, chemical engineering, geochemistry, oceanography, boiler engineering,[3] petroleum engineering,[4] oil recovery system,[3] and food engineering.[5]

Phase equilibria, like solid−liquid equilibria, in electrolyte solutions are of crucial importance in such industrial processes as wastewater treatment, desalination, and crystallization (see refs 6 and 7 as examples of the treatment). The prediction of the freezing point is especially important for freeze concentration (FC) and eutectic freeze concentration (EFC). The latter is a novel and promising separation and concentration technique to recover simultaneously ice and salt crystals with high purities by operating at eutectic conditions.[8] Therefore, accurate models describing thermodynamic behavior in phases of these systems are required for analysis, designing, and optimizing processes and equipment.[4] Thermodynamic models based on parameters determined from the most accurate experimental data, like the data from freezing point depressions,[9] isopiestic equilibrium,[10] vapor pressures,[11] cell potential differences,[12−15] and calorimetric method[16] for binary salt systems provide the reliable predictions of the thermodynamic properties of pure and, with some additional parameters, mixed solutions. Pitzer's virial coefficient model,[2] which uses still primarily osmotic and activity coefficient data at a fixed temperature for parametrization, is widely applied to interpret the thermodynamic properties of electrolyte solutions. Ordinarily the parameter estimation has been performed at 298.15 K and based on the isopiestic method because of the generality of this experimental technique. It is also the most accurate method for this purpose in addition to the best electrochemical methods in case the latter methods can be used. At the freezing point of the solution, also the determination of the exact value of this temperature is a very accurate method and it is in accuracy comparable to those of the isopiestic method and the best electrochemical methods. The problem that the method is not isothermal is not a serious one when rather dilute solutions are only considered (for a uniunivalent electrolyte, the limit of the best accuracy is the molality of about 0.5 mol·kg^{-1}, see below). The relevant thermodynamic properties determined for the freezing points of the solutions associate in these conditions within experimental error with the temperature of 273.15 K. It seems to us that this source of accurate thermodynamic data is not utilized in the thermodynamic literature as thoroughly as it is possible.

In the present study, the parameter values for the Pitzer equations at 273.15 K have been determined for sodium and potassium chloride solutions using freezing point data, and the resulting values are tested with all relevant thermodynamic data available in the literature. Additionally, the predicted freezing

Received: November 29, 2013
Revised: February 17, 2014
Accepted: March 5, 2014
Published: March 5, 2014

dx.doi.org/10.1021/ie404042h | *Ind. Eng. Chem. Res.* 2014, 53, 5608−5616

points in the sets used in the parameter estimation were compared to those obtained with the commonly used Pitzer parameters together with their temperature dependencies.

THEORY

At the freezing point T_f of an electrolyte solution, the following equilibrium is attained

$$\text{A (in electrolyte solution)} \rightleftarrows \text{A (as solid)} \tag{1}$$

where A refers to the solvent (water in this case). The condition for the equilibrium is

$$\mu_A(T_f, \text{in solution}) = \mu_A^*(T_f) + RT_f \ln a_A = \mu_A^*(s, T_f) \tag{2}$$

where μ_A^* and μ_A designate the chemical potential of pure solvent (asterisk symbol, $*$) and that of the solvent in solution, respectively, and a_A is the activity of the solvent. At T_f, the molar Gibbs energy of the fusion for the solvent is

$$\Delta G_{m,fus}(A, T_f) = \mu_A^*(T_f) - \mu_A^*(s, T_f) \tag{3}$$

On the other hand

$$\Delta G_{m,fus}(A, T_f) = \Delta H_{m,fus}(A, T_f) - T_f \Delta S_{m,fus}(A, T_f) \tag{4}$$

where H refers to the enthalpy and S refers to the entropy. At the freezing point of the pure solvent (i.e., at T_f^*), we have

$$\Delta S_{m,fus}(A, T_f^*) = \Delta H_{m,fus}(A, T_f^*)/T_f^* \tag{5}$$

where $\Delta H_{m,fus}(A, T_f^*)$ is the enthalpy of the fusion at that temperature. To simplify the notations, we define that $\Delta H^* = \Delta H_{m,fus}(A, T_f^*)$ and $\Delta S^* = \Delta S_{m,fus}(A, T_f^*)$. The temperature dependence for the molar enthalpy and entropy of fusion can be expressed as

$$\Delta H_{m,fus}(A, T_f) = \Delta H^* + \Delta C_{p,m}(T_f - T_f^*) \tag{6}$$

$$\Delta S_{m,fus}(A, T_f) = \frac{\Delta H^*}{T_f^*} + \Delta C_{p,m} \ln\left(\frac{T_f}{T_f^*}\right) \tag{7}$$

where

$$\Delta C_{p,m} = C_{p,m}^*(A, l) - C_{p,m}^*(A, s) \tag{8}$$

where $C_{p,m}$ refers to the molar heat capacity at a constant pressure. The difference between the heat capacities is the theoretically problematic quantity in the thermodynamic treatment of the freezing point data. The following very accurate temperature dependence of $C_{p,m}$ for ice is available in the literature (see ref 17),

$$\frac{C_{p,m}^*(A, s)}{J\cdot K^{-1}\cdot mol^{-1}} = 38.107 + 0.14034\cdot\left(\frac{T}{K} - 273.15\right) \tag{9}$$

and it can be used in the range from 269.53 K to 273.15 K. The heat capacity of the liquid water below zero degree Celsius is not a quantity that can be experimentally determined in a very accurate way. This fact limits the high-precision theoretical treatment of the freezing point data only to dilute solutions where the variation of $C_{p,m}^*(A, l)$ with respect to the temperature has no significant effect on the results. It is verified below that this limit is about 0.5 mol·kg^{-1}. The following equation can be derived using eqs 4−7

$$-R \ln a_A = y = \Delta H^*\left(\frac{1}{T_f} - \frac{1}{T_f^*}\right) + \Delta C_{p,m}\left[\frac{(T_f - T_f^*)}{T_f} - \ln\left(\frac{T_f}{T_f^*}\right)\right] \tag{10}$$

and it is possible to calculate directly the values of quantity y from the experimental freezing point data. Let us define the freezing point depression (ΔT_f) in the following ordinary way

$$\Delta T_f = T_f^* - T_f \tag{11}$$

The definition of the osmotic coefficient of the solvent ($= \phi$) is based on the solvent activity in solutions of a uniunivalent electrolyte as follows

$$\ln a_A = -2mM_A\phi \tag{12}$$

where m is the molality of the solution and M_A is the molar mass of solvent (for water it is 0.018015 kg·mol^{-1}). Using eqs 10, 11, and 12, the following equation can be derived for ΔT_f

$$\Delta T_f = \frac{2RT_f^* M_A m\phi}{2RM_A m\phi + \frac{\Delta H^*}{T_f^*}} + \frac{\Delta C_{p,m}\Delta T_f + \Delta C_{p,m}(T_f^* - \Delta T_f)\ln\left(\frac{T_f^* - \Delta T_f}{T_f^*}\right)}{2RM_A m\phi + \frac{\Delta H^*}{T_f^*}} \tag{13}$$

In the present calculations, the following values were used in this equation: $T_f^* = 273.15$ K, $\Delta H^* = 6009.5$ J·mol^{-1} (Osborne et al.[18]), and $\Delta C_p = 37.87$ J·K^{-1}·mol^{-1} (Osborne[17] and Osborne et al.[18]). This equation requires iterative calculations, and the corresponding equation has been previously used in the thermodynamic considerations of NaCl and KCl solutions based on more empirical Hückel equation to describe the nonideality.[19,20]

In this connection, it is shown that the temperature dependence of $\Delta C_{p,m}$ has no effect on the results below a molality of 0.5 mol·kg^{-1}. Let us consider the NaCl solution at this molality as an example. The freezing-point depression of this solution at this molality is about 1.69 K. The following approximate equation was derived here for the molar heat capacities of liquid water in the range from 273.15 K to 283.15 K based on the experimental values of Osborne et al.[18]

$$\frac{C_{p,m}^*(A, l)}{J\cdot K^{-1}\cdot mol^{-1}} = 75.951 - 0.04556\cdot\left(\frac{T}{K} - 273.15\right) \tag{14}$$

This equation applies also to the extrapolation to temperatures below zero degrees Celsius. Archer and Carter[21] have measured a large amount of heat capacity values of liquid water below zero and some of these experimental data are presented in Figure A-2 (Appendix 2) in their paper and these data seem to be the most reliable set available for this quantity in these conditions. At 270 K in their Table 3,[21] they suggest a value of 76.059 J·K^{-1}·mol^{-1} and in Figure A-2 the individual values at this temperature vary from (75.915 to 76.149) J·K^{-1}·mol^{-1}. The predicted value from eq 14 is 76.095 J·K^{-1}·mol^{-1}, and it thus agrees quite well with the experimental values. Using eqs 9 and 14, the following equation can be presented for $\Delta C_{p,m}$ in eq 8

dx.doi.org/10.1021/ie404042h | Ind. Eng. Chem. Res. 2014, 53, 5608−5616

Table 1. Values of the Pitzer Parameters for eqs 16 and 17 at 273.15 K in NaCl and KCl solutions and the Temperature Dependencies[a] of the Values of Pitzer and Mayorga at 298.15 K

β^0	β^1	C^ϕ	$10^4(d\beta^0/dT)_p$	$10^4(d\beta^1/dT)_p$	$10^5(dC^\phi/dT)_p$
		NaCl			
0.0765[b]	0.2664[b]	0.00127[b]	7.159	7.005	−10.54
0.0585[c]	0.2489[c]	0.00391[c]			
0.0532[d]	0.2496[d]	0.0044[d]			
0.0442[e]	0.1893[e]	0.0061[e]			
0.0396[f]	0.2801[f]				
0.0379[g]	0.2801[g]	0.00698[g]	15.44[g]	−5.44[g]	−2.29[g]
		KCl			
0.04835[b]	0.2122[b]	−0.00084[b]	5.794	10.71	−5.095
0.03386[c]	0.1854[c]	0.000434[c]			
0.0234[f]	0.1919[f]				
0.0239[g]	0.1919[g]	0[g]	9.78[g]	8.12[g]	−3.36[g]

[a]Taken from ref 16. [b]Determined by Pitzer and Mayorga[25] at 298.15 K. [c]Calculated values using the parameters of Pitzer and Mayorga and their temperature dependencies given in the table. [d]Calculated values using the parameters of Pitzer and Mayorga and their temperature dependencies given by Silvester and Pitzer.[23] [e]Parameter values obtained from the equations suggested by Thurmond and Brass.[24] [f]Recommended in the present study for dilute solution (where m < 0.5 mol·kg^{-1}). [g]Recommended in the present study for less dilute solution up to a molality of 1.5 mol·kg^{-1}.

$$\frac{\Delta C_{p,m}}{J\cdot K^{-1}\cdot mol^{-1}} = 37.844 - 0.1859\cdot\left(\frac{T}{K} - 273.15\right) \quad (15)$$

For the NaCl solution where the molality is 0.5 mol·kg^{-1}, the value of $\Delta C_{p,m}$ from eq 15 is 38.158 J·K^{-1}·mol^{-1}. With this value, the second term on the right-hand side of eq 13 (the only term containing $\Delta C_{p,m}$ in this equation) has a value of 0.00903 K, and with the used value of $\Delta C_{p,m}$ = 37.87 J·K^{-1}·mol^{-1}, it is 0.00896 K. The error is in the fifth digit and it is not experimentally obtainable.

In the present study, the Pitzer equations are used in the treatment of nonideality. For the osmotic coefficient in an aqueous solution of a uniunivalent electrolyte, the Pitzer equation has the form

$$\phi = 1 - \frac{A_\phi\sqrt{m}}{1 + b\sqrt{m}} + (\beta^0 + \beta^1 e^{-\alpha\sqrt{m}})(m/m^o) + C^\phi(m/m^o)^2 \quad (16)$$

where m^o = 1 mol·kg^{-1} and A_ϕ is the Debye–Hückel constant which depends on the temperature. According to Archer and Wang,[22] its value at 273.15 K and at 101.325 kPa is 0.37642 (mol·kg^{-1})$^{-1/2}$. The following common Pitzer parameter values are now used in eq 16: b = 1.2 (mol·kg^{-1})$^{-1/2}$ and α = 2.0 (mol·kg^{-1})$^{-1/2}$. In this equation, β^0, β^1, and C^ϕ are the parameters that depend on the electrolyte, and they are determined in the present study for 273.15 K for NaCl and KCl solutions. In the literature are also given four equations for the temperature dependences of the Pitzer parameters of these two electrolytes, i.e., those of Silvester and Pitzer for both NaCl and KCl,[16] that of Silvester and Pitzer for NaCl,[23] and that of Thurmond and Brass for NaCl.[24] The parameter values calculated from these equations for 273.15 K are given in Table 1. The most important Pitzer parameter values at 298.15 K (i.e., those determined by Pitzer and Mayorga[25]) are additionally included in the table. In refs 26, 27, and 28 where almost all existing reliable thermodynamic data at the latter temperature have been considered, these values were proved to be reliable. The Pitzer equation for the activity coefficients (γ) of a uniunivalent electrolyte with the generally accepted parameter values has the form

$$\ln\gamma = f^\gamma + B^\gamma(m/m^o) + (3/2)C^\phi(m/m^o)^2 \quad (17)$$

where

$$f^\gamma = -A_\phi\left[\frac{\sqrt{m}}{1 + 1.2\sqrt{m/m^o}} + \frac{2\sqrt{m^o}}{1.2} \times \ln(1 + 1.2\sqrt{m/m^o})\right] \quad (18)$$

$$B^\gamma = 2\beta^0 + \frac{\beta^1 m^o}{2m}\left[1 - e^{-2\sqrt{m/m^o}} \times \left(1 + 2\sqrt{m/m^o} - 2\frac{m}{m^o}\right)\right] \quad (19)$$

RESULTS AND DISCUSSION

Determination of Pitzer Parameters for Dilute Solutions and Tests of the Resulting Equation. In dilute solutions, eq 16 is valid without the C^ϕ term and the parameters for NaCl and KCl are first determined for the case. It will be shown in what follows that the resulting two-parameter equation applies up to a molality of 0.5 mol·kg^{-1}. The following method seems to be simple and fully reliable for estimating the parameters β^0 and β^1: To solve experimental β^0 values, it is possible to arrange eq 16 without the C^ϕ term in the following form using eq 12 and quantity y in eq 10

$$\beta^0 = \frac{ym^o}{2RM_A m^2} - \frac{m^o}{m} + \frac{A_\phi m^o}{\sqrt{m}(1 + b\sqrt{m})} - \beta^1 e^{-\alpha\sqrt{m}} \quad (20)$$

Probably the most accurate set of the freezing-point data available in the literature for NaCl and KCl solutions is the one measured by Scatchard and Prentiss[9] in both cases. The experimental points in the range from (0.0788 to 0.486) mol·kg^{-1} were used in the estimation for NaCl solutions and in the range from (0.0767 to 0.486) mol·kg^{-1} for KCl solutions. Thus, 11 points were included in the former estimation and 10 points in the latter. For the calculations based on eq 20, the value of parameter β^1 must also be estimated. For this quantity, the value was chosen that gives the least value for the standard

deviation about the mean value of the experimental β^0 values. In this way, the following parameters were obtained: β^0(NaCl) = 0.0396, β^1(NaCl) = 0.2801, β^0(KCl) = 0.0234, and β^1(KCl) = 0.1919. The standard deviation for the estimated β^0 parameters is 0.002 in both cases.

The new parameter values were first tested with the data used in the parameter estimation. The experimental freezing point depressions from Scatchard and Prentiss[9] were reproduced with the new model using eqs 13 and 16. The errors calculated by

$$e_T = \Delta T_f \text{ (observed)} - \Delta T_f \text{ (predicted)} \quad (21)$$

are then presented as a function of the molality. The resulting error plots for both salts are shown in Figure 1. These plots

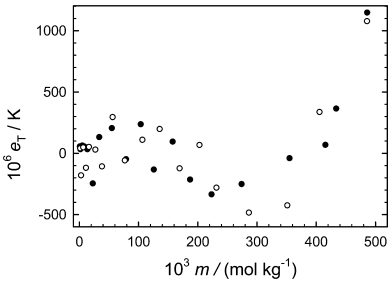

Figure 1. Plot of e_T (eq 21), the deviation between the observed and predicted freezing-point depressions in NaCl solutions (symbol ●) and KCl solutions (○) as a function of molality m. The observed values have been measured by Scatchard and Prentiss[9] and the predicted values were determined from eq 13, where eq 16 with β^0(NaCl) = 0.0396, β^1(NaCl) = 0.280, β^0(KCl) = 0.0234, β^1(KCl) = 0.192, and C^ϕ(NaCl) = C^ϕ(KCl) = 0 was used for the osmotic coefficients.

reveal that the new Pitzer models apply well to the experimental data used in the estimation. Almost all absolute errors are smaller than 0.001 K and they form a random pattern in both cases. Then, the NaCl parameters were tested with the other freezing point data existing for NaCl solutions. The results are presented in Figure 2 and its presentation corresponds exactly to that of Figure 1. The data from the following sources were included in the tests: Gibbard and Gossmann[29] (5 points), Harkins and Roberts[30] (9), Momicchioli et al.[31] (11), and Craft and van Hook[32] (23). Only the last set in this list consists of really high-precision data in these dilute solutions but all of these data support almost within their precision the suggested Pitzer parameters. The test results of the new KCl parameters with the other existing data are presented in the same way in graphs A and B of Figure 3. Graph A contains the results from the high precision data and graph B from the remainder of the data. The following studies were included in the KCl tests: Garnsey and Prue[33] (21 points), Brown and Prue[34] (15), Adams[35] (6), Chiorboli et al.[36] (10), Jones and Bury[37] (11), Karagunis et al.[38] (8), Damköhler and Weinzierl[39] (11), Menzel[40] (7), and Cavallaro et al.[41] (11). The data in graph A support excellently the new parameter values because almost all absolute errors are smaller than 0.0004 K. Also the data in graph B support well the new Pitzer parameters but some of the data sets in this graph seem to give results that are not in a full agreement with the other data (i.e., the data

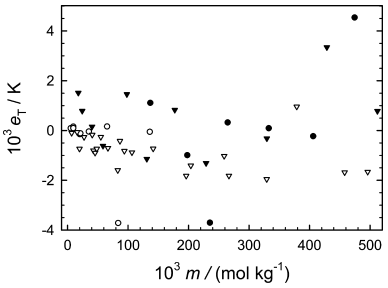

Figure 2. Plot of e_T (eq 21), the deviation between the observed and predicted freezing-point depressions in NaCl solutions as a function of molality m. The observed values have been measured by Gibbard and Gossmann[29] (symbol ●), Harkins and Roberts[30] (○), Momicchioli et al.[31] (▼), and Craft and Van Hook[32] (▽) and the predicted values were determined from eq 13, where eq 16 with β^0 = 0.0396, β^1 = 0.280, and C^ϕ = 0 was used for the osmotic coefficients.

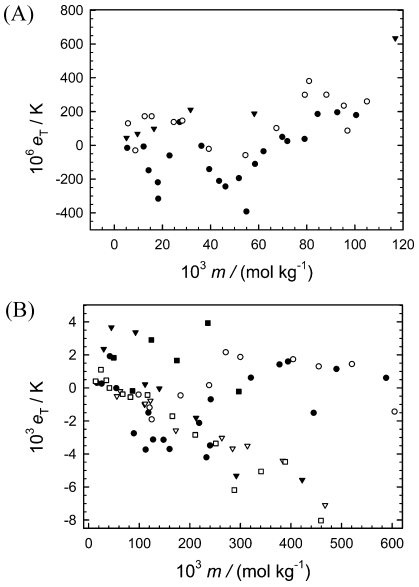

Figure 3. Plot of e_T (eq 21), the deviation between the observed and predicted freezing-point depressions in KCl solutions as a function of molality m. The observed values have been measured by Garnsey and Prue[33] (graph A, symbol ●), Brown and Prue[34] (A, ○), Adams[35] (A, ▼), Chiorboli et al.[36] (B, ●), Jones and Bury[37] (B, ○), Karagunis et al.[38] (B, ▼), Damköhler and Weinzierl[39] (B, ▽), Menzel[40] (B, ■), and Cavallaro et al.[41] (B, □) and the predicted values were determined from eq 13, where eq 16 with β^0 = 0.0234, β^1 = 0.192, and C^ϕ = 0 was used for the osmotic coefficients.

from refs 38, 39, and 41). In the cases of the sets from refs 38 and 39 this disagreement is, however, mainly due to the lower precision of the measurements as the results from the more concentrated solutions reveal (see below the results in Figure 7).

dx.doi.org/10.1021/ie404042h | Ind. Eng. Chem. Res. 2014, 53, 5608−5616

It is also possible to test of the new Pitzer equations for NaCl and KCl solutions using electrochemical data. Both Harned and Nims[42] and Harned and Cook[43] measured at low temperatures the concentration cells of the following type

$$\mathrm{Ag(s)|AgCl(s)|MCl(aq,}\ m_1\mathrm{)|}$$
$$\mathrm{M(Hg)|MCl(aq,}\ m_2\mathrm{)|AgCl(s)|Ag(s)} \quad (22)$$

where M(Hg) is the alkali metal amalgam electrode. In the set of Harned and Nims, the temperature T was 273.45 K, M was Na, the molality of the reference solution was m_1 = 0.1 mol·kg^{-1}, the molality of the tested solution (= m_2) varied from 0.05 to 4.0 mol·kg^{-1}, and three of these molalities were smaller than 1.0 mol·kg^{-1}. In the set of Harned and Cook, T = 273.15 K, M = K, m_1 = 0.05 mol·kg^{-1}, m_2 varied from 0.1 to 4.0 mol·kg^{-1}, and five of these molalities were smaller than 1.0 mol·kg^{-1}. The cell potential difference (cpd) for the cells of this kind can be calculated from

$$E = -\frac{2RT}{F}\ln(m_2/m_1) - \frac{2RT}{F}\ln(\gamma_2/\gamma_1) \quad (23)$$

These eight points were predicted using the new Pitzer equations for the activity coefficients (see eq 17). For the NaCl data at 273.45 K, the value of 0.3766 (mol·kg^{-1})$^{-1/2}$ was used for A_ϕ. The resulting cpd errors, defined by

$$e_E = E(\mathrm{observed}) - E(\mathrm{predicted}) \quad (24)$$

are given in Figure 4 as a function of molality m_2. The amalgam cell data can be explained within 0.6 mV with the new Pitzer parameters in the molalities used in the tests and these data support thus well the new parameters.

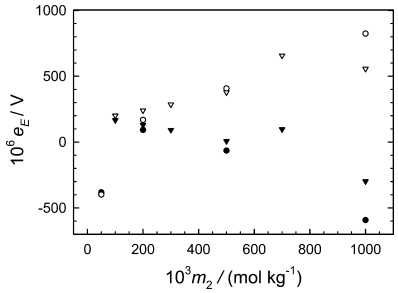

Figure 4. Plot of e_E (eq 24), the deviation between the observed and predicted cell potential difference (cpd) from the concentration cell data measured on cell 22 by Harned and Nims[42] (T = 273.45 K, M = Na, m_1 = 0.1 mol·kg^{-1}) and by Harned and Cook[43] (T = 273.15 K, M = K, m_1 = 0.05 mol·kg^{-1}) as a function of molality m_2. The predicted cpd was calculated by using eq 23 where eq 17 with the new Pitzer parameters for NaCl solutions (β^0 = 0.0396, β^1 = 0.280, C^ϕ = 0, symbol ●) and for KCl solutions (β^0 = 0.0234, β^1 = 0.192, C^ϕ = 0, ▼) and with the literature Pitzer parameters[16,25] for NaCl solutions (β^0 = 0.0585, β^1 = 0.2489, C^ϕ = 0.00391, o) and for KCl solutions (β^0 = 0.03386, β^1 = 0.1854, C^ϕ = 0.000434, ▽) was used for the activity coefficients (see Table 1).

Determination of Pitzer Parameters for Less Dilute Solutions and Tests of the Resulting Equation. In the less dilute solutions, the following equation is a valid parameter β^0

$$\beta^0 = \frac{ym^o}{2RM_A m^2} - \frac{m^o}{m} + \frac{A_\phi m^o}{\sqrt{m}\,(1 + b\sqrt{m})} - \beta^1 e^{-\alpha\sqrt{m}} - \frac{C^\phi m}{m^o} \quad (25)$$

This equation is used here in the determination of the Pitzer parameters from the data of Scatchard and Prentiss[9] for more concentrated NaCl and KCl solutions. In the evaluations, it is assumed that parameter β^1 has the same value as those used for dilute solutions, that is, β^1(NaCl) = 0.280 and β^1(KCl) = 0.192. The reason for this choice is that we previously have obtained good results with the Pitzer equation in aqueous hydrochloric acid solutions up to high molalities at various temperatures using this assumption (see ref 44). The experimental points in the range (0.0788 to 1.277) mol·kg^{-1} were used in the estimation for NaCl solutions and in the range (0.0767 to 1.246) mol·kg^{-1} for KCl solutions. Thus, in the former estimation were included 20 and in the latter 19 points. The calculations based on eq 22 are close to those used for dilute solutions. The value of parameter C^ϕ was chosen that gives the least value for the standard deviation about the mean value of the experimental β^0 values. In this way, the following parameters were obtained: β^0(NaCl) = 0.0379, C^ϕ(NaCl) = 0.00698, β^0(KCl) = 0.0239, and C^ϕ(KCl) = 0. The standard deviation for the estimated β^0 parameters are 0.002 and 0.0015, respectively.

The new parameter values were tested using the same data sets as those for dilute solutions in case they also contain data from the more concentrated solutions. The resulting error plots for the sets[9] used in the parameter estimation are shown in Figure 5. These plots correspond exactly to the plots presented in Figures 1 to 3 for dilute solutions and reveal that the new Pitzer models apply well to these data because no higher absolute errors than 0.003 K are observed. Then, the NaCl parameters were tested with the data from the sets of Gibbard and Gossmann,[29] Momicchioli et al.,[31] and Craft and van Hook,[32] and the results are presented in Figure 6. Finally, the KCl parameters were tested with the sets of Chiorboli et al.,[36] Jones and Bury,[37] Karagunis et al.,[38] Damköhler and

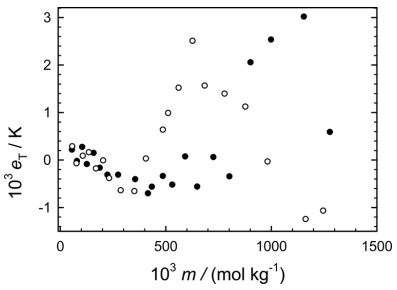

Figure 5. Plot of e_T (eq 21), the deviation between the observed and predicted freezing-point depressions in NaCl solutions (symbol ●) and KCl solutions (○) as a function of molality m. The observed values have been measured by Scatchard and Prentiss[9] and the predicted values were determined from eq 13, where eq 16 with β^0(NaCl) = 0.0379, β^1(NaCl) = 0.280, C^ϕ(NaCl) = 0.00698, β^0(KCl) = 0.0239, β^1(KCl) = 0.192, and C^ϕ(KCl) = 0 was used for the osmotic coefficients.

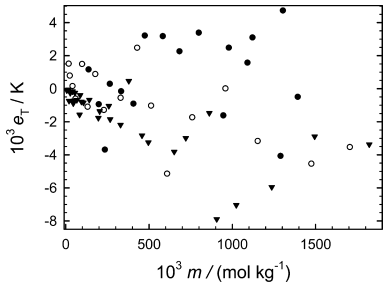

Figure 6. Plot of e_T (eq 21), the deviation between the observed and predicted freezing-point depressions in NaCl solutions as a function of molality m. The observed values have been measured by Gibbard and Gossmann[29] (symbol ●), Momicchioli et al.[31] (○), and Craft and Van Hook[32] (▼), and the predicted values were determined from eq 13, where eq 16 with $\beta^0 = 0.0379$, $\beta^1 = 0.280$, and $C^\phi = 0.00698$ was used for the osmotic coefficients.

Weinzierl,[39] and Menzel,[40] and the results are shown in Figure 7. All of these data support almost within their precision the suggested Pitzer parameters for the less dilute NaCl and KCl solutions.

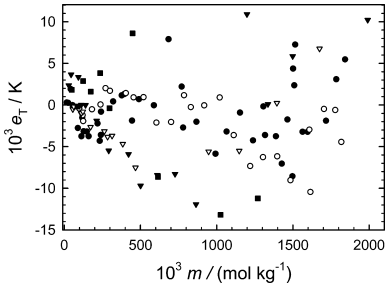

Figure 7. Plot of e_T (eq 21), the deviation between the observed and predicted freezing-point depressions in KCl solutions as a function of molality m. The observed values have been measured by Chiorboli et al.[36] (●), Jones and Bury[37] (○), Karagunis et al.[38] (▼), Damköhler and Weinzierl[39] (▽), and Menzel[40] (■) and the predicted values were determined from eq 13, where eq 16 with $\beta^0 = 0.0239$, $\beta^1 = 0.192$, and $C^\phi = 0$ was used for the osmotic coefficients.

The values of the Pitzer parameters at 273.15 K from Silvester and Pitzer[16,23] and from Thurmond and Brass,[24] based on calorimetric data, are shown in Table 1. These values were also tested with the data of Scatchard and Prentiss[9] for NaCl and KCl solutions in the same way as the new parameter values. The results are shown in Figure 8. The parameter values of Silvester and Pitzer[16] were also tested with the galvanic cell data of Harned and Nims[42] (NaCl solutions) and with those of Harned and Cook[43] (KCl solutions) near to or at the temperature of 273.15 K. These results are presented in Figure 4 in the same way as the results for the new parameter values. The error plots in Figures 4 and 8 show that the literature parameters do not apply to these data as well as the values obtained in the present study. Therefore, it seems to us that the Pitzer parameters for low temperatures can be determined more accurately from the freezing point data than from the

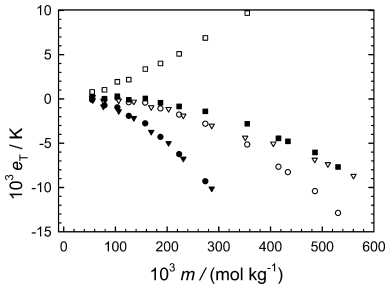

Figure 8. Plot of e_T (eq 21), the deviation between the observed and predicted freezing-point depressions in NaCl and KCl solutions as a function of molality m. The observed values have been measured by Scatchard and Prentiss[9] and the predicted values were determined from eq 13, where eq 16 with the parameter values shown in Table 1 were used. Symbols: ●, NaCl, Pitzer and Mayorga,[25] 298.15 K; ○, NaCl, Silvester and Pitzer,[16] 273.15 K; ▼, KCl, Pitzer and Mayorga,[25] 298.15 K; ▽, KCl, Silvester and Pitzer,[16] 273.15 K; ■, NaCl, Silvester and Pitzer,[23] 273.15 K; □, NaCl, Thurmond and Brass,[24] 273.15 K.

calorimetric data. According to the considerations presented above, the high-precision freezing point data (where the experimental errors are often quite close to 0.0001 K) give the thermodynamic quantities (as if they are isothermally determined) at 273.15 K within their full precision up to about 0.5 mol·kg^{-1}. Therefore, it is clear that the calorimetric data (where results from various temperatures are needed) cannot compete in accuracy with these data. In Table 1 are also given the temperature derivatives that were obtained from the present results at 273.15 K and from the values of Pitzer and Mayorga at 298.15 K for these three parameters of both salts.

Recommended Activity and Osmotic Coefficients. On the basis of the evidence provided by the tests of the present study (see Figures 1 to 7), the suggested Pitzer parameters explain well the freezing point depressions available for NaCl and KCl solutions. New tables (Tables S1 and S2, these tables are given in the Supporting Information) of the values of thermodynamic properties in solutions of these salts at 273.15 K were based on these equations. The Pitzer equations determined for the more concentrated solutions were used in the calculation of the values of the activity quantities in these tables. The values from the two-parameter Pitzer equations for dilute solutions are reported in parentheses in case they are different from the former values. In these tables, additionally, the predicted freezing point depressions are tabulated based on the new parameters and they were compared to the values obtained previously[19,20] by using the Hückel equations for describing the nonideality. The agreement between these values is always good.

The activity and osmotic coefficients for NaCl and KCl solutions at 273.15 K in Supporting Information, Tables S1 and S2 are also compared to the values presented in the literature for these quantities in Tables 2 and 3, respectively. In both of these tables, the activity coefficients from the text-book of Harned and Owen[45] were included and these values were based on the electrochemical data of Harned and Nims[42] and Harned and Cook.[43] In Table 2, the values from multiparameter equations of Pitzer et al.,[46] Clarke and Glew,[47] and Archer[48] were also included for NaCl solutions, as well as in Table 3 the osmotic coefficients for KCl solutions from the multiparameter

dx.doi.org/10.1021/ie404042h | Ind. Eng. Chem. Res. 2014, 53, 5608−5616

Table 2. Results of the Comparison of the Values Presented for the Activity Coefficients (γ) and Osmotic Coefficients (ϕ) in Aqueous Sodium Chloride Solutions at 273.15 K as Functions of the Molality (m)[a]

m/m^o	γ^a	γ(H and O)[b]	γ(PPB)[c]	γ(C and G)[d]	γ(Arc)[e]	ϕ^a	ϕ(PPB)[c]	ϕ(C and G)[d]	ϕ(Arc)[e]
0.1	0.7813	0.781	0780	0.77998	0.7796	0.9325	0.932	0.93184	0.9316
0.2	0.7343	0.731		0.73269		0.9213		0.92056	
0.5	0.6717	0.671	0.672	0.67159	0.6706	0.9098	0.912	0.91128	0.9108
1.0	0.632	0.6375	0.635	0.63501	0.6340	0.912	0.917	0.91610	0.9157
1.5	0.618	0.626		0.62475		0.922		0.93123	

[a]The present values. They were calculated up to 0.5 mol·kg^{-1} using the Pitzer parameters of β^0 = 0.0396, β^1 = 0.2801, and C^ϕ = 0, and above this molality using those of β^0 = 0.0379, β^1 = 0.2801, and C^ϕ = 0.00698 (see text). [b]Taken from ref 45. [c]Taken from ref 46. [d]Taken from ref 47. [e]Taken from ref 48.

Table 3. Results of the Comparison of the Values Presented for the Activity Coefficients (γ) and Osmotic Coefficients (ϕ) in Aqueous Potassium Chloride Solutions at 273.15 K as Functions of the Molality (m)[a]

m/m^o	γ^a	γ(H and O)[b]	γ(S and P)[c]	ϕ^a	ϕ(Arc)[d]	ϕ(S and P)[c]
0.1	0.7707	0.768	0.7717	0.9262	0.9253	0.9269
0.2	0.7172	0.717	0.7193	0.9108		0.9124
0.5	0.6421	0.642	0.6475	0.8910	0.8907	0.8956
1.0	0.586	0.588	0.596	0.879	0.8813	0.888
1.5	0.554	0.563	0.570	0.874		0.889

[a]The present values. They were calculated up to 0.5 mol·kg^{-1} using the Pitzer parameters of β^0 = 0.0234, β^1 = 0.1919, and C^ϕ = 0, and above this molality using those of β^0 = 0.0239, β^1 = 0.1919, C^ϕ = 0 (see text). [b]Taken from ref 45. [c]The activity using the Pitzer parameters β^0 = 0.03386, β^1 = 0.1854, and C^ϕ = 0.000434, see Table 1 and refs 16 and 25. [d]Taken from ref 49.

equation of Archer.[49] All of these complicated equations apply to high temperatures and pressures. In general, the agreement in the tables is quite good with the new values which are closely associated with the experimental accuracy of the high-precision freezing point data. This result is an expected one because the best freezing-point data are normally included in the data set used in the parameter estimation for these complicated equations. In Table 3 are also given the activity and osmotic coefficients calculated using the Pitzer parameters presented in Table 1 for the case where the temperature dependencies of these parameters are given by Pitzer and Silvester[16] for KCl solutions. According to the test results with the real experimental data in Figure 8, it is not a surprise that these parameter values do not predict the results obtained by the new parameter values as well as the other equations tested in Tables 2 and 3.

CONCLUSIONS

Pitzer parameters for NaCl and KCl solutions were determined for 273.15 K by a new calculation method from the best freezing point data available in the literature, and all other reliable data for this quantity were used in the tests of the resulting parameters. It is proved here that the accuracy of the new two-parameter Pitzer equations are affected by no means by the fact that the freezing point data are not isothermal and that these equations apply within experimental error up to a molality of 0.5 mol·kg^{-1}. The results obtained with the new Pitzer equations are compared to those obtained by the corresponding equations where the parameter values have been determined using calorimetric data from the values obtained at 298.15 K. These values were tested with both the freezing point data and the cell-potential difference data. The latter data are, however, only scarcely available for 273.15 K. The new parameter values apply better to the data from both sources. New activity and osmotic coefficients were calculated at rounded molalities for 273.15 K and these results were compared to the values presented in the commonly used thermodynamic tables and to those obtained from the general literature equations with many parameters for the properties of NaCl and KCl solutions at various temperatures and pressures.

Experimental data associated with the solid−liquid equilibrium, for example, the freezing points of aqueous solutions, form an important thermodynamic background in the design of the separation and purification processes and equipment for desalination and freeze crystallization, especially eutectic freezing crystallization. Furthermore, it is important that this background should be developed as firm as possible. Therefore, a robust thermodynamic model presented in this work for sodium and potassium chloride solutions is of great importance because it applies to the existing wide experimental data within the errors associated with the best measurements (in the best cases close to within 0.0001 K). Sodium and potassium chloride solutions are examples of the salts whose solutions have been thoroughly investigated. It seems important that the corresponding high-quality models will be recalculated in the near future for solutions of all salts which have been so far reliably measured in the literature.

ASSOCIATED CONTENT

Supporting Information

Tables S1 and S2 as described in the text. This material is available free of charge via the Internet at http://pubs.acs.org.

AUTHOR INFORMATION

Corresponding Author

*Fax: +358 5 621 2350. E-mail: jpartane@lut.fi.

Notes

The authors declare no competing financial interest.

ACKNOWLEDGMENTS

The authors are indebted to the Academy of Finland (Project No. 260141) and to the Graduate School and Research Foundation of Lappeenranta University of Technology for financial support.

REFERENCES

(1) Robinson, R. A.; Stokes, R. H. *Electrolyte Solutions*, 2nd ed.; Butterworths Scientific Publications: London, 1959; pp 185−189.

(2) Pitzer, K. S. Thermodynamics of electrolytes. I. Theoretical basis and general equations. *J. Phys. Chem.* **1973**, *77*, 268−277.

(3) Schreiber, D. R.; DeWyse, K.; Schreiber, L. C.; Tung, T. Enthalpies of dilution of some aqueous transition metal sulfate solutions at 25 °C. *J. Solution Chem.* **1999**, *28*, 567−573.

(4) Haghighi, H.; Chapoy, A.; Tohidi, B. Freezing point depression of electrolyte solutions: Experimental measurements and modeling using cubic-plus-association equation of state. *Ind. Eng. Chem. Res.* **2008**, *47*, 3983−3989.

(5) Rahman, M. S.; Guizani, N.; Al-Khaseibi, M.; Al-Hinai, S. A.; Al-Maskri, S. S.; Al-Hamhami, K. Analysis of cooling curve to determine the end point of freezing. *Food Hydrocolloids* **2002**, *16*, 653−659.

(6) Marliacy, P.; Hubert, N.; Schuffenecker, L.; Solimando, R. Use of Pitzer's model to calculate thermodynamic properties of aqueous electrolyte solutions of Na_2SO_4 + NaCl between 273.15 and 373.15 K. *Fluid Phase Equilib.* **1998**, *148*, 95−106.

(7) Mohs, A.; Decker, S.; Gmehling, J. The solid−liquid equilibrium of the binary system H_2O−DMSO and the influence of a salt (NaCl, KCl) on the thermodynamic behavior. Correlations using a revised LIQUAC model. *Fluid Phase Equilib.* **2011**, *304*, 12−20.

(8) van der Ham, F.; Witkamp, G. J.; de Graauw, J.; van Rosmalen, G. M. Eutectic freeze crystallization simultaneous formation and separation of two phases. *J. Cryst. Growth* **1999**, *198/199*, 744−748.

(9) Scatchard, G.; Prentiss, S. S. The freezing points of aqueous solutions. IV. Potassium, sodium and lithium chlorides and bromides. *J. Am. Chem. Soc.* **1933**, *55*, 4355−4362.

(10) Robinson, R. A. The vapour pressures of solutions of potassium chloride and sodium chloride. *Trans. R. Soc., New Zealand* **1945**, *75*, 203−217.

(11) Gibbard, H. F., Jr.; Scatchard, G.; Rousseau, R. A.; Creek, J. L. Liquid−vapor equilibrium of aqueous sodium chloride, from 298 to 373 K and from 1 to 6 mol kg^{-1}, and related properties. *J. Chem. Eng. Data* **1974**, *19*, 281−288.

(12) Janz, G. J.; Gordon, A. R. The thermodynamics of aqueous solutions of sodium chloride at temperatures from 15−45° from e. m. f. measurements on cells with transference. *J. Am. Chem. Soc.* **1943**, *65*, 218−221.

(13) Brown, A. S.; MacInnes, D. A. The determination of activity coefficients from the potentials of concentration cells with transference. I. Sodium chloride at 25°. *J. Am. Chem. Soc.* **1935**, *57*, 1356−1362.

(14) Hornibrook, W. J.; Janz, G. J.; Gordon, A. R. The thermodynamics of aqueous solutions of potassium chloride at temperatures from 15−45° from e. m. f. measurements on cells with transference. *J. Am. Chem. Soc.* **1942**, *64*, 513−516.

(15) Shedlovsky, T.; MacInnes, D. A. The determination of activity coefficients from the potentials of concentration cells with transference. III. Potassium chloride. IV. Calcium chloride. *J. Am. Chem. Soc.* **1937**, *59*, 503−506.

(16) Silvester, L. F.; Pitzer, K. S. Thermodynamics of electrolytes. X. Enthalpy and effects of temperature on the activity coefficients. *J. Solution Chem.* **1978**, *7*, 327−337.

(17) Osborne, N. S. Heat of fusion of ice. A revision. *J. Res. Natl. Bur. Stand.* **1939**, *23*, 643−646.

(18) Osborne, N. S.; Stimson, H. F.; Ginnings, D. C. Measurements of heat capacity and heat of vaporization of water in the range 0 to 100 °C. *J. Res. Natl. Bur. Stand.* **1939**, *23*, 197−260.

(19) Partanen, J. I.; Minkkinen, P. O. Activity and osmotic coefficients of dilute sodium chloride solutions at 273 K. *J. Chem. Eng. Data* **1991**, *36*, 432−435.

(20) Partanen, J. I.; Minkkinen, P. O. Activity and osmotic coefficients of dilute potassium chloride solutions at 273 K. *Acta Chem. Scand.* **1992**, *46*, 116−121.

(21) Archer, D. G.; Carter, R. W. Thermodynamic properties of the NaCl + H_2O system. 4. Heat capacities of H_2O and NaCl(aq) in cold-stable and supercooled states. *J. Phys. Chem. B* **2000**, *104*, 8563−8584.

(22) Archer, D. G.; Wang, P. The dielectric constant of water and Debye−Hückel limiting law slopes. *J. Phys. Chem. Ref. Data* **1990**, *19*, 371−411.

(23) Silvester, L. F.; Pitzer, K. S. Thermodynamics of electrolytes. 8. High-temperature properties, including enthalpy and heat capacity, with application to sodium chloride. *J. Phys. Chem.* **1977**, *81*, 1822−1828.

(24) Thurmond, V. L.; Brass, G. W. Activity and osmotic coefficients of NaCl in concentrated solutions from 0 to −40 °C. *J. Chem. Eng. Data* **1988**, *33*, 411−414.

(25) Pitzer, K. S.; Mayorga, G. Thermodynamics of electrolytes. II. Activity and osmotic coefficients for strong electrolytes with one or both ions univalent. *J. Phys. Chem.* **1973**, *77*, 2300−2308.

(26) Partanen, J. I.; Minkkinen, P. O. Thermodynamic activity quantities in aqueous sodium and potassium chloride solutions at 298.15 K up to a molality of 2.0 mol kg^{-1}. *Acta Chem. Scand.* **1993**, *47*, 768−776.

(27) Partanen, J. I.; Minkkinen, P. O. A critical comparison of the equations presented for activities in aqueous sodium and potassium chloride solutions at 298.15 K. *J. Chem. Eng. Data* **1994**, *39*, 432−437.

(28) Partanen, J. I; Covington, A. K. Re-evaluation of the thermodynamic activity quantities in aqueous sodium and potassium chloride solutions at 25 °C. *J. Chem. Eng. Data* **2009**, *54*, 208−219.

(29) Gibbard, H. F., Jr.; Gossmann, A. F. Freezing points of electrolyte mixtures. I. Mixtures of sodium chloride and magnesium chloride in water. *J. Solution Chem.* **1974**, *3*, 385−393.

(30) Harkins, W. D.; Roberts, W. A. The freezing-point lowerings in aqueous solutions of salts and mixtures of salts and of a salt with a nonelectrolyte. *J. Am. Chem. Soc.* **1916**, *38*, 2676−2679.

(31) Momicchioli, F.; Devoto, O.; Grandi, G.; Cocco, G. Thermodynamic properties of concentrated solutions of strong electrolytes. I. Activity coefficients of water from freezing-point depressions for alkali chlorides. *Ber. Bunsen. Phys. Chem.* **1970**, *74*, 59−66.

(32) Craft, Q. D.; Van Hook, W. A. Isotope effects in aqueous systems. VI. Partial molal free energies in NaCl−H_2O−D_2O by freezing-point measurements. The heat of fusion of D_2O. *J. Solution Chem.* **1975**, *4*, 923−947.

(33) Garnsey, R.; Prue, J. E. Cryoscopic determination of osmotic coefficients for ammonium chloride and bromide. *Trans. Faraday Soc.* **1966**, *62*, 1265−1270.

(34) Brown, P. G. M.; Prue, J. E. A study of ionic association in aqueous solutions of bi-bivalent electrolytes by freezing-point measurements. *Proc. R. Soc. London, Ser. A* **1955**, *232*, 320−336.

(35) Adams, L. H. The measurement of freezing-point depression of dilute solutions. *J. Am. Chem. Soc.* **1915**, *37*, 481−496.

(36) Chiorboli, P.; Momicchioli, F.; Grandi, G. Cryoscopical measurements of strong electrolyte solutions. I. The equilibrium method for measuring freezing points with a resistance platinum thermometer. *Boll. Sci. Fac. Chim. Ind. Bologna* **1966**, *24*, 133−151.

(37) Jones, E. R.; Bury, C. R. The freezing-points of concentrated solutions. Part I. Experimental methods and the freezing-points of potassium chloride solutions. *Philos. Mag., Ser. [7]* **1927**, *3*, 1032−1037.

(38) Karagunis, G.; Hawkinson, A.; Damköhler, G. Zur Individualität der osmotischen Koeffizienten bei Alkalihalogeniden. *Z. Phys. Chem. A* **1930**, *151*, 433−466.

(39) Damköhler, G.; Weinzierl, J. Zur Individualität der osmotischen Verhaltens der Alkalihalogenide. *Z. Phys. Chem.* **1934**, *167*, 71−86.

(40) Menzel, H. Eine neue Thermometerform zur Kryoskopie wässriger Lösungen. *Z. Elektrochem.* **1927**, *33*, 63−69.

(41) Cavallaro, L.; Indelli, A.; Pancaldi, G. On some improvements on a cryoscopic precision apparatus and on the control of a thermocouple (in Italian). *La Ricerca Scientifica* **1953**, *23*, 2237−2243.

(42) Harned, H. S.; Nims, L. F. The thermodynamic properties of aqueous sodium chloride solutions from 0 to 40°. *J. Am. Chem. Soc.* **1932**, *54*, 423−432.

(43) Harned, H. S.; Cook, M. A. The thermodynamics of aqueous potassium chloride solutions from electromotive force measurements. *J. Am. Chem. Soc.* **1937**, *59*, 1290−1292.
(44) Partanen, J. I.; Juusola, P. M.; Vahteristo, K. P.; de Mendonça, A. J. G. Re-evaluation of the activity coefficients of aqueous hydrochloric acid solutions up to a molality of 16.0 mol·kg^{-1} using the Hückel and Pitzer equations at temperatures from 0 to 50 °C. *J. Solution Chem.* **2007**, *36*, 39−59.
(45) Harned, H. S.; Owen, B. B. *The Physical Chemistry of Electrolytic Solutions*, 3rd ed.; Reinhold Publishing Corporation: New York, 1958; pp 726−727.
(46) Pitzer, K. S.; Peiper, J. C.; Busey, R. H. Thermodynamic properties of aqueous sodium chloride solutions. *J. Phys. Chem. Ref. Data* **1984**, *13*, 1−102.
(47) Clarke, E. C. W.; Glew, D. N. Evaluation of the thermodynamic functions for sodium chloride from equilibrium and calorimetric measurements below 154 °C. *J. Phys. Chem. Ref. Data* **1985**, *14*, 489−610.
(48) Archer, D. G. Thermodynamic properties of the NaCl + H_2O system: II. Thermodynamic properties of NaCl(aq), NaCl·$2H_2O$(cr), and phase equilibria. *J. Phys. Chem. Ref. Data* **1992**, *21*, 793−829.
(49) Archer, D. G. Thermodynamic properties of the KCl + H_2O system. *J. Phys. Chem. Ref. Data* **1999**, *28*, 1−17.

ACTA UNIVERSITATIS LAPPEENRANTAENSIS

679. STRAND, ELSI. Enhancement of ultrafiltration process by pretreatment in recovery of hemicelluloses from wood extracts. 2016. Diss.

680. TANNINEN, PANU. Press forming of paperboard – advancement of converting tools and process control. 2015. Diss.

681. VALTONEN, PETRI. Distributed energy resources in an electricity retailer's short-term profit optimization. 2015. Diss.

682. FORSSTRÖM-TUOMINEN, HEIDI. Collectiveness within start up-teams – leading the way to initiating and managing collective pursuit of opportunities in organizational contexts. 2015. Diss.

683. MAGUYA, ALMASI. Use of airborne laser scanner data in demanding forest conditions. 2015. Diss.

684. PEIPPO, JUHA. A modified nominal stress method for fatigue assessment of steel plates with thermally cut edges. 2015. Diss.

685. MURASHKO, KIRILL. Thermal modelling of commercial lithium-ion batteries. 2016. Diss.

686. KÄRKKÄINEN, TOMMI. Observations of acoustic emission in power semiconductors. 2016. Diss.

687. KURVINEN, EMIL. Design and simulation of high-speed rotating electrical machinery. 2016. Diss.

688. RANTAMÄKI, JUKKA. Utilization of statistical methods for management in the forest industry. 2016. Diss.

689. PANOVA, YULIA. Public-private partnership investments in dry ports – Russian logistics markets and risks. 2016. Diss.

690. BAHARUDIN, EZRAL. Real-time simulation of multibody systems with applications for working mobile vehicles. 2016. Diss.

691. MARTIKAINEN, SOILI. Development and effect analysis of the Asteri consultative auditing process – safety and security management in educational institutions. 2016. Diss.

692. TORVINEN, PEKKA. Catching up with competitiveness in emerging markets – An analysis of the role of the firm's technology management strategies. 2016. Diss.

693. NORONTAUS, ANNUKKA. Oppisopimuskoulutus yritysten tuottamana koulutuspalveluna: tavoitteista vaikutuksiin. 2016. Diss.

694. HALMINEN, OSKARI. Multibody models for examination of touchdown bearing systems. 2016. Diss.

695. TALONPOIKA, ANNA-MARIA. Financial working capital – management and measurement. 2016. Diss.

696. INKINEN, HENRI. Intellectual capital, knowledge management practices and firm performance. 2016. Diss.

697. YANG, XIAOCHEN. Development of a welding production quality control and management system model for China. 2016. Diss.

698. LEMINEN, VILLE. Leak-proof heat sealing of press-formed paperboard trays. 2016. Diss.

699. LAAKSONEN, LAURI. Spectral retinal image processing and analysis for ophthalmology. 2016. Diss.

700. OINONEN, MINNA. Management of customer co-development in business-to-business markets. 2016. Diss.

701. ALATALO, SARA-MAARIA. Hydrothermal carbonization in the synthesis of sustainable porous carbon materials. 2016. Diss.

702. UZHEGOV, NIKITA. Design and material selection of high-speed rotating electrical machines. 2016. Diss.

703. RICHTER, CHRIS. Digital collaborations and entrepreneurship – the role of shareconomy and crowdsourcing in the era of smart city. 2016. Diss.

704. JAFARI, SHILA. Investigation of adsorption of dyes onto modified titanium dioxide. 2016. Diss.

705. PATEL, YOGINI. Computational modelling of non-equilibrium condensing steam flows in low-pressure steam turbines. 2016. Diss.

706. LEVCHUK, IRINA. Titanium dioxide based nanomaterials for photocatalytic water treatment. 2016. Diss.

707. AMOUR, IDRISSA. Variational ensemble kalman filtering applied to data assimilation problems in computational fluid dynamics. 2016. Diss.

708. SHESTAKOVA, MARINA. Ultrasound-assisted electrochemical treatment of wastewaters containing organic pollutants by using novel Ti/Ta2O5-SnO2 electrodes. 2016. Diss.

709. OLEKSIIENKO, OLGA. Physico-chemical properties of sol-gel synthesized titanosilicates for the uptake of radionuclides from aqueous solutions. 2016. Diss.

710. PATALA, SAMULI. Advancing sustainability-oriented innovations in industrial markets. 2016. Diss.

711. KUORIKOSKI, TERO. Kohti resonoivaa urheilujohtamista – Tavoitteen muodostuminen urheilun kentässä. 2016. Diss.

712. LAHTELA, VILLE. Improving the properties of solid Scots pine (Pinus sylvestris) wood by using modification technology and agents. 2016. Diss.

713. NEVARANTA, NIKO. Online time and frequency domain identification of a resonating mechanical system in electric drives. 2016. Diss.

714. FANG, CHAO. Study on system design and key technologies of case closure welding for ITER correction coil. 2016. Diss.

715. GARCÍA PÉREZ, MANUEL. Modeling the effects of unsteady flow patterns on the fireside ash fouling in tube arrays of kraft and coal-fired boilers.

716. KATTAINEN, JARI. Heterarkkisen verkostoyhteistyön johtamistarpeet verkoston muotoutumisvaiheessa. 2016. Diss.